# Long term trends of halogenated trace gases, hydrocarbons, alkyl nitrates and of the oxidative capacity of the atmosphere

Mike J. Newland

May 2013

A thesis submitted for the degree of Doctor of Philosophy
University of East Anglia, Norwich, UK

*"…the solution of an intellectual problem comes about in a way not very different from what happens when a dog carrying a stick in its mouth tries to get through a narrow door: it will go on turning its head left and right until the stick slips through…And of course though a head with brains in it has far more skill and experience in these turnings and twistings than an empty one, yet even for it the slipping through comes as a surprise, it is something that just suddenly happens…"*

**The Man Without Qualities, Robert Musil**

# Preface

I set about this work with no knowledge of halons or of alkyl nitrates, two words that would come to dominate my thinking during the subsequent three and a half (and a bit!) years. I had no knowledge of modeling and scant understanding of atmospheric chemistry, in short I was ill equipped to begin such an endeavour. Yet by fair winds and good fortune I find myself already at the end of my journey, having produced that which lies open before you, and added my first brick to the great and endless wall that is human knowledge.

During these years past I have experienced the highs and lows of research — frustrating weeks and months spent, not in the search for an answer to any scientific question but merely trying to understand how the tools to do the job work. At those times one despairs of ever achieving anything worthwhile and science herself is a distant city wreathed in cloud.

I spent two years wrestling with the explanation of one graph and then one day, unlooked for, there (perhaps!) was the answer staring back at me. And these are the days that make it worthwhile, when I imagine I hear the call of nature (not like that, no, not like that either, sorry, Nature). Rarely has something rung more true with me than the quote by Robert Musil on the previous page. A similar quote, by Albert Einstein, has been eyeing me recently from a mug on the desk beside me, "*It is not that I am so smart, it's just that I stay with problems longer.*" I often don't even know what question I'm trying to answer but sit patiently at my desk waiting, as if sat beside a lake fishing, knowing that if I can just cast into vaguely the right area with a bit of patience eventually, perhaps, I'll hook something.

This thesis has shown me that answers are found not by having the most complex model, or by the output of reams of data, but by the careful analysis of a small amount of real world measurements. And having faith that these measurements are trying to tell me something, whispering to me, then shouting, '**Look, it's obvious you fool!**', as I sit there staring dumbly at my screen, oblivious to the cries.

I finish with a minor diversion into the dangerous territories of orthography. A bone of some contention between Claire and I (and the English and the Americans) is the spelling of the various participles of the verb, to model. All I shall say is that model is trochaic. To double the 'l' when using a participle would, to my ears, make it iambic. This would be ridiculous.

# Acknowledgements

The first thanks must go to my primary supervisor, Claire Reeves, for giving me the opportunity to do the research contained herein. I could not have hoped for a better supervisor, her door has always been open and she has always been willing to discuss at length ideas, problems or any random thoughts that happen to pop into my head. Thanks also go to Bill Sturges my secondary supervisor, particularly for guidance on the workings of the firn model and to Johannes Laube for his general advice and prodigious paper output!

Thanks to those who have provided the measurements for my work including: Johannes Laube, David Oram, Chris Hogan, Dave Worton and Detlev Helmig and the general NEEM community. For I am just a lowly modeler and without measurements from those who venture out into the real world I would just be sat at my desk making things up. I have been very fortunate to find myself in a group in which I have been 'the modeler' and hence to have found my way on to several papers. Thanks to all those who have included my work in their papers and to the co-authors of the halons paper.

Thanks to the Norfolk Terrace C crew, ENV 0.32ers, 01.37 W and K, the upstairs people, the downstairs people, to all the old folk, the new folk and to all those who have been there the whole time.

Thanks to the UEA institutions: Café Direct, purveyor of questionable lattes, you have provided a place for reflection and the ingestion of the thoughts of the great; and the UFO, your noodles were out of this world.

Thanks to the Lyndhurstian email group that continues in its own happy way no matter where we all are. To Will for his knowledge of the sun, to Rob for his knowledge of the sea, and to Matt for his knowledge of everything else.

Many thanks must go to those who brought me to the point of even considering a PhD, in particular Derek Vance at the University of Bristol for renewing my interest in learning. Also to Heidi Mader at Bristol and Sue Turner at UEA for finding me dissertation topics which guided me down the route of divining the past from the study of ice.

Finally, thanks to all those who have gone before me. I did a little research to create an academic genealogy of doctoral supervisors (see overleaf) which has served to both inspire and encourage me. Well, I wouldn't want to let Liebig and Ørsted down would I?

# Academic Genealogy

**1800**

**Hans Christian Ørsted**
*University of Copenhagen 1799*

**Freiherr Justus Von Liebig**
*University of Erlangen 1822*

**Edvard A. Scharling**
*Technical University of Denmark 1839*

**Sir Benjamin C. Brodie**
*University of Giessen 1850*

**A. G. Vernon Harcourt**
*University of Oxford 1859*

**H. P. J. Julius Thomsen**
*University of Uppsala 1877*

**Sir John Conroy**
*University of Oxford 1868*

**1900**

**Prof. J. N. Brønsted**
*University of Copenhagen 1908*

**Sir Harold Brewer Hartley**
*University of Oxford 1901*

**R. P. Bell F.R.S.**
*University of Copenhagen 1932*

**Prof. E. F. Caldin**
*University of Oxford*

**Prof. S. A. Penkett**
*University of Leeds 1963*

**Dr. C. E. Reeves**
*University of East Anglia 1989*

**2000**

**Mike Newland**
*University of East Anglia 2013*

*Source: academictree.org*

# Abstract

Atmospheric trends of a series of ozone depleting substances (halons) and greenhouse gases (PFCs, $SF_5CF_3$, HFC-227ea) are reported using measurements from Cape Grim, Tasmania. A two-dimensional global atmospheric chemistry transport model is used to derive global annual emission histories of these long lived gases. Emissions of the halons are found to have decreased since peaking in the 1990s. There is still some considerable uncertainty in the remaining banks of the halons caused by uncertainties in their atmospheric lifetimes and possibly in the reported production data. The contribution of the halons to total tropospheric bromine is predicted to fall from current mixing ratios of about 8.1 ppt to about 3 ppt by 2060 assuming reported lifetimes to be correct. Emissions of the higher perfluorocarbons (PFCs) ($C_4F_{10}$, $C_5F_{12}$, $C_6F_{14}$ and $C_7F_{16}$) have decreased since peaking in the 1990s, with the exception of $C_7F_{16}$, emissions of which have remained stable since the 1990s. Emissions of $C_3F_8$ have also decreased since the 1990s; those of $C_2F_6$ appear to be increasing though this disagrees with recent work of other groups. However the growth rate of the radiative forcing of the atmosphere from the PFCs reported herein has been relatively constant for the past decade largely because of increasing emissions of c-$C_4F_8$. Emissions of $SF_5CF_3$ appear to have ceased in the mid-2000s seeming to confirm the source of the gas as being from production of certain fluorochemicals by the company 3M. Emissions of the hydrofluorocarbon (HFC) HFC-227ea have increased rapidly since the mid-1990s.

Long term trends of six alkanes (ethane, propane, n-butane, iso-butane, n-pentane and iso-pentane) and six alkyl nitrates (methyl, ethyl, 2-propyl, 2-butyl, 2+3-pentyl and 3-methyl-2-butyl) have been derived from measurements from firn air from the two Greenland sites, NEEM and North GRIP. These suggest that alkane mixing ratios peaked in the Arctic around 1980 and that alkyl nitrate mixing ratios in the Arctic peaked in the early 1990s. A detailed chemical mechanism has been developed in a 2-D atmospheric model to investigate the tropospheric chemistry relevant to the production of alkyl nitrates. Using this model, long term emission histories of the alkanes have been derived. These suggest that alkane emissions from Europe, North America and Russia roughly halved between 1980 and the early 2000s while those from Asia roughly doubled. A historic trend of the changing photochemical age of air masses reaching the Arctic has been derived and used as a proxy for changing OH concentrations in the mid-high latitude northern hemisphere. This suggests that OH concentrations decreased from 1950 to about 1975, increased from 1975 to 1995 and have subsequently decreased again. This trend appears to correlate with the trend in the growth rate of methane in the atmosphere over the past sixty years. Using a box model the chemistry of the alkyl nitrate system both in background air and polluted air masses has been investigated, focusing on the response of the system to varying levels of atmospheric NO, OH and $HO_2$. It appears that the observed historic trends of the alkyl nitrates are a result of both changing OH and NO concentrations.

# Acronyms

| | |
|---|---|
| **AGAGE** | Advanced Global Atmospheric Gases Experiment |
| **EDGAR** | Emission Database for Global Atmospheric Research |
| **GWP** | Global Warming Potential |
| **HFC** | Hydrofluorocarbon |
| **HO$_x$** | OH + HO$_2$ |
| **HTOC** | Halons Technical Options Committee |
| **IPCC** | Intergovernmental Panel on Climate Change |
| **IUPAC** | International Union of Pure and Applied Chemistry |
| **JPL** | Jet Propulsion Laboratory (NASA) |
| **MARC** | Model for Alkyl nitrate Related Chemistry |
| **NEEM** | North Greenland Eemian Ice Drilling Project |
| **NGRIP / North GRIP** | North Greenland Ice Core Project |
| **NMVOC** | Non-methane Volatile Organic Compounds |
| **NOAA** | National Oceanic and Atmospheric Administration |
| **NO$_x$** | NO + NO$_2$ |
| **NO$_y$** | NO$_x$ + oxidation products of NO$_x$ |
| **ODP** | Ozone Depletion Potential |
| **ODS** | Ozone Depleting Substance |
| **PFC** | Perfluorocarbon |
| **RETRO** | RE-analysis of the TROpospheric chemical composition over the past 40 years |
| **RH** | Formula of generic alkane |
| **RONO$_2$** | Formula of generic alkyl nitrate |
| **UEA** | University of East Anglia |
| **WMO** | World Meteorological Organisation |

# Contents

# Chapter 1

# Introduction

# 1  Introduction

The effects of man's activities on the chemistry of the atmosphere have repeatedly been brought to the public's attention during the second half of the twentieth century as humans have continued to perturb its natural state. From local air pollution in cities in the 1950s, to acid rain in the 1980s, the ozone hole in the 1990s, and anthropogenically induced climate change today, atmospheric chemistry issues have been among the most pressing of environmental concerns.

These issues have all been brought to the attention of the public because of the effect which they have had on human health or on the environment. Smog, occurring in cities due to emissions from transport, is of concern because of the presence of secondary pollutants, such as ozone, which in high concentrations can cause respiratory problems and are toxic to plants. Acid rain, caused by high emissions of sulfur dioxide into the atmosphere, reduces the pH of rainwater making it toxic to plants, and reduces the pH in rivers and lakes damaging these ecosystems; it also causes erosion to buildings. The destruction of the stratospheric ozone layer, by the release of chlorine and bromine containing compounds into the atmosphere, is of concern because it serves to protect all life on Earth from the harmful effects of ultraviolet radiation from the sun. Global warming and the associated climate change, has effects which are manifold and yet to be fully comprehended, hence the complexity of the issue and the reason that it is a problem which is likely to be with us for many centuries into the future.

As scientists we are called upon by society to investigate these issues, to identify them before they cause irreparable damage, to understand their mechanisms and thus to propose solutions to them which can then be acted on by government, and then to continue to monitor the situation as we, as a society, seek to remedy the problems that we have caused.

Since the 1956 Clean Air Act in the UK, a response to the great smog of 1952 in London, societies have been attempting to solve atmospheric chemistry problems on regional, national and international scales. However while the causes and mechanisms behind such problems are fairly rapidly identified (or often already understood), the solutions are often far less straightforward. Since the problems are generally a result of industrial activities, society must weigh up the cost of the possibility of retarding economic growth against its concern for the environment and the health effects of the problem.

In some situations this has been relatively straightforward, such as the replacement of chlorofluorocarbons (CFCs), which deplete stratospheric ozone, with compounds which have similarly desirable chemical and physical properties but which when released to the atmosphere have no effect on ozone. For other issues, such as society's reliance on global warming inducing fossil fuels as an energy source for both industry and transport, a solution has proved incredibly challenging, especially in a world in which the population continues to grow and becomes ever more affluent, thus increasing its energy usage demands.

The work presented in this thesis covers many of these issues including gases which deplete stratospheric ozone, anthropogenic greenhouse gases which contribute to global warming, pollutants which contribute to local and regional smog episodes, hydrocarbons and $NO_x$.

This chapter introduces the reader to the basic concepts which will be covered in more detail in the following chapters. First the basic structure of the atmosphere is defined. Then the chemistry of the troposphere and the issues pertaining to the greenhouse effect are discussed. Next the chemistry of the stratosphere and ozone related chemistry is discussed. The use of models to represent global atmospheric chemistry is discussed and then the use of firn air to reconstruct atmospheric histories is examined. Finally the thesis rationale is presented at the end of the chapter explaining further the aims and objectives of the work. More specific introductions to each long lived gas studied are given in Chapters 4 and 5 and to the chemistry of the alkanes and alkyl nitrates at the beginning of Chapter 6.

## 1.1    Structure of the Atmosphere

### 1.1.1   Temperature

The atmosphere can be split into four defined regions. Beginning at the surface these are: the troposphere, the stratosphere, the mesosphere and the thermosphere. The boundaries between these layers occur at $8 - 18$ km for the tropopause (dependent on latitude and season), $45 - 55$ km for the stratopause and $80 - 90$ km for the mesopause. These boundaries are generally defined by temperature: temperature decreases with altitude in the troposphere, there is then a temperature inversion above the tropopause and temperatures increase with altitude in the stratosphere before decreasing again in the mesosphere and increasing again in the thermosphere. This thesis will be solely concerned with the troposphere and the stratosphere.

The troposphere is characterised by rapid mixing both vertically and horizontally. This mixing is driven by convective transport caused by the temperature profile of the troposphere decreasing with altitude. This profile comes about because the main source of heat in the troposphere is radiation from the Earth's surface. As hot air rises from the surface it expands and cools due to falling pressure.

The stratosphere is characterised by very slow vertical mixing because of the temperature inversion which prevents the convective transport observed in the troposphere. The source of the heating in the stratosphere are the reactions of ozone which are discussed further in Section 1.4.

### 1.1.2 Pressure

The air pressure at a given point in the atmosphere is simply a result of the amount of molecules above that point, as is shown from the derivation of pressure as force divided by area, and force as mass multiplied by acceleration (i.e. gravity). Hence the higher the altitude, the lower the pressure. This is expressed mathematically using the hydrostatic equation (Equation 1.1) (Seinfeld and Pandis, 2006).

$$\frac{dp(z)}{dz} = -\rho(z)g$$

(E1.1)

where $p$ is pressure, $z$ is height, $\rho(z)$ is the air density at height $z$, and $g$ is acceleration due to gravity.

From a combination of the ideal gas law $pV = nRT$ and $V = m / \rho$, where $M_{air}$ is the average molecular weight of air (28.97 g mol$^{-1}$), $R$ is the molar gas constant (8.314 m$^2$ kg s$^{-2}$ K$^{-1}$ mol$^{-1}$) and $T(z)$ is the temperature at a given height, this can be expressed as Equation 1.2.

$$\frac{dp(z)}{dz} = -\frac{M_{air}gp(z)}{RT(z)}$$

(E1.2)

This can then be re-written in integral form as,

$$p(z) \quad = \quad p_0 \, e^{-z/H} \tag{E1.3}$$

where $H = RT/M_{air}\, g$ and is known as the scale height. This is the height over which the mass of the atmosphere decreases by a factor of $e$ (2.718). In the lower atmosphere $H$ is equal to roughly 8 km (Seinfeld and Pandis, 2006).

### 1.1.3   Amount of a Substance

The most basic way of expressing the amount of a substance in a given volume of the atmosphere is the number of molecules of that substance found in a cubic centimetre, known as the number density. This is a useful number for calculations but it can be difficult to comprehend the exact meaning of a number which is often on the order of $10^6 - 10^{12}$. It is often more useful to know the number of molecules relative to the total number of molecules in that volume of air. This is expressed in terms of a ***molar mixing ratio***. A mixing ratio of 1 part per million means that in every million molecules, there is one molecule of that substance. Commonly used mixing ratio units are parts per million (ppm), parts per billion (ppb) and parts per trillion (ppt).

### 1.1.4   Radiation

The Earth receives short wave radiation from the sun. The amount of energy received as radiation is known as the solar constant ($S_0$) and remains fairly stable with time at about 1362 W m$^{-2}$ (Seinfeld and Pandis, 2006). A part of this incoming radiation is reflected directly back to space both by atmospheric constituents (e.g. clouds and aerosols) and from the surface. The rest of the energy is absorbed, again by both atmospheric constituents (clouds, aerosols and gases) and at the surface. Most of this absorbed energy is then re-radiated back into the atmosphere at a longer wavelength.

The average temperature at the surface of the Earth ($T_e$) can be calculated by combining two equations (Equations 1.4 and 1.5) (Seinfeld and Pandis, 2006). The first of these gives the radiation flux received from the sun at the surface of the Earth ($F_S$), which depends on the solar constant and the mean albedo of the surface (the amount of radiation which is reflected

4

from the surface, $R_p$), the second gives the amount of radiation emitted by the Earth ($F_L$) which depends on the temperature at the surface and the Stefan-Boltzmann constant ($\sigma = 5.67 \times 10^{-8} \text{ W m}^{-2} \text{ K}^{-4}$).

$$F_S = \frac{S_0}{4}(1 - R_p) \tag{E1.4}$$

$$F_L = \sigma T_e^4 \tag{E1.5}$$

Assuming the system to be in equilibrium (i.e. that the amount of incoming radiation from the sun is equal to the outgoing radiation from the Earth), these two equations can be combined to give Equation 1.6.

$$T_e = \left( \frac{(1 - R_p) S_0}{4\sigma} \right)^{1/4} \tag{E1.6}$$

Assuming a mean global albedo of 0.3, Equation 1.6 yields a mean surface temperature of 255K, with a mean global albedo of 0.15 (the earth without clouds) it yields a mean surface temperature of 268K (Seinfeld and Pandis, 2006). These are both well below the observed mean surface temperature of the Earth in the twenty first century of 288K (IPCC, 2007).

This difference is accounted for by the presence of the Earth's atmosphere. The atmosphere absorbs some of the long wave radiation emitted by the Earth and re-emits it in all directions; some is lost to space but some is re-radiated back to the surface. This effect, known as the ***greenhouse effect*** shifts the equilibrium of the Earth system towards warmer temperatures and accounts for the difference between the observed mean global surface temperature and that calculated using Equation 1.6 (Seinfeld and Pandis, 2006). Only atmospheric species which absorb in the wavelength range of the radiation emitted by the Earth contribute to this effect. The most important of these species are $H_2O$, $CO_2$ and $CH_4$ (IPCC, 2007). The enhancement of this effect by the release of anthropogenic greenhouse gases since the industrial revolution is discussed further in Section 1.3.

## 1.2    Tropospheric Chemistry

The chemistry of trace gases in the troposphere is dominated by reaction with the hydroxyl radical (OH). The distribution of OH is in turn largely controlled by atmospheric methane ($CH_4$) and carbon monoxide (CO) distributions (e.g. Wayne, 2006). This is because they are both present in the atmosphere at high mixing ratios and have long atmospheric lifetimes.

### 1.2.1    The Hydroxyl Radical

The hydroxyl radical (OH) is the main driver of oxidative chemistry in the troposphere. The reason for this lies in its non-reactivity towards the major atmospheric constituents, $N_2$, $O_2$, and $H_2O$. This means that it is present in the atmosphere at concentrations that enable it to react with most of the trace gases in the troposphere. Although it is only present at fairly low mixing ratios (<0.05 ppt), most OH reactions involve catalytic cycles which lead to the regeneration of the radical somewhere in the chain enabling a small amount of OH to remove large amounts of trace gases (e.g. Seinfeld and Pandis, 2006). This continual removal of large hydrocarbons and other pollutants from the atmosphere has led to OH having the moniker of the 'global detergent' attached to it.

Due to the short lifetime and low atmospheric mixing ratios of the OH radical it has historically proved very difficult to measure directly (e.g. Seinfeld and Pandis, 2006). Additionally the relevance of such point measurements for considering global lifetimes of long lived gases, well mixed through the atmosphere, is questionable for an atmospheric species whose mixing ratios vary so much spatially and temporally. It has been found to be both easier and more useful to define the atmospheric concentrations of OH in terms of the effect which its presence has on other species within the atmosphere. The species most commonly used for this technique has been methyl chloroform ($CH_3CCl_3$) (e.g. Prinn et al., 1992). Knowing the sources of methyl chloroform and its reaction rate with OH, and having calculated lifetimes with respect to its other sinks, the mean OH concentration can then be derived. This global mean was later improved upon by others (e.g. Spivakovsky et al., 2000; von Kuhlmann et al., 2001) to provide a more useful zonal mean concentration of OH. These lifetime studies have suggested a mean global tropospheric concentration of OH of about $1 \times 10^6$ molecules $cm^{-3}$. This method of calculating zonal mean OH mixing ratios is explored

further in Section 2.4. Direct measurements of the OH radical by techniques such as laser induced fluorescence have measured similar concentrations, on the order of $10^5$ - $10^7$ molecules cm$^{-3}$, but these are highly variable spatially and temporally (e.g. Stone et al., 2012).

The production of the OH radical in the troposphere begins with the photolysis of an ozone molecule ($O_3$) by a photon with energy hv. This produces excited oxygen atoms, $O(^1D)$. These generally collide with a third body, M (typically $N_2$ or $O_2$) which removes energy and converts the excited $O(^1D)$ atoms to ground-state $O(^3P)$ atoms. These then react with $O_2$ and M to give back an $O_3$ molecule. This is a null cycle, i.e. there is no net change in $O_3$ mixing ratio. However, some of the $O(^1D)$ atoms produced from the photolysis of ozone can go on to react with water vapour ($H_2O$) to produce two OH radicals (Figure 1.1).
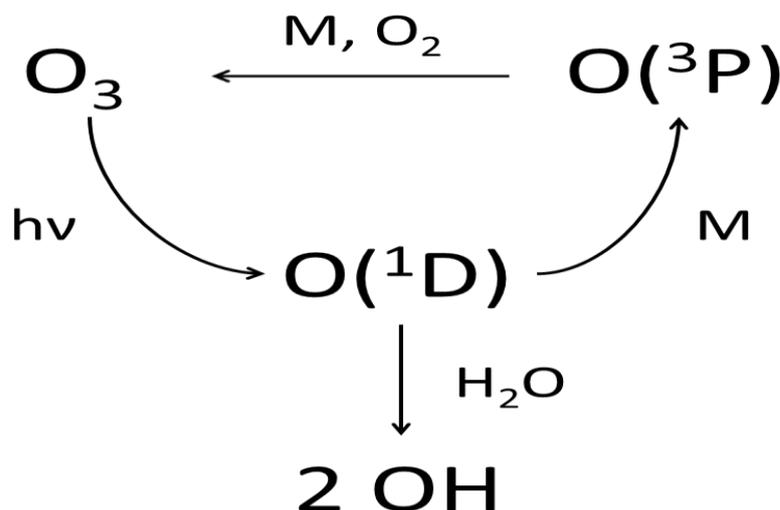


**Figure 1.1** Formation of two hydroxyl radicals (OH) from the photolysis of ozone in the presence of water vapour.

The amount of $O(^1D)$ that is converted to OH radicals in Figure 1.1 depends on the local concentration of water vapour, i.e. the relative humidity. At 298K at mid-latitudes at noon roughly 5% of $O(^1D)$ atoms are converted to OH radicals at 10% relative humidity. At 80% relative humidity this increases to a 40% conversion rate (Seinfeld and Pandis, 2006).

### 1.2.2 NO$_x$ Cycles and Ozone

The two atmospheric traces gases nitric oxide (NO) and nitrogen dioxide (NO$_2$) are collectively known as NO$_x$. They exist in a state of equilibrium with rapid interconversion between the two molecules in the troposphere. The main reaction converting NO$_2$ to NO is the photolysis of NO$_2$. This reaction also produces an O($^3$P) atom which rapidly reacts with O$_2$ to form ozone. This reaction is the only significant source of ozone in the troposphere but most of the ozone created in this way is rapidly converted back to O$_2$ and O($^3$P) by reaction with an NO radical (Figure 1.2). The other main oxidation pathway for NO is by reaction with peroxy radicals.
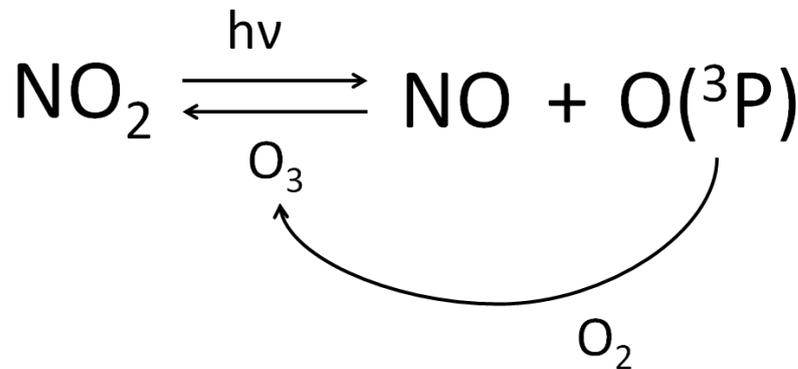


**Figure 1.2** Simplified NO$_x$ and ozone system

The relationship between O$_3$ and NO$_x$ can be described by looking at the rates of change of each molecule in the system based on the assumption that the system presented in Figure 1.2 is a closed system. This is a reasonable assumption since the inter-conversion of NO$_x$ occurs much faster than ozone reacts with other species in the atmosphere when sunlight is present. Equation 1.7 shows the rate equation of NO$_2$ using the simplified system shown in Figure 1.2.

$$\frac{d[NO_2]}{dt} = k_{NO+O_3}[O_3][NO] - j_{NO_2}[NO_2] \qquad (E1.7)$$

where [$X$] denotes the concentration of a given molecule in units of molec cm$^{-3}$, $k_{x+y}$ represents the reaction rate of the molecules $X$ and $Y$ in units of cm$^3$ molec$^{-1}$ s$^{-1}$, and $j_x$ represents the rate of loss due to photolysis of the molecule $X$ in units of s$^{-1}$. Since we assume

the system to be in steady state then the rate of change of $NO_2$ is equal to zero. Hence Equation 1.7 can be rearranged to demonstrate Equation 1.8.

$$[O_3] \quad = \quad \frac{j_{NO_2}\,[NO_2]}{k_{NO+O_3}\,[NO]} \tag{E1.8}$$

Equation 1.8 is known as the photostationary state relationship or the Leighton relationship and shows that, presuming photolysis to be active, if the mixing ratio of two of the three species, NO, $NO_2$, and $O_3$, in the atmosphere is known at a given moment then that of the other species can be calculated.

### 1.2.3  Tropospheric Ozone

The main sink of the OH radical in the atmosphere is reaction with carbon monoxide (CO) which converts the OH radical to a hydroperoxy radical ($HO_2$). Figure 1.3 shows the effect that the presence of $HO_2$ has on the $NO_x$ relationship described in Section 1.2.2.
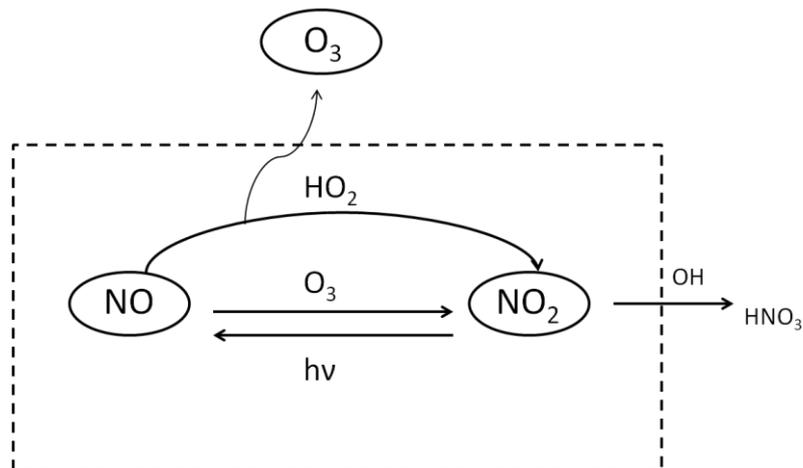


**Figure 1.3**  The effect of the presence of the hydroperoxy radical ($HO_2$) on the $NO_x - O_3$ system shown in Figure 1.2 (Wayne, 2006).

It is seen that, whereas in Figure 1.2 $O_3$ was created by the photolysis of $NO_2$ and used up again in the oxidation of NO, in Figure 1.3 NO can be oxidised by $HO_2$ rather than $O_3$. This means that the photolysis of $NO_2$ has effectively created a molecule of $O_3$. So, the higher the

$HO_2$ mixing ratios, the greater this production source of ozone will be. The rate of ozone production by this route is then equal to the rate of the reaction of NO with $HO_2$ (since for every NO molecule reacting with $HO_2$, a molecule of ozone is 'formed', or rather, not destroyed).

The rate at which a given system (or air mass) produces ozone is termed the ozone production efficiency (OPE). In the system shown in Figure 1.3 the OPE can be defined in terms of the amount of ozone created ($P_{O3}$) per molecule of $NO_x$ removed ($L_{NOx}$) from the system. Figure 1.3 shows that ozone production is determined by the amount of $HO_2$ reacting with NO, i.e. $k_{HO2+NO}[HO_2][NO]$ and $NO_x$ is removed from the system by reaction of $NO_2$ with OH to form nitric acid ($HNO_3$), i.e. $k_{OH+NO}[OH][NO_2]$ . So the OPE can be defined by Equation 1.9.

$$OPE \quad = \quad \frac{P_{O_3}}{L_{NO_x}} \quad = \quad \frac{k_{HO_2+NO}\,[HO_2][NO]}{k_{OH+NO_2}\,[OH][NO_2]} \qquad\qquad \text{(E1.9)}$$

where $P_{O3}$ is the production rate of ozone and $L_{NOx}$ is the rate of loss of $NO_x$.

Equation 1.9 assumes that ozone production is $NO_x$ limited, however as discussed in Section 1.2.5 this is not always the case. Particularly in urban environments ozone production is often limited by the availability of the hydrocarbon precursors rather than $NO_x$.

### 1.2.4   Methane oxidation

Methane ($CH_4$) is present in the troposphere at high mixing ratios because of large emissions and a slow sink. Methane has a wide range of emission sources many of which are anthropogenic. The main anthropogenic sources are associated with fossil fuel production and use, landfills, biomass burning, ruminants and rice farming, with the main natural source emissions from wetlands (Denman and Brasseur, 2007). The main sink of methane is by reaction with the OH radical but this is relatively slow so methane maintains a fairly constant mixing ratio in the atmosphere with only small seasonal variations. The global mean mixing ratio of methane has risen from about 715 ppb in pre-industrial times to about 1800 ppb in 2012 due to increasing atmospheric sources (e.g. Dlugockencky et al., 2012).

The oxidation of CH$_4$ begins with reaction with the OH radical (Reaction 1.1). This forms a methyl peroxy radical (CH$_3$O$_2$) which then reacts with either NO (Reaction 1.2) or HO$_2$ to ultimately form formaldehyde (HCHO) via the alkoxy radical (CH$_3$O). The formaldehyde is then photolysed or reacts with OH to form CO (Reaction 1.3). The oxidation of methane leads to the production of ozone because of the production of peroxy radicals which limit the loss of ozone by reaction with NO. The chain that leads to the maximum ozone yield is summarised below, this chain requires high levels of NO$_x$ (but not so high that the NO$_2$ + OH reaction acts to remove OH from the system – see Figure 1.3) so that the reaction of CH$_3$O$_2$ happens preferentially with NO rather than HO$_2$. It is seen that there is a yield of four peroxy radicals (three HO$_2$ and one CH$_3$O$_2$) which leads to the 'production' of four molecules of ozone.

$$CH_4 + OH \xrightarrow{\ O_2\ } CH_3O_2 + H_2O \tag{R1.1}$$

$$CH_3O_2 + NO \xrightarrow{\ O_2\ } HCHO + HO_2 + NO_2 \tag{R1.2}$$

$$HCHO + h\nu \xrightarrow{\ 2O_2\ } CO + 2HO_2 \tag{R1.3}$$

$$3(HO_2 + NO \rightarrow NO_2 + OH) \tag{R1.4}$$

$$4(NO_2 + h\nu \xrightarrow{\ O_2\ } NO + O_3) \tag{R1.5}$$

$$\textit{Net Reaction}: \ \textbf{CH}_4 + \textbf{8O}_2 \ \rightarrow \ \textbf{CO} + \textbf{H}_2\textbf{O} + \textbf{2OH} + \textbf{4O}_3 \tag{R1.6}$$
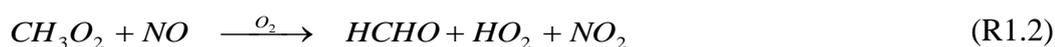
### 1.2.5 Photochemical Smog

The formation process of photochemical smog was first recognised by Haagen-Smit (1952) in the 1950s. One of the main constituents of this smog was ozone, which we have already seen is formed as a result of the oxidation of NO$_2$ in the presence of peroxy radicals (HO$_2$ and RO$_2$).

Most volatile organic compounds (VOCs) follow a similar oxidation path to that of methane; reaction with OH forms a peroxy radical which can then react with NO to form an aldehyde or ketone or with HO$_2$ to form a hydroperoxide. The end product of all of these chains is HCHO which goes on to form CO.

When NO$_x$ and hydrocarbons react to form O$_3$ there is competition between the hydrocarbon and the NO$_2$ to react with the OH radicals. Hence the ozone formation potential of a given air

mass depends on the initial ratio of VOC:NO$_x$. When the ratio of the rate constants, $k_{HC+OH}$ / $k_{NO2+OH}$ (~5.5) of these two reactions is equal to the ratio of VOC:NO$_x$ then OH has a similar tendency for both reactions. If the initial ratio of VOC:NO$_x$ is lower than 5.5 then OH will react preferentially with NO$_2$ to form HNO$_3$ retarding the formation of ozone, hence any further increase of NO$_x$ in the system will not lead to more ozone being produced. This system is said to be VOC limited (i.e. the amount of ozone produced depends on the amount of hydrocarbon and not the amount of NO$_x$). If the initial ratio is above 5.5 then the system is said to be NO$_x$ limited since increasing the amount of hydrocarbon will have no further effect on ozone production unless NO$_x$ is also increased. This is shown in Figure 1.4, an ozone isopleth plot, which demonstrates these limitations.
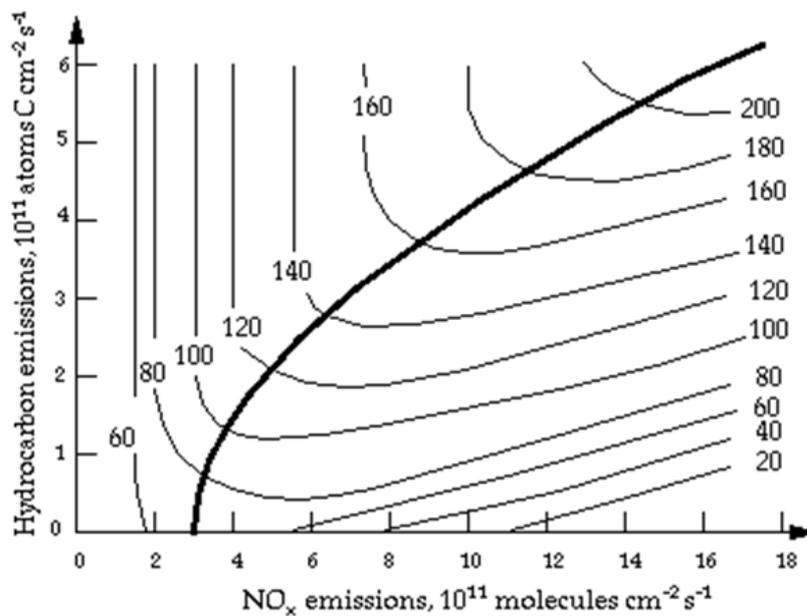


**Figure 1.4** Ozone isopleth plot showing contours of ozone mixing ratio in ppb as a function of emission rates of NO$_x$ and hydrocarbons (Jacob 1999, adapted from Sillman et al., 1990).

Generally the background atmosphere will be a NO$_x$ limited environment with regard to ozone production because of high levels of VOC emissions from plants and because VOCs generally have a longer atmospheric lifetime than NO$_x$ (e.g. Finlayson-Pitts and Pitts, 1999). Whereas urban areas are generally VOC limited because of the very high levels of NO$_x$. As air masses are transported away from urban areas they will move from being VOC limited to

$NO_x$ limited as the $NO_x$ is more quickly depleted than the VOCs (e.g. Finlayson-Pitts and Pitts, 1999).

### 1.2.6 Non-methane Hydrocarbons

Due to the importance of methane ($CH_4$) to atmospheric chemistry, its far greater atmospheric abundance and its relative inertness compared to most other hydrocarbons, it is often considered separately from them and hence all other hydrocarbons are often referred to as ***Non-Methane HydroCarbons*** (NMHCs). NMHCs play an important role in tropospheric chemistry influencing the mixing ratios of $HO_x$, $NO_x$ and Cl in the troposphere and being involved in the formation of tropospheric ozone (Haagen-Smit, 1952). Most NMHCs follow a similar oxidation mechanism to that of methane (Reactions $1.1 - 1.6$). The final products of this chain are HCHO, leading to CO and ultimately to $CO_2$. These products are reached through a series of intermediate carbonyl compounds such as aldehydes (RCHO) and ketones (R'C(O)R). The OH radical tends to be regenerated throughout this process while the greater number of peroxy radicals involved in the oxidation chain, the more NO is converted to $NO_2$.

Alkanes are a class of saturated hydrocarbons with the general chemical formula $C_nH_{2n+2}$. The sources, sinks and seasonality of the non-methane alkanes are discussed below with regards to their study in Chapters 5 and 6 of the thesis.

#### *1.2.6.1* ***Alkane Sources***

The atmospheric mixing ratios of the alkanes have increased greatly during the past 100 years due to the widespread use of fossil fuels in power generation and road transport and a rapidly increasing global population. However there are also natural emissions of these species from the oceans, biomass burning and volcanoes.

Ethane is the most abundant non-methane alkane in the atmosphere with estimated global sources of 9.2 Tg yr^{-1} (EDGAR v2.0, Olivier et al., 1999a). The major anthropogenic sources of ethane are emissions from natural gas extraction and distribution and emissions from biomass burning. Propane has greater estimated emissions, 10.5 Tg yr^{-1} (EDGAR v2.0, Olivier et al., 1999a) but has a shorter lifetime and so a lower atmospheric abundance than ethane. Its main sources are related to natural gas distribution and the petrochemical industry (Reimann and Lewis, 2007). The major anthropogenic sources of the butanes and pentanes are

the combustion of fossil fuels and leakage and evaporation during oil and natural gas production (Friedrich and Obermeier, 1999). The emissions given by EDGAR v2.0 (Olivier et al., 1999a) for the butanes and pentanes were 14.1 and 12.3 Tg yr$^{-1}$ respectively (Pozzer et al., 2010). The sources of the higher alkanes are mainly associated with their use as solvents and with fossil fuel evaporation (Reimann and Lewis, 2007). The majority of anthropogenic emissions, about 91.5% for the butanes and pentanes, (EDGAR v3.2, van Aardenne et al., 2005), are in the northern hemisphere.

The largest natural source of $\geq$C2 alkanes to the atmosphere is from biomass burning (which has both a natural and an anthropogenic component). Pozzer et al. (2010) used the Global Fire Emissions Database (GFED) and emissions factors from Andreae and Merlet (2001) to calculate global emissions in 2000 of 2.76 and 0.86 Tg yr$^{-1}$ for ethane and propane respectively. They also calculated emissions of 1.1 Tg yr$^{-1}$ for the $\geq$C4 alkanes.

The oceans are another natural source of alkanes to the atmosphere. The annual mean fluxes of the C4 – C5 alkanes from the oceans to the atmosphere are reported as $0.3 \times 10^7$ molecules cm$^{-2}$ s$^{-1}$ for iso-butane and iso-pentane and $0.5 \times 10^7$ molecules cm$^{-2}$ s$^{-1}$ for n-pentane in Broadgate et al. (1997) in studies from the North Sea. Similar numbers were obtained by Plass-Dulmer et al. (1995) for studies from 50°N to 35°S and by Broadgate (1995) in the Southern Ocean. From these flux rates global emissions were estimated to be 0.54 and 0.35 Tg yr$^{-1}$ for ethane and propane respectively (Plass-Dulmer et al., 1995) and 0.21 and 0.09 Tg yr$^{-1}$ for the butanes and pentanes respectively (Broadgate et al., 1997). Additionally studies in the Southern Ocean marine boundary layer, where the impact of anthropogenic sources is negligible due to the short lifetime of the C4 – C5 alkanes, suggest that the observed atmospheric mixing ratios of 1 – 10 pptv could be entirely accounted for by a marine oceanic source (Lewis et al., 2001). These mixing ratios are a little lower than those observed by NOAA at South Pole of 10 – 15 pptv (Pozzer et al., 2010). The mechanism of production of alkanes in the ocean has been postulated to be photodegradation of organic matter from phytoplankton (Wilson et al. 1970).

Biogenic emissions of the $\geq$C2 alkanes are thought to be insignificant compared to their global budget (Kesselmeier and Staudt, 1999).

There has been the suggestion of a volcanic emission source by Etiope and Ciccioli (2009) who estimate global annual emissions of 2 – 4 and 1.0 – 2.4 Tg for ethane and propane respectively.

### 1.2.6.2    Alkane Sinks

The major atmospheric sink of the alkanes is reaction with the OH radical. However reaction with atomic chlorine could also be important in certain situations as the reaction rate of alkanes with Cl is almost 100 times greater than that with OH. Hopkins et al. (2002) showed that while air masses with a UK origin displayed hydrocarbon ratios characteristic of processing by the OH radical, those with Arctic origins displayed ratios characteristic of chlorine chemistry even in the summer months when OH would be expected to be at a maximum.

The reaction of alkanes with the OH radical proceeds by abstraction of an H-atom from the C-H bond and follows the same oxidation chain as methane. If a carbon atom is attached to only one other carbon atom it is said to be a primary carbon, if it is attached to two other carbon atoms, it is said to be secondary, and if it is attached to three other carbon atoms it is said to be tertiary. The rate constants for the abstraction of a hydrogen atom are slower for secondary and tertiary carbons compared to primary carbons, i.e. a hydrogen is more likely to be abstracted from a primary carbon.

### 1.2.6.3    Alkane Seasonality

The atmospheric lifetimes of the alkanes vary considerably depending on latitude and time of year. This is because the main sink is reaction with the OH radical, the concentration of which varies spatially and temporally because of its photochemical production mechanism and its very short lifetime. Swanson et al. (2003) report global tropospheric lifetimes for n-butane and iso-butane of 5.5 and 5.7 days based on reaction with an average global OH field of $1.0x10^6$ molecules cm$^{-3}$ (typical Greenland summer concentrations). Using a typical winter time OH concentration of $1.0x10^5$ molecules cm$^{-3}$ the lifetimes are 59 and 60 days.

Measurements of the $\geq$C2 alkanes show large seasonal variations of the mixing ratio at a given latitude (e.g. Swanson et al., 2003; Pozzer et al., 2010). These have a greater amplitude in the northern hemisphere from where the majority of emissions come. The seasonal cycles have late winter maxima and summer minima in both hemispheres. The maxima, at background sites, are on the order of a few hundred ppt for C4 – C5 in the northern hemisphere and the minima on the order of 10 – 20 ppt. This variation is thought to be mainly due to the variation in the sink strength (reaction with OH and Cl) rather than seasonal

changes in the source strength, with fossil fuel combustion and oil and gas production thought to be fairly constant throughout the year (Jobson et al., 1994, Poisson et al., 2000).

### 1.2.7 NO$_y$ and Reservoir Species

Many of the cycles considered so far occur very rapidly, with the atmospheric lifetimes of the species involved often on the order of seconds (e.g. NO$_x$). However NO$_x$ can also form less reactive species with lifetimes on the order of days to months. The oxidation products of NO$_x$ include nitric acid (HNO$_3$), nitrous acid (HONO), the nitrate radical (NO$_3$), dinitrogen pentoxide (N$_2$O$_5$), peroxyacetyl nitrate (PAN – RC(O)OONO$_2$) and alkyl nitrates (RONO$_2$). Along with NO$_x$ these species are known collectively as NO$_y$. These can be particularly important when considering the possible effects of the emissions of high levels of NO$_x$ in urban areas on the remote troposphere. These areas are too far away from urban areas to be affected by the direct transport of NO$_x$, however the less reactive forms of NO$_y$ can be transported from regions of high NO$_x$ (urban areas) to those of low NO$_x$ where they can be broken down releasing the NO$_x$ and perturbing the NO$_x$ mixing ratios in the background troposphere.

The organic nitrates are a family of NO$_y$ species with the general formula RONO$_2$. The largest component of the organic nitrates in the troposphere is generally PAN. This was found to be ubiquitous throughout the atmosphere, particularly in the Arctic where it was discovered to be a major component of the 'Arctic haze' recognised in the 1980s by Barrie (1986). PAN is formed by reaction of the peroxyacetyl radical (CH$_3$C(O)O$_2$) with NO$_2$. The main loss process for PAN is thermal decomposition. Since the photolysis loss is relatively independent of altitude, the lifetime of PAN increases with increasing altitude in the troposphere (ie. decreasing temperature) from a few hours at the surface to a few weeks in the upper troposphere. By this means PAN acts a reservoir for NO$_x$ transporting it to remote areas of the atmosphere. The tropospheric chemistry of the alkyl nitrates, another such reservoir species, is discussed separately in Section 1.2.8 below.

### 1.2.8 Alkyl Nitrates

Alkyl nitrates are a class of organic nitrates with at least one –ONO$_2$ group attached to an alkyl group. They are a part of the group collectively known as NO$_y$ or 'odd' nitrogen (see

Section 1.2.7). Species within this group provide a transport reservoir for the short lived $NO_x$ compounds due to their relatively longer lifetimes. This allows $NO_x$ to be transported from polluted areas to remote background sites. Alkyl nitrates have been reported as making up only a few percent of the $NO_y$ budget in urban and rural areas (Shepson et al., 1993; Thornberry et al., 2001), however due to their relatively long lifetimes and their continued production during transport of polluted air masses, as alkanes are converted to alkyl nitrates (e.g. Bertman et al., 1995), they can comprise up to tens of percent of the $NO_y$ budget in polar regions and in the remote marine troposphere (Talbot et al., 2000). Therefore alkyl nitrates could potentially be a substantial source of $NO_x$ in remote background regions contributing to tropospheric ozone formation in these regions.

The general formula of the mono-nitrates (i.e. those with only one nitrate group attached) is $C_nH_{2n+1}ONO_2$. A shorthand nomenclature was designed by Fischer et al. (2000) whereby the number of carbons in the molecule is preceded by a number representing the position of the nitrate group and this is preceded by the positions of any alkyl groups which branch off of the main carbon chain. The alkyl group is represented by M for methyl and E for ethyl. The abbreviations for the molecules referred to in this study are shown in Table 1.1.

**Table 1.1** Nomenclature and abbreviations of the alkyl nitrates used in this study.

| Alkyl Nitrate | Chemical Formula | Abbreviation |
|---|---|---|
| Methyl nitrate | $CH_3ONO_2$ | C1 |
| Ethyl nitrate | $CH_3CH_2ONO_2$ | C2 |
| 1-propyl nitrate | $CH_3(CH_2)_2ONO_2$ | 1C3 |
| 2-propyl nitrate | $CH_3CH(ONO_2)CH_3$ | 2C3 |
| 1-butyl nitrate | $CH_3(CH_2)_3ONO_2$ | 1C4 |
| 2-butyl nitrate | $CH_3CH(ONO_2)CH_2CH_3$ | 2C4 |
| 1-pentyl nitrate | $CH_3(CH_2)_4ONO2$ | 1C5 |
| 2-pentyl nitrate | $CH_3CH(ONO_2)(CH_2)_2CH_3$ | 2C5 |
| 3-pentyl nitrate | $CH_3CH_2CH(ONO_2)CH_2CH_3$ | 3C5 |
| 3-methyl-2-butyl nitrate | $CH_3CH(ONO_2)CH(CH_3)CH_3$ | 3M2C4 |

### 1.2.8.1 Photochemical Production of Alkyl nitrates

The main production mechanism for the $\geq$C3 alkyl nitrates is the gas phase oxidation of alkanes by OH in the presence of $NO_x$. These alkyl nitrates are therefore generally associated with polluted air masses. Oxidation of the parent alkane (RH) to the alkyl radical (R·) is followed by reaction with molecular oxygen to form a peroxy radical (Reaction 1.8). The peroxy radical then reacts with an NO molecule to form either the alkoxy radical and $NO_2$ (Reaction 1.9a) or the alkyl nitrate (1.9b). The terminology $\alpha_1$ and $\alpha_3$ are used for the branching ratios of Reactions 1.7 and 1.9 to maintain consistency with previous work (e.g. Reeves et al., 2007; Worton et al., 2012).

$$RH + OH \xrightarrow{\alpha_1} R\cdot + H_2O \tag{R1.7}$$

$$R\cdot + O_2 \rightarrow RO_2 \tag{R1.8}$$

$$RO_2 + NO \xrightarrow{1-\alpha_3} RO + NO_2 \tag{R1.9a}$$

$$RO_2 + NO \xrightarrow{\alpha_3} RONO_2 \tag{R1.9b}$$
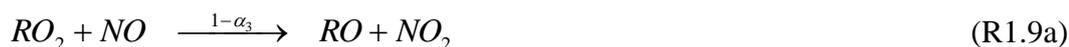
For the $\geq$C3 alkanes there is more than one site from which the H atom can be abstracted in Reaction 1.7 and so a range of peroxy radicals can be formed. The branching ratios for this reaction ($\alpha_1$) tend to favour the formation of the secondary peroxy radicals over primary and tertiary (Table 1.2).

It has already been seen that the conversion of NO to $NO_2$ (Reaction 1.9a) can lead to the production of ozone. For this reason it has been postulated that alkyl nitrates can be used as tracers of ozone production (e.g. Reeves et al., 2007).

**Table 1.2** Branching ratios for the formation of alkyl nitrate precursor peroxy radicals from parent alkanes (http://mcm.leeds.ac.uk/MCM) in 2011.

| Alkane | Peroxy Radical | Branching Ratio $(\alpha_1)$ |
|---|---|---|
| **propane** | 1-propyl | 0.264 |
| | 2-propyl | 0.736 |
| **n-butane** | 1-butyl | 0.127 |
| | 2-butyl | 0.873 |
| **n-pentane** | 1-pentyl | 0.083 |
| | 2-pentyl | 0.568 |
| | 3-pentyl | 0.349 |
| **iso-pentane** | 3-methyl-2-butyl | 0.297 |

There are two possible pathways for Reaction 1.9. The dominant pathway, 1.9a, involves the conversion of NO to $NO_2$ by reaction with the peroxy radical yielding an alkoxy radical. This reaction has a branching ratio $(1 - \alpha_3)$. In the secondary pathway, 1.9b, which has a branching ratio $\alpha_3$, the peroxy radical reacts with NO to form an alkyl nitrate. The yield of this secondary pathway increases with increasing carbon chain length (Table 1.3). At low atmospheric NO concentrations the reaction of peroxy radicals with each other or with $HO_2$ will begin to compete with Reaction 1.9 and so the efficiency of this reaction will be reduced. Roberts et al. (1998) estimate this will begin to occur when the NO concentration falls below 100 – 200 ppt.

Since the yield of alkyl nitrates from Reaction 1.9 increases with chain length but the mixing ratios of the alkanes tends to decrease with chain length, propyl and butyl nitrates are generally present at the highest concentrations in polluted air (Beyersdorf et al., 2010).

**Table 1.3** Branching ratios for the formation of alkyl nitrates from their precursor peroxy radicals and NO (http://mcm.leeds.ac.uk/MCM) in 2011.

| Alkyl Nitrate | Branching Ratio ($\alpha_3$) |
|:---:|:---:|
| C1 | 0.001 |
| C2 | 0.009 |
| 1C3 | 0.02 |
| 2C3 | 0.042 |
| 1C4 | 0.033 |
| 2C4 | 0.09 |
| 1C5 | 0.052 |
| 2C5 | 0.129 |
| 3C5 | 0.131 |
| 3M2C4 | 0.141 |

### 1.2.8.2 *Alternative Sources of Alkyl nitrates*

Another photochemical pathway has been shown to become important for the production of the lower alkyl nitrates in polluted air. Reaction 1.10 shows the reaction of the alkoxy radical, formed in Reaction 1.9a, with $NO_2$.

$$RO + NO_2 \quad \rightarrow \quad RONO_2 \tag{R1.10}$$

This photochemical pathway has been shown to become dominant over Reaction 1.9b for the production of methyl nitrate in polluted air masses where $NO_x$ mixing ratios exceed 40 ppb (Archibald et al., 2007). This reaction is only likely to be important for methyl nitrate rather than the higher nitrates because of the very small branching ratio ($\alpha_3$) for the production of methyl nitrate via the reaction of the peroxy radical with NO.

An oceanic source for C1 – C3 alkyl nitrates was first postulated by Atlas et al. (1993) during the SAGA campaign in which it was observed that elevated mixing ratios of methyl and ethyl

nitrates correlated well with equatorial regions of high productivity. This has since been confirmed by field measurements (e.g. Chuck et al., 2002; Blake et al., 2003; Dahl et al., 2005). Chuck et al. (2002) estimate an annual emission flux from equatorial Atlantic and Pacific Ocean regions of 230 and 68 Gg yr$^{-1}$ for methyl and ethyl nitrate respectively. The oceanic source of $\geq$C4 alkyl nitrates is insignificant compared to anthropogenic sources (Blake et al., 2003).

The production mechanism of the alkyl nitrates is thought to be by the reaction ROO + NO in the aqueous phase with the peroxy radical coming from the photolysis of coloured dissolved organic matter (CDOM) and the NO coming from the photolysis of nitrite (Dahl et al., 2003). Direct emission from algae (Chuck et al., 2002) or from bacteria at depth (Dahl et al., 2007) has also been postulated.

Alkyl nitrates also have a biomass burning source (Friedli et al., 2001; Simpson et al., 2002). Simpson et al. (2002) report emissions of C1 – C4 alkyl nitrates from savanna fires in Australia, with methyl nitrate being primarily emitted during the 'flaming' stage and ethyl – butyl nitrates mainly emitted during the 'smouldering' stage. They estimate global emissions from this source to be on the order of 8 Gg yr$^{-1}$.

### 1.2.8.3    *Alkyl Nitrate Sinks*

The main loss processes for the alkyl nitrates are oxidation by the OH radical and photodissociation (e.g. Talukdar et al., 1997a, 1997b). The importance of the OH sink relative to photolysis increases with increasing carbon chain length to become the dominant loss process in C5 alkyl nitrates and above (Roberts and Fajer, 1989).

The lifetimes of the alkyl nitrates vary with latitude and season due to the seasonality of the OH sink and photolysis. Clemitshaw et al. (1997) report a range of lifetimes with respect to OH and to photolysis. Photolysis lifetimes vary from about ten days for butyl and pentyl nitrate in the summer to 1 – 2 years in the winter at 65°N with lifetimes also decreasing with altitude. The lifetimes due to reaction with OH ($\tau_{OH}$) at 65°N range from tens of years in winter to about 10 days in the summer. $\tau_{OH}$ increases with altitude as the OH concentration decreases. At the equator $\tau_{OH}$ is similar all year round, on the order of a few days.

Photolysis of the alkyl nitrates is thought to yield the peroxy radical and $NO_2$ (IUPAC, 2010), i.e. effectively a reversal of Reaction 1.9b. The products of the reaction of alkyl nitrates with

OH are less well constrained. The reaction proceeds via H-atom abstraction (IUPAC, 2010) but the exact products are dependent on the branching of the alkyl nitrate (Aschmann et al., 2011). Aschmann et al. (2011) observed high yields of acetone and acetaldehyde during the OH initiated oxidation of 3-methyl-2-butyl nitrate and the release of $NO_2$. However they also note that the $NO_2$ may remain locked into intermediate species if the alkyl nitrates go on to form multifunctional species such as carbonyl nitrates.

### 1.2.8.4 *Global Atmospheric Distribution of Alkyl nitrates*

There have been a number of studies of the latitudinal and seasonal variations of alkyl nitrates in marine air (Blake et al., 2003), in the Arctic (Swanson et al., 2003) and in the Antarctic (Beyersdorf et al., 2010).

Blake et al. (2003) report extensive measurements of C1 – C4 alkyl nitrates from the Pacific between 45°N and 72°S during the PEM-Tropics A and B projects. This study observed an equatorial band between about 8°N and 13°S in which the oceans are a source of alkyl nitrates. The highest mean methyl and ethyl nitrate measurements were found in this region. The highest mixing ratios of 2-propyl nitrate were found in the most northerly regions of the study (i.e. 40-45°N) but it also showed significantly elevated mixing ratios in the same equatorial band as the C1 – C2 nitrates. The high mixing ratios in the northern mid-latitudes are explained by production from anthropogenic polluted outflow. 2-butyl nitrate showed almost no enhancement in equatorial regions and again had the highest mixing ratios in the most northerly regions of the study.

Swanson et al. (2003) and Beyersdorf et al. (2010) observe a strong seasonality of alkyl nitrate mixing ratios in the Arctic and Antarctic respectively. Polar alkyl nitrate mixing ratios show a similar seasonality to the alkanes, with a spring-time peak just before polar sunrise and lows in the summer time. Winter time mixing ratios of 2-propyl and 2-butyl nitrate are about 10 ppt, while methyl and ethyl nitrate are about 5 – 6 ppt. In the summer 2-propyl and 2-butyl nitrate mixing ratios fall close to zero, while methyl and ethyl nitrate mixing ratios fall to about 3 ppt. The amplitude of the seasonal cycle reflects the reaction rate with OH, i.e. it increases with increasing carbon number.

## 1.3 Greenhouse Gases

### 1.3.1 The Anthropogenic Greenhouse Effect

In Section 1.1.4 the radiative balance of the Earth system was discussed and it was seen that the observed temperature at the surface of the Earth is dependent on the greenhouse effect caused by the presence of molecules in the atmosphere which absorb and re-emit long wave radiation emitted from the surface of the Earth.

Two of the largest contributors to the natural greenhouse effect are the gases $CO_2$ and $CH_4$ (IPCC, 2007). Since the industrial revolution human activity has added significantly to the global mean mixing ratios of both of these gases. Global $CO_2$ mixing ratios have increased by over 30% from about 280 parts per million (ppm) before the industrial revolution to about 392 ppm in 2012 (e.g. Conway et al., 1994). Global $CH_4$ mixing ratios have increased by more than 150% from about 700 parts per billion (ppb) in pre-industrial times to about 1825 ppb in 2012 (Dlugokencky et al., 2012). This increase in greenhouse gases increases the total energy present in the Earth system and shifts the radiative equilibrium towards higher temperatures. This has led to the effect known as *Global Warming*, i.e. an increase in the mean global temperature at the surface of the Earth. The mean global surface temperature increased by about 0.8 K between 1900 and 2000 (IPCC, 2007).

### 1.3.2 Global Warming Potential

The effect of increasing the atmospheric mixing ratio of a particular gas is a complex problem and is dependent on the precise wavelength bands in which it absorbs, the amount of radiation emitted by the Earth in this wavelength band, and on the mixing ratios of species in the atmosphere which already absorb at that wavelength. Hence the effect of increasing the amount of a particular gas in the atmosphere is not linear but tends to become increasingly less as atmospheric mixing ratios increase and absorption at particular wavelength bands 'fills up' (e.g. Seinfeld and Pandis, 2006).

The effect of certain gases is particularly large because they absorb in what is known as the atmospheric window. This is a region of the wavelength spectrum in which, before the industrial revolution, there were very few species in the atmosphere which absorbed in that region and so almost all of the radiation emitted from the Earth at these wavelengths was lost to space (e.g. Seinfeld and Pandis, 2006).

The radiative forcing of a factor in the atmosphere is defined in the most recent IPCC report (IPCC, 2007) as the 'rate of energy change per unit area of the globe as measured at the top of the atmosphere', expressed in $W\ m^{-2}$. For a given atmospheric species the radiative forcing effect is often expressed in terms of $W\ m^{-2}\ ppb^{-1}$. Greenhouse gases will have positive radiative forcing effects, increasing the amount of energy in the earth system, whereas factors such as sulphate aerosol can have negative effects (IPCC<,2007). The radiative forcing effect of a particular molecule depends on the region of the spectrum in which the gas absorbs and the strength of this absorption.

The Global Warming Potential (GWP) of a gas is a concept which attempts to quantify the total effect of the emission of a given amount of a particular gas on radiative forcing compared to a reference gas (hence GWP is dimensionless) (IPCC, 1990). It is a similar concept to the radiative forcing effect but takes into account the atmospheric lifetime of the species. GWPs are defined for a given time horizon so that species which have a short atmospheric lifetime may have a large effect over a 5 year time horizon but a negligible effect over a 100 year time horizon. The most common time horizon reported is 100 years and the most common reference gas is $CO_2$.

### 1.3.3   Perfluorocarbons

The perfluorocarbons (PFCs) are a group of fully fluorinated carbon compounds. The most abundant group of these in the atmosphere are the perfluoroalkanes with the general formula $C_nF_{2n+2}$. These compounds have atmospheric lifetimes on the order of thousands of years (Table 1.1) due to their chemical inertness. In addition the PFCs have very high global warming potentials (Table 1.4), on the order of 10,000 times that of $CO_2$, due to strong absorption in the infra-red region of the spectrum. The combination of these two properties means that although these compounds currently contribute only a very small amount to the total anthropogenic radiative forcing of the atmosphere, they cannot be ignored because their emission is effectively a permanent change to the radiative forcing of the atmosphere.

**Table 1.4** Atmospheric lifetimes and global warming potentials of the PFCs studied in this work.

| Chemical Formula | Atmospheric Lifetime [a] (years) | Global Warming Potential [b] |
|:---:|:---:|:---:|
| $CF_4$ | > 50,000 | 7,390 |
| $C_2F_6$ | > 10,000 | 12,200 |
| $C_3F_8$ | 2,600 | 8,830 |
| $C_4F_{10}$ | 2,600 | 8,860 |
| c-$C_4F_8$ | 3,200 | 10,300 |
| $C_5F_{12}$ | 4,100 | 9,160 |
| $C_6F_{14}$ | 3,100 | 9,300 |
| $C_7F_{16}$ | ~3000 | - [c] |

[a] Montzka and Reimann et al. (2011)

[b] 100 year time horizon (Forster and Ramaswamy, 2007)

[c] Not reported.

$CF_4$ is the only PFC to have any significant natural source (Harnisch et al., 1996). Pre-industrial background mixing ratios of $CF_4$ have been estimated using stratospheric air (Harnisch et al., 1996a, 1996b), firn air and ancient glacial ice (Khalil et al., 2003; Worton et al., 2007; Mühle et al., 2010), with early estimates being around $40 - 44$ ppt (Harnisch et al., 1996a, 1996b; Khalil et al., 2003) and more recent estimates giving lower mixing ratios of 34-35 ppt (Worton et al., 2007; Mühle et al., 2010). $C_2F_6$ has been reported to have a negligible natural source, with reported estimates of a pre-industrial background of < 0.3 ppt (Worton et al., 2007) and $0.1 \pm 0.02$ ppt (Mühle et al., 2010). These natural sources are likely to be geochemical (Harnisch et al., 1996; Deeds et al., 2008). Measurements from firn air suggest that all other PFCs are entirely anthropogenic (e.g. Oram et al., 2012; Laube et al., 2012), i.e. pre-industrial mixing ratios were indistinguishable from zero.

The main anthropogenic sources of the PFCs are the aluminium industry and the electronics industry with some additional use in fire protection devices and as refrigerants. Table 1.5 shows the various reported usages of the PFCs studied in this work.

**Table 1.5** Emission sources of the perfluorocarbons

| Emission Source | Chemical Formula |
| --- | --- |
| Primary Aluminium Production | $C_2F_6$ |
| CVD Chamber Cleaning | $C_2F_6$, $C_3F_8$, c-$C_4F_8$ |
| Plasma Etching | $C_2F_6$, $C_3F_8$, c-$C_4F_8$ |
| Refrigeration / Air Conditioning | $C_2F_6$, $C_3F_8$, $C_5F_{12}$ |
| Heat Transfer Fluids and Electronics Testing | $C_5F_{12}$, $C_6F_{14}$, $C_7F_{16}$ |
| Fire Extinguishing | c-$C_4F_8$, $C_4F_{10}$ |

During the process of primary aluminium smelting, periods occur known as 'anode effects' when the level of aluminium oxide drops below a threshold level for electrolysis. During these periods $CF_4$ and $C_2F_6$ are emitted as a by-product (e.g. Worton et al., 2007). It has recently been reported that new smelter designs being used in China may have continuous emissions of these two PFCs even during normal operating conditions (Rand and Marks, 2011).

PFCs have been used in the electronics industry since the 1980s due to their combination of desirable chemical and physical properties: inert, high dielectric strengths, non-flammable and non-toxic. The primary use is in the semi-conductor industry as a fluorine source for chemical vapour deposition (CVD) chamber cleaning (70%) and plasma etching of silicon wafers (20-30%) (Harte et al., 2011). The main PFC used for these processes is $C_2F_6$, some of which is converted to $CF_4$ in the cleaning process. Emission reductions can be achieved particularly by changing the CVD chamber cleaning gas to higher PFCs (e.g. $C_3F_8$, c-$C_4F_8$), oxygenated PFCs or $NF_3$ (though even the use of $NF_3$ still leads to some emissions of $CF_4$ as the fluorine reacts with any carbon present).

The higher PFCs ($C_5F_{12}$, $C_6F_{14}$, $C_7F_{16}$) are liquids at room temperature and have been reported to be used since the early 1950s for cooling electronics in the military and have been used in commercial cooling applications since the 1970s (EPA, 2008). They are used as heat transfer fluids (HTFs) for high power electronics because of their high dielectric strengths, electrical resistivity and thermal stability. Emissions are due to leakages and evaporative losses (Tuma and Tousignant, 2001). Since the mid-1990s PFCs have begun to be replaced as HTFs by a group of compounds known as segregated hydrofluoroethers (HFEs). These have similar

chemical properties to the PFCs but have atmospheric lifetimes on the order of 10 years (Montzka and Reimann, 2011) giving them GWPs on the order of 100 times lower than those of the PFCs.

Other uses of the PFCs include as refrigerants and in air conditioning units ($C_2F_6$, $C_3F_8$, $C_5F_{12}$) and in fire protection applications ($C_4F_{10}$, c-$C_4F_8$) making use of their chemical inertness.

PFCs are included in the suite of gases controlled by the Kyoto protocol. However voluntary efforts have been made by both the aluminium industry and the electronics industry to reduce their emissions of the gases. The International Aluminium Institute Board introduced a goal of reducing PFC emissions by 80% per tonne of aluminium produced by 2010 from a baseline of 1990 emissions. It met this target in 2006 and introduced a further target of reducing emissions by at least 50% from 2006 values by 2020. The International Aluminium Institute report that global emissions fell from an average of 4.93 tonnes of $CO_2$ equivalent (TCE) in 1990 to 0.70 TCE in 2008, with total PFC emissions falling from 96 million TCE to less than 28 million TCE during the same period even though primary aluminium production doubled (IAI Survey, 2005). In 1999 the World Semiconductor Council and the U.S. semiconductor industry approved voluntary agreements to reduce PFC emissions by 10% from mid-1990s values by 2010 using various abatement technologies and alternative gases for chamber cleaning (primarily $NF_3$). This goal was achieved in the U.S. in 2003 despite an increase in the demand for silicon wafers. The achievement of this goal by the global industry is reliant on a switch to new fabrication facilities with better technologies.

Several sinks have been suggested for $CF_4$ and $C_2F_6$ including VUV (vacuum ultra-violet – 100 – 200 nm) photolysis and high energy ion reactions in the mesosphere (Morris et al., 1995), and destruction in high temperature combustion processes at the surface (Cicerone, 1979; Ravishankara et al., 1993) .

### 1.3.4   $SF_5CF_3$

The presence of trifluoromethyl sulfur pentafluoride ($SF_5CF_3$) in the atmosphere was first reported by Sturges et al. (2000). The gas has a global mean radiative forcing of 0.59 W m$^{-2}$ ppbv$^{-1}$ (Nielsen et al., 2002), making it the most powerful greenhouse gas, per molecule, yet discovered, though at current atmospheric concentrations the contribution to global warming

is minimal compared to other gases. Atmospheric concentrations of $SF_5CF_3$ were close to zero in the 1960s (Sturges et al., 2000) suggesting that the gas is entirely anthropogenic in origin.

Following the identification of $SF_5CF_3$ in the atmosphere work was done by several groups to try to identify the sources of the gas. Research focused on possible links to $SF_6$ since the two gases are chemically similar and display similar growth curves. One of the sources suggested by Sturges et al. (2000) was as a breakdown product of $SF_6$ in high voltage equipment. Huang et al. (2005) showed that $SF_5CF_3$ could indeed be formed as breakdown product of $SF_6$ under spark discharge conditions in the presence of HFC-23 and HFC-32. It has also been proposed that the molecule could be formed in the atmosphere by a recombination reaction of the $SF_5^+$ and $CF_3^+$ radicals either via a three body reaction or assisted by aerosols (Carrier et al., 2007). Work by Buys (2009) in which air was sampled a couple of metres downwind from potentially leaking electric switch gear found that concentrations of $SF_5CF_3$ and $SF_6$ were not elevated above background atmospheric levels. The only reported industrial use for $SF_5CF_3$ is as a dielectric gas in high energy radar equipment (McCulloch, 2003).

The only source of $SF_5CF_3$ to the atmosphere to have been confirmed is as a by-product of the manufacture of certain 3M fluorochemicals (Santoro, 2000). The electrofluorination process used for the manufacture of these perfluorooctanyl substances, eg. perfluorooctane sulfonyl fluoride (POSF) and products was used by 3M from the 1950s (personal communication, Santoro, 2010). However in 2000 3M agreed to a voluntary phase out of POSF related products, largely due to pressure from the US Environmental Protection Agency, which it completed in 2002 (3M website). The two main production plants of POSF for 3M were in Decatur, Alabama and Antwerp, Belgium (Paul et al., 2009).

Stratospheric profiles suggest a lifetime for $SF_5CF_3$ on the order of 1000 years (Sturges et al., 2000). A similar lifetime was determined by Miller et al. (2002). Morris et al. (1995) determined a lower limit for the lifetime of long-lived greenhouse gases, such as $SF_5CF_3$, for which the primary determining factor of the lifetime is the transport time of the gas from the Earth's surface to the mesosphere, of 800 years (Chim et al., 2003). $SF_5CF_3$ does not undergo oxidation reactions in the troposphere (Kennedy and Mayhew, 2001) and with no excited state below 8eV ($\lambda > 155$nm), it is not broken down in the stratosphere by UV or VUV photolysis (Chim et al. 2001; 2003) and the sole removal method is by reaction with photons (Lyman-$\alpha$), small cations or electrons in the mesosphere. $SF_5CF_3$ displays a similar vertical profile to $SF_6$ (Sturges et al. 2000) and there is a good correlation between $SF_6$ and $SF_5CF_3$ in stratospheric air samples, suggesting similar loss mechanisms for the two gases (Buys, 2009).

### 1.3.5  HFCs

The use of hydrofluorocarbons (HFCs) has grown rapidly as production of first chlorofluorocarbons (CFCs) and later their replacements, hydrochlorofluorocarbons (HCFCs), have been controlled under the Montreal protocol. HFCs are viewed as preferable replacements to their fore-runners as they contain no chlorine or bromine and therefore have ozone depleting potentials of virtually zero (IPCC/TEAP, 2005), consequently there are currently no restrictions on the production of HFCs (IPCC/TEAP, 2005). However there are concerns about the relatively high global warming potential (GWP) of HFCs – HFC-227ea has an estimated GWP of 3,220 (Forster and Ramaswamy, 2007). The C-H bond is susceptible to reaction with OH and hence this is the main breakdown reaction of the HFCs. Because of this HFCs are mostly broken down in the troposphere and so have relatively short lifetimes compared to CFCs. However HFC-227ea is one of the longer lived HFCs with a reported lifetime of 38.9 years (Montzka and Reimann, 2011).

The presence of 1,1,1,2,3,3,3 heptafluoropropane (HFC-227ea; $CF_3CHFCF_3$) in the atmosphere was first reported in the literature by Laube et al. (2010) based on observations from firn and from aircraft and balloon flights. The gas is thought to have been introduced in the early 1990s as one of the host of replacements for ozone depleting CFCs. Laube et al. (2010) report northern hemisphere atmospheric mixing ratios for HFC-227ea in mid-2009 of about 0.6 ppt from aircraft and balloon flights with an inter-hemispheric gradient of at least 1.1 (Laube et al., 2010). Though this is still a very low atmospheric concentration, the growth rate has increased from an average of 0.002 ppt $a^{-1}$ during the period 1995 – 1998 to 0.056 ppt $a^{-1}$ during the period 2004 – 2007. This growth rate will likely increase further as CFCs and HCFCs continue to be replaced by HFCs and other gases.

IPCC/TEAP (2005) reported the main demand for HFC-227ea in 2002 to be for use in fire protection devices (3 Gg $a^{-1}$) followed by medical aerosols (1 Gg $a^{-1}$) and foams (0.1 Gg $a^{-1}$), with emissions related to these uses of 0.3, 1 and 0.01 Gg $a^{-1}$ respectively. They report an expected rise of emissions of HFC-227ea to 4 Gg $a^{-1}$ by 2015 but exact estimates are difficult as there are currently only two reported producers of HFC-227ea (in USA and Russia) (IPCC/TEAP, 2005) and so industry does not have to give production estimates.

## 1.4    Stratospheric Chemistry

The chemistry of the stratosphere is dominated by the reactions of ozone. The presence of ozone in the stratosphere, though at very low mixing ratios, is vital to the chemistry of the stratosphere, of the troposphere and to the presence of life on Earth. The catalytic creation and destruction of ozone is the main source of heat in the stratosphere. The ozone layer absorbs most of the radiation received by the Earth in the UVB region of the spectrum (280 – 315 nm) preventing this radiation from reaching the troposphere. If there were no ozone layer, UVB radiation would alter tropospheric chemistry and, at the surface, would increase the risk of cancers in animals and be damaging to plant life and single celled organisms.

Ozone is involved in various chemical cycles in the stratosphere, the first of which was proposed by Chapman (1930). The production of ozone (Reaction 1.13) involves the breakdown of $O_2$ by photolysis (Reaction 1.11) and the recombination of the products, O, with $O_2$ (Reaction 1.12). The ozone is lost by photolysis (Reaction 1.14) and by reaction with O atoms (Reaction 1.15).

$$O_2 + h\nu \quad \rightarrow \quad O + O \tag{R1.11}$$

$$2[O + O_2 + M] \quad \rightarrow \quad O_3 + M \tag{R1.12}$$

$$\textit{Net Ozone Production : } \quad \textbf{3O}_2 + \textbf{h}\nu \quad \rightarrow \quad \textbf{2O}_3 \tag{R1.13}$$

$$O_3 + h\nu \quad \rightarrow \quad O + O_2 \tag{R1.14}$$

$$O + O_3 \quad \rightarrow \quad 2O_2 \tag{R1.15}$$

$$\textit{Net Ozone Loss : } \quad \textbf{2O}_3 + \textbf{h}\nu \quad \rightarrow \quad \textbf{3O}_2 \tag{R1.16}$$

$M$ is a third body ($N_2$ or $O_2$) required to stabilise the product of Reaction 1.12. It is seen that the net result of Reactions 1.13 and 1.16 is that ozone is neither created nor destroyed.

By the 1960s it was realised that the Chapman cycle over-predicts the observed mixing ratios of ozone in the stratosphere by a factor of two. Hence an additional source of ozone destruction was needed to explain the observations. Over the coming decade a series of

catalytic cycles were proposed to account for this additional destruction. In the early 1970s Crutzen (1970) and Johnston (1971) proposed a role for $NO_x$ in stratospheric ozone chemistry. The most basic of these reactions can be written generally as below, where $X =$ NO, OH or Cl.

$$X + O_3 \ \rightarrow \ XO + O_2 \tag{R1.17}$$

$$XO + O \ \rightarrow \ X + O_2 \tag{R1.18}$$

$$\textit{Net Reaction:} \ \ O_3 + O \ \rightarrow \ 2O_2 \tag{R1.19}$$

### 1.4.1   $NO_x$ Cycles

$NO_x$ is present in the stratosphere mainly due to surface emissions of $N_2O$ which is broken down in the stratosphere. The resulting $NO_x$ leads to the destruction of $O_3$ in a catalytic cycle in which NO is regenerated (Reactions $1.20 - 1.22$).

$$NO + O_3 \ \rightarrow \ NO_2 + O_2 \tag{R1.20}$$

$$NO_2 + O \ \rightarrow \ NO + O_2 \tag{R1.21}$$

$$\textit{Net Reaction:} \ \ O_3 + O \ \rightarrow \ 2O_2 \tag{R1.22}$$
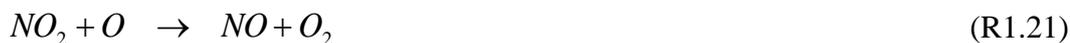
### 1.4.2   $HO_x$ Cycles

Another catalytic cycle, which was proposed by Bates and Nicolet (1950), involves the $HO_x$ family (H, OH, $HO_2$). The main sources of $HO_x$ to the atmosphere are the reactions of $H_2O$ and $CH_4$ with $O(^1D)$. The main catalytic $HO_x$ cycles are shown below.

$$OH + O_3 \ \rightarrow \ HO_2 + O_2 \tag{R1.23}$$

$$HO_2 + O \ \rightarrow \ OH + O_2 \tag{R1.24}$$

$$\textit{Net Reaction:} \ \ O_3 + O \ \rightarrow \ 2O_2 \tag{R1.25}$$

$$OH + O_3 \quad \rightarrow \quad HO_2 + O_2 \qquad\qquad (R1.26)$$

$$HO_2 + O_3 \quad \rightarrow \quad OH + 2O_2 \qquad\qquad (R1.27)$$

***Net Reaction :*** $\; \boldsymbol{2O_3 \quad \rightarrow \quad 3O_2}$ $\qquad\qquad$ (R1.28)

### 1.4.3   Chlorine Cycles

Further catalytic cycles involving halogens were proposed by Molina and Rowland (1974). These were associated with the burgeoning large scale use of halogen containing compounds, used generally because of their low reactivity and low toxicity. However it was realised that these compounds were being transported to the stratosphere where they were broken down by short wavelength radiation and involved in the catalytic destruction of ozone (Molina and Rowland, 1974). The basic cycle is shown below (Reactions 1.29 – 1.31).

$$Cl + O_3 \quad \rightarrow \quad ClO + O_2 \qquad\qquad (R1.29)$$

$$ClO + O \quad \rightarrow \quad Cl + O_2 \qquad\qquad (R1.30)$$

***Net Reaction :*** $\; \boldsymbol{O_3 + O \quad \rightarrow \quad 2O_2}$ $\qquad\qquad$ (R1.31)
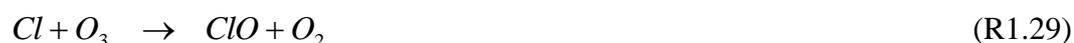
### 1.4.4   Reservoir Species and Termination

The catalytic reactions shown in Sections 1.3.1 – 1.3.3 are terminated when the $NO_x$, $HO_x$ or $ClO_x$ species react to form less reactive 'reservoir' species. These species can either act as temporary buffers to the catalytic cycles (e.g. $ClONO_2$) or can result in the permanent removal of the species from the stratosphere as a portion is transported back to the troposphere and lost there (e.g. $HNO_3$ and HCl). As much as 99% of the stratospheric active chlorine can be stored as $ClONO_2$ and HCl (Seinfeld and Pandis, 2006).

### 1.4.5  Bromine Cycles

Bromine is on average $60 - 65$ times more effective than chlorine per molecule at depleting ozone (Daniel and Velders, 2007). This is for two reasons, firstly bromine containing species tend to be photolysed at longer wavelengths than those containing chlorine and so have shorter lifetimes in the stratosphere, secondly the lack of a reservoir species to buffer the reaction of atomic bromine with ozone. The bromine analogues of the two most important reservoir species for chlorine (HBr and $BrONO_2$) have much shorter lifetimes than their counterparts HCl and $ClONO_2$.

### 1.4.6  Ozone Depleting Substances and ODPs

The Ozone Depletion Potential (ODP) of a gas is a concept used to quantify the ability of a given amount of that gas released at the Earth's surface to break down stratospheric ozone, relative to a reference gas, CFC-11. These ODPs are generally calculated using two dimensional models (e.g. Daniel and Velders, 2011) and then averaged over the whole atmosphere to give a single value for each gas. Specific ODPs for the ozone depleting substances investigated in this work are discussed in the relevant sections of Chapter 3.

### 1.4.7  Halons

The halons are a family of fully halogenated, bromine containing compounds. In 2008 they contributed about 8.3 ppt of the total 22.5 ppt of inorganic bromine ($Br_y$) in the stratosphere (with another $0.4 - 0.9$ ppt contributed by controlled usage of methyl bromide and the remainder by natural sources of methyl bromide and by very short lived substances (VSLS)) (Montzka and Reimann, 2011).

Halons were produced from the 1950s until the end of 2009 and are used mainly in fire extinguishing equipment and explosion protection applications because of their highly inert chemical nature. The two main halons produced for these purposes were H-1211 ($CBrClF_2$) and H-1301 ($CBrF_3$). A third halon, H-2402 ($CBrF_2CBrF_2$), was produced and used mainly in the Soviet Union (McCulloch, 1992). H-1202 ($CBr_2F_2$) is thought to have had very little direct use but was produced as a by-product from over-bromination during H-1211 manufacture (HTOC, 1999). Table 1.6 summarises the halons reported in this work, their atmospheric lifetimes, ODPs and their main uses.

**Table 1.6** Summary of the halons reported in this work

| Name | Chemical Formula | Atmospheric lifetime [a] (years) | ODP [b] | Main use |
|---|---|---|---|---|
| H-1211 | $CBrClF_2$ | 16 | 7.9 | Portable fire extinguishers |
| H-1301 | $CBrF_3$ | 65 | 15.9 | Fixed fire extinguishers and explosion protection |
| H-2402 | $CBrF_2CBrF_2$ | 20 | 13.0 | Portable and fixed fire extinguishers |
| H-1202 | $CBr_2F_2$ | 2.9 | - [c] | Very little reported usage |

[a] Montzka and Reimann (2011)

[b] Daniel and Velders (2011)

[c] Not reported

The halons have relatively long atmospheric lifetimes (H-1211 – 16 years, H-1301 – 65 years, H-2402 – 20 years, H-1202 – 2.9 years (Montzka and Reimann, 2011)). They are mainly broken down by photolysis. This occurs almost entirely in the troposphere for H-1202, in both the troposphere and the stratosphere for H-1211 and H-2402 and almost entirely in the stratosphere for H-1301. The bromine released from breakdown in the stratosphere contributes to stratospheric ozone depletion, with bromine being 60 – 65 times more effective than chlorine at depleting ozone on a per molecule basis (Daniel and Velders, 2007). Because of this, production of halons for non-essential use in non-Article 5 countries (i.e. North America, Europe, Australia and Japan) was banned under the Montreal Protocol in 1994 and production for use in Article 5 countries was banned from 2010. However halons continue to be released to the atmosphere from the existing installed capacity and from users with critical use exemptions (CUEs) such as civil aviation and military applications. Significant halon supply for CUE comes from recycling (HTOC, 2011). H-1301 is still being produced as a chemical feedstock for the production of the pesticide Fipronil (HTOC, 2011).

Previous studies of the halons in air extracted from deep firn snow (Butler et al., 1999, Sturrock et al., 2002; Reeves et al., 2005) have shown them to be entirely anthropogenic in origin with concentrations near zero in the early 1960s. Atmospheric mixing ratios of the halons increased rapidly from the late 1970s up to the late 1990s (Butler et al., 1999; Fraser et

al., 1999; Sturrock et al., 2002). They have since levelled off or begun to decline, with the exception of H-1301 which continues to grow (based on data reported up to 2008) (Reeves et al, 2005; Montzka and Reimann, 2011).

Though halons are no longer being produced they are still being released to the atmosphere due to the existing 'halon bank'. That is, the halons which remain unused in equipment and so are yet to be either released or destroyed. Countries have been encouraged to recycle excess or unwanted halon banks rather than destroying them where possible in order to provide adequate supplies for essential use in military equipment and other applications where new technologies cannot readily be introduced to replace the use of halons. This is a particular problem with H-2402 as it is required by countries (particularly India) which bought Russian military equipment which relies on H-2402. Though Russia and Ukraine have a reasonably large bank of H-2402, the export of ozone depleting substances is prohibited in both countries.

The replacements for H-1301, which was mainly used in fixed fire extinguishing systems, include HFC-227ea, HFC-23, $CO_2$ systems and inert gas systems (HTOC, 2006). The replacements for H-1211, which was mainly used for portable fire extinguishers include ABC powder, foam and $CO_2$ systems (HTOC, 2006).

## 1.5    Atmospheric Modeling

Modeling physical and chemical systems is now an integral part of geophysical studies. Models are generally used in problems where a series of integration steps are required to be performed. A series of calculations that would take days to perform by hand can be run with a computer model in a matter of seconds. The greater the complexity of a model (i.e. the more simultaneous integrations required), the longer it will take to run for a given time period. As computer processors become more powerful with each passing year the capabilities of models become ever greater. However models are still limited by processing power. Consequently a trade-off must be made between model complexity, i.e. the number of processes and chemical reactions represented, and the spatial and temporal resolution of the model.

The efficacy of a model is tested by comparison of the model output to real world measurements, or metrics, from the system which the model is trying to reproduce. It will generally be the case for every component of the model that it has been tested against relevant metrics. It is only once this has been satisfactorily achieved that the results of the model, with

regard to the problem that it is being used to investigate, can be viewed as having any degree of validity.

### 1.5.1 Chemical Transport Models

A chemical transport model by definition aims to represent the transport in the atmosphere and the chemistry relevant to the problem. Beyond this they can be as simple or as complex as needed, from a two box model, representing transport between the two hemispheres, to a high resolution three dimensional model. The model will consist of a set of fixed parameters such as the transport scheme, the chemical mechanism (i.e. how the species within the model react with each other), the temperature and pressure profiles, the photolysis scheme and any number of other parameterisations relevant to the problem. There will be a set of variables which are the subject of the integration calculations updating their concentrations in the model at each time step based on their chemical reactions and physical transport within the model domain. These variables can either be initialised with a given concentration at the start of the model run, input to the model during the run as emissions, or created by processes within the model. The changing concentrations of these variables with time can then be output in order to investigate the problem. Figure 1.5 summarises the typical elements of a chemical transport model.

#### *1.5.1.1* ***Model Chemistry***

The chemical solver in the model will solve a series of first order ordinary differential equations. These are in the form of the rate equation (Equation 1.10) for the given reaction (Reaction 1.32).

$$A + OH \quad \xrightarrow{k} \quad B \tag{R1.32}$$

$$\frac{d[A]}{dt} \quad = \quad k\,[OH][A] \tag{E1.10}$$
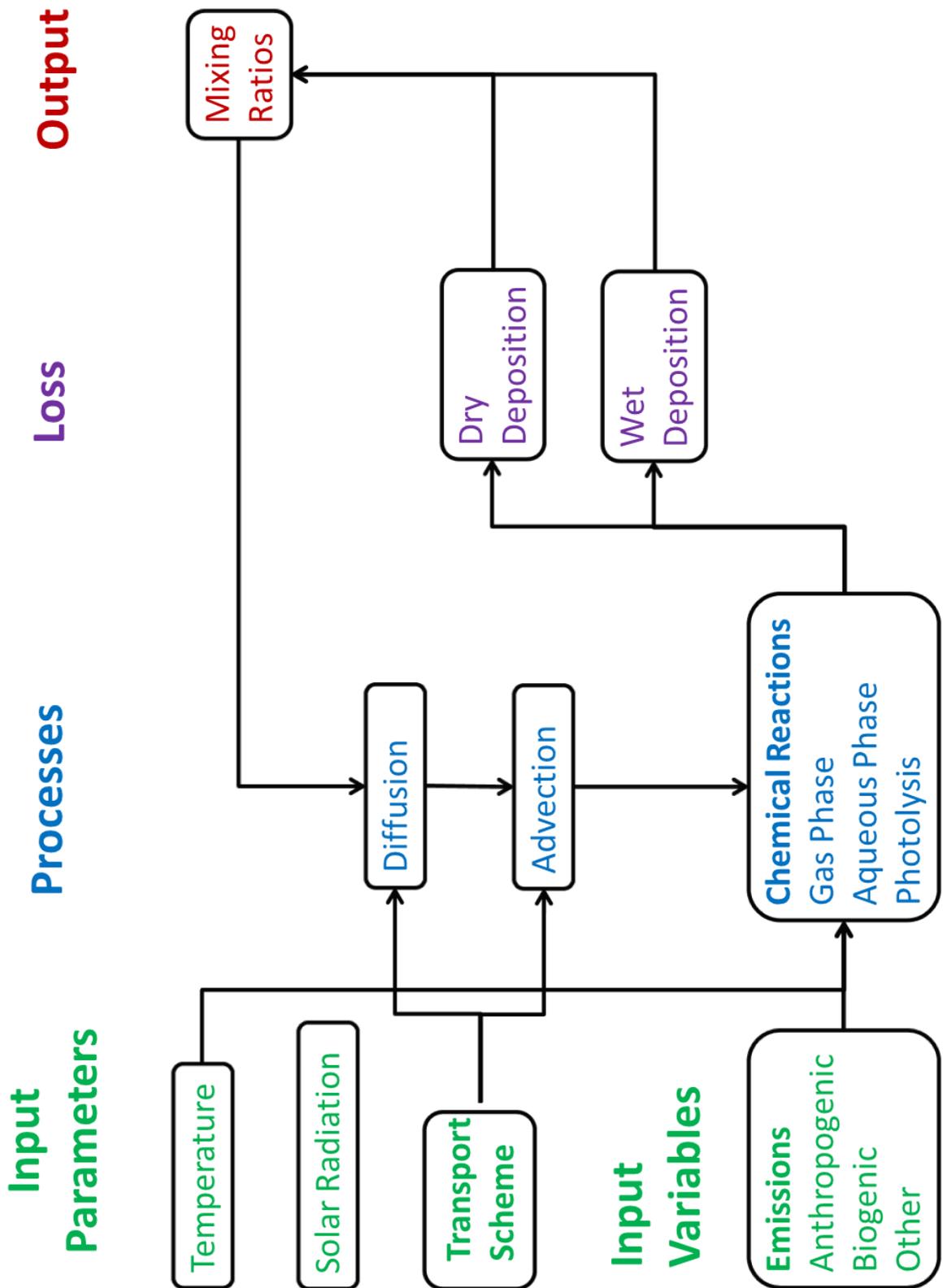
**Figure 1.5**  A general scheme for a chemical transport model

The explicit solution to Equation 1.10 is shown in Equation 1.11.

$$[A]_t \quad = \quad [A]_0 e^{-k[OH]t} \tag{E1.11}$$

For use in a chemical model a solver is required to satisfy several requirements (e.g. Jacobson, 2005). It must provide solutions to the differential equations that are accurate, this accuracy can be checked for a given time step by reducing the time step and checking that the same result is obtained. It must be stable, i.e. the difference between the model calculated value and the exact solution to the differential equation must not increase with time during the model run. It must conserve mass in the model domain, i.e. if the chemical equations are written in such a way that each element should be preserved during chemical reactions, the solutions to the equations must reflect this. The solutions to the equations must be positive. The ideal solver should run as fast as possible while still satisfying these requirements.

The vastly different lifetimes of some of the species in the atmosphere (from microseconds to thousands of years) create problems when choosing a time step over which the model should integrate the equations. This time step must be short enough to accurately represent changes to the species with the shortest lifetime in the model. However the shorter the time step, t, the greater the computational processing power required, i.e. the slower the model will run. To overcome this problem a variety of different integration schemes have been developed which provide semi-implicit solutions to the equations rather than an explicit solution such as would be obtained by solving Equation 1.11. These allow time steps to be used which are much longer than the lifetime of the shortest lived species but still remain stable. The chemical solver used in FACSIMILE, the language in which the atmospheric model used in this work is written, uses the semi-implicit method Gear's solution (Gear, 1971).

### 1.5.1.2 *Model Transport*

Transport of a species within the atmosphere is a function of two parameters advection and diffusion. Advection is transport with the mean fluid flow, i.e. in the atmosphere movement of a species in the mean direction of the wind. Diffusion is a random molecular movement which acts in all directions and tends to smooth out local differences in concentration of a species. This transport is solved within a model by the use of a set of diffusion coefficients in each

dimension for each cell. These constrain the rate of transport between adjacent cells in the model. Transport schemes can either be designed to recreate a mean inter-annual transport for a given location and then annually repeated or can use real meteorological data to define the advective transport.

The transport scheme in a model can be tested by the the use of inert tracer species with well known emission magnitudes and locations. These are emitted into the model and then the model output for these species is compared to measurements at various global locations (e.g. Hough, 1989).

### 1.5.2  2-D Global Modeling

A two-dimensional global atmospheric model will have dimensions of latitude and altitude. This is because the mixing time of a species in the troposphere around a latitudinal band is on the order of two to three weeks. Therefore if the lifetimes of the species of interest are longer than this, then the averaging out in a particular model cell will be a fair representation of the homogeneity of the majority of the atmosphere. This is not the case for latitudinal transport which, across hemispheres, can take on the order of years.

However often the lifetimes of many of the species within a chemical transport model are on the order of hours to a few days (e.g. $NO_x$). This leads to large scale spatial variations in the mixing ratios of these species in the real atmosphere, often a few orders of magnitude. In a two-dimensional model it is not possible to represent these large longitudinal variations which occur for such species as they are averaged out around a latitudinal band. As such the mixing ratio in each latitudinal band represents an integration of remote background, rural and urban mixing ratios. However for problems involving non-linear chemistry, such as the sensitivity of ozone production to the local $NO_x$ concentrations, this averaging out of mixing ratios around a latitudinal band becomes a problem.

## 1.6    Firn Air

Firn is the part of an ice pack below the freshly fallen, uncompressed snow and above the region where air becomes trapped in bubbles. This zone can be a few tens of metres to a few hundred metres deep depending on snow accumulation rates at the site. Figure 1.6 shows a schematic of the structure of a firn column.

Air trapped within firn can be extracted and used to recreate atmospheric histories of gases (e.g. Schwander et al., 1993), which again can range from tens of years to hundreds of years. The main advantage of firn air compared to that trapped within bubbles in ice cores is that a far greater quantity of air can be extracted from the firn. This allows for analysis of trace gases which are present in too low concentrations to be detected in the small quantities of air extracted from ice cores.
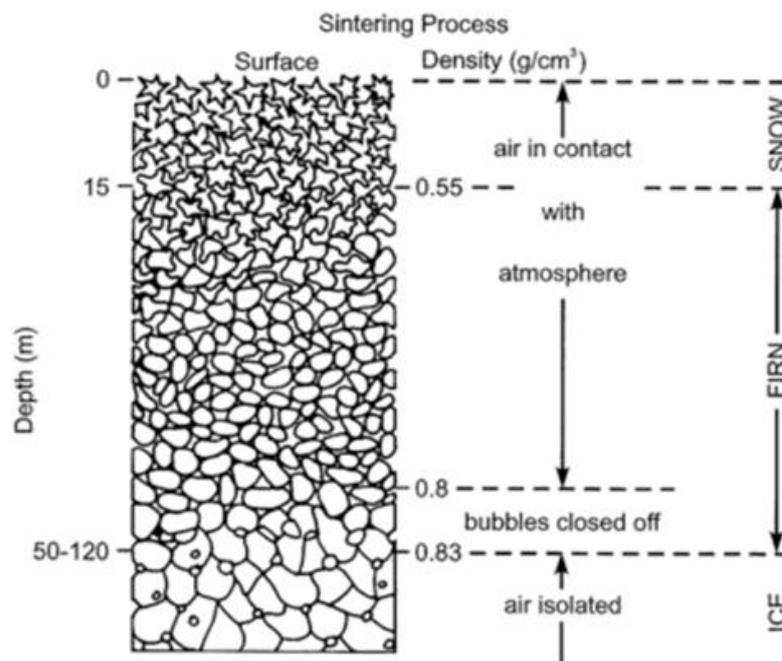


**Figure 1.6** Schematic of firn column (Raynaud, 1992)

The air within the firn is still effectively connected to the atmosphere and to other air within the firn, consequently the air at any given depth is representative of a range of ages (Figure 1.7). Therefore the concentration-depth profile of a gas measured in the firn air is not easily translated into an atmospheric history of the gas. Two sorts of models are available to try to de-convolute an atmospheric history from a firn profile. Direct models require the input of a hypothetical atmospheric scenario and create a modeled concentration-depth profile based on this scenario which can then be compared to the measured profile (Trudinger et al., 1997). Inverse models attempt to use the measured firn profile to back out an atmospheric profile (Rommelaere et al., 1997; Martinerie et al., 2009).
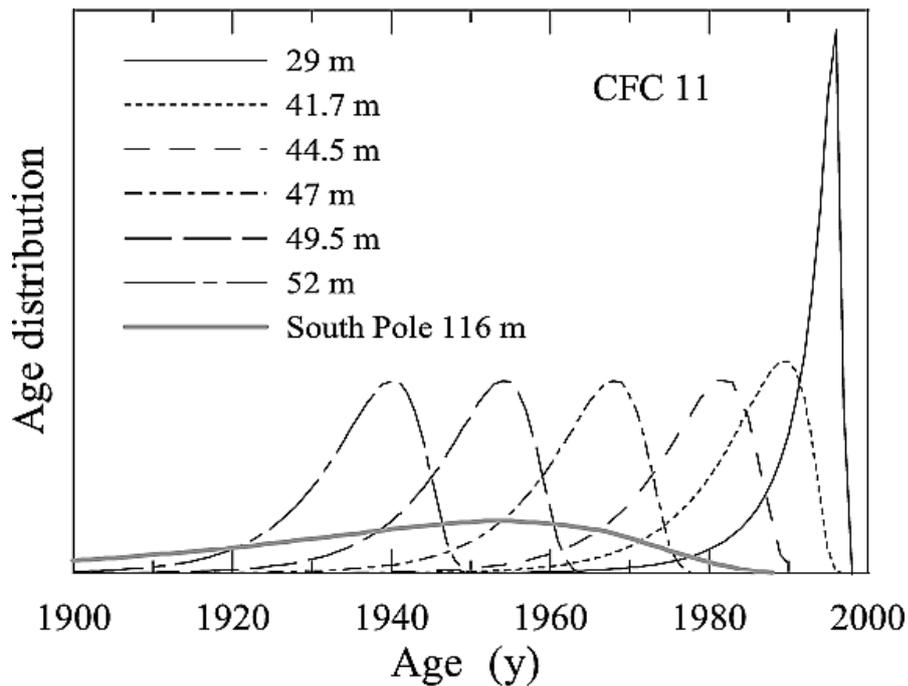
**Figure 1.7** Example of age distribution of a species with depth in a firn profile (Trudinger et al., 2002).

## 1.7    Scientific Justification

This final section of the introduction provides a justification of the need for the work undertaken during this research and the methods used and a rationale for the presentation of the findings in this thesis.

### 1.7.1   Long Lived Gases

When the depletion of the stratospheric ozone layer was discovered the scientific community quickly recognised this to be an issue which required co-operation at an international level to be able to control. The production and use of many ozone depleting substances (e.g. CFCs, halons) were banned under the international treaty the Montreal Protocol (1987) and its subsequent amendments, to which all UN member states are signed up. The Montreal Protocol has been effective in controlling the emission of banned ozone depleting substances and hence prevented potentially catastrophic levels of ozone depletion which could have had damaging consequences for all life on earth (e.g. Montzka and Reimann, 2011).

The emission of many greenhouse gases ($CO_2$, $CH_4$, $N_2O$, $SF_6$, HFCs, and PFCs) are controlled under another international agreement, the Kyoto Protocol (1997) and its subsequent amendments. Rather than an outright ban on usage, such as for ODSs under the

Montreal Protocol, signatory countries have emission reduction targets. The Kyoto Protocol has proved far less effective than the Montreal Protocol at imposing its intended emission controls (e.g. Forster and Ramaswamy, 2007). The reasons for this are manifold. Among them are that there have been no economically viable replacements found for the reliance on fossil fuels for energy and transport (leading to emissions of $CO_2$ and $CH_4$); and that, though the concept of greenhouse gases and the greenhouse effect are relatively well understood scientifically, the issue of global warming and its effects on climate cover a broad spectrum of science of which certain areas provide conflicting research. These two problems make unilateral political co-operation very difficult to achieve since it is widely viewed that a 'solution to climate change' would be very costly and governments are unwilling to devote large amounts of money to solving the issue when so many of the potential effects are unknown. Consequently the United States has not ratified the treaty and Canada has pulled out having previously ratified it. Other major contributors to greenhouse gas emissions such as China and India fall into the category of 'developing countries' who, though signed up, bear no binding emission targets (though many developing countries have now signed up to voluntary targets).

Atmospheric concentrations of many ODSs and greenhouse gases are now continually monitored by global networks of measurement stations. The requirement for this continued monitoring is both to be quickly aware of new emissions of these gases and to confirm or improve upon our understanding of their sources and sinks. An atmospheric model, used in conjunction with measurements of atmospheric mixing ratios of long lived gases from well mixed background air, can be used to establish a historical record of the global emissions of these ODSs and greenhouse gases. This record can show whether or not emissions continue to fall as required under the Montreal and Kyoto Protocols. Additionally, as the presence of ODSs and greenhouse gases that are not covered by either of the protocols is discovered in the atmosphere, the atmospheric model can be used to establish the emissions history of these substances which can be used to inform policy on the need for controls on these previously uncontrolled substances.

In this thesis, measurements from the southern hemisphere background site Cape Grim, Tasmania are presented, from which an archive of clean air samples dating back to 1978 is available. The historical trends in mixing ratios are analysed with discussion of reasons for changing atmospheric mixing ratios and emissions. The measurements are used to derive annual global emissions of each of the trace gases. The derived 'top-down' emissions are also

compared to 'bottom-up' estimates (calculated using reported industry usage and various extrapolations based on factors such as population and degree of industrialisation) in order to verify the usage of such trace gases reported by industry. For the halons, the derived emissions are used, together with reported production from industry, to estimate the remaining quantity of halons. This should be decreasing since halons should no longer be being produced having been banned under the Montreal Protocol. For the PFCs and H-1202 the measurements from Cape Grim are used in conjunction with northern hemisphere measurements from firn air in order to try to constrain the latitudinal distribution of emissions.

For the modeling work presented in Chapters 3 and 4, the gases all have atmospheric lifetimes > 10 years (with the exception of HFC-227ea), with the lifetimes of the PFCs on the order of thousands of years. For such species a 2-D model (latitude and altitude) with a relevant transport scheme is adequate for deriving global emissions from measured time series (e.g. Hough, 1989). This is because the species become well mixed around latitude bands within a few weeks and so any longitudinal variation in atmospheric mixing ratios are rapidly lost. The use of a measurement site in the southern hemisphere mid-latitudes (Cape Grim, Tasmania) further ensures that the measured air is well mixed with respect to species emitted in the northern hemisphere.

The atmospheric model can also be used to calculate tropospheric lifetimes of the species within it. These tropospheric lifetimes can then be used in conjunction with data on lifetimes with regard to other sinks (e.g. stratospheric) to give total atmospheric lifetimes for the species. In this way updated atmospheric lifetimes of the halons are calculated in the thesis as well as local, seasonally dependent lifetimes for the alkanes and alkyl nitrates.

### 1.7.2   Tropospheric Chemistry and Composition

Since the industrial revolution (and probably before), the activity of humans has had a measurable impact on the composition of the atmosphere both locally and globally.

Locally, generally in cities, this has led to issues of poor air quality which can lead to health problems for humans, animals and plants. Emissions of hydrocarbons and $NO_x$ together in high concentrations leads to the production of photochemical smog (Haagen-Smit, 1952). One of the major constituents of this smog is ozone. High levels of ozone can cause respiratory problems in humans and are toxic to plants, similarly $NO_y$ compounds such as $NO_2$ and PAN

can also lead to respiratory problems, and irritation of the eyes and carbon monoxide is toxic in high concentrations (e.g. World Health Organisation, 2003). Furthermore ozone is a greenhouse gas and increases in levels of tropospheric ozone in the atmosphere are thought to be responsible for between 5 – 16 % of the global temperature increase since pre-industrial times (Forster and Ramaswamy, 2007).

Globally, human emissions to the atmosphere have led to an amplification of the natural greenhouse effect, leading to the issue of anthropogenically induced global warming. Increasing the amount of energy in the earth system will lead to changes in the earth's climate. While this is recognised as a serious problem, with undisputed effects such as sea level rise (from the dual effects of the volumetric increase of water and glacier melt), due to the complex and interlinked nature of the system many of the effects of increasing the surface temperature of the earth are very poorly constrained and there are likely many more as yet unpredicted effects.

An atmospheric model is used to derive northern hemisphere emissions of the alkanes. It also investigates the sources of the alkanes and the alkyl nitrates measured in the Arctic.

The emission trends of the alkanes derived from the Greenland firn air will be the first top-down emission trends to be published and will provide a comparison to existing bottom-up derived trends. The work on the alkyl nitrates builds on already published work (Worton, 2012) in both extending the atmospheric record of the alkanes and alkyl nitrates (by the use of data from the NEEM site in conjunction with that from North GRIP) and in further developing the discussion of the reasons behind the observed trends in Arctic mixing ratios of the alkyl nitrates.


### 1.8    Thesis Rationale

The main goals of this thesis are split into two areas. Chapters 3 and 4 report the use of a two-dimensional atmospheric model to derive annual global emissions of a series of long lived ozone depleting and greenhouse gases. In Chapters 5 and 6 measurements of alkanes and alkyl nitrates from firn air in Greenland are used in conjunction with a firn model, a two-dimensional atmospheric model and a one-box model. These are used to explore the transport of pollutants to the Arctic, historic emission trends of the alkanes, the chemistry of the alkyl nitrate system, and the historic oxidative capacity of the atmosphere in the northern hemisphere.

These two topics both contribute to our understanding of past, current and future atmospheric composition. They reveal the effects of anthropogenic influences on the composition of the atmosphere.

# Chapter 2

# Methodologies

## 2  Methodologies

Chapter 2 will discuss the various sources of the data used in this work and some of the methods of analysis. It will also discuss the structure of the atmospheric models and the firn air model used in this work. Finally the methodologies of using the model to derive global emissions and steady state atmospheric lifetimes, the development of a chemical mechanism for use in one-box modeling of the alkyl nitrate system, and the use of the firn model to derive the atmospheric history of a gas are discussed.

The measurement sources include air samples collected both directly from the air and from within firn. All measurements used in this work were kindly provided by others, either through unpublished data or through publically available data sets; I was involved in neither sample collection nor analysis. Brief details of the collection methods and sample analysis methods for the unpublished data are included herein with references to the full analysis details and a summary is given in Table 2.1.

### 2.1    Sample Collection

#### 2.1.1   Cape Grim

Between 1978 and 1995 a series of approximately 65 samples of background air were collected at Cape Grim, Tasmania (40.41°S, 144.41°E) (Figure 2.1). These form the Cape Grim air archive. The samples were collected in electro-polished stainless steel canisters and passivated aluminium cylinders and were only taken during baseline atmospheric conditions (with prevailing winds from the south-westerly sector) so as to be representative of background conditions rather than sampling air coming from the landmasses of mainland Australia or Tasmania (Fraser et al., 1991; Weeks et al., 1992; Langenfelds et al., 1996). Analysis of trace gases (CFC-11, CFC-12, CFC-113, $CH_3CCl_3$, $CCl_4$, $N_2O$ and $CH_4$) in the air archive show agreement with measurements made *in situ* at Cape Grim (Cunnold et al., 1994, Prinn et al., 1995, Oram, 1999) to within 2% (Oram et al., 1995), suggesting that the archive samples contain air representative of ambient air at Cape Grim and that the storage process leads to no significant changes in concentrations of these species. Subsamples of the main archive were sent to UEA in stainless steel canisters to be analysed (Oram, 1999). Comparison of the mean ratios of the trace gases CFC-11, CFC-12, CFC-113, $CHCl_3$,

$CH_3CCl_3$, $CCl_4$, $N_2O$ and $CH_4$ in the sub-samples to the parent archive suggested that there was no loss during the transfer process.

Since 1994, samples have been collected directly into 3 litre electro-polished or Silco-steel treated stainless steel canisters (e.g. Oram et al., 2012) and sent to UEA for analysis.

## 2.1.2   NEEM

Firn air samples were collected at the NEEM site, Greenland (77.45°N, 51.07°W, 2484m a.s.l) (Figure 2.1) between 14th and 30th July 2008. Samples were collected from two boreholes, the 'EU' hole, sampled using the firn air system of the University of Bern (Schwander et al., 1993), and the 'US' hole, sampled using the US firn air system (Battle et al., 1996). The exact sampling procedure is detailed in the 'NEEM firn air sampling field report' (Schwander et al., 2008).
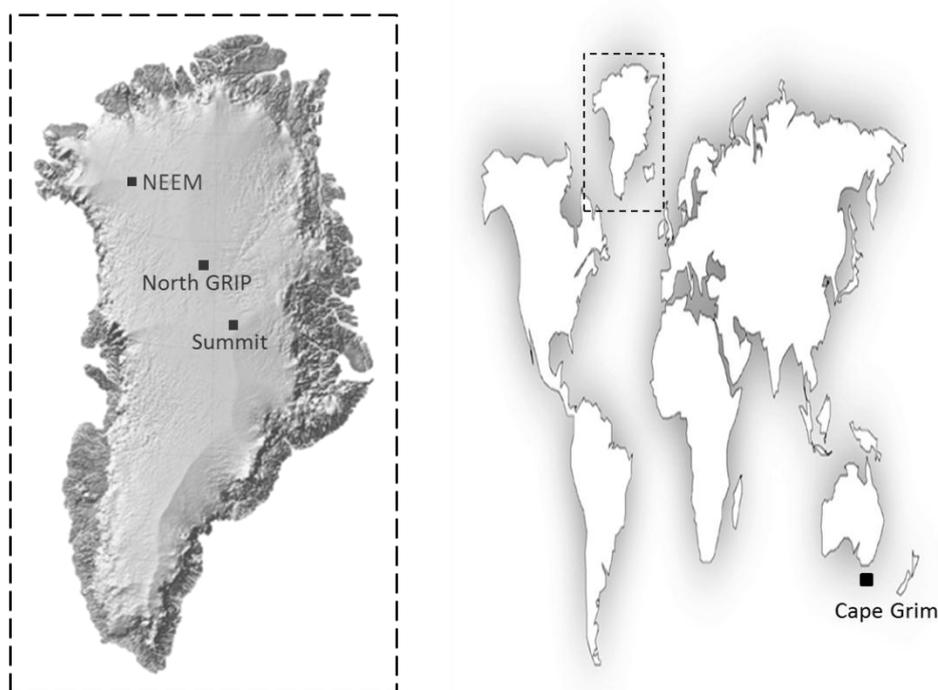


**Figure 2.1** The sites of air sample collection, Cape Grim, Tasmania, and firn air sample collection, NEEM, Greenland.

## 2.2 Sample Analysis

### 2.2.1 Long Lived Gases

Measurements of atmospheric trace gases made at the University of East Anglia (UEA) have generally used one of two setups.

The first uses a Micromass Autospec gas chromatograph combined with a tri-sector mass spectrometer (GC-MS) operated in single ion mode with the gases separated on a KCl-passivated alumina ($Al_2O_3$/KCl) PLOT column (see Fraser et al., 1999 and Oram et al., 2012 for further details). The second setup uses a Micromass/Waters Autospec gas chromatograph combined with a high sensitivity tri-sector (EBE) mass spectrometer (GC-MS) operated in EI-SIR (Electron Impact-Selected Ion Recording) mode. The gases are separated on an Agilent GS GasPro column (see Laube et al., 2010 for further details).

Samples were analysed for the halons on the first system up to 2004 with measurements provided by D. Oram. Subsequently the second system was used with measurements provided by J. Laube. For $SF_5CF_3$ and c-$C_4F_8$ samples were analysed on the first system up to 2006 and then on the second system after this with measurements again provided by D. Oram and J. Laube. The PFCs (except c-$C_4F_8$), and HFC-227ea were exclusively analysed on the second system and provided by J. Laube.

### 2.2.2 Alkanes and Alkyl nitrates

Firn air samples from the 'EU' hole at NEEM were analysed for alkanes at the Max Planck Institute Laboratory (MPI) by gas chromatography with flame ionisation detection (GC-FID) (see Baker et al., 2010 for further details) and the measurements were provided by Angela Baker. The Institute of Arctic and Alpine Research (INSTAAR) analysed samples from both the 'EU' and 'US' holes at NEEM for alkanes by GC-FID (see Pollmann et al., 2008 for further details), with the measurements provided by D. Helmig.

The firn air samples from the 'EU' hole at NEEM were analysed for alkyl nitrates by Chris Hogan at UEA using a GC-MS in Negative Ion Chemical Ionisation mode (GC-NICI-MS) (e.g. Worton et al., 2008; Hogan, 2012).

**Table 2.1** Method of analysis of the measurements used in this work

| Species | Source | Analysis Location | Analysis Method |
|---|---|---|---|
| **Halons** | Cape Grim | UEA | GC-MS (EI) |
| | NEEM | UEA | GC-MS (EI) |
| **PFCs** | Cape Grim | UEA | GC-MS (EI) |
| | NEEM | UEA | GC-MS (EI) |
| **c-C$_4$F$_8$** | Cape Grim | UEA | GC-MS (EI) |
| | NEEM | UEA | GC-MS (EI) |
| **SF$_5$CF$_3$** | Cape Grim | UEA | GC-MS (EI) |
| **HFC-227ea** | NEEM | UEA | GC-MS (EI) |
| **Alkanes** | NEEM | MPI | GC-FID |
| | NEEM | INSTAAR | GC-FID |
| **Alkyl Nitrates** | NEEM | UEA | GC-MS (NICI) |

## 2.3 Data Sources

### 2.3.1 Global Monitoring Networks

There are two major global networks monitoring atmospheric trace gas mixing ratios both *in–situ* and from flask samples. These networks are administered by NOAA/ESRL GMD (National Oceanic and Atmospheric Administration Earth System Research Laboratory Global Monitoring Division) and AGAGE (Advanced Global Atmospheric Gases Experiment) and provide high frequency measurements of the majority of the ozone depleting gases controlled by the Montreal Protocol and the greenhouse gases controlled by the Kyoto Protocol.

AGAGE have been monitoring trace gases since 1978 (e.g. Prinn et al. 2000) and now take air samples at five stations (Mace Head, Ireland (MHD); Trinidad Head, California (THD); Ragged Point, Barbados (RGP); Cape Matatula, American Samoa (SMO); Cape Grim,

Tasmania (CGO)) while collaborating with a further six stations. The stations are all situated on the coast or at mountain sites in order to mainly sample background air rather than local pollution events. AGAGE currently make data publically available for 33 compounds via their site, http://agage.eas.gatech.edu/data.htm.

NOAA/ESRL currently operates six baseline observatories (located to receive mainly background air) (Barrow, Alaska (BRW); Trinidad Head, California (THD); Summit, Greenland (SUM); Mauna Loa, Hawaii (MLO); American Samoa (SMO); South Pole, Antarctica (SPO)) monitoring a wide range of trace gases. In addition to these baseline observatories NOAA/ESRL host data from a large number of other observatories around the globe at their public data archive, http://www.esrl.noaa.gov/gmd/dv/data/.

## 2.3.2   Bottom-up Emissions Estimates

Bottom-up emission estimates are calculated using various sociological parameters, such as population and level of industrialisation, and information provided by industry. The two sources of bottom-up emission estimates used in this work are EDGAR (Emissions Database for Global Atmospheric Research) and HTOC (Halons Technical Options Committee).

The latest version of EDGAR (EDGAR v4.2) (e.g. van Aardenne et al., 2005 (EDGAR v32-FT2000)) provides annual emission estimates of all of the Kyoto Protocol gases as well as ozone precursor gases and acidifying air pollutants at a resolution of $0.1°$ x $0.1°$ for the period 1970 – 2008. It also reports the same emissions by country. These data are available at http://www.edgar.jrc.ec.europa.eu.

HTOC is a Technical Options Committee (TOC) of the Technology and Environmental Assessment Panel (TEAP) of the Ozone Secretariat of the United Nations Environmental Programme (UNEP). They provide quadrennial assessment reports on the state of the halons industry which contain bottom-up production and emissions estimates of H-1301 and H-1211 by region as well as estimates of the remaining banks of H-1301, H-1211 and H-2402. The most recent of these reports was published in 2011 (HTOC, 2011).

### 2.3.3 Emissions Data from Reanalysis Projects

The RETRO project was an attempt to produce the first global long-term reanalysis simulation of tropospheric chemistry (Schultz and Rast, 2007). The RETRO model integrations included the pollutant species: ozone, carbon monoxide, $NO_x$, nitric acid and volatile organic compounds (VOCs); compounds important for tropospheric oxidation: ozone, hydroxyl, hydrogen peroxide, carbon monoxide and methane; and compounds involved in radiative forcing: methane, ozone and water vapour. The project used data from the European Centre for Medium Range Weather Forecasts (ECMWF) reanalysis project ERA-40 (Uppala et al., 2005) for the meteorological and transport parameters within the simulations. An ensemble approach was adopted for the project using five different models to try to avoid certain biases that any particular model may have. The emission data sets produced from the RETRO project contain monthly gridded emission data at a 0.5°x0.5° resolution for the years 1960 – 2000.

The data from the HYDE project (van Aardenne et al, 2001) is an attempt to create an historic anthropogenic emissions data set for $CO_2$, CO, $CH_4$, NMVOCs, $SO_2$, $NO_x$, $N_2O$ and $NH_3$. The data are available at ten year intervals from 1890 – 1990 at a 1°x1° resolution. The data are based on estimates from the Emission Database for Global Atmospheric Research (EDGAR 2.0) (Olivier et al, 1999a). Emissions are calculated from historical activity statistics and selected emission factors for each species. Anthropogenic emissions are split in to three groups: energy/industry, agriculture/waste and biomass burning.

### 2.3.4 Atmospheric Reaction Rate Data

The majority of the kinetic reaction rates and photochemical data used in the full chemistry model were taken from the IUPAC Subcommittee for Gas Kinetic Data Evaluation (http://www.iupac-kinetic.ch.cam.ac.uk; Atkinson et al., 2004; Atkinson et al., 2006; Atkinson et al., 2008). If the required data were not provided by IUPAC then data were taken from the NASA / JPL 'Chemical Kinetics and Photochemical Data for Use in Atmospheric Studies: Evaluation No. 17' (Sander et al., 2011). Both these sources consider the full range of literature available on each reaction and provide a recommendation based on a synthesis of this data. There are sometimes minor differences between the recommendations of each organisation.

## 2.4  The Atmospheric Model

A two-dimensional atmospheric chemistry transport model was used for the work with the long lived gases in Chapters 3 and 4 to derive annual global emissions using the measurements from Cape Grim and to explore the reported atmospheric lifetimes of the gases. The model was also used to derive emissions of the hydrocarbons presented in Chapter 5 from firn air measurements at NEEM.

### 2.4.1  History of Model

The 2-D atmospheric chemical transport model used in this work is a simplified version of that originally developed by Adrian Hough at the Harwell Laboratory of AEA Environment and Energy in the late 1980s, hereafter referred to as Hough-91. The transport scheme of the model is described in Hough (1989), the chemical mechanism in Hough (1991) and the photolysis algorithm in Hough (1988a).

The model was originally developed to investigate the distribution, budgets and trends of trace gases in the troposphere. It was used in particular for investigating the budgets and distributions of ozone precursors and tropospheric ozone distribution (e.g. Hough and Derwent, 1990; Hough and Johnson, 1991; Johnson and Derwent, 1996; Derwent, 1996). A version of the model with the same transport and photolysis schemes but a much simplified chemical mechanism has since been used to investigate the global emissions of long lived gases (e.g. Fraser et al., 1999; Reeves et al., 2005; Laube et al., 2010; Sturges et al., 2012; Oram et al., 2012; Laube et al., 2012).

### 2.4.2  Physical Structure

The model grid is split into twenty-four latitudinal bands and twelve vertical levels, totalling two hundred and eighty-eight cells. The cells are all of equal volume so that each cell contains the same amount of material in each band. Hence cells at the equator have a smaller latitudinal width than those at the poles. The latitudinal boundaries of each cell and the pressure and number density at each level are shown in Tables 2.2 and 2.3.

**Table 2.2** Grid boundaries and mid points of the latitudinal cells in the model.

| Horizontal Cell No. [a] | Cell Boundaries (°) | Cell Mid-Point (°) |
|:---:|:---:|:---:|
| 1, 24 | 90.0 – 66.4 | 73.4 |
| 2, 23 | 66.4 – 56.4 | 61.0 |
| 3, 22 | 56.4 – 48.6 | 52.3 |
| 4, 21 | 48.6 – 41.8 | 45.1 |
| 5, 20 | 41.8 – 35.7 | 38.7 |
| 6, 19 | 35.7 – 30.0 | 32.8 |
| 7, 18 | 30.0 – 24.6 | 27.3 |
| 8, 17 | 24.6 – 19.5 | 22.0 |
| 9, 16 | 19.5 – 14.5 | 17.0 |
| 10, 15 | 14.5 – 9.6 | 12.0 |
| 11, 14 | 9.6 – 4.8 | 7.2 |
| 12, 13 | 4.8 – 0.0 | 2.4 |

[a] Cells 1 – 12 are southern hemisphere, 13 – 24 are northern hemisphere.

**Table 2.3** Height, pressure and number density of the twelve vertical levels in the model.

| Vertical Level | Mid-Height (km) | Air Pressure (hPa) | Number Density ($\times 10^{-18}$ $cm^{-3}$) |
|:---:|:---:|:---:|:---:|
| 12 | 23 | 40.99 | 1.37 |
| 11 | 21 | 54.11 | 1.81 |
| 10 | 19 | 71.44 | 2.39 |
| 9 | 17 | 94.32 | 3.15 |
| 8 | 15 | 124.51 | 4.16 |
| 7 | 13 | 164.38 | 5.50 |
| 6 | 11 | 217.02 | 7.26 |
| 5 | 9 | 286.50 | 9.04 |
| 4 | 7 | 378.24 | 11.29 |
| 3 | 5 | 499.35 | 14.15 |
| 2 | 3 | 659.24 | 17.78 |
| 1 | 1 | 870.32 | 22.39 |

The upper boundary condition is governed by the ratio of the mixing ratio of the species at 25 km, to that in the top box of the model (23 km). This is only important for long lived species, for which there is a diffusive loss from the model domain, or for species which have sources above the model domain, such as ozone and $NO_x$.

The atmospheric circulation scheme used in the model is an interpolation on to the model grid of the two-dimensional circulation derived by Plumb and Mahlman (1987) which was based on the output of a three dimensional General Circulation Model (Mahlman et al., 1980). The

scheme splits the transport into a transport stream function (u) and an eddy diffusion tensor (K). The concentration of the species in each grid cell is then varied with time according to Equation 2.1.

$$\frac{dc_i}{dt} + div(c_i u) = S_i + div(KN grad\left(\frac{c_i}{N}\right))$$
(E2.1)

where $c_i$, concentration of species; $u$, zonally averaged wind field; $S_i$, net source and sink; $K$, eddy diffusion tensor; $N$, atmospheric molecular number density.

The transport coefficients from Plumb and Mahlman (1987) described a conservative and completely closed transport scheme up to 33 km. Hough-91 has an upper boundary at 24 km and so had to compress this conservative transport scheme in the upper layers. This was achieved by interpolating the transport coefficients between 0 and 16 km directly on to the grid, then assuming the pressure at 24 km to be zero and adjusting the pressures between 16 km and 24 km accordingly so that the transport coefficients of Plumb and Mahlman (1987) between 16 km and 33 km could be interpolated on to the Hough-91 grid of 16 – 24 km. In all other respects and for all other calculations the pressures remain as shown in Table 2.3.

The model is written using the programming language FACSIMILE (Curtis and Sweetenham, 1987) and the differential equations are assembled and integrated using the Gear's method (1971). The mixing ratios of the input species in the model are driven entirely by the emissions, the loss processes and the transport with no redistribution of the burden to ensure that mixing ratios agree with observations.

The fixed temperature field used was compiled by Barnett and Corney (1985, 1986) based on the data of Oort (1983). Values for each cell are read in at the mid-point of each month and sine interpolated in between these times.

The surface layer of the model has three different surface types, land, ocean and ice which affect emission and deposition rates. However there is no explicit topography in the model.

### 2.4.3 Photolysis Scheme

The photolysis scheme within the model is a two-stream isotropic multiple scattering algorithm involving absorption by molecular oxygen and ozone, Rayleigh scattering, Mie

scattering, surface albedo and three cloud layers developed by Hough (1988a). The model considers radiation in the wavelength range 200 – 660 nm. This range is chosen because wavelengths shorter than 200 nm are completely absorbed above 24 km (the vertical extent of the model domain), while wavelengths longer than 660 nm have little effect on the atmospheric photochemistry considered in the model.

Uncertainties in the scheme are introduced by each of the processes considered. The treatment of clouds (e.g. Wild et al., 2000; Tie et al., 2003), Rayleigh scattering (e.g. Dickerson et al., 1997; Liao et al., 2003; Martin et al., 2003; Tie et al., 2005), and Mie scattering (e.g. Wild et al., 2000) within atmospheric models have all been the subject of much work since the development of the photolysis scheme used in this model. However these parameters have been left unchanged in consideration of the difficulty of improving them when considering the uncertainties inherently associated with the two-dimensional nature of the model. However the solar flux is a parameter which can be examined more closely and for which longitudinal variation is not an issue. This is discussed further below.

### 2.4.3.1    *Solar Flux*

The incident solar photon flux at the top of the model domain is calculated in the model for each wavelength band by inputting the flux at the top of the atmosphere (TOA) and then attenuating this flux by absorption by molecular oxygen and ozone above the model domain. Changes in the recommended values of these four parameters (TOA solar flux, column ozone above the model, absorption cross sections of ozone and molecular oxygen) since the development of Hough-91 are examined in turn below.

The TOA flux input to Hough-91 was taken from the WMO review of 1986 (Hough, 1988a). This was based on the compilation of a series of ground based observation data sets (Wehrli, 1985). Since this time a number of studies have reported solar spectra based on both satellite data (e.g. Haigh et al., 2010) and modelling studies (e.g. Lean et al., 2005; Krivova et al., 2007).

The TOA solar photon flux used in Hough-91 has been replaced in MARC by data from the NRLSSI (Naval Research Laboratory Solar Spectral Irradiance) model (Lean et al., 2005). This is an empirical model derived from observational correlations between 0 and 100,000 nm from 1950 to 2011. The NRLSSI dataset was recommended for use in the SPARC 2010 CCMVal (Chemistry Climate Model Validation) project (Eyring et al., 2010). Between 120

and 300 nm this model has been partly designed to give good agreement with observations provided by the UARS/SOLSTICE satellite instrument. Above 300 nm the data is based only on modeling. A mean of the values between the solar maxima of 2002 and the minima of 2008 has been taken.

Figure 2.2 shows a comparison of the percentage difference in the flux from NRLSSI to that used in Hough-91. It also compares to that derived by the model SATIRE (Krivova et al., 2007) to demonstrate the differences in current modeled datasets. The region in which the NRLSSI data is most different to that of the data used in Hough-91 is for wavelengths shorter than 240 nm and longer than 640 nm. This increase in short wavelength radiation can be expected to have an effect on photolysis in the uppermost levels of the model in the stratosphere.
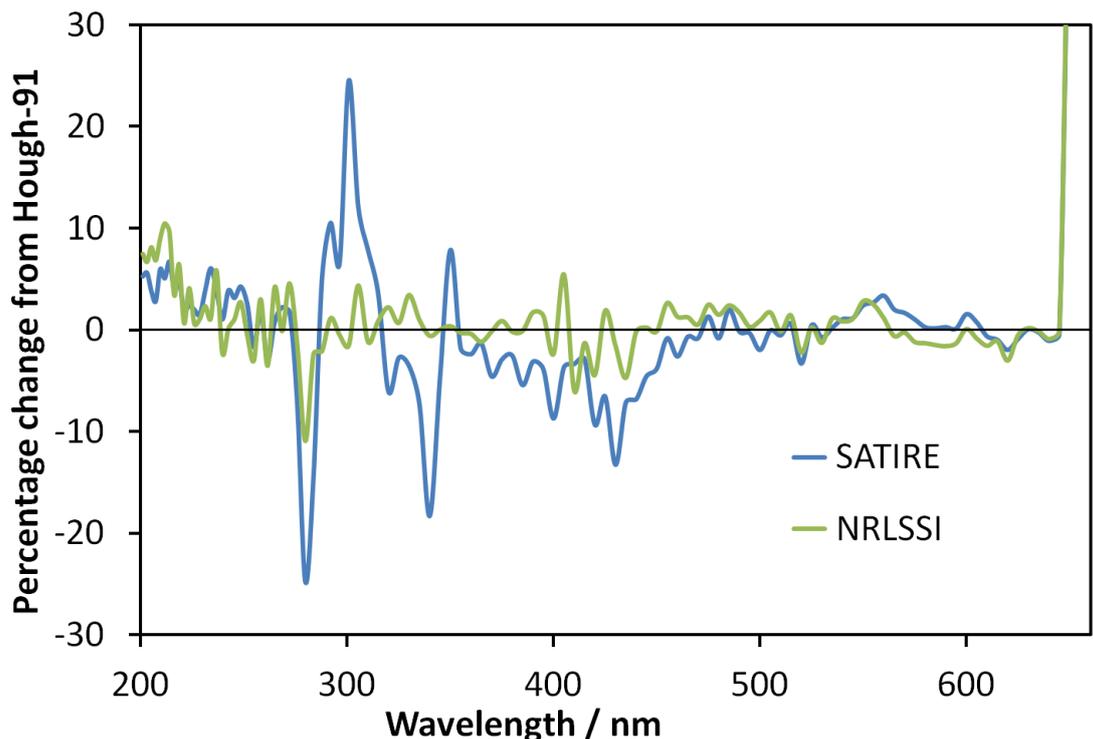


**Figure 2.2** A comparison of the NRLSSI and SATIRE modeled datasets for the solar photon flux incident at the top of the atmosphere to the data used in Hough-91 (WMO, 1986).

### 2.4.3.2 *Ozone Column*

The photolysis rates calculated within the model are sensitive to the ozone column above the model domain (as well as the mixing ratios within the model domain) as ozone absorbs much of the shorter wavelength radiation between the top of the atmosphere and the top of the model (24 km).

The ozone column values above the model domain for Hough-91 were taken from the WMO review of 1986 based on data from the SBUV spectrometer on the satellite NIMBUS-7. Stratospheric ozone has decreased significantly since the early 1980s (e.g. Douglass and Fioletov, 2011), when the observations reported in WMO 1986 were made.

An alternative ozone column was investigated using the ozone climatology of UGAMP (Li and Shine, 1999). This climatology is derived from ozone measurements from a variety of sources including the SBUV, SAGE II, SME and TOMS satellite based instruments as well as ozonesondes and provided at a latitudinal resolution of 2.5 degrees. Five years of data are provided to account for stratospheric inter-annual variability such as the quasi-biannual oscillation. However this is not seen as important for MARC and so a mean of ozone during the two modes of the QBO was taken.

However neither the original ozone column from Hough-91 nor the UGAMP ozone climatology represent the trend in stratospheric ozone from 1970 – 2009 and hence both have uncertainties associated with them in terms of the absolute ozone column values. So although the effects of the UGAMP climatology are shown in Figure 2.2 for comparison with Hough-91, the original Hough-91 ozone column was retained in MARC.

### 2.4.3.3 *Absorption Cross Sections*

Since Hough-91 there have also been some changes to the recommended values of the absorption cross section of ozone in the region of 200 – 230 nm (Atkinson et al., 2004). These have mainly served to decrease the solar photon flux at the top of the model (Figure 2.3). Likewise there have been changes to the recommended absorption cross-section of molecular oxygen (Atkinson et al., 2004). These have increased the solar flux at the top of the model.

The main effect of the changes in the four parameters which control the incident solar flux at the top of the model domain is in the ultraviolet region below 220 nm. Figure 2.3 shows the incident solar photon flux at the top of the model domain for a solar zenith angle of zero and

compares each change separately to a base case which uses all the original values from Hough-91. This shows that, with the exception of the changes to the absorption cross-section of ozone, the other changes all increase the flux in this wavelength region. The overall effect of these changes is to increase the solar photon flux in this region and hence to increase photolysis rates near the top of the model domain.
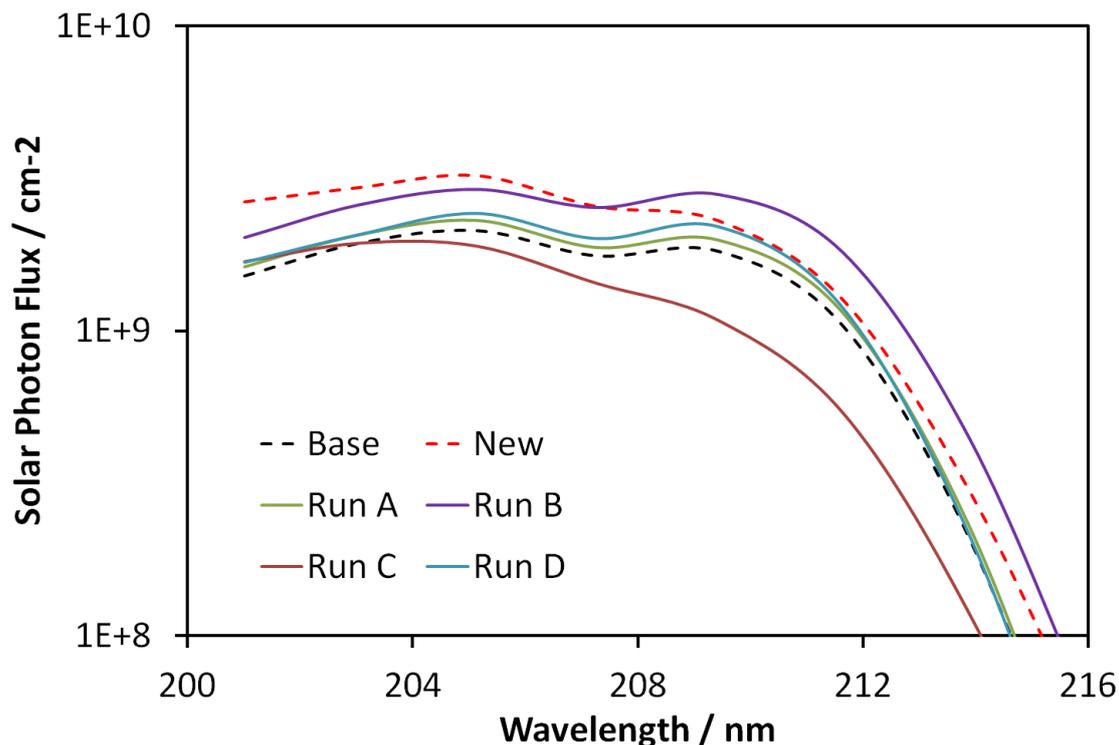


**Figure 2.3** Incident solar photon flux at the top of the model domain (24 km). A comparison of the original flux from Hough-91 ('Base') to adjustments of the TOA solar flux (Run A), the ozone column above the model domain (Run B), the absorption cross section of ozone (Run C), and the absorption cross section of oxygen (Run D). 'New' combines all the adjustments.

### 2.4.4   Chemical Mechanism

The 2-D atmospheric model uses a fixed OH field. This is based on modeling by Hough (1991) using a model with a full tropospheric chemistry scheme. It has been scaled in this work to give a lifetime for methyl chloroform, with respect to reaction with OH, of 6.1 years, as given by the most recent WMO review (Montzka and Reimann, 2011), using a reaction rate of $1.2 \times 10^{-12} e^{(-1440/T)}$ (Atkinson et al., 2008).

The OH concentrations are input monthly for each cell and interpolated in between these times using a sine smoothing function. The reaction rates of the long lived gases with OH are taken from Sander et al. (2011). However for the halons (Chapter 3) the loss due to photolysis is more than 20 times greater than the loss to reaction with OH for all halons. For the PFCs and $SF_5CF_3$ (Chapter 4) there is no reaction with OH.

### 2.4.4.1 Alkyl Nitrate Chemistry in the 2-D Atmospheric Model

A fixed $NO_x$ field was implemented into the 2-D atmospheric model to study the formation, loss and transport of the alkyl nitrates at a simple scale. Like the OH field this was based on a full chemistry model run by Hough and Johnson (1990). Loss of the alkyl nitrates was by reaction with OH and photolysis. This, in conjunction with the fixed OH field used in the 2-D model, allowed the production and transport of alkyl nitrates to the Arctic to be investigated in Chapters 5 and 6. The alkanes and alkyl nitrates studied in this work were all explicitly described in the model with oxidation of the alkane giving a peroxy radical and reaction of the peroxy radical with NO giving an alkyl nitrate.

### 2.4.5 Model Validation

### 2.4.5.1 Model Transport

The original model transport scheme was validated against the long lived inert tracers [85]Kr, CFC-11 and CFC-12 (Hough, 1989). This validation showed that mass was conserved during the integration of the transport equations. Use of established emissions of the tracer [85]Kr (emitted only in the northern hemisphere) produced sensible interhemispheric gradients. Use of bottom-up emission estimates of CFC-11 and CFC-12 showed a very good agreement between model output and measured values in the southern hemisphere with differences of <1%. The agreement in the northern hemisphere was within 5%. The greater difference in the northern hemisphere reflects the measurement sites being closer to the emission sources hence the species are less well mixed through the atmosphere than when tey reach the southern hemisphere. The model transport scheme has also been validated for use with the long lived gases CFC-11 and CFC-12 (emitted mainly in the northern hemisphere) in Reeves et al. (2005) in which model output for the southern hemisphere site Cape Grim was seen to agree with measurements to within 5%. In a multi-model intercomparison study of Jacob et al.

(1997) used the short lived tracer $^{222}$Rn to evaluate the model transport of 16 3-D models and 4 2-D models, including the Hough-91 model. It was shown that the 2-D models do well at recreating concentrations of the tracer in the lower troposphere as observed in the 3-D models but are less good when comparing to vertical profiles. However this should not be a problem for the work presented in this thesis as all measurement sites are ground based.

However in later work with the model the values of the vertical eddy diffusion coefficient, $K_{zz}$ in the stratosphere were reduced by Johnson and Derwent (1996) and Derwent (1996). This was seen to give modeled profiles of ozone in the lower stratosphere that agreed better with observations. It has also been suggested in Shia et al. (1998) that the horizontal eddy diffusion coefficient, $K_{yy}$, should be reduced in the region of the tropical lower stratosphere to create an observed subtropical barrier. This would reduce the transport between mid-latitudes and the tropics in the stratosphere.

### 2.4.5.2    *Hydroxyl Radical*

The hydroxyl radical (OH) is the most important species driving oxidative chemistry in the troposphere. Local OH concentrations in the atmosphere are governed by its sources and sinks, with photolysis of ozone (created by hydrocarbon and $NO_x$ emissions) being the main source, and reaction with $CH_4$ and CO being the main sinks.

Since OH concentrations are difficult to measure directly in the atmosphere, many studies have looked instead at the oxidative effects of the radical. There have been various ways of defining the OH burden within a region of the atmosphere used previously including: a volume weighted approach and reaction with a gas with well defined sources and sinks such as methane ($CH_4$) or methyl chloroform ($CH_3CCl_3$) (Lawrence et al., 2001).

Figure 2.4 shows the OH fields derived from global modeling work by Spivakovsky et al. (2000), von Kuhlmann (2001) and Emmons et al. (2010) (MOZART-4). The values presented are annual mean values for the twelve regions shown, from 90° to 30° and 30° to the equator and for three different pressure heights. Though the absolute values differ somewhat between the three models, there are some general trends common to all three. It is seen that mean annual mixing ratios are higher in the subtropical regions than in the mid-high latitudes. Surface values are higher in the northern hemisphere than for their corresponding regions in the southern hemisphere. This is because of the greater emissions of hydrocarbons and $NO_x$ in

the northern hemisphere which, as discussed above, are key to the photochemical creation of the hydroxyl radical.

**Spivakovsky** — $10^6[OH]$ mol/cm³

| | 90S | 30S | 0 | 30N | 90N |
|---|---|---|---|---|---|
| 250hPa | 0.64 | 1.43 | 1.36 | 0.64 | |
| 500hPa | 0.72 | 2.00 | 1.99 | 0.88 | |
| 750hPa | 0.47 | 1.44 | 1.52 | 0.76 | |
| Surface | | | | | |

**MOZART-4** — $10^6[OH]$ mol/cm³

| | 90S | 30S | 0 | 30N | 90N |
|---|---|---|---|---|---|
| 250hPa | 0.54 | 1.05 | 1.26 | 0.72 | |
| 500hPa | 0.53 | 1.39 | 1.59 | 0.72 | |
| 750hPa | 0.42 | 1.25 | 1.37 | 0.77 | |
| Surface | | | | | |

**von Kuhlmann** — $10^6[OH]$ mol/cm³

| | 90S | 30S | 0 | 30N | 90N |
|---|---|---|---|---|---|
| 250hPa | 0.36 | 0.82 | 0.96 | 0.52 | |
| 500hPa | 0.46 | 1.48 | 1.61 | 0.72 | |
| 750hPa | 0.51 | 1.51 | 1.76 | 0.86 | |
| Surface | | | | | |

**Hough-91** — $10^6[OH]$ mol/cm³

| | 90S | 30S | 0 | 30N | 90N |
|---|---|---|---|---|---|
| 250hPa | 0.43 | 1.13 | 1.24 | 0.47 | |
| 500hPa | 0.70 | 1.88 | 2.07 | 0.83 | |
| 750hPa | 0.52 | 0.89 | 1.11 | 0.79 | |
| Surface | | | | | |

**Figure 2.4** Annual mean OH burden from MOZART-4 (Emmons et al, 2010), Spivakovsky et al. (2000) (from Emmons et al, (2010)), von Kuhlmann (2001) and the scaled Hough-91 (see text).

Figure 2.4 also shows a comparison of the annual mean OH concentrations used in the model in this work (Hough-91) using the altitudes $0 - 2$ km, $2 - 6$ km and $6 - 10$ km as analogues for the pressure heights used in the other work. Note that the OH concentrations have been scaled up by 6% from the original Hough-91 model. This is to give methyl chloroform the recommended global lifetime of 6.1 years with respect to OH (Montzka and Reimann, 2011) in the model.

It is seen in Figure 2.4 that in the surface layer the scaled annual mean [OH] concentration in Hough-91 tends to fall within the range of the other three models for the two mid-high latitude regions and to have estimates $20 - 30$ % lower for the two tropical regions. In the upper regions of the model Hough-91 is seen to generally be within the range of the other models.

### 2.4.5.3 *Calculating Mean [OH] with Methyl Chloroform*

Methyl chloroform ($CH_3CCl_3$) is a man-made trace gas which was produced for use as a solvent until production was banned under the Montreal Protocol in 1991 (Montzka and Reimann et al., 2011). The main atmospheric sink of $CH_3CCl_3$ is reaction with OH. It has a total atmospheric lifetime of 5.0 years (Montzka and Reimann, 2011). It is believed that the minor sinks of $CH_3CCl_3$ (loss in the stratosphere and to the oceans) are reasonably well constrained and hence a lifetime with respect to reaction with OH can be inferred, this is 6.1 years (Montzka and Reimann et al., 2011). Using this lifetime and a series of measurements of changing $CH_3CCl_3$ mixing ratios at different sites, [OH] can be estimated using Equation 2.2 which describes the rate of change of $CH_3CCl_3$ in the atmosphere. This also requires knowing the emissions of $CH_3CCl_3$, uncertainties in these emissions have called the accuracy of this method into question in the past (e.g. Krol and Lelieveld, 2003), but since emissions have now fallen to virtually zero it is now believed that the method provides a very accurate way to determine [OH] (e.g. Montzka et al., 2011).

$$d[CH_3CCl_3]/dt \; = \; E - (k_{OH}[OH][CH_3CCl_3] + L_{strat} + L_{oc.}) \qquad \text{(E2.2)}$$

where $L_{strat}$ = loss to stratosphere and $L_{oc.}$ = loss to the ocean.

Because the lifetime of methyl chloroform with respect to OH is believed to be well constrained, it is often used to validate global OH concentrations in models.

The problem with validating [OH] using the lifetime of a certain gas is that there is an implication that [OH] has not changed interannually unless a lifetime is given for a specified year or a lifetime range is given. The question of whether or not OH concentrations have varied significantly interannually in the northern hemisphere is explored further in Chapter 6.

## 2.5    Derivation of Steady State Atmospheric Lifetimes

The global lifetime of a molecule ($\tau_{atm}$) in the atmosphere can be defined as the time taken to lose 1 - 1/e (~63%) of its global atmospheric burden. At steady state it can be calculated as the atmospheric burden, $B$ (molecules), of the molecule divided by the loss, $L$ (molecules s$^{-1}$) (Equation 2.3).

$$\tau_{atm} \ = \ \frac{B}{L} \qquad\qquad (E2.3)$$

The steady state lifetime of a species can be calculated by two different methods within the 2-D atmospheric model. For both methods the model is first run to steady state, that is, emissions are kept constant and the emissions and loss of the species within the model domain gradually tend towards equality (the larger the loss within the model the quicker this occurs).

The first method (Equation 2.4) then considers the burden of the species and equates $L$ in Equation 2.3 to annual emissions ($E$), molecules cm$^{-3}$ s$^{-1}$, within the model domain. The burden is divided by the annual emissions, which at steady state is equal to the loss, to give a steady state lifetime.

$$\tau_{atm} \ = \ \frac{B}{E} \qquad\qquad (E2.4)$$

The second method (Equation 2.5) considers the loss rate of the species in each cell ($[L]$) within the model. A weighted mean is then taken of all of the loss rates. This weighting is given by the percentage of the total burden of the species in each particular cell ($[X]/B$, where $[X]$ = concentration in model cell (molecules cm$^{-3}$), $B$ = global burden (molecules cm$^{-3}$)).

$$\tau_{atm} \ = \ \overline{\Sigma[L]^{-1} \cdot \frac{[X]}{B}} \qquad\qquad (E2.5)$$

It is also noted that model calculated steady state lifetimes using Equation 2.5 are not the same as the instantaneous lifetime (i.e. the time it would take for the global burden of the molecule to decrease by 1 - 1/e if emissions were to cease) of the molecule in the atmosphere at any given moment. This will be dependent on the atmospheric history of the species prior to the measurement time. If the burden of the molecule is increasing (i.e. $E > L$), then the

instantaneous lifetime calculated would be longer than the steady state lifetime, if it is decreasing (i.e. $E < L$) it would be shorter. For Equation 2.5, if the burden is increasing then $[X]/B$ will be larger at the surface and smaller at higher altitudes than at steady state and vice-versa if the burden is decreasing (assuming a surface source). The effect of these differences on the instantaneous lifetime compared to the steady state lifetime will be dependent on the region of the atmosphere for which the majority of the loss occurs for a given species.

### 2.5.1   Partial Atmospheric Lifetimes

For the atmospheric lifetimes calculated above, the loss term, $L$, represents the total loss of the species from all sinks. Thus Equations 2.4 and 2.5 give total atmospheric lifetimes. If different loss processes are considered separately then a lifetime with respect to each particular loss process can be calculated. This is done simply by replacing the loss term in Equation 2.5 with a partial loss term (e.g. $L_x$ and $L_y$). The total atmospheric lifetime can be calculated from the combination of the sum of the inverse of the lifetimes (Equation 2.6). Another application for Equation 2.6 is its use if both the total atmospheric lifetime and some of the partial lifetimes are known. Equation 2.6 can then be used to calculate the lifetime with respect to the remaining sink(s).

$$\frac{1}{\tau_{atm}} = \frac{1}{\tau_x} + \frac{1}{\tau_y} \qquad\qquad \text{(E2.6)}$$

Steady state partial lifetimes can be calculated in the 2-D atmospheric model by including or removing the relevant sinks. The model can also be used to calculate partial lifetimes with respect to a particular region of the atmosphere (e.g. the troposphere or the stratosphere) rather than with respect to a particular sink. To calculate the tropospheric lifetime only loss processes within the troposphere are switched on. There is no loss in the stratosphere and no loss from the top of the model. Unlike for the calculation of the total lifetimes using Equations 2.4 and 2.5 there is no burden above the model domain to be considered since there is no diffusive loss from the top of the model and the whole burden above the troposphere is effectively compressed into the upper part of the model domain. Hence the tropospheric lifetime calculated in this way can be considered to be a 'true' lifetime. However the lifetime

calculated depends on the definition of the tropopause, i.e. the altitude below which loss processes occur. This can vary between 8 and 17 km depending on latitude and season. The easiest way to treat the tropopause within the model is to set it at a defined height for the whole latitudinal range. A more accurate method would be to either code in variation with latitude and season based on observations or to define a chemical tropopause based on the concentrations of a given species, most likely ozone. In Chapter 3 it is shown that varying the height of the tropopause for the halons from 12 km to 16 km changes the calculated tropospheric lifetime by less than 5%.

To calculate the stratospheric lifetime, loss processes in the troposphere are switched off. If the main loss process for the species of study is above the model domain then the derived stratospheric (and total) lifetime is dominated by the chosen value of the ratio of the species at 25 km (above the model domain) to that in the top box of the model (23 km). This ratio governs the diffusion across the upper boundary just as diffusion is treated in the rest of the cells throughout the model. For species with no photochemical loss in the model domain then the lifetime is completely dependent on this value. There are generally very few measurements to constrain this value since it is above the altitude at which research aircraft fly, though there are some limited data from balloon flights. Stratospheric lifetimes calculated using the model suffer from the same limitations, of not having the burden above the model domain included in the calculation, as total atmospheric lifetimes.

For shorter lived species ($\tau < 1$ year) a steady state global lifetime cannot be calculated as the loss rate varies considerably throughout the year dependent on the latitude and the season. However a regional lifetime can be calculated using a similar method to that above. The model is run to steady state with the loss processes only active for a given latitude band. These changing lifetimes can be represented in a Hovmöller plot of time against latitude. These are used for the alkanes and alkyl nitrates in Chapter 6 of this work.

## 2.6    Derivation of Annual Global Emissions

The main use of the 2-D atmospheric model for long lived species in this work is the derivation of global emissions based on measurements. The model has two main adjustable input functions, the total global annual emissions of a species and the latitudinal distribution of these emissions. The emissions distribution is generally based on bottom-up emissions estimates (see Section 2.7). This distribution can remain fixed through the model run or be

varied if the location of emissions are believed to have changed (e.g. movement of halon emissions from Europe/North America to China following the implementation of the Montreal Protocol).

Having fixed the emissions distribution, an inversion technique is performed in which a set of atmospheric measurements (generally from Cape Grim in this work) are used to constrain the annual emissions. This is an iterative process in which, starting with an *a-priori* emissions scenario, the model output at the latitude of the measurement site is compared to an approximate mean of the measurements. The emissions are then adjusted for each year to improve the fit of the model output to the measurements. This process is repeated until the model output from the emissions scenario provides a good fit to the measurements (Figure 2.5).

The emissions derived in this way are a function not only of the measurements but also of the fixed model parameters. These include the transport scheme, the reaction rates of the species with e.g. OH or photolysis, the fixed OH field used in the model and the incident solar radiation and its transfer and absorption in the atmosphere. These assumptions are used to define the uncertainties in the derived emission scenarios presented in this work.
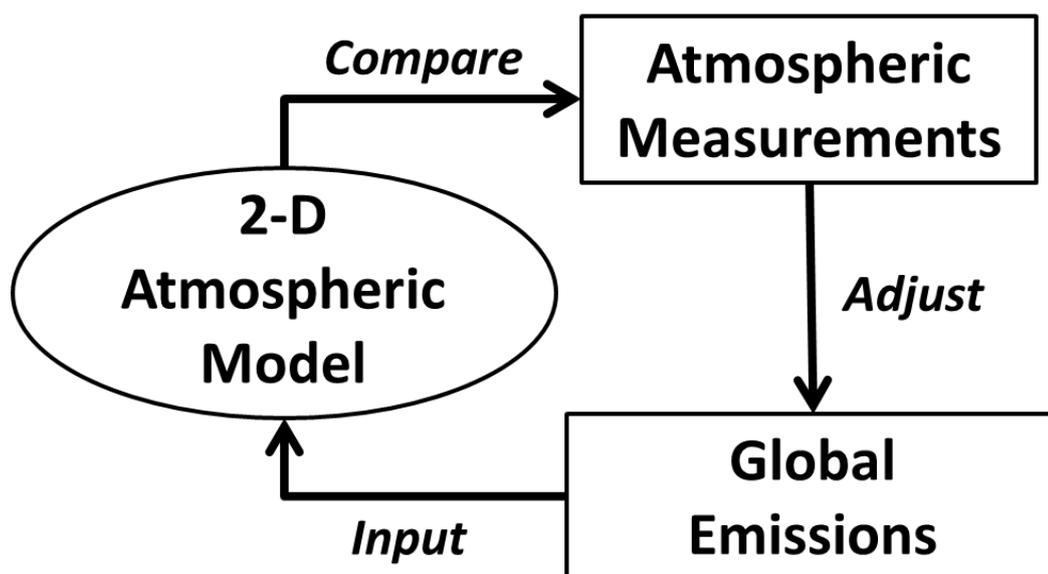


**Figure 2.5** Schematic of the process by which global emissions are derived from atmospheric measurements for long lived gases.

### 2.6.1   Measurement Sites

For measurement sites which are above 2 km altitude (i.e. in the second vertical level of the model, such as Summit, Greenland), it is questionable whether the model output for the lowest level or the second level should be used. This issue arises because there is no topography defined within the model. Swanson et al. (2003) note that the similarities of measured seasonal alkane profiles at Barrow, Alaska (11 m a.s.l) and Summit (3216 m a.s.l) suggest that Summit can be generally be assumed to be "representative of a surface site". For a large ice sheet such as Greenland or the Antarctic, this is perhaps unsurprising, one would not expect surface sites to be receiving free tropospheric air, whereas a mountain based site, at which the boundary layer air can flow around the base of the mountain, may be expected to generally be sampling air representative of the free troposphere (e.g. Pico Mountain, Azores (Helmig et al., 2008); Jungfraujoch, Switzerland (Nyeki et al., 1998)).

## 2.7   Latitudinal Emission Distributions

Before adjusting the emissions to fit the measurements, the latitudinal distribution of the emissions within the model must be chosen. This distribution can be held fixed throughout the model run, or varied inter-annually or intra-annually depending on the available information for the species. The emissions distributions are generally based on reported bottom-up estimates of emission such as EDGAR or HTOC. The specific distributions used for each species are discussed in the relevant chapters.

The model can also be used to constrain the emissions distribution if measurements are available at more than one site, especially if northern and southern hemisphere sites are available. Mixing ratios can be expected to be higher closer to the source of the emissions and to 'lead' the trend observed at sites further from the source. This technique is used to investigate the emissions distribution of H-1202 in Chapter 4.

## 2.8   One Box Modeling

A one box model was developed to investigate the dependencies of the alkane-alkyl nitrate system studied in Chapter 6. This was written using the programming language FACSIMILE. A chemical mechanism was developed to represent the chemistry relevant to the problem.

### 2.8.1   Chemical Mechanism

The chemical mechanism to be developed has to represent the chemistry that governs the production and loss of the hydrocarbons and alkyl nitrates. These include the formation of the peroxy radical from oxidation of the hydrocarbon, the competition of NO and $HO_2$ for reaction with the peroxy radical and the subsequent reactions of the alkyl nitrates, hydroperoxides and aldehydes formed from these reactions. The chemical reactions described by the model are detailed in Table 2.4.

In Chapter 6 the one-box model is used in two different ways, firstly with the majority of species at fixed concentrations to investigate the sensitivity of alkyl nitrate production to changes in one variable independent of others. Secondly allowing the majority of species to vary to investigate the interdependence of different variables on each other and how this relates to the production of the alkyl nitrates.

The chemistry scheme has been largely built from scratch using Jacobson (2005) and Emmons et al. (2010) for reference as well as the original Hough-91 model. The reaction rates and products have mostly been taken from IUPAC (http://www.iupac-kinetic.ch.cam.ac.uk; Atkinson et al., 2004; Atkinson et al., 2006; Atkinson et al., 2008).

Reactions of the alkanes methane, ethane, propane, butane and pentane are explicitly described in the model. In Table 2.4 reactions of the $\geq$ C2 alkanes are written as RH, where R represents the relevant number of methyl groups. Aldehydes are written as R'CHO, where R' represents R less one methyl group.

There are no emissions in to the box model during the model run. It is run with all species at given initial concentrations. These concentrations can be fixed throughout the run or varied depending on the question being investigated.

**Table 2.4** Reactions included in the chemical mechanism used in the one-box modeling in Chapter 6.

| Reactants | Products |
|---|---|
| **$O_x$ and $HO_x$ reactions** | |
| $HO_2 + HO_2$ | $H_2O_2$ |
| **$NO_x$ reactions** | |
| $NO + O_3$ | $NO_2$ |
| $NO + HO_2$ | $NO_2 + OH$ |
| $NO_2 + OH$ | $HNO_3$ |
| **$NO_y$ reactions** | |
| $CH_3ONO_2 + OH$ | $0.5.HCHO + 0.5.NO_2 + 0.5.HO_2 + 0.5.HNO_3 + 0.5CH_3OOH$ |
| $RONO_2 + OH$ | $0.5.R'CHO + 0.5.NO_2 + 0.5.HO_2 + 0.5.HNO_3 + 0.5ROOH$ |
| **Organic reactions** | |
| $CO + OH$ | $HO_2$ |
| $CH_4 + OH$ | $CH_3O_2$ |
| $CH_3O_2 + HO_2$ | $CH_3OOH$ |
| $CH_3O_2 + HO_2$ | $HCHO + HO_2$ |
| $CH_3O_2 + NO$ | $0.999.HCHO + 0.999.HO_2 + 0.999.NO_2 + 0.001.CH_3ONO_2$ |
| $CH_3O_2 + CH_3O_2$ | $CH_3OH + HCHO$ |
| $CH_3O_2 + CH_3O_2$ | $2.HCHO + 2.HO_2$ |
| $RH + OH$ | $RO_2$ |
| $RO_2 + HO_2$ | $ROOH$ |
| $RO_2 + NO$ | $0.991.CH_3CHO + 0.991.HO_2 + 0.991.NO_2 + 0.009.C_2H_5ONO_2$ |
| $RO_2 + NO_2$ | $C_2H_5O_2NO_2$ |
| $HCHO + OH$ | $CO + HO_2$ |
| $RCHO + OH$ | $RC(O)O_2$ |
| $CH_3OOH + OH$ | $0.4.HCHO + 0.4.OH + 0.6.CH_3O_2$ |
| $ROOH + OH$ | $0.75.R'CHO + 0.75.OH + 0.25.RO_2$ |
| $HCOOH + OH$ | $HO_2$ |
| **Photolysis** | |
| $NO_2$ | $NO + O_3$ |
| $HCHO$ | $CO + 2.HO_2$ |
| $HCHO$ | $CO + H_2$ |
| $CH_3CHO$ | $CH_4 + CO$ |
| $CH_3CHO$ | $CH_3O_2 + HO_2 + CO$ |
| $C_2H_5CHO$ | $C_2H_5O_2 + HO_2 + CO$ |
| $CH_3OOH$ | $HCHO + HO_2 + OH$ |
| $C_2H_5OOH$ | $HCHO + HO_2 + OH$ |
| $CH_3COCH_3$ | $CH_3C(O)O_2 + CH_3O_2$ |
| $CH_3COCH_3$ | $2.CH_3O_2 + CO$ |
| $CH_3ONO_2$ | $HCHO + HO_2 + NO_2$ |
| $RONO_2$ | $R'CHO + HO_2 + NO_2$ |

## 2.9 Firn Modeling

### 2.9.1 Model Structure

Firn models can be used to derive the atmospheric history of a gas from measurements of air trapped in the firn. The firn model used for this study was a direct model developed at LGGE, Grenoble and is based upon that described by Rommelaere et al. (1997) and further developed by Martinerie et al. (2009). The behaviour of the gas within the firn, the extent and rate at which the gas diffuses through it, depends on the diffusivity profile of the firn, the diffusivity coefficient of the gas and on the gravitational fractionation (caused by the molecular weight) of the gas. Such profiles are different for every site. Furthermore the air at any given depth in the firn is representative of a range of ages because of the inter-connected nature of the firn.

For modeling, the firn diffusion profiles (i.e. how much a gas can diffuse at a given depth in the firn) are constrained using a series of reference gases with well known atmospheric histories. The concentration-depth profile of a given gas in the firn is a function of its atmospheric history, its diffusion coefficient and the diffusion profile. Since three of these variables are known (i.e. the concentration-depth profile, the atmospheric history and the diffusion coefficient) the diffusion profile can be calculated. The use of a range of reference gases provides a better constraint on the diffusion profile.

At NEEM the reference gases used were ($CO_2$, $CH_4$, $SF_6$, HFC-134a, CFC-11, CFC-12, CFC-113 and $CH_3CCl_3$) as well as $^{14}CO_2$ and $\delta^{15}N_2$ (Buizert et al., 2012). The model has been tuned to these data for NEEM by Patricia Martinerie and Emmauel Witrant at the Laboratoire de Glaciologie and Géophysique de l'Environnement, Grenoble (LGGE). For North GRIP the reference gases used were $CO_2$ and $CH_4$.

Each gas has a different diffusion rate through the firn based on its molecular structure. The diffusion coefficient of each gas is calculated relative to a reference gas, generally $CO_2$. Different methods have been reported for the calculation of these diffusion coefficients (e.g. Chen and Othmer, 1962; Fuller et al., 1966). All of the diffusion coefficients used in the firn modeling in this work were calculated using the method of Fuller et al. (1966) based on the sum of the Le Bas molar volumes of the molecule, except for the modeling of HFC-227ea from Laube et al. (2010) which used the Chen and Othmer method.

The diffusion coefficients used for the firn modeling for each molecule within this work are given in Table 2.6.

**Table 2.5** Diffusion coefficients used for the firn modeling in this thesis

| Molecule | Diffusion Coefficient (relative to $CO_2$) | Measured Arctic Seasonal Amplitude [b] |
|---|---|---|
| H-1202 | 0.514 | - |
| $C_2F_6$ | 0.541 | - |
| $C_3F_8$ | 0.461 | - |
| c-$C_4F_8$ | 0.449 | - |
| $C_4F_{10}$ | 0.408 | - |
| $C_5F_{12}$ | 0.371 | - |
| $C_6F_{14}$ | 0.342 | - |
| $C_7F_{16}$ | 0.319 | - |
| $SF_5CF_3$ | 0.467 | - |
| HFC-227ea | 0.465 [a] | - |
| Ethane | 0.827 | 0.59 |
| Propane | 0.657 | 1.09 |
| n-butane | 0.560 | 1.31 |
| iso-butane | 0.560 | 1.36 |
| n-pentane | 0.495 | 1.46 |
| iso-pentane | 0.495 | 1.51 |
| Methyl nitrate | 0.695 | 0.25 |
| Ethyl nitrate | 0.587 | 0.33 |
| 2-propyl nitrate | 0.517 | 0.69 |
| 2-butyl nitrate | 0.467 | 0.81 |
| 2+3-pentyl nitrates | 0.428 | 0.84 |
| 3-methyl-2-butyl nitrate | 0.428 | 0.96 |

[a] Taken from Laube et al. (2010) and calculated by Chen and Othmer (1962) method. [b] From Worton et al. (2012).

### 2.9.2 Derivation of Atmospheric History

For short lived species, such as the alkanes and alkyl nitrates the mixing ratios of which fall to near zero in the summer months, derived atmospheric mixing ratios represent an annual mean. For these species a further step is required to fit the model output to the measurements in the upper part of the firn, which represents the seasonal changes of the mixing ratios during the first year after entrainment in the firn. To fit this variation a seasonal amplitude (Table 2.6) of the observed mixing ratios in the Arctic from Swanson et al. (2003) was applied to the annual mean of the most recent year (after Worton et al., 2012).
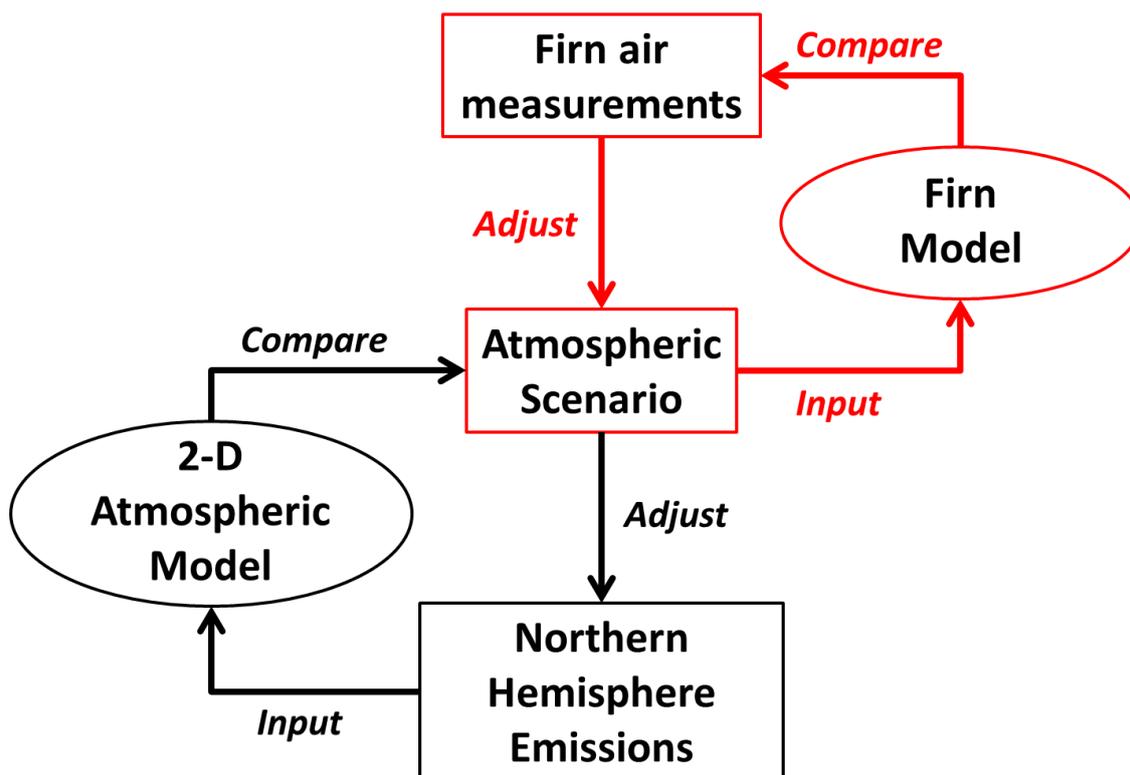
**Figure 2.6** Schematic of the process by which atmospheric scenarios are derived from firn air measurements using the firn model and subsequently northern hemisphere emissions (for short lived gases) are derived using the atmospheric model.

Having derived an atmospheric scenario from the firn this can then be used to derive emissions of the measured species using the 2-D atmospheric model (Figure 2.6), following the process outlined in Section 2.6. For gases with atmospheric lifetimes of less than a year the derived emissions are representative of northern hemisphere emissions (if northern hemisphere firn sites are used) as there will be no significant inter-hemispheric transport.

# Chapter 3

# Halons

# 3  Halons

Chapter 3 reports the atmospheric records of the halons between 1978 and 2011 from measurements at Cape Grim and compares these trends to those reported by NOAA and AGAGE. Global annual emissions of the halons are derived using the 2-D atmospheric model. These are compared to those reported using a top-down approach by NOAA and AGAGE and the bottom-up estimates of HTOC (Halons Technical Options Committee). The contribution of the halons to total tropospheric bromine is explored and extrapolated to 2060, to investigate the future effect of the halons on tropospheric bromine. The source and seasonality of H-1202 emissions are investigated. Finally the implications for the banks and the cumulative emission of an alternative set of steady state atmospheric lifetimes are discussed.

## 3.1 Introduction

The halons are ozone depleting gases that have been used since the 1950s for fire protection purposes due to their chemical inertness, originally in the military and later in commercial applications (HTOC, 1999). The production of the gases has been banned under the Montreal Protocol since 1994 in non-Article 5 countries and since 2010 in Article 5 countries. However there are still emissions of the halons from critical use exemptions which have been unable to find viable alternatives for fire protection.

Air samples have been collected regularly at Cape Grim since 1978. These air samples have been analysed for four halons: H-1301 ($CBrClF_2$), H-1211 ($CBrF_3$), H-2402 ($CBrF_2CBrF_2$) and H-1202 ($CBr_2F_2$), at UEA using the experimental setups detailed in Chapter 2. This record has been reported between 1978 and 1998 in Fraser et al. (1999) and more recently up to 2011 in Newland et al. (2013).

## 3.2 Atmospheric Modeling

### 3.2.1  Model Setup

The 2-D atmospheric model was used to model the long lived gases in Chapters 3 and 4. The only loss processes that affect the gases studied in these two chapters are reaction with OH

and photolysis. For the halons the rate of loss to reaction with OH is seen to be at least twenty times smaller than the loss to photolysis at all times.

The OH concentrations are fixed and do not vary interannually. The OH field is based on results from a full chemistry model run by Hough (1991) that has then been scaled to give a lifetime for methyl chloroform, with respect to reaction with OH, of 6.1 years, as given by the most recent WMO review (Montzka and Reimann, 2011), using a reaction rate of $1.2 \times 10^{-12} e^{(-1440/T)}$ (Atkinson et al., 2008). The OH concentrations are input monthly for each cell and interpolated in between these times using a sine smoothing function.

For the photolysis, the absorption cross sections are calculated for each grid box as a function of seasonally varying temperature for the wavelengths $200 - 660$ nm. For the halons they are the mean of the temperature dependent absorption cross sections reported by Gillotay and Simon (1989), Gillotay et al. (1988) and Burkholder et al. (1991).

The diffusive loss from the top of the model is governed by defining the ratio of the mixing ratio of a particular species in the top box of the model (i.e. at 23 km in the atmosphere) to that of the species in a box directly above the model domain (i.e. 25 km). This loss represents any loss processes that occur above the model domain. For the initial runs, which derived the emissions reported in Section 3.4 of this chapter, the value of the ratio of the concentration of H-1211, H-1301 and H-2402 in the top box of the model (23 km) to that of a box above the model domain (25 km) was fixed so that, in combination with the loss from photolysis and reaction with OH, the steady-state lifetimes of the halons within the model domain were equal to those given in Montzka and Reimann (2011) (H-1211 – 16 years, H-1301 – 65 years, H-2402 – 20 years). To achieve these steady-state lifetimes values of 0.952 (H-1211), 0.736 (H-1301) and 0.820 (H-2402) were used for this ratio. For H-1202, the lifetime reported in Montzka and Reimann (2011) was originally derived by Fraser et al. (1999) using the same model used in this work. However due to changes in the calculation of absorption cross-sections, the lifetime of H-1202 within the model domain is revised to 2.6 years.

The ratio was later changed in a further set of runs in order to adjust the lifetimes to alternative values. This is discussed fully in Section 3.8.

### 3.2.2 Latitudinal Distribution of Emissions

The latitudinal distribution of halon *production* changed considerably during the early – mid-1990s when the Montreal Protocol came into force banning the further production of halons in non-Article 5 countries. The major area of production since 1994 has been south-east Asia, namely China (HTOC, 2006). However the *emission* distribution would not have changed so dramatically since the use of halons for fire protection applications was phased out gradually in non-Article 5 countries with some use for critical exemptions still on-going.

H-2402 was produced almost exclusively in Russia and former Soviet countries (HTOC, 2011). Emissions of H-2402 are now limited largely to these countries and to countries which use ex-Soviet military equipment.

The emissions distributions used in the model for H-1211 and H-1301 were varied according to the reported regional annual emissions of these halons in HTOC (2011). The distribution used for H-1202 emissions was the same as that of H-1211 since the emissions appear to be co-located (see Section 3.5). H-2402 emissions were assumed to have a constant distribution throughout the period over which the model was run based on their use in Russia and former Soviet-bloc countries.

The annual emissions input to the model were adjusted so that the model output for the box representing 35.7°S − 41.8°S reproduced the measurements from Cape Grim (40.4°S). The model has previously been shown to reproduce southern hemispheric observations to within about 5% for gases emitted mostly in the northern hemisphere and for which there have been well reported emission inventories such as CFC-11 and CFC-12 (e.g. Reeves et al. 2005).

## 3.3 Cape Grim Mixing Ratio Time Series

The mixing ratios of the four halons measured at Cape Grim between 1998 and 2011 are shown in Figures 3.1 – 3.4. The output from the model run using the 'best fit' emissions scenarios (shown in Section 3.4) is also shown as a red line through the measurements. Measurements by NOAA and AGAGE at Cape Grim are also shown in Figures 3.1 – 3.4 where available. The entire records from Cape Grim (1978 – 2011) are shown as insets in the main panels. The measurements made using the first analytical method (Al-PLOT column, Autospec) have previously been reported by Fraser et al. (1999) for the period 1978-1998

however the mixing ratios of H-1211 and H-1301 are presented here on the NOAA-2006 gravimetric calibration scale as opposed to the UEA volumetric scale used in Fraser et al. (1999). The measurements made using the first method between 1999 and 2004 and those using the current methods (GasPro column, Autospec-Premier) have not been previously reported. It is evident that the data obtained from the two different analytical setups agree very well and can be combined to make a single continuous record.

Table 3.1 shows the mean mixing ratios of the halons between January and June 2011 at Cape Grim and the mean growth rates during the periods 1985 – 1999 (when the mixing ratios were all increasing), 1999 – 2005 (when growth rates began to slow or turn over) and 2005 – 2011 (when the mixing ratios of three of the halons were decreasing).

**Table 3.1.** Mean mixing ratios of the halons at Cape Grim for January to June 2011, and mean growth rates for the periods 1985 – 1999, 1999 – 2005 and 2005 – 2011.

| Halon | Mean Mixing Ratio Jan – June 2011 (ppt) | Mean growth rate (ppq yr$^{-1}$) | | |
|:---:|:---:|:---:|:---:|:---:|
| | | **1985 – 1999** | **1999 – 2005** | **2005 – 2011** |
| **H-1211** | 3.98 ±0.04 | 186 ± 14 | 67 ± 24 | -42 ± 16 |
| **H-1301** | 3.15 ±0.03 | 139 ± 7 | 54 ± 21 | 29 ± 17 |
| **H-2402** | 0.39 ±0.01 | 16 ± 1.5 | 0 ± 1.7 | -3.3 ± 2.5 |
| **H-1202** | 0.020 ±0.001 | 2.2 ± 0.1 | -1.7 ± 0.2 | -2.6 ± 0.2 |

### 3.3.1   H-1211

The mixing ratio of H-1211 grew rapidly during the 1980s and 1990s from 1.2 – 1.4 ppt (parts per trillion) in 1985 to 3.9 ppt at the end of 1999 at an average growth rate of 0.19 ppt yr$^{-1}$. The growth rate began to slow after 1999 and mixing ratios reached a maximum of 4.2 ppt in 2004 – 2006. Thereafter the concentrations at Cape Grim began to slowly decline to a mean mixing ratio in the first half of 2011 of 4.0 ppt.

NOAA report a similar trend in mixing ratios for H-1211 from measurements by GC-MS of Cape Grim background samples (mean of flask pairs) between 1998 and mid-2011 (Montzka and Elkins, 2012). These measurements are about 1% higher than UEA

measurements between 1998 and 2003 and about 1% lower between 2003 and 2011. The mixing ratios reported by AGAGE from *in-situ* baseline measurements by GC-MS at Cape Grim since 1998 (http://agage.eas.gatech.edu) display a similar trend to those reported here but are consistently about 2 – 3% higher. This is most likely caused by differences in calibration scales (see Section 2.2.2).
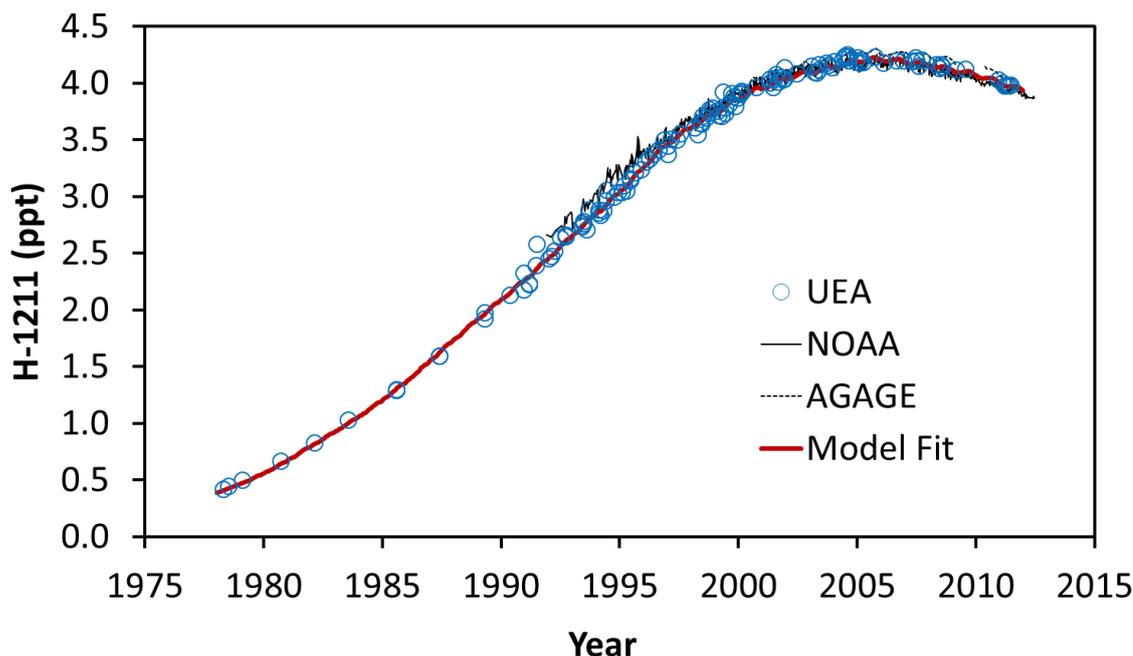


**Figure 3.1 H-1211:** Measured mixing ratios (ppt) from Cape Grim archive at UEA – blue circles. Model fit – red line. Measured mixing ratios (ppt) from Cape Grim archive by AGAGE – grey line.

### 3.3.2   H-1301

The H-1301 mixing ratio grew steadily from a mean of 0.7 – 0.8 ppt in 1985 to a mean of 2.6 – 2.7 ppt in 1999 at an average growth rate of 0.14 ppt yr$^{-1}$. The mean mixing ratio in the first half of 2011 was 3.15 ppt with a mean growth rate since 2000 of 0.045 ppt yr$^{-1}$. H-1301 is the only one of the halons reported here to have atmospheric mixing ratios that are still increasing. This continued growth is consistent with predictions in Fraser et al. (1999) and Montzka and Fraser (2003) which show H-1301 mixing ratios peaking around 2020 before beginning to decline.

The mixing ratios reported by NOAA from GC-ECD (electron capture detection) measurements on Cape Grim flask pair mean samples are almost 5% higher than those of UEA between 1998 and 2000 but then steadily converge with those reported here during 2001 and 2002 and from 2003 the two trends are virtually identical up to the middle of 2006 when NOAA's ECD measurements stopped (Montzka and Elkins, 2012). Since 2004 NOAA have also measured the flask samples by GC-MS. These mixing ratios agree very well with those reported here (S. Montzka, personal communication, 2012). The baseline mixing ratios reported by AGAGE since 1998, measured by GC-MS *in-situ* at Cape Grim (http://agage.eas.gatech.edu/), are consistently about 3% higher than those reported here (presumably caused by differences in the calibration scales) with the exception of a period between 2001 and 2003 during which the AGAGE measurements show a high degree of variability.
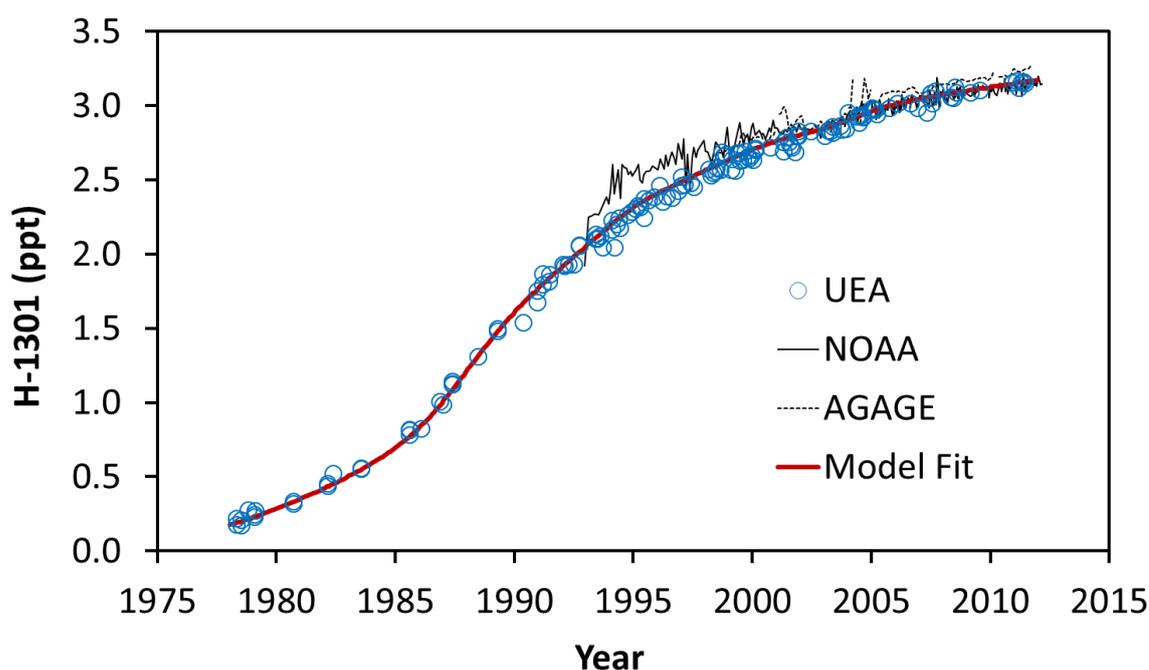


**Figure 3.2 H-1301:** Measured mixing ratios (ppt) from Cape Grim archive at UEA – blue circles. Model fit – red line. Measured mixing ratios (ppt) from Cape Grim archive by AGAGE – grey line.

### 3.3.3   H-2402

The mixing ratio of H-2402 increased from about 0.21 ppt in 1985 to a mean of 0.42 ppt in 1999 at a mean growth rate of 0.016 ppt yr$^{-1}$. The mixing ratio levelled off during the late

1990s – early 2000s at a peak of 0.42 – 0.44 ppt. It began to fall around 2005 and reached a mean of 0.39 ppt during the first half of 2011.

NOAA reports measurements of H-2402 from 2004 onwards and for a brief period from 1995 to the start of 1997. The declining trend since 2004 agrees well with the trend observed in this work but the mixing ratios reported by NOAA are consistently 10 – 15% higher. This is again probably caused by a calibration difference since the UEA measurements are presented on the UEA volumetric scale.

AGAGE H-2402 data are not currently available from the publically-accessible data archive (http://agage.eas.gatech.edu), but monthly global means were presented in Montzka and Reimann (2011) and are very similar to those reported by NOAA in Montzka and Reimann (2011).
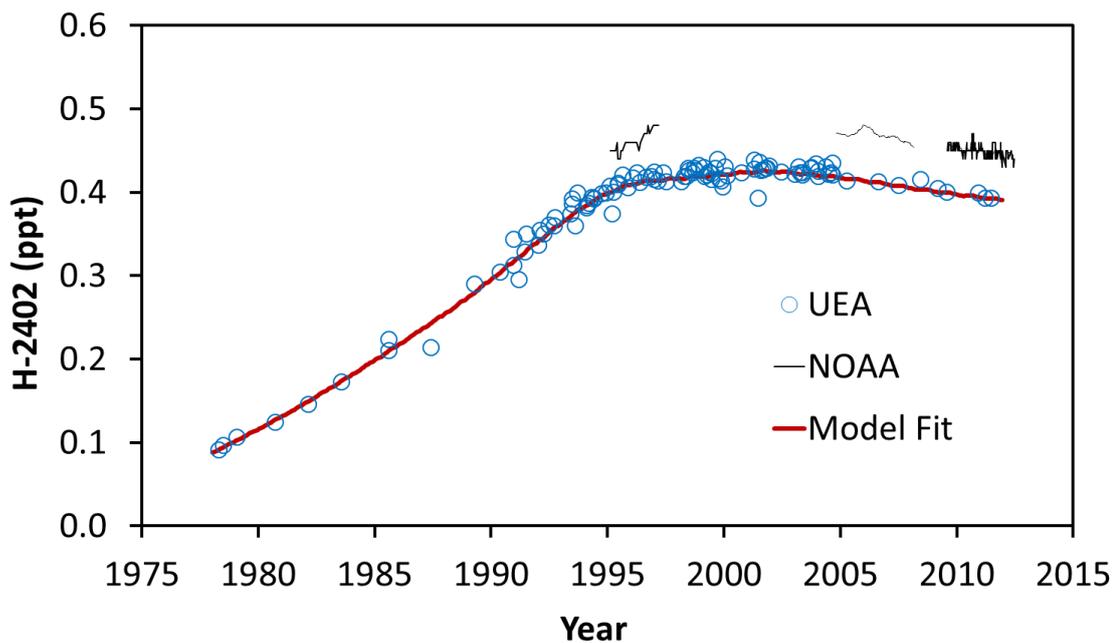


**Figure 3.3 H-2402:** Measured mixing ratios (ppt) from Cape Grim archive at UEA – blue circles. Model fit – red line.

### 3.3.4  H-1202

The mixing ratio of H-1202 at Cape Grim grew from an annual mean of 14 – 15 ppq (parts per quadrillion) in 1985 to a mean of 45 ppq in 1999 with a mean growth rate of 2.2 ppq yr[-]

[1]. The mean annual mixing ratio remained fairly stable between 1999 and 2001 and has since fallen sharply to a mean mixing ratio of about 20 ppq in the first half of 2011.

UEA is the only institution to have reported measurements of H-1202.

H-1202 shows a pronounced seasonal cycle because of its short lifetime (3.0 years). This is discussed further in Section 3.5.
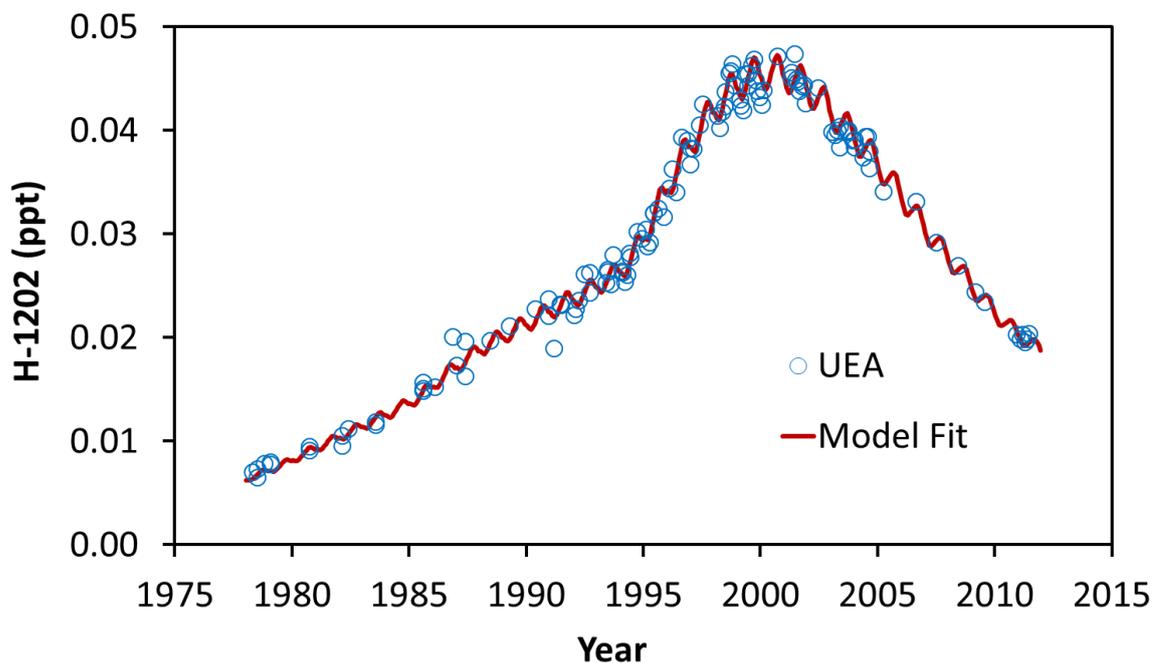


**Figure 3.4 H-1202:** Measured mixing ratios (ppt) from Cape Grim archive at UEA – blue circles. Model fit – red line.

## 3.4 Emissions

The annual global emissions of the halons, as derived from the model runs in Figures 3.1 – 3.4, are shown in Figures 3.5 – 3.8. The emissions are derived using an inversion technique using the measurements from Cape Grim presented in the preceding section. The model output at the latitude of the Cape Grim site (40.41°S, 144.41°E) was compared to the measurements. The emissions were then adjusted for each year to improve the fit of the model output to the measurements. This process was repeated until the model output from the emissions scenarios (Figures 3.5 – 3.8) provided a good fit to the measurements.

Also shown, where available, are the emissions reported by NOAA and AGAGE (Montzka and Reimann, 2011), both derived using a one box atmospheric model with global measurements, and the emissions derived using a 12-box model in conjunction with AGAGE measurements (from the Cape Grim archive air before 2004 and global measurements thereafter (Montzka and Reimann, 2011)). Finally the bottom up estimates of HTOC are shown (HTOC, 2011); these emission estimates are calculated based on emissions modeling taking into account industry reported production, usage and destruction.

Uncertainties in the measurements and fitting the model output to those measurements, the atmospheric lifetimes of the halons, and in the model transport all contribute to uncertainties in the model derived emissions. Figures 3.5 − 3.8 show the annual emissions estimated in this work with error bars based on the measurement errors associated with each individual data point and errors in the transport within the model (which are taken as a constant 5% throughout the run based on previous work with the model − the model has previously been shown to reproduce southern hemispheric observations to within about 5% for gases emitted mostly in the northern hemisphere and for which there have been well reported emission inventories such as CFC-11 and CFC-12 (Reeves et al. 2005)). These errors should allow comparison with other top-down derived emissions (i.e. NOAA and AGAGE), assuming that the same atmospheric lifetimes were used. Errors associated with the lifetimes of the halons are not shown in these Figures; a discussion of lifetimes and uncertainties is presented in Section 3.8.

### 3.4.1   H-1211

The model derived annual emissions of H-1211 are 3.0 Gg in 1978, they then increase at an average growth rate of 0.58 Gg yr$^{-1}$ to maximum emissions of 12.8 Gg in 1995. Emissions have since decreased at an average rate of 0.52 Gg yr$^{-1}$ to 5.0 Gg in 2010.
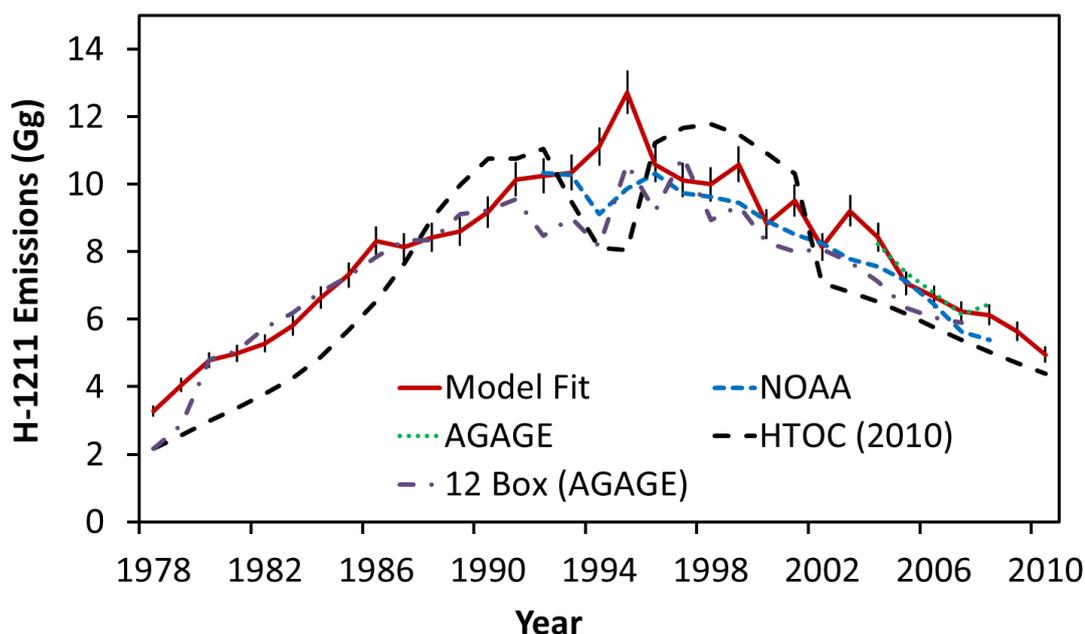
**Figure 3.5 H-1211:** Model derived annual emissions (Gg) from Cape Grim measurements using NOAA scale – red line. NOAA one box model derived emissions (WMO 2010) – blue short dashed line. AGAGE 12-box model derived emissions (WMO 2010) – green dotted line. Annual emissions reported by HTOC (2010) – black long dashed line.

The emissions derived here show a similar trend to those derived by NOAA and AGAGE. The cumulative emissions derived from the model for the period 1979 – 2009, shown in Table 3.2, are 253 Gg compared to those using the AGAGE measurements and a 12-box model which are 11% lower at 225 Gg. The emissions reported by HTOC are similar to those reported here with cumulative emissions for the period 1979 – 2009 of 234 Gg, 8% lower than those derived in this work and 4% higher than those derived by AGAGE.

Figure 3.5 shows emissions of H-1211 are 3.0 Gg in 1978 suggesting that there have been significant emissions prior to this time. Extrapolating emissions back to zero in the 1963 using an exponential growth curve, adjusted to reach the 1978 mixing ratio at Cape Grim, leads to cumulative emissions prior to 1978 of 13.4 Gg. This is significantly more than those reported by HTOC prior to 1978 of 8.1 Gg.

The cumulative emissions derived from the model for the period 1995 – 2008 are about 5% lower than those reported by HTOC for the same period, 112 and 118 Gg respectively. The cumulative emissions reported by NOAA and AGAGE lie between these two values at 117 and 114 Gg respectively.

3.4.2  H-1301

The model derived annual emissions of H-1301 in 1978 are 1.5 Gg. Annual emissions then increase gradually to 2.5 Gg in 1984 at an average rate of 0.17 Gg yr$^{-1}$ before a more rapid increase up to a maximum of 6.0 Gg in 1987 at a rate of 1.2 Gg yr$^{-1}$. They then decline steadily to annual emissions between 2007 and 2010 of 1.8 – 1.9 Gg.

The NOAA record shows a great deal of variability and though it agrees with the general decline in recent years, the exact features are often quite different. The AGAGE emissions display far less variability and a more similar trend. Emissions derived by both AGAGE and HTOC display a steady rise from 1978 to the mid-late 1980s, whereas we derive a slower growth in the early 1980s followed by a steep increase beginning around 1985. This was also commented on in Fraser et al. (1999).

The cumulative emissions derived in this work for the period 1979 – 2009 (97 Gg) (Table 3.2) are similar to those of HTOC (99 Gg) and those derived using a 12-box model with AGAGE measurements (96 Gg).
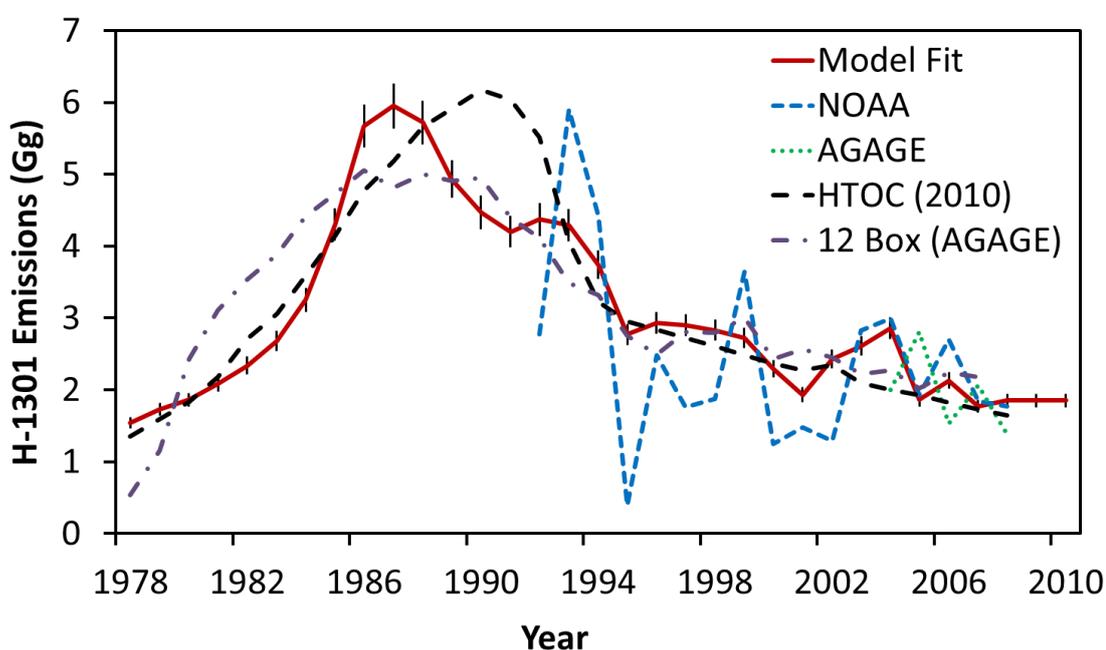


**Figure 3.6 H-1301:** Model derived annual emissions (Gg) from Cape Grim measurements using NOAA scale – red line. NOAA one box model derived emissions (WMO 2010) – blue short dashed line. AGAGE 12-box model derived emissions (WMO 2010) – green dotted line. Annual emissions reported by HTOC (2010) – black long dashed line.

H-1301emissions are seen to have levelled off after 2006. This could be a compensation for the fact that the model fit shows a large decline in emissions between 2004 and 2006. However recent measurements from Cape Grim, up to June 2011, confirm that mixing ratios are increasing again.

One so urce of the emissions could be associated with the production of H-1301 as a chemical feedstock. Both China and France are still producing H-1301 for use as a chemical feedstock for the pesticide Fipronil. A UNEP report (UNEP, 2009) reported the production of almost 0.6 Gg of H-1301 in China in 2008 and HTOC 2010 reports approximately 0.4 Gg per year of production in France since the mid-1990s. However production in France is reported to lead to only $6x10^{-4}$ Gg of fugitive H-1301 being emitted (HTOC, 2007). This tiny amount cannot account for the continued emissions of H-1301 of 1.7 Gg in 2010. This suggests that there could be another unreported source of H-1301 emissions.

Figure 3.6 shows emissions of H-1301 in 1978 are 1.6 Gg. Prior to this cumulative emissions derived using the atmospheric model and assuming an exponential growth curve from zero at 1963, adjusted to match the Cape Grim measurement in 1978, are 4.7 Gg compared to 4.3 Gg reported by HTOC.

The cumulative emissions derived from the model for the period 1995-2008 are similar to those of NOAA, 28 and 29 Gg respectively. Those of HTOC for the same period are slightly higher at 32 Gg and AGAGE are considerably higher at 37 Gg.

### 3.4.3 H-2402

The model derived annual emissions are 0.9 Gg in 1978 and increase steadily up to a peak of 1.9 Gg in 1990 at a growth rate of 0.08 Gg $yr^{-1}$. They then decline to 1.0 Gg in 1996 and remain around this level until 2000. They then begin to decline again to 0.7 Gg in 2006 and have remained around this level up to 2010.
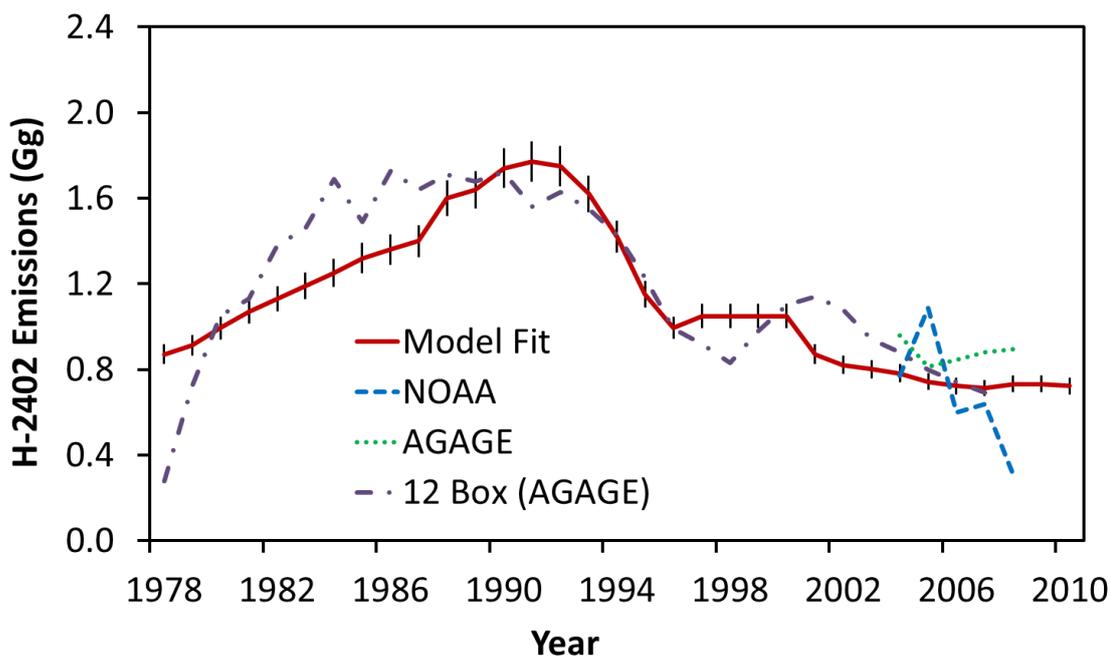
**Figure 3.7 H-2402:** Model derived annual emissions (Gg) from Cape Grim measurements using NOAA scale – red line. NOAA one box model derived emissions (WMO 2010) – blue short dashed line. AGAGE 12-box model derived emissions (WMO 2010) – green dotted line.

The emissions derived by AGAGE for the period 1979 – 2009 (Table 3.2) using a 12 box model display a very similar trend and calculate very similar cumulative emissions for the period 1979 – 2009 of 36 Gg compared to 35 Gg in this work. HTOC does not report annual emissions of H-2402.

The decline in emissions of H-2402 begins after 1991. Since the gas was used mainly in the Soviet Union it would be expected that emissions would decrease significantly after the fall of the Soviet Union in 1991 and the concomitant reduction in the size of the military and in industrial activity.

Cumulative emissions of H-2402 prior to 1978 are calculated using the model extrapolating an exponential growth curve back to zero in 1963 adjusted to match the Cape Grim measurement in 1978 as 3.9 Gg.

3.4.4   H-1202

The model derived annual emissions of H-1202 are 0.16 Gg in 1978. They increase steadily up to 0.52 Gg in 1993 at a rate of 0.024 Gg yr$^{-1}$ and then increase steeply to a peak of 0.84 Gg in 1997 before declining to 0.26 Gg in 2010.
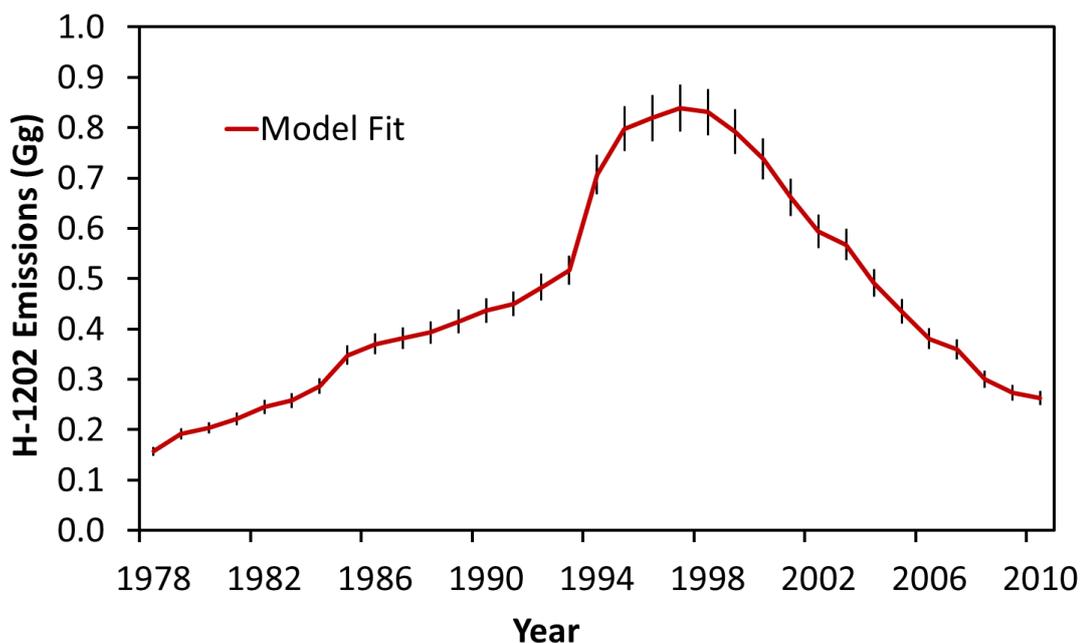


**Figure 3.8 H-1202:** Model derived annual emissions (Gg) from Cape Grim measurements.

Figure 3.8 shows annual emissions of H-1202 are 0.15 Gg in 1978. Extrapolating emissions back to zero in 1963 and adjusting for the Cape Grim measurement in 1978 gives cumulative emissions prior to 1978 of 0.69 Gg. However this is the most sensitive of the halons to the chosen start date for emissions due to its short lifetime (2.9 years). Likewise the derived emissions have the greatest possibility for error based on the chosen OH reactivity and photolysis rates.

UEA is the only institution that measures H-1202 and so there are no reported emissions from NOAA or AGAGE. The reasons for the emissions trend are discussed in Section 3.5.

**Table 3.2** Estimates of the cumulative emissions of the halons between 1963 and 2010 reported by HTOC (bottom-up estimate) and calculated in this work using firstly the lifetimes reported by Montzka and Reimann (2011) and secondly the alternative lifetimes calculated in this work (Section 3.8). Also shown are the banks of H-1211 and H-1301 that are calculated by subtracting the specific estimates of the cumulative emission from the estimates of cumulative production as reported by HTOC (HTOC, 2011).

*Using $\tau_{atm}$ Montzka and Reimann (2011)[a]*

| Reference | Cumulative Emissions (Gg) | | | | Banks (Gg) | |
|---|---|---|---|---|---|---|
| | H-1211 | H-1301 | H-2402 | H-1202 | H-1211 | H-1301 |
| This Work | 276 | 106 | 42 | 16 | 37 | 43 |
| HTOC | 248 | 106 | - | - | 65 | 43 |

*Using alternative $\tau_{atm}$ [b]*

| | Cumulative Emissions (Gg) | | | | Banks (Gg) | |
|---|---|---|---|---|---|---|
| | H-1211 | H-1301 | H-2402 | H-1202 | H-1211 | H-1301 |
| Using alternative $\tau_{atm}$ | 290 | 101 | 46 | 16 | 24 | 48 |
| Uncertainty range | 262 – 319 | 99 – 103 | 42 – 49 | 13 – 19 | -5 – 52 | 47 – 50 |

[a] Except H-1202 (lifetime from this work). [b] See Section 3.8 and Table 3.4.

## 3.5 H-1202

### 3.5.1 Seasonality of H-1202

UEA is the only institution that measures H-1202 and hence there is less information on its behaviour in the atmosphere than for the other halons. Its emission sources are unclear as there are no reported direct emissions by HTOC. It displays a seasonal behaviour in the Cape Grim air with summer minima and winter maxima caused by the seasonality of the photolysis sink. During the steep gradient changes in mean inter-annual mixing ratios this seasonal cycle is somewhat masked but between 1998 and 2000 there are high resolution measurements and a fairly stable annual average mixing ratio allowing the seasonality to be examined.

The intra-annual variation of the measured mixing ratios during the period 1998 – 2000 was de-trended from the inter-annual trend by comparison to a cubic fit to the measurements

between 1995 and 2005 (Figure 3.9). A cubic fit to this de-trended data shows the amplitude of the seasonal cycle observed to be about 8%, with an R-squared value of 0.69 (Figure 3.10). Also shown in Figure 3.10 is the behaviour of the atmospheric model through the same period. This seasonal amplitude of 8% agrees well with the reported seasonality in Fraser et al. (1999) (about 7%) which uses a similar method on the Cape Grim samples between 1990 and 1998. A fit to the 2001 – 2008 measurements, using the same technique, shows the same seasonal amplitude but with a much lower R-squared value of only 0.14. This is because of the lower resolution of the data and the more variable mixing ratios as the mean annual mixing ratio is in sharp decline.
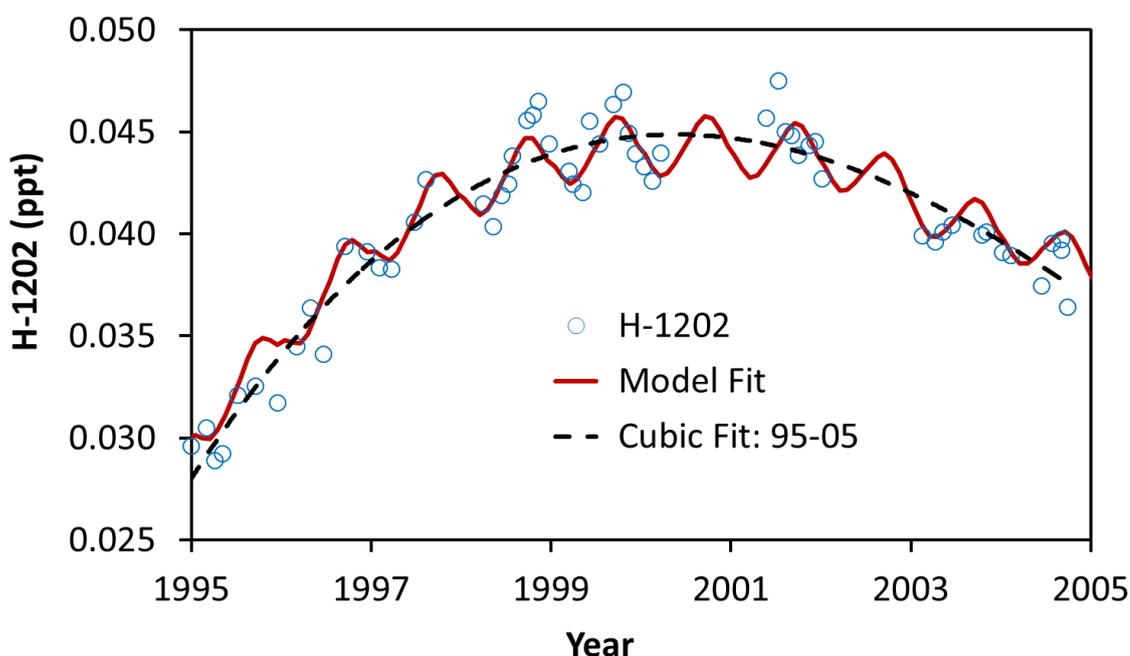


**Figure 3.9** Detail from Figure 3.4 showing the model fit and a cubic fit to measured H-1202 mixing ratios between 1995 and 2005.

The model appears to do a good job of recreating the seasonal amplitude. However if the uppermost and lowermost measured values are taken, then the seasonal amplitude would be about 12% and the model would be seen to be underestimating it. A model run was performed in which the photolysis rates (the main sink of H-1202) were doubled (Run B - Figure 3.10). It is seen that this gives a better fit to the higher measured values. A larger photolysis rate would have a great impact on emissions as photolysis is the major sink. A doubling of the

photolysis rate would require almost a doubling of emissions to fit to the Cape Grim measurements.
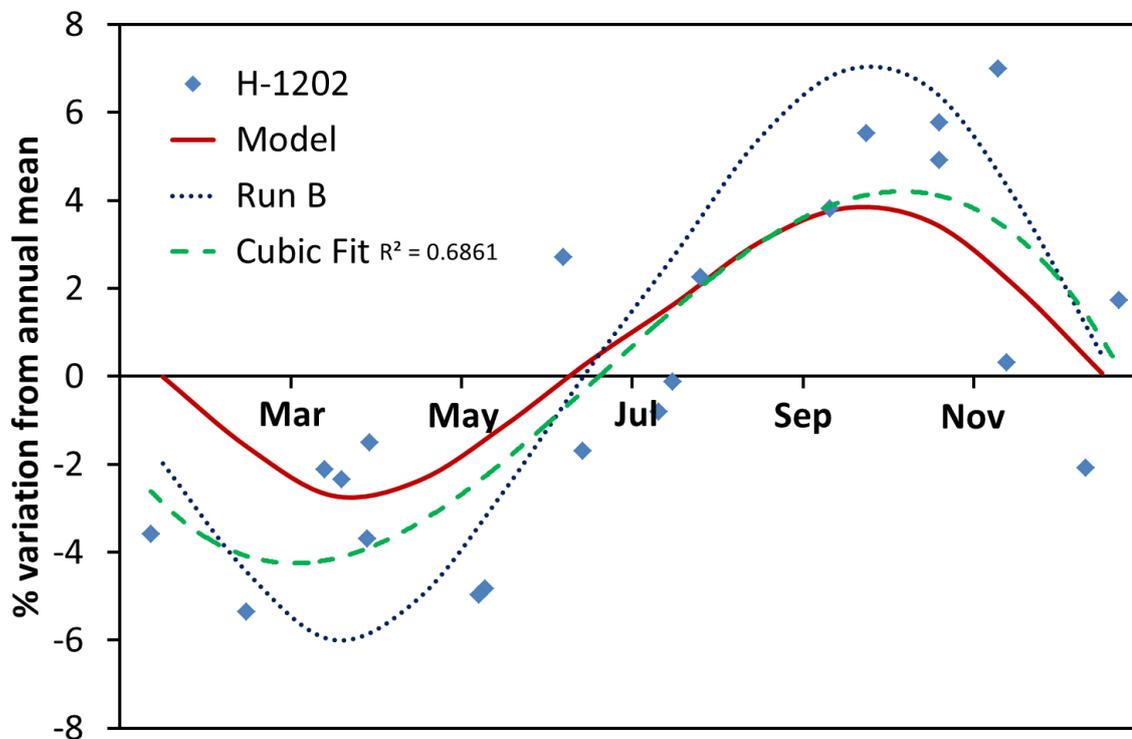


**Figure 3.10** A comparison between a cubic fit (green dashed line) to the measured mixing ratios of H-1202 between 1998 and 2000, the seasonal model output (red line) at Cape Grim and the seasonal model output with the photolysis rates doubled (yellow dotted line).

### 3.5.2 Latitudinal Emissions Distribution of H-1202

The emissions distribution of H-1202 is assumed to be equivalent to that of H-1211 production. This is because unlike the other halons, H-1202 has negligible reported direct usage (e.g. Fraser et al., 1999) and is produced mainly as an unwanted by-product caused by over-bromination during the production of H-1211 (Reeves et al., 2005).

H-1202 has a relatively short atmospheric lifetime (2.9 years – Montzka et al., 2011) and hence the atmospheric mixing ratio at any given latitude is sensitive to the emissions distribution. Using a measurement site in the northern hemisphere as well as Cape Grim, the emissions distribution can be better constrained.

Measurements of H-1202 in the firn at NEEM, Greenland, taken in the summer of 2008, are used for a northern hemisphere constraint (Figure 3.11). The atmospheric model was first run, with an emissions distribution, based on the industrial distribution from Hough (1991) – Run A and global emissions were adjusted to fit the measurements from Cape Grim. The atmospheric model output for the Arctic was then run through a direct firn model and the output compared to the firn profile (Figure 3.11). It is seen that mixing ratios in the main part of the profile are over estimated by about 50% using this scenario.

The emissions distribution was then changed to Run B. This is similar to the scenario 'Run A+F' reported in Reeves et al. (2005) to give the best fit to the firn profile of H-1202 at NGRIP (taken in 2001). However in this work the Hough (1991) distribution is used until 1992 reflecting the time of production of H-1211 moving mainly to non-Article 5 countries (Figure 3.12). The emissions are then moved to being between 19°N and 36°N, the model boxes representing China and South East Asia. This reflects the region where the majority of the production took place after 1992 as reported by HTOC (2011). This gives a much better fit to the firn measurements overestimating them by less than 5%. This is the scenario which was used to derive the emissions in Section 3.4.
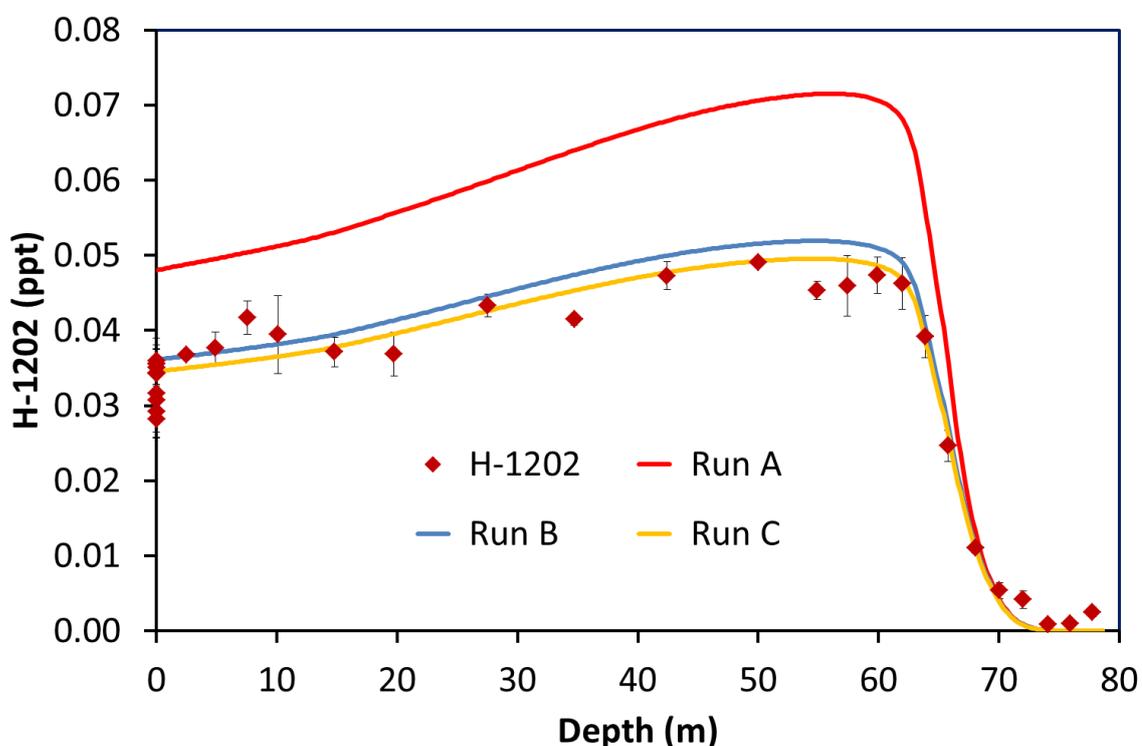


**Figure 3.11 H-1202**: Firn profile from NEEM, Greenland

A further run (Run C) was performed to try to give an even closer fit to the firn profile. This run was the same as Run B except that after 1992 an arbitrary 5% of emissions were in the southern hemisphere. This adjustment reduces the global emissions reported in Section 3.4 by 4% and reduces northern hemisphere mixing ratios slightly hence giving the best fit to the firn profile. However there is no reason to suggest that there should be recent emissions of H-1202 in the southern hemisphere.

### 3.5.3   Source of H-1202

It was found during an audit in 2002 of Chinese plants producing H-1211, that the production of H-1202 during H-1211 production was about 20 to 30 kg per tonne of H-1211 (E. Pedersen, personal communication, 2002). However all the H-1202 produced was supposed to be captured and fed back in to the H-1211 production process (E. Pedersen, personal communication, 2002).

Figure 3.12 shows a comparison of H-1211 production (as reported by HTOC (2011)) and the ratio of the model derived H-1202 emissions to this production. This ratio is seen to gradually fall during the period between 1975 and 1990, when non-Article 5 countries were the major producers of H-1211. This was presumably caused by improvements in the production efficiency of H-1211 in these countries. Assuming all H-1202 emissions to be from H-1211 production the emissions per Gg of H-1211 were between 20 and 25 tonnes. This value is in good agreement with the values reported above.

The ratio begins to rise in the early 1990s as production of H-1211 moves from non-Article 5 countries to China and South Korea. In the mid-1990s, when all production has moved to Article 5 countries, emissions stabilise at about 50-60 tonnes of H-1202 emitted per Gg of H-1211 produced. However as production of H-1211 begins to decline, this ratio begins to increase again. Presumably the production is not becoming less efficient in Article 5 countries and so the explanation must be either that there is more production of H-1211 than is being reported to HTOC, or that there is an alternative source of H-1202 emissions.

Model derived emissions for H-1202 of 0.32 Gg in 2008 (Section 3.4.4) would equate to H-1211 production of 5.3 Gg assuming H-1202 emissions of 60 tonnes per Gg of H-1211 produced. This compares to the reported emissions of South Korea (the only known producer after China stopped H-1211 production in 2005) of around 1000 ODP tonnes per year of H-

1211 and H-1301 which equates to a maximum possible H-1211 production (assuming no H-1301 production) of 0.33 Gg (based on an ODP of 3.0 (Montzka et al., 2011)). This suggests that either there is an alternative source of H-1202 emissions or that there is continuing production of H-1211.
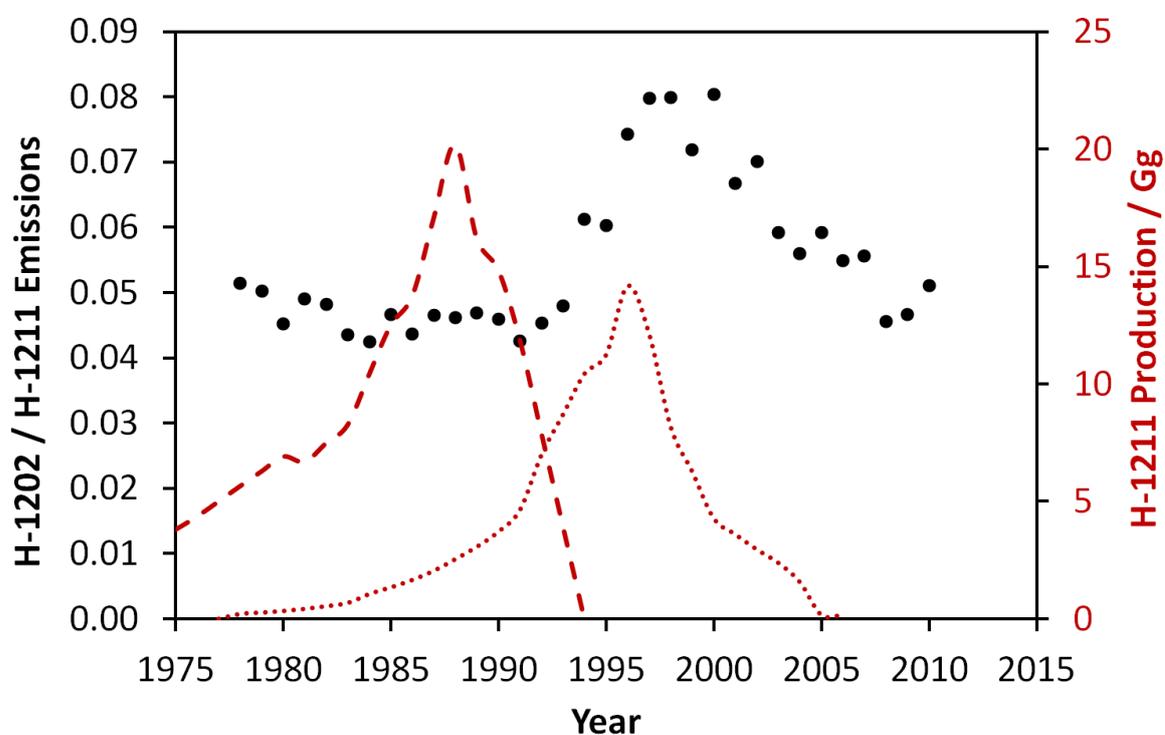


**Figure 3.12** The ratio of model derived emissions of H-1202 to H-1211 (see Figures 3.5 & 3.8) (black circles). Also shown is production of H-1211 in non-Article 5 countries (red dashed line) and Article 5 countries (red dotted line) (HTOC, 2010).

## 3.6 Halon Banks

The production of halons for direct use has ceased globally as of January 1$^{st}$ 2010 (HTOC, 2011) with the People's Republic of China stopping production of H-1211 by the end of 2005 and H-1301 by the end of 2009 and the Republic of Korea halting production of both by the end of 2009 (HTOC, 2011). There is still some limited production of H-1301 for use as a chemical feedstock in the preparation of the fertilizer Fipronil. Such usage is not controlled under the Montreal protocol.

Assuming no resumption of production, emissions will continue to fall year on year. However many countries have their own halon recycling programs whereby unused halons can be

collected and reused in equipment which still requires the gases and so it is likely that halon use for essential purposes will persist for some time. The European Union introduced a regulation in 2000 requiring the decommissioning of all halon systems by the end of 2003 with the exception of some specified critical uses (HTOC, 2011).

The banks at the end of 2010, as estimated by HTOC (2011), for H-1211, H-1301 and H-2402 were 65 Gg, 42.5 Gg and 2.3 Gg respectively. Since H-1202 has been mainly emitted as a by-product of H-1211 production, and has very limited application, if any, as a fire retardant, any remaining bank must be very small. With the cessation of H-1211 production in China at the end of 2005 (HTOC, 2011) and Korea at the end of 2009, emissions of H-1202 should be expected to rapidly fall to near zero.

## 3.7 Total Tropospheric Bromine

The total bromine compound mixing ratio (the sum of methyl bromide, the halons and very short lived bromine species) in the troposphere peaked at 16 - 17 ppt around 1998 and by 2008 had declined to 15.7 ± 0.2 ppt (Montzka et al., 2011). This decline has been attributed mainly to a decrease in the emissions of methyl bromide (Montzka et al., 2011). The measurements from Cape Grim show that during the period 2002 - 2011 the H-1211 mixing ratio has fallen slightly and that of H-1301 has risen slightly. Consequently there has been a small increase in the contribution to tropospheric bromine mixing ratios from the halons, from 7.5 ppt at the end of 2002 to 7.8 ppt at the end of 2010.

Figure 3.13 shows the contribution of the halons to tropospheric bromine mixing ratios at Cape Grim extrapolated to 2060. The emissions from 1978 to 2010 are those derived in Section 3.4. Emissions after 2010 are based on the reported  banks from HTOC (2011) and the bank release fraction (the proportion of the remaining bank released per year) reported in WMO 2010 (H-1211 – 0.075, H-1301 – 0.04, H-2402 – 0.08)(Daniel and Velders, 2011). H-1202 is not shown in Figure 3.13 as its contribution is negligible and with its short lifetime will become even more so in the near future. It is seen that after 2025, H-1301 becomes the main halon contributing to tropospheric bromine. This is because of its long atmospheric lifetime. By 2060 it is contributing almost 80% of the total 3.4 ppt of bromine from the halons. However with the continued production of H-1301 for use as a chemical feedstock, and emissions beginning to increase again, this should be viewed as a best case scenario.
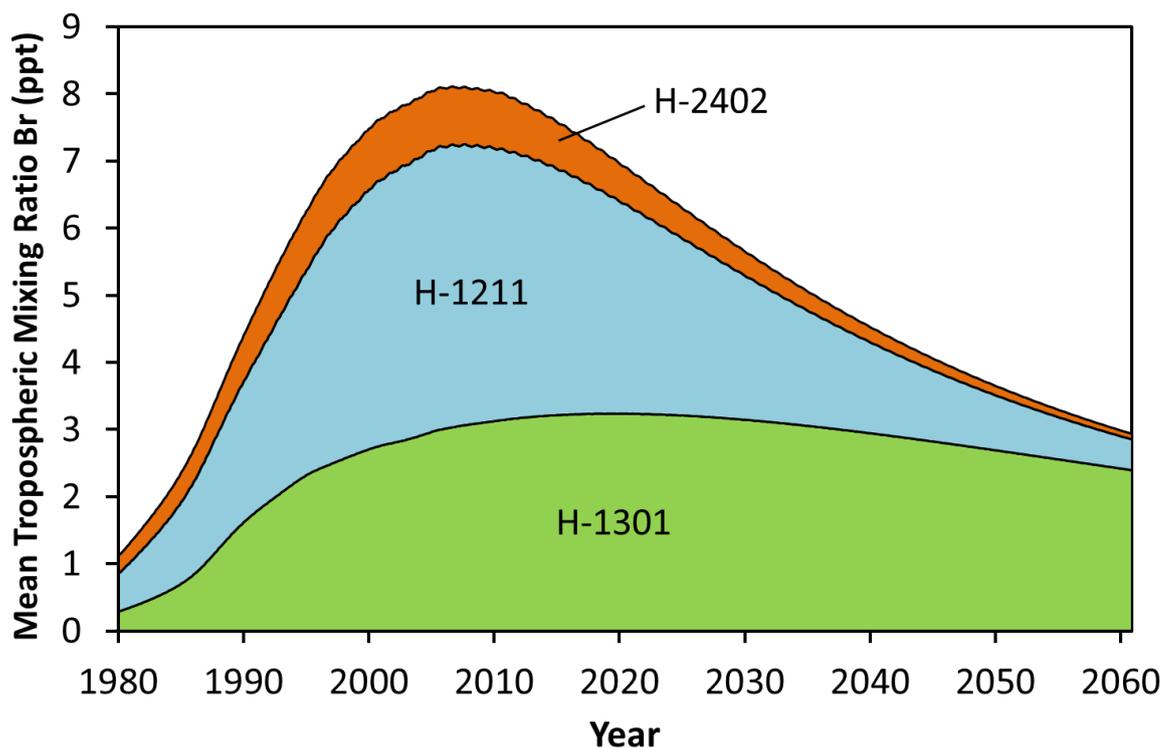
**Figure 3.13** The contribution of each of the halons to global mean tropospheric bromine mixing ratios as modelled for the period 1978 – 2060. From 1978 to 2010 the emissions used to model the halon mixing ratios are those derived in Section 3.4. Emissions after 2010 are based on banks from HTOC (2011) and bank release fractions from Daniel and Velders (2011).

## 3.8 Atmospheric Lifetimes

The emissions of H-1211, H-1301 and H-2402 derived in Section 3.4 are based on atmospheric lifetimes for the molecules of 16, 65 and 20 years respectively, as given by Montzka and Reimann (2011). These lifetimes were all originally derived by Burkholder et al. (1991) using a 1-D photochemical model extending to an altitude of 60 km. There have been various other estimates of the tropospheric, stratospheric and total lifetimes, in particular the recent re-evaluation of the stratospheric lifetimes of H-1211 and H-1301 by Laube et al. (2013). Here we evaluate the atmospheric lifetimes for the halons using the 2-D atmospheric model and considering the stratospheric lifetimes reported in Laube et al. (2013). The implications of such changes on the model derived emissions and on the sizes of the remaining halon banks are considered in Section 3.8.4.

### 3.8.1   Tropospheric Lifetimes

The modeled tropospheric lifetimes ($\tau_{trop}$) are calculated by running the model to steady state and then dividing the global atmospheric burden of the molecule by the global emissions. The model was run with the photolysis and OH sinks only active in the troposphere and the diffusive loss from the top of the model switched off (i.e. the only model sinks are in the troposphere). A range of tropospheric lifetimes were calculated by changing the defined height of the tropopause ($Z_{trop}$). These are shown in Table 3.3. The uncertainties associated with the absorption cross-sections used were also investigated. The cross-sections measured by Gillotay and Simon (1989), Gillotay et al. (1988) and Burkholder et al. (1991) generally agree to within 10% at room temperature though this error tends to increase at wavelengths longer than 265 nm. At low temperatures the agreement is generally within 20% but again differences tend to increase at wavelengths longer than 265 nm. Tropospheric lifetimes were calculated with the photolysis rates adjusted by $\pm 20\%$ for $Z_{trop} = 14$ km (Table 3.3). This estimate is considered to account for both uncertainties in the absorption cross sections and other uncertainties in the photolysis rates calculated by the model such as the solar photon flux and attenuation of the flux by molecular oxygen and ozone. Errors in the rate constant for reaction with the hydroxyl radical and in the OH field are not considered since this loss is at least 20 times smaller than photolysis for all four halons.

It is seen that the given height of the tropopause does not affect the calculated tropospheric lifetimes greatly. Moving the tropopause from 12 km to 16 km changes the H-1211 tropospheric lifetime from 25.6 years to 24.6 years, the H-2402 lifetime from 42.9 to 39.1 years and the H-1202 lifetime from 3.1 to 2.9 years. H-1301 has a tropospheric lifetime greater than 10,000 years for all studied tropopause heights. The tropospheric lifetime of H-1211 calculated here, $25 - 26$ years, agrees reasonably with the value of 23 years calculated by Burkholder et al. (1991), while that of H-2402 is slightly higher ($39 - 43$ versus $<34$ years) and that of H-1202 slightly lower ($2.9 - 3.1$ versus 3.2 years), compared to Burkholder et al. (1991).

Adjusting the photolysis rates by 20% has a relatively large effect on the tropospheric lifetimes giving a tropospheric lifetime range for H-1211 of 21.0 years to 30.9 years, for H-2402 of 34.0 to 50.8 years and for H-1202 lifetime of 2.5 to 3.7 years.

**Table 3.3** Tropospheric ($\tau_{trop}$) and stratospheric ($\tau_{strat}$) lifetimes of the halons calculated in the model. Tropospheric lifetimes vary based on the defined height of the tropopause ($Z_{trop}$), with uncertainties due to ±20% photolysis rates also given at $Z_{trop}$ = 14 km. Stratospheric lifetimes vary based on the diffusive loss from the top of the model which is determined by the ratio of the mixing ratio of the given molecule at 25 km to that in the top model box (23 km) (F). Uncertainties due to ±20% photolysis rates are given for representative values of F for each halon (see Section 3.8).

| Model Run | H-1211 | H-1301 | H-2402 | H-1202 |
|---|---|---|---|---|
| | $\tau_{trop}$ (yr) | | | |
| $Z_{trop}$ = 12 km | 25.6 | >10000 | 42.9 | 3.11 |
| $Z_{trop}$ = 14 km | 25.0 | >10000 | 40.7 | 3.00 |
| ($\sigma$ ±20%) | (21.0 – 30.9) | ( - ) | (34.0 – 50.8) | (2.51 – 3.72) |
| $Z_{trop}$ = 16 km | 24.6 | >10000 | 39.1 | 2.92 |
| | $\tau_{strat}$ (yr)[a] | | | |
| F = 1.0 | 50.2 | 370 | 50.0 | 27.2 |
| F = 0.8 | 39.5 | 75.9 | 39.3 | 24.4 |
| ($\sigma$ ±20%) | - | (74.0 – 78.0) | - | - |
| F = 0.5 | 33.6 | 47.5 | 33.4 | 22.3 |
| F = 0.2 | 30.9 | 39.5 | 30.7 | 21.2 |
| ($\sigma$ ±20%) | - | - | (29.3 – 32.2) | (19.5 – 23.3) |
| F = 0.0 | 29.8 | 36.8 | 29.6 | 20.7 |
| ($\sigma$ ±20%) | (28.7 – 31.1) | - | - | - |

[a] Stratospheric lifetimes are only calculated for $Z_{trop}$ = 14 km (stratospheric lifetimes at $Z_{trop}$ = 12 km and 16 km can be inferred using the total lifetime (Table 3.4) and the tropospheric lifetime).

### 3.8.2 Stratospheric Lifetimes

To calculate the stratospheric lifetimes ($\tau_{strat}$) the photolysis and OH sinks were only active in the stratosphere and the effect of a range of values for F (the ratio of the mixing ratio of the molecule above the model domain (25 km) to that in the top box (centred on 23 km) which governs the diffusive loss from the top of the model – representing all loss processes above the model domain) was investigated (Table 3.3). The stratospheric lifetime calculated in this way is an approximation since the atmospheric burden above the model domain is not known and so cannot be included in the calculation. However use of a 1-D atmospheric model

extending up to 50 km suggests that this is less than 1.5% of the total atmospheric burden for H-1211 and H-1301 at steady state with no tropospheric loss.

The stratospheric lifetimes calculated using the full range of possible values for F are presented in Table 3.3. The value of F can, however, be compared to actual measurements of the halons at 23 and 25 km. Very few such measurements at these altitudes exist, but we do have measurements from three mid-latitude balloon flights; two from Aire sur l'Adour, France in October 1994 and March 1999, and one from Gap, France in June 1997, and a tropical balloon flight from Teresina, Brazil. The mid-latitude data are previously unpublished, but were collected and analysed in essentially identical manner to other balloon flights from the same series reported by Pfeilsticker et al. (2000). The tropical measurements were reported by Laube et al. (2008). For H-1211, based on three flights, the mean value of F for H-1211 was 0.21 with a standard deviation of 0.01. For H-1301, based on four flights, the mean value of F was 0.74 with a standard deviation of 0.1. For H-2402 only one flight detected the molecule above 25 km and gave a value for F of 0.19. H-1202 was not detected above 25 km on any of the flights.

The stratospheric steady state lifetimes of H-1211 and H-1301 have recently been re-evaluated by Laube et al. (2013) based on tracer analysis using samples collected by the high altitude research aircraft, M55 Geophysica, and a range of balloon flights. Laube et al. (2013) applied a relative method to calculate stratospheric lifetimes using CFC-11 as a reference tracer. For this method the stratospheric lifetime of CFC-11 must be known and Laube et al. (2013) derived two sets of halon lifetimes relative to a CFC-11 lifetime of 45 years (as recommended in Montzka and Reimann, 2011) and of 60.1 years. The latter is justified as recent work has suggested a steady state lifetime of 56 – 64 years (Douglass et al. 2008). This is acknowledged in Montzka and Reimann (2011) as they note that, "evidence is emerging that the lifetimes for some important ODSs (e.g., CFC-11) may be somewhat longer than reported in past assessments". As shown in Table 3.4 we here use the stratospheric halon lifetimes reported in Laube et al. (2013) relative to a CFC-11 lifetime of 60.1 years, i.e. 36 (32 – 41) years for H-1211 and 82 (75 – 93) years for H-1301.

**Table 3.4** Tropospheric ($\tau_{trop}$), stratospheric ($\tau_{strat}$), and total atmospheric ($\tau_{atm}$) lifetimes of the halons reported in the literature and calculated in this work.

| Reference | H-1211 | H-1301 | H-2402 | H-1202 |
|---|---|---|---|---|
| | $\tau_{trop}$ (yr) | | | |
| Burkholder et al. (1991) | 23 | >397 | <34 | 3.2 |
| This work[a] | **25** | **>10000** | **41** | **3.0** |
| | (21 – 31) | ( - ) | (34 – 51) | (2.5 – 3.7) |
| | $\tau_{strat}$ (yr) | | | |
| Volk et al. (1997) | 26 ±5 | - | - | - |
| Laube et al. (2013)[b] | 27 (+4,-3) | 62 (+7,-6) | - | - |
| Laube et al. (2013)[c] | 36 (+5,-4) | 82 (+11,-7) | - | - |
| This work | **36 (+5,-4)** [d] | **82 (+11,-7)** [d] | **31**[e] | **21**[e] |
| | (32 – 41) | (75 – 93) | (29 – 34)[f] | (19 – 23)[f] |
| | $\tau_{atm}$ (yr) | | | |
| Burkholder et al. (1991)[g] | 16 | 65 | <20 | 3.3 |
| Butler et al. (1998) | 11[h] | - | - | - |
| This work[a,d] | **15** | **82**[i] | **17** | **2.6** |
| | (13 – 18) | (75 – 93) | (16 – 20) | (2.2 – 3.2) |

[a] See Section 3.8 and Table 3.2 for further details. [b] Based on a lifetime for CFC-11 of 45 years. [c] Based on a lifetime for CFC-11 of 60.1 years. [d] The stratospheric lifetimes of H-1211 and H-1301 from Laube et al. (2013) for a CFC-11 lifetime of 60.1 years are used. [e] For F = 0.2. [f] Based on ±20% photolysis rates and F = 0.0 – 0.5. [g] These are the values reported in Montzka and Reimann (2011) with the exception of H-1202. [h] A combination of the stratospheric lifetime (based on correlation with age) of Volk et al. (1997) and the tropospheric lifetime of Burkholder et al. (1991). [i] The stratospheric lifetime from Laube et al. (2013) is considered a total atmospheric lifetime as H-1301 has negligible loss in the troposphere.

The value of the ratio F required to be used in the model to give the stratospheric lifetimes from Laube et al. (2013) was examined. For H-1211 a value of 0.65 was required, and for H-1301 a value of 0.828. For H-1301 this is within the 1σ range of the balloon measurements reported here. For H-1211 this is outside the 1σ range but it is noted that a value for F of 0.2, as suggested by the balloon data, gives a stratospheric lifetime of 31 years, this is in between

the two lifetimes (based on a CFC-11 lifetime of 45 and 60.1 years) reported by Laube et al. (2013).

There have been no stratospheric lifetimes derived from measurements for H-2402 or H-1202. Consequently the value of F used for the estimate of the stratospheric lifetime of H-2402 was constrained using the one relevant balloon flight. For H-1202 there are no relevant balloon flight data but it seems likely that mixing ratios are decreasing rapidly with height at this height and so a value for F of 0.2, as measured for H-1211 and H-2402, was used for the estimate of stratospheric lifetime.

### 3.8.3   Total Atmospheric Lifetimes

The total atmospheric lifetimes ($\tau_{atm}$) are calculated by combining the inverse of the tropospheric and stratospheric lifetimes. The tropospheric lifetimes used for the alternative total lifetimes are those calculated for $Z_{trop}$ = 14 km. For H-1211 and H-1301 the stratospheric lifetimes derived by Laube et al. (2013) relative to a CFC-11 lifetime of 60.1 years were used. For H-2402 and H-1202 the stratospheric lifetimes calculated in the model, with the value of F constrained by the balloon data as described above, were used.

This gives total atmospheric lifetimes of 15 (13 – 18) years for H-1211, 82 (75 – 93) years for H-1301, 17 (16 – 20) years for H-2402, and 2.6 (2.2 – 3.2) years for H-1202. This is likely to be a maximum lifetime for H-2402 since, unlike for H-1211 and H-1202, Burkholder et al. (1991) did not extrapolate the absorption cross sections to wavelengths longer than 320 nm due to the non-systematic nature of the cross sections calculated between 300 – 320 nm. Uncertainty ranges are calculated by combining the uncertainties in the tropospheric and the stratospheric lifetimes given in Table 3.4. Note that the uncertainties in the stratospheric lifetimes do not take account of the uncertainty in the choice of lifetime of CFC-11 used.

### 3.8.4   Effects on Cumulative Emissions and Banks

The top-down emissions of H-1211, H-1301 and H-2402 derived in Section 3.4 would be altered by the alternative lifetimes reported in Section 3.8. The decreased lifetimes of H-1211 and H-2402, compared to those reported in Montzka and Reimann (2011), would require higher global emissions to fit the measurements. Likewise the increased lifetime of H-1301 would require lower emissions to fit the measurements. The model was run with the

alternative lifetimes; the cumulative emissions (1963 – 2010) derived for H-1211 increased by 14 Gg to 290 Gg, for H-1301 they decreased by 5 Gg to 101 Gg and for H-2402 they increased by 4 Gg to 46 Gg (Table 3.5).

These alternative cumulative emissions have implications for the estimates of the banks. Calculating the banks using the alternative cumulative emissions would mean that the H-1211 bank was 24 Gg, 63% lower than that estimated by HTOC and the H-1301 bank would be 48 Gg compared to 43 Gg estimated by HTOC (Table 3.5). The cumulative emissions of H-2402 would be 4 Gg higher but this cannot be directly compared to the bank reported by HTOC as they do not report production of H-2402 and their estimate of the bank is not a direct calculation of production less emissions.

The estimate of 24 Gg for the remaining H-1211 bank suggests that at current annual emission rates (5.7 and 5.0 Gg in 2009 and 2010) the bank of H-1211 would be used up within the next five years. Given the current estimated rate of emissions it seems unlikely that the bank is so small. If we had used the lower limit of the uncertainty range of the atmospheric lifetime for H-1211 (i.e. 13 years, see Table 3.4 and Section 3.8.3), the derived cumulative emissions would have been greater than the reported production giving a bank of -5 Gg (Table 3.5). Similarly, if we had chosen the stratospheric lifetime of H-1211 of 27 years determined by Laube et al (2013) for a CFC-11 lifetime of 45 years, this would also have given an atmospheric lifetime of 13 years and again lead to a negative value for the calculated bank. This suggests that an atmospheric lifetime of H-1211 of 14 years or less is inconsistent with the reported cumulative production. Clearly large uncertainties in the lifetime of H-1211 remain, which affect top-down estimates of the emissions, but it raises the question as to the accuracy of the reported production.

For H-1301, using the atmospheric lifetime of 82 years gives a bank 13% larger than that estimated by HTOC, which has implications for the decline of tropospheric bromine (see below).

**Table 3.5** The effect of using different CFC-11 lifetimes to calculate the stratospheric lifetime of H-1211 and H-1301 (using the Laube et al. (2013) method – Section 3.8.2) on the total lifetimes, cumulative emissions and remaining banks of H-1211 and H-1301.

| | H-1211 | | | H-1301 | | |
|---|---|---|---|---|---|---|
| $\tau_{CFC-11}$ (years) | $\tau_{H-1211}$ (years) | Cumulative Emissions (Gg) | Bank (Gg) | $\tau_{H-1301}$ (years) | Cumulative Emissions (Gg) | Bank (Gg) |
| 45 | 13 | 319 | -5 | 62 | 107 | 42 |
| 52.5 | 14 | 304 | 10 | 72 | 104 | 45 |
| 60.1 | 15 | 290 | 24 | 82 | 101 | 48 |

### 3.8.5 Effects on Total Tropospheric Bromine

Figure 3.14 shows (dashed dot line) the extrapolation to 2060 of the halons contribution to total tropospheric bromine using release fractions based on the banks calculated from our top-down cumulative emissions derived using the alternative atmospheric lifetimes given in Table 3.4. These bank release fractions were calculated by dividing emissions of the halon in 2010 by the calculated bank at the end of 2009 (H-1211 – 0.18, H-1301 – 0.055). For H-2402 the same bank and bank release fractions are used as used in the scenarios plotted in Figure 3.14 because a revised bank cannot be calculated since no production data has been reported.

With an even smaller H-1211 bank than in the other scenarios presented in Figure 3.14, the tropospheric bromine burden from the halons is predicted to initially fall more quickly in the coming decades but by 2060 all three scenarios converge. H-1301 contributes 50% even earlier, in 2017. With the larger H-1301 bank, H-1301 is calculated to contribute almost 95% of the total bromine from the halons in 2060.
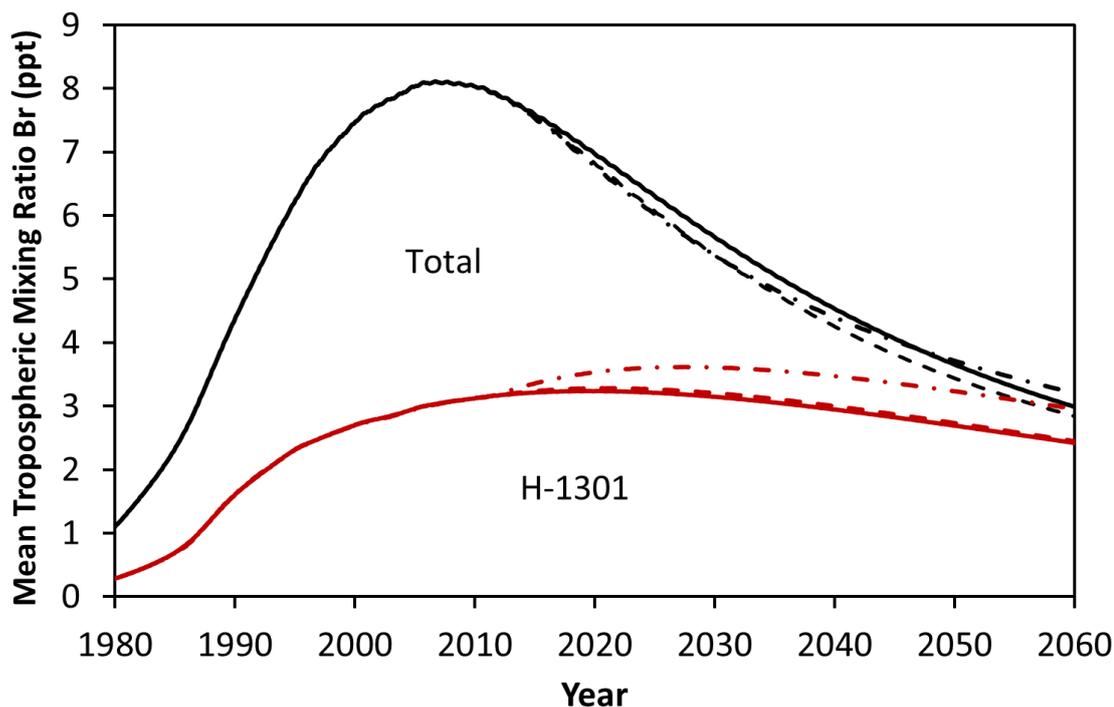
**Figure 3.14** The contribution of each of the halons to global mean tropospheric bromine mixing ratios as modelled for the period 1978 – 2060. From 1978 to 2010 the emissions used to model the halon mixing ratios are based on the measurements in Section 3.3. From 2010: the solid line is the scenario presented in Figure 3.13 with emissions based on banks from HTOC (2011) and bank release fractions from Daniel and Velders (2011); the dashed line uses emissions based on banks and bank release fractions calculated in this work using atmospheric lifetimes reported in Montzka and Reimann (2011) (dashed line); the dot-dash line uses emissions based on banks and bank release fractions calculated in this work using the alternative atmospheric lifetimes calculated in this section.

## 3.9 Conclusions from Atmospheric Modeling of Halons

The work in this chapter has used a 2-D atmospheric model, constrained with measurements of background air from Cape Grim, to determine the global annual emissions of four halons between 1978 and 2010. Additionally the model has been used to investigate the atmospheric lifetimes of the halons and to predict the future atmospheric trends of the halons to 2060. The main conclusions from this work are listed below.

(i)  Atmospheric mixing ratios of the four halons reported here all grew rapidly from the late-1970s. H-2402 mixing ratios peaked around 1995 and have since slowly declined. H-1211 and H-1202 mixing ratios peaked around 2000 with H-1211 having since declined very slowly and H-1202 having declined

rapidly. The growth rate of H-1301 has slowed since around 1995 but mixing ratios are still increasing.

(ii)     The atmospheric mixing ratios of H-1211, H-2402 and H-1202 are all likely to continue to decline due to the cessation of halon production. The mixing ratio of H-1301 should begin to decline during the 2020s.

(iii)    The contribution of the halons to total tropospheric bromine (TTB) at Cape Grim peaked at 8.1 ppt in 2007 − 2008 and had fallen to 7.9 ppt by mid-2011.

(iv)     Currently H-1211 is the main halon contributing to TTB. This will change to H-1301 by 2025 because of the longer lifetime of H-1301 compared to the other halons. The total contribution from the halons to TTB in 2060 is predicted to be about 3.0 ppt, 38% of that in 2010.

(v)      Emissions of all of the halons have declined since peaking in the late-1980s to mid-1990s but the decline has slowed in recent years with no significant changes in emissions of H-1301 and H-2402 between 2006 and 2010.

(vi)     Halon emissions have not fallen to zero even though there has been no production since 2010. This is because of existing stocks of halons ('banks') which can continue to be used due to exemptions under the Montreal Protocol.

(vii)    H-1202 emissions appear not to have declined to zero, as would be expected if they are only emitted as a by-product of H-1211 production. This could be because there is unreported production of H-1211, because H-1202 is being used in military aircraft, or because H-1211 stocks are contaminated with a small amount of H-1202.

(viii)   Alternatives to the currently recommended lifetimes for the halons are calculated using the atmospheric model based partly on recently reported new stratospheric lifetimes. These are 15 years for H-1211 (WMO 2010 recommendation of 16 years), 82 years (65) for H-1301, 17 years for H-2402 (20), and 2.6 years (2.9) for H-1202. Using these alternative lifetimes affects

the calculated sizes of the remaining halon banks but has little effect on the long term declining trend of halon mixing ratios in the atmosphere.

# Chapter 4

# Fully Fluorinated Gases

# 4  Fully Fluorinated Gases

Chapter 4 reports the atmospheric histories of seven perfluorocarbons (PFCs), trifluoromethyl sulfur pentafluoride ($SF_5CF_3$) and a hydrofluorocarbon (HFC) measured in air samples from Cape Grim. These histories are compared to measurements from firn air at NEEM. The firn air is also used to investigate the emissions distributions of the gases. Global annual emissions of the nine gases from 1978 – 2010 are derived from the Cape Grim measurements using the 2-D atmospheric model. Finally the effects on global radiative forcing of the reported gases are discussed.

## 4.1  Introduction

The nine compounds reported in this chapter are all fully fluorinated except for HFC-227ea. Unlike chlorinated and brominated compounds, which break down in the stratosphere leading to destruction of stratospheric ozone, fluorinated compounds are more stable and hence tend to have very long atmospheric lifetimes. This means that they are not of concern in the destruction of stratospheric ozone. However many of them are strongly absorbing in the infrared region of the spectrum and hence have very high global warming potentials (GWPs) and very high radiative efficiencies. The lifetimes, GWPs, and radiative efficiencies of the species reported in this chapter are shown in Table 4.1.

Air samples from Cape Grim have been analysed for seven PFCs: $C_2F_6$, $C_3F_8$, c-$C_4F_8$, $C_4F_{10}$, $C_5F_{12}$, $C_6F_{14}$ and $C_7F_{16}$, trifluoromethyl sulfur pentafluoride ($SF_5CF_3$) and 1,1,1,2,3,3,3-heptafluoropropane (HFC-227ea) at UEA using the experimental setups detailed in Chapter 2. These records have been reported in Oram et al. (2012) (c-$C_4F_8$), Laube et al. (2012) ($C_4F_{10}$, $C_5F_{12}$, $C_6F_{14}$ and $C_7F_{16}$), Sturges et al. (2012) ($SF_5CF_3$) and Laube et al. (2010) (HFC-227ea).

**Table 4.1**  Atmospheric lifetimes, global warming potentials and radiative efficiencies of the compounds reported in Chapter 4.

| Chemical Formula | Atmospheric Lifetime [a] (years) | Global Warming Potential [b] | Radiative Efficiency (W m$^{-2}$ ppb$^{-1}$) [b] |
|---|---|---|---|
| $C_2F_6$ | 10,000 | 12,200 | 0.26 |
| $C_3F_8$ | 2,600 | 8,830 | 0.26 |
| c-$C_4F_8$ | 3,200 | 10,300 | 0.32 |
| $C_4F_{10}$ | 2,600 | 8,860 | 0.33 |
| $C_5F_{12}$ | 4,100 | 9,160 | 0.41 |
| $C_6F_{14}$ | 3,200 | 9,300 | 0.49 |
| $C_7F_{16}$ | ~3000 | - | - |
| $SF_5CF_3$ | 650 – 950 | 17,700 | 0.57 |
| HFC-227ea | 38.9 | 3,220 | 0.26 |

[a] Montzka and Reimann (2011)

[b] 100 year time horizon (Forster and Ramaswamy, 2007)


## 4.2    Atmospheric Modeling

### 4.2.1    Model Setup

The model set up used was the same as that for the halons (see Section 3.2). The atmospheric loss processes of the PFCs and $SF_5CF_3$ are not known with suggested losses being photolysis and high energy ion reactions in the mesosphere (Morris et al., 1995), or destruction at the surface in high temperature combustion processes (Cicerone, 1979; Ravishankara et al., 1993). Their lifetimes in the model were entirely constrained by the diffusive loss from the top of the model which was adjusted for each of them to give the lifetime reported in Montzka and Reimann (Table 4.1) within the model domain.

For HFC-227ea, the lifetime within the model domain was constrained by the reaction rate with OH taken from Atkinson et al. (2008) of $5.3 \times 10^{-13}$.exp(-1770/T) (which gives a lifetime with respect to OH of 46.5 years, compared to 44.5 years in Montzka and Reimann (2011)) and the diffusive loss from the top of the model to give a stratospheric lifetime of 450 years (within the range calculated in Laube et al. 2010 from compact correlation with CFC-12). This gives an overall lifetime of 42.1 years, compared to that from Montzka and Reimann (2011) of 38.9 years.

## 4.2.2 Latitudinal Distribution of Emissions

Emissions of $C_2F_6$ (as well as $CF_4$ which is not reported here) are associated with the process of primary aluminium smelting as well as with the electronics industry (e.g. Worton et al., 2007). The rest of the PFCs reported herein are used in the electronics industry (e.g. ISMI, 2005), in fire protection (e.g. IPCC/TEAP, 2005) or in cooling of high power electronics (EPA, 2008).

The emissions distribution used for all of the PFCs, with the exception of $C_2F_6$, was that of $C_6F_{14}$ reported by EDGAR for the year 2005. Though EDGAR reports emissions of all of the PFCs studied in this chapter, it is seen in Section 3 of this chapter that these reported emissions are grossly underestimated for some of the PFCs. The trend of $C_6F_{14}$ emissions reported by EDGAR agrees well with that derived from the Cape Grim measurements in Section 3 and so this distribution was used for the atmospheric modeling. Because of the different source of $C_2F_6$ emissions (the aluminium industry has a large presence in the southern hemisphere (e.g. Worton et al. (2007)) a different emissions distribution was used for the atmospheric modeling. This was based on a mean of the emissions distribution reported by EDGAR for the period 1980 – 2005. The $C_2F_6$ emission distribution is explored further in Section 3 of this chapter using measurements from the firn air at NEEM.

The emissions distribution used for the atmospheric modeling of $SF_5CF_3$ was based on the locations of the two main reported production sites of perfluorooctanyl substances by 3M, Decatur, Alabama and Antwerp, Belgium (see Section 4 of this chapter for further details).

The emission distribution for the atmospheric modeling of HFC-227ea was based on the reported emissions of EDGAR in 2005.

## 4.2.3 Emission Uncertainties

Uncertainties in the annual emissions of the PFCs and $SF_5CF_3$ were calculated by combining a mean measurement uncertainty for each year with a 5% uncertainty associated with the modeling. The model has previously been shown to recreate background measurements in the southern hemisphere of long lived gases with well known atmospheric histories (e.g. CFC-11 and CFC-12) and emissions mainly in the northern hemisphere to within 5% (Reeves et al., 2005). This error is assumed to account for uncertainties in the transport scheme within the model. Uncertainties in the lifetime of the PFCs are not considered because the lifetime is so

long (thousands of years) compared to the period of study that it will have an insignificant effect on the calculated emissions.

Uncertainties in the annual emissions of HFC-227ea were calculated by combining uncertainties in the firn model output from NEEM with uncertainties in the reaction rate of HFC-227ea with OH and uncertainties in the OH field used in the model (based on uncertainties in the reaction rate of $CH_3CCl_3$ with OH – see Chapter 2 for how the OH field is defined).

## 4.3    Perfluorocarbons

### 4.3.1    Cape Grim Mixing Ratio Time Series

The long term trends of the mixing ratios of the PFCs measured from the Cape Grim air archive are shown in Figures 4.1 to 4.4. Measurements by AGAGE from Cape Grim are also shown for $C_2F_6$ and $C_3F_8$. These are a combination of in-situ measurements and prior to 2004 measurements from archived air samples (Mühle et al., 2010). The model fit to the measured mixing ratios is shown as a solid red line in Figures 4.1 to 4.4. Table 4.2 shows the mixing ratios of the PFCs in 2010 and the growth rates from 1978 – 1995 and from 1995 – 2011. These periods were chosen as this is around the time that emissions of PFCs from the electronics industry begin to become significant.

**Table 4.2** Mixing ratios (ppt) of the PFCs at Cape Grim in December 2010 and growth rates (ppq a$^{-1}$) for the periods 1978 – 1995 and 1995 – 2011.

| PFC | Cape Grim mixing ratio: Dec 2010  (ppt) | Mean growth rate 1978 – 1995 (ppq a$^{-1}$) | Mean growth rate 1995 – 2010  (ppq a$^{-1}$) |
|---|---|---|---|
| $C_2F_6$ | 3.8 | 76 | 106 |
| $C_3F_8$ | 0.5 | 5.9 | 21 |
| c-$C_4F_8$ | 1.2 | 28 | 24 |
| $C_4F_{10}$ | 0.18 | 5.1 | 4.8 |
| $C_5F_{12}$ | 0.14 | 3.8 | 3.6 |
| $C_6F_{14}$ | 0.25 | 4.3 | 10.3 |
| $C_7F_{16}$ | 0.14 | 2.0 | 5.6 |
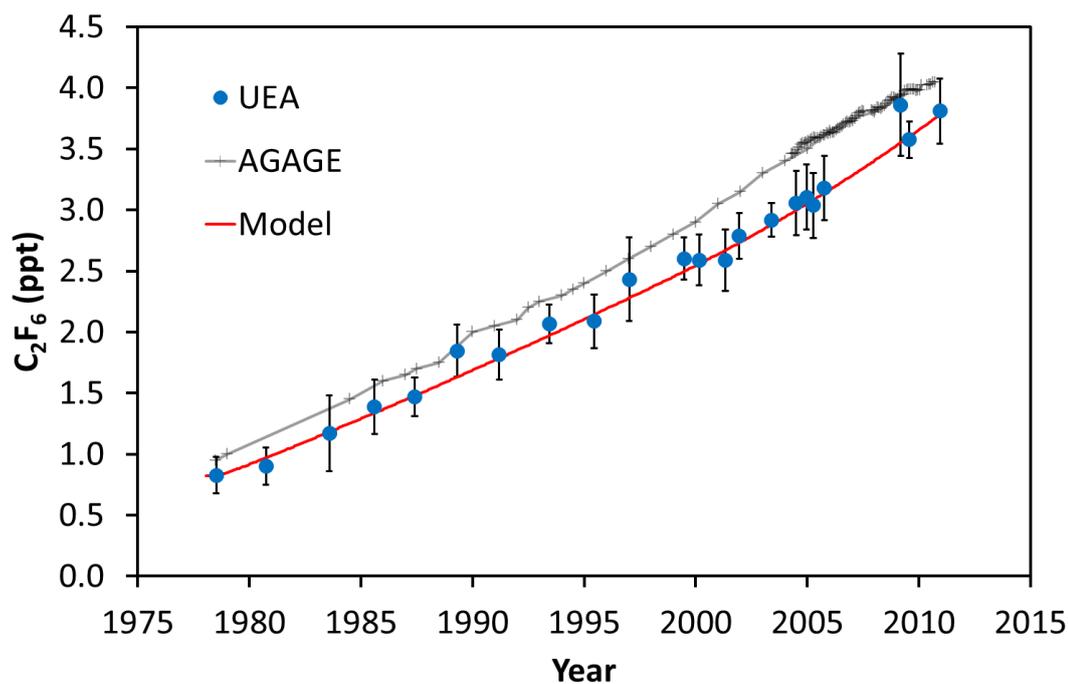
**Figure 4.1 $C_2F_6$:** Measured mixing ratios (ppt) from Cape Grim - UEA (blue circles), AGAGE (grey crosses and line). Model fit to the UEA measured mixing ratios (red line).

The mixing ratio of $C_2F_6$ in 1978 at Cape Grim was about 0.8 ppt (Figure 4.1). It then increased steadily up to 2001 with an average growth rate of 80 ppq $a^{-1}$, which increased to 120 ppq $a^{-1}$ thereafter, leading to a mixing ratio at the end of 2010 of about 3.8 ppt. The measurements from the Cape Grim archive by AGAGE give mixing ratios which are consistently about 15% higher than those measured at UEA. This constant offset suggests a calibration difference between the two datasets.

The mixing ratios of $C_3F_8$ increased steadily up to the mid-1990s with a growth rate of about 6 ppq $a^{-1}$ (Figure 4.2). It then increased sharply at a rate of about 25 ppq $a^{-1}$ up to the mid-2000s before slowing down again slightly reaching a mixing ratio of about 0.55 ppt in 2010. The agreement between the UEA measurements and those of AGAGE is much better for $C_3F_8$ than $C_2F_6$. The AGAGE measurements are again slightly higher but with a maximum discrepancy of less than 5%.

The mixing ratio of c-$C_4F_8$ is about 0.35 ppt in 1978 (Figure 4.3). It increases steadily through the 1980s with a growth rate of about 30 ppq $a^{-1}$. The growth rate then falls to 15 ppq $a^{-1}$
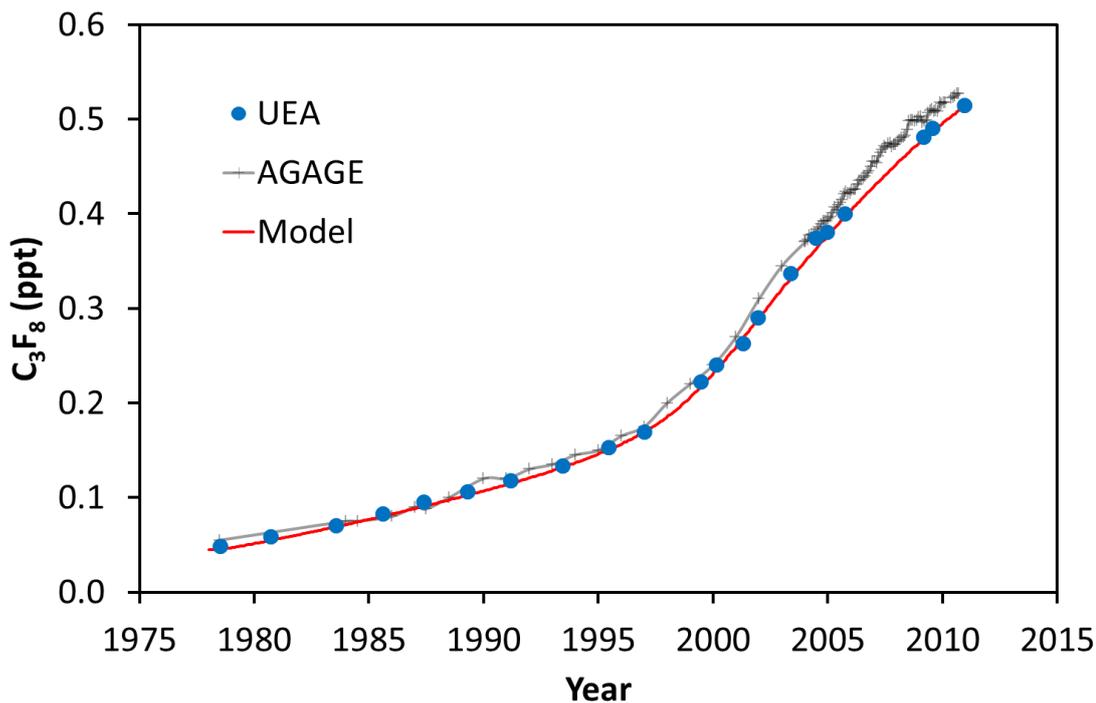
**Figure 4.2 C$_3$F$_8$:** Measured mixing ratios (ppt) from Cape Grim - UEA (blue circles), AGAGE (grey crosses and line). Model fit to the UEA measured mixing ratios (red line).
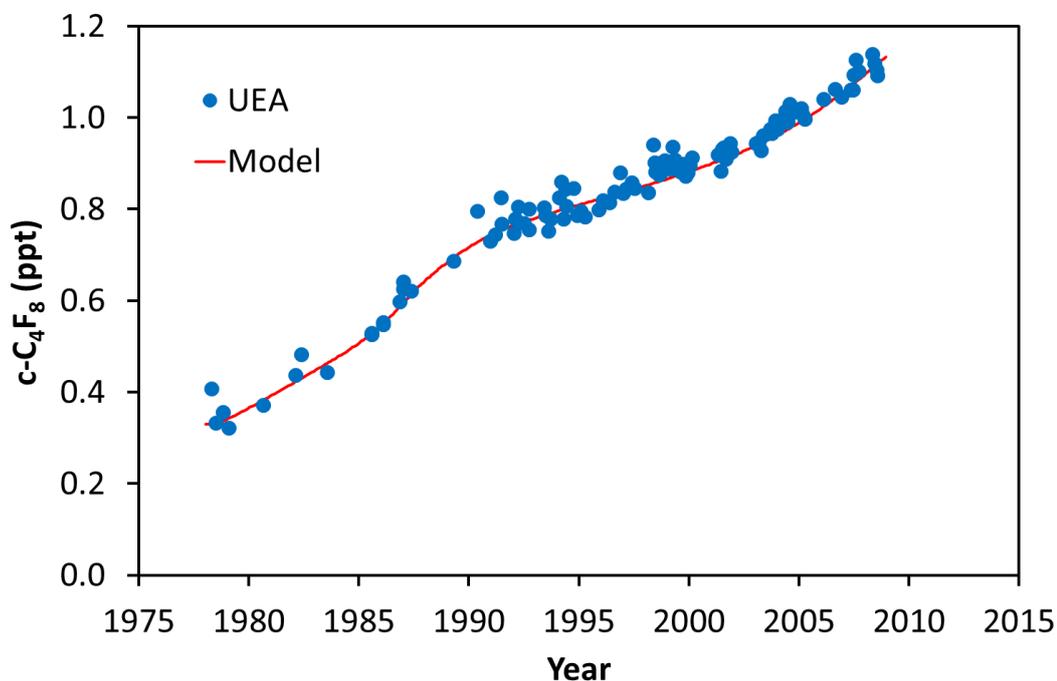


**Figure 4.3 c-C$_4$F$_8$:** Measured mixing ratios (ppt) from Cape Grim (blue circles). Model fit to the measured mixing ratios (red line).

during the 1990s before gradually increasing through the 2000s up to about 40 ppq a$^{-1}$ giving a mixing ratios of about 1.1 ppt in 2010.

The mixing ratio of $C_4F_{10}$ grew steadily at about 5 – 6 ppq a$^{-1}$ up to 2001 (Figure 4.4). This growth rate has since declined to 3 ppq a$^{-1}$ with a mixing ratio at the end of 2010 of about 0.18 ppt.

The mixing ratio of $C_5F_{12}$ (Figure 4.4) behaved in a very similar fashion to $C_4F_{10}$ with a growth rate of 5 ppq a$^{-1}$ between 1985 and 2001 which then decreased to 2 ppq a$^{-1}$ by 2010 to give a mixing ratio at the end of 2010 of about 0.15 ppt.

The $C_6F_{14}$ mixing ratio (Figure 4.4) steadily increased at an average growth rate of 3 ppq a$^{-1}$ up to the early 1990s before increasing rapidly for ten years at about 17 ppq a$^{-1}$ and then increasing more slowly again at 8 ppq a$^{-1}$ up to a mixing ratio at the end of 2010 of about 0.26 ppt.

The mixing ratio of $C_7F_{16}$ (Figure 4.4) increased steadily from the early 1980s to the end of 2010 at an average growth rate of 3 ppq a$^{-1}$ to a mixing ratio at the end of 2010 of 0.11 ppt.
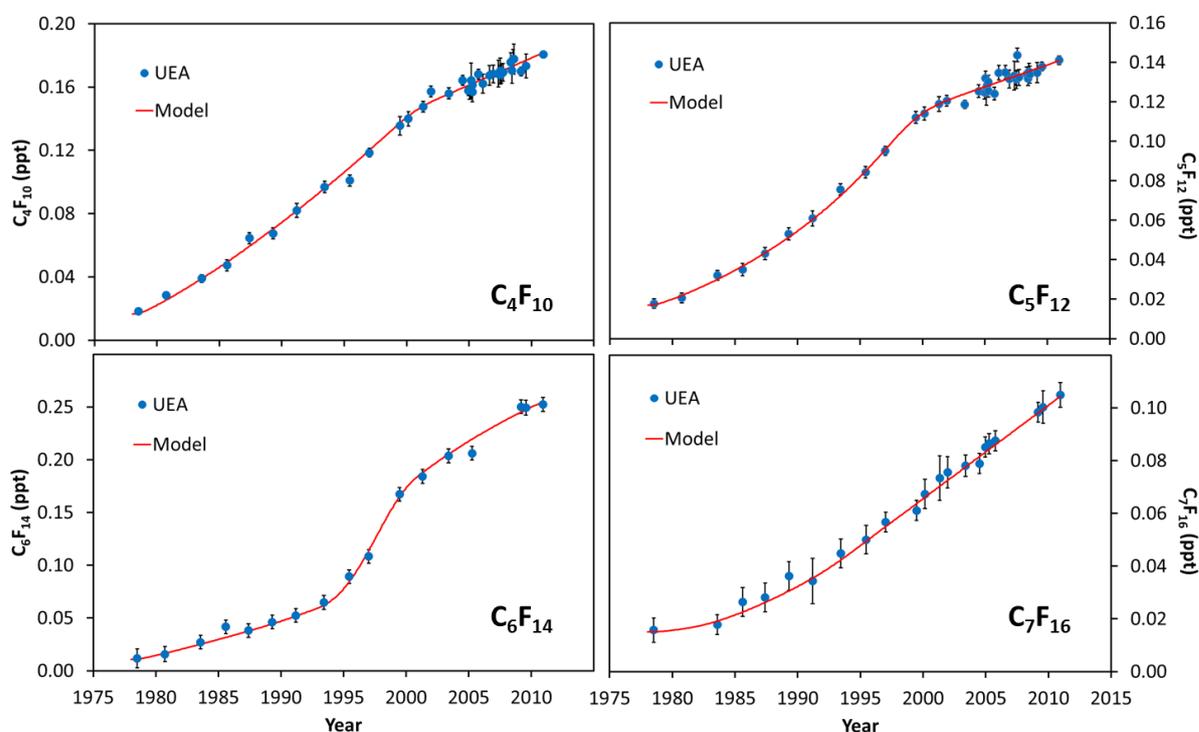


**Figure 4.4** Measured mixing ratios (ppt) from Cape Grim (blue circles) of the higher PFCs ($C_4F_{10}$, $C_5F_{12}$, $C_6F_{14}$, $C_7F_{16}$). Model fits to the measured mixing ratios (red line).

### 4.3.2 PFCs in NEEM Firn Air

The measured concentration-depth profiles of the PFCs from firn air samples at NEEM, Greenland are shown in Figures 4.5 to 4.8. These measurements are compared to output from the firn model which was obtained using various scenarios described below.

**Table 4.3** Conditions of five model runs used to model the PFCs in the NEEM firn air.

| Model Run | Emissions Distribution [a] | Initial Emissions Year | Initial mixing ratio (ppt) |
|-----------|---------------------------|------------------------|----------------------------|
| A | $C_6F_{14}$ | 1960 | 0 |
| B | $C_6F_{14}$ | 1960 | 0.25 ($C_2F_6$); 0.12 ($C_3F_8$) |
| C | $C_2F_6$ | 1960 | 0.25 ($C_2F_6$) |
| D | $C_6F_{14}$ | 1970 | 0 |
| E | $C_2F_6$ [b] | 1960 | 0.25 ($C_2F_6$) |

[a] Emissions distributions reported by EDGAR for 2005 for $C_6F_{14}$ and the mean distribution of 1980 – 2005 for $C_2F_6$ (see Section 2.2 of this chapter). [b] Based on the $C_2F_6$ distribution but with increased southern hemisphere emissions.

For all scenarios the 2-D atmospheric model was run from 1978 to 2008 with emissions derived from the Cape Grim measurements (Sections 3.1 and 3.3 of this chapter). The mixing ratio in the model prior to 1978 was held constant either at a background value or at zero. Table 4.3 summarises the conditions used for each model run.

Run A used an atmospheric model run with an emissions distribution the same as that given for $C_6F_{14}$ in 2005 by EDGAR. Mixing ratios were linearly interpolated from zero at 1960 to the initial Cape Grim mixing ratio in 1978.

Run B, performed for $C_2F_6$ and $C_3F_8$, assumes a background concentration prior to 1960 of 0.25 ppt for $C_2F_6$ and 0.12 ppt for $C_3F_8$ and then linearly interpolates from this mixing ratio in 1960 to the initial Cape Grim mixing ratio in 1978.

Run C, performed for $C_2F_6$, assumes a background concentration of 0.25 ppt before 1960 and uses an emission distribution derived from the average reported EDGAR emissions for $C_2F_6$ between 1980 and 2005.

Run D, performed for the higher PFCs, is equivalent to Run A but interpolates mixing ratios from a zero mixing ratio at 1970 rather than 1960.

Run E, performed for $C_2F_6$ is equivalent to Run C but adjusts the amount of emissions from the southern hemisphere to get the best fit to the measurements in the firn.
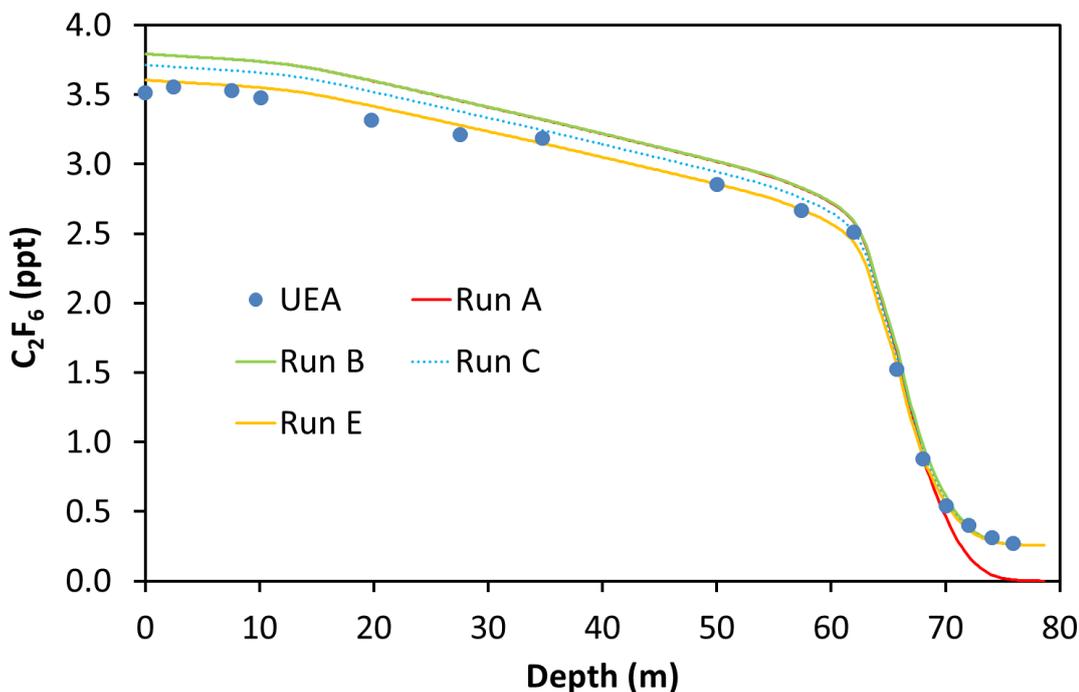


**Figure 4.5 $C_2F_6$:** Measured concentration-depth profile from the firn air at NEEM (blue circles). Runs A, B, C and E are output from the firn model based on input from atmospheric model runs with different initial conditions (see Table 4.3).

The model output for Run A shows a good fit for all the PFCs except $C_2F_6$ and $C_3F_8$. The measured mixing ratios near the base of the firn are indistinguishable from zero for these compounds. For $C_2F_6$ and $C_3F_8$ the mixing ratios near the base appear to be non-zero. Since the deepest measurements in the firn at NEEM represent air with a mean age dating back to before the middle of the twentieth century (Buizert et al., 2012) it seems likely that these backgrounds represent a natural source of these two compounds. Hence Run B was performed with an assumed background equal to that which is seen near the base of the firn. For $C_2F_6$ this was taken as 0.25 ppt and $C_3F_8$ as 0.13 ppt. A background mixing ratio of around 0.25 ppt for $C_2F_6$ agrees well with that reported by Worton et al. (2007) of <0.3 ppt, whereas Mühle et

al. (2010) report a background of $0.1\pm0.02$ ppt. The background mixing ratio of $C_3F_8$ in Figure 4.6 appears to be about 0.12 ppt. Mühle et al. (2010) report no detectable background for $C_3F_8$ in Greenland firn with a detection limit of 0.02 ppt.
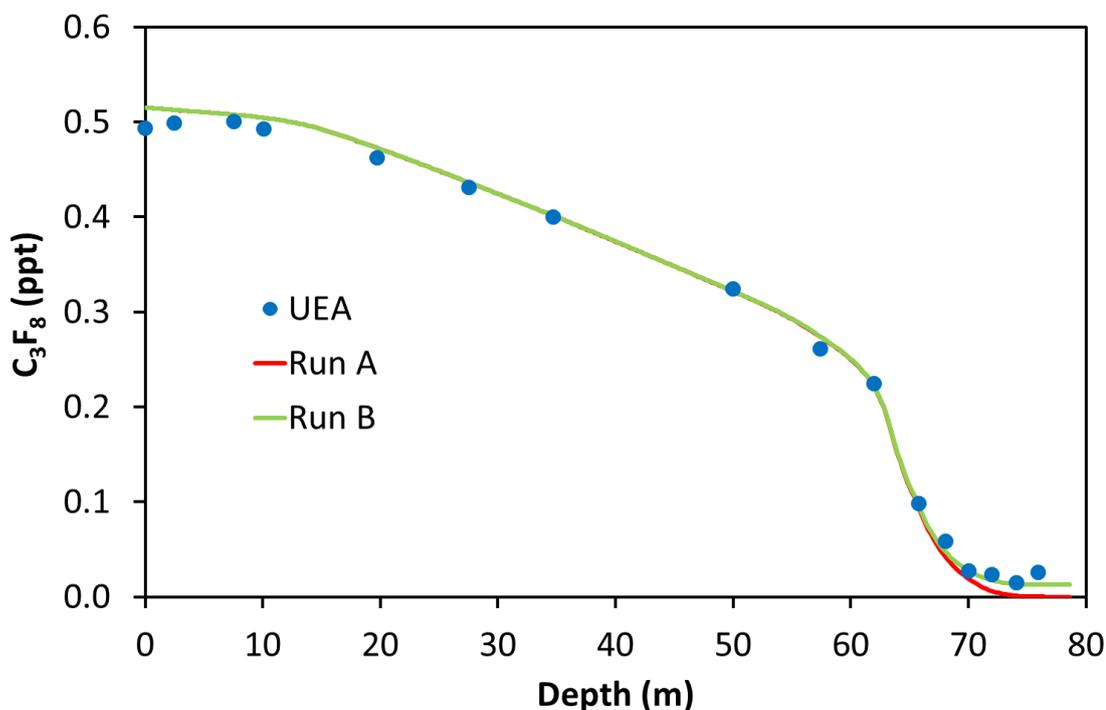


**Figure 4.6 $C_3F_8$:** Measured concentration-depth profile from the firn air at NEEM (blue circles). Runs A and B are output from the firn model based on input from atmospheric model runs with different initial conditions (see Table 4.3).

Run C was performed for $C_2F_6$ with an emission distribution derived from an average of the reported emissions of $C_2F_6$ between 1980 and 2005 by EDGAR. This gives 7.5% of emissions in the southern hemisphere. It is unsurprising that emissions of $C_2F_6$ should have a different distribution to those of the other PFCs since unlike them, whose emission is solely associated with the electronics industry, a large proportion of the $C_2F_6$ emissions are associated with the aluminium industry (e.g. Worton et al., 2007), which has significant sources in the southern hemisphere (IAI, 2005). Run C is seen to improve the fit to the measurements compared to Run B using the $C_6F_{14}$ distribution but still does not completely fit the data. So further runs were performed in which the emissions in the southern hemisphere were increased so that the model output fit the measurements at NEEM well. Run E, which had 20% of emissions in the southern hemisphere, is shown in Figure 4.8.
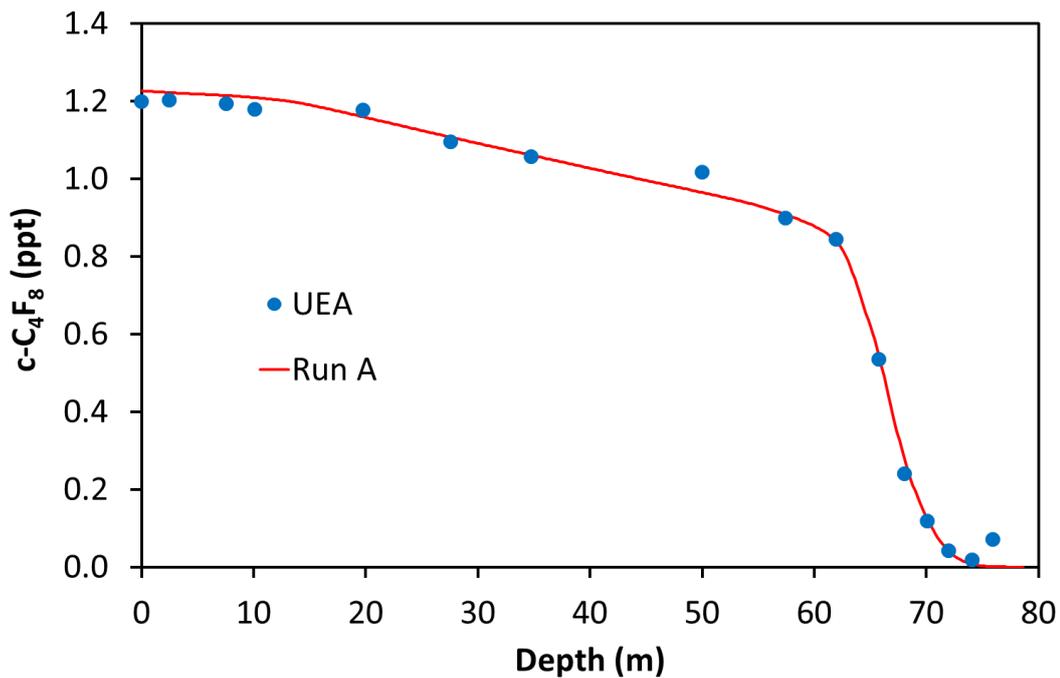
**Figure 4.7 c-C$_4$F$_8$:** Measured concentration-depth profile from the firn air at NEEM (blue circles). Run A is output from the firn model based on input from an atmospheric model run (see Table 4.3).
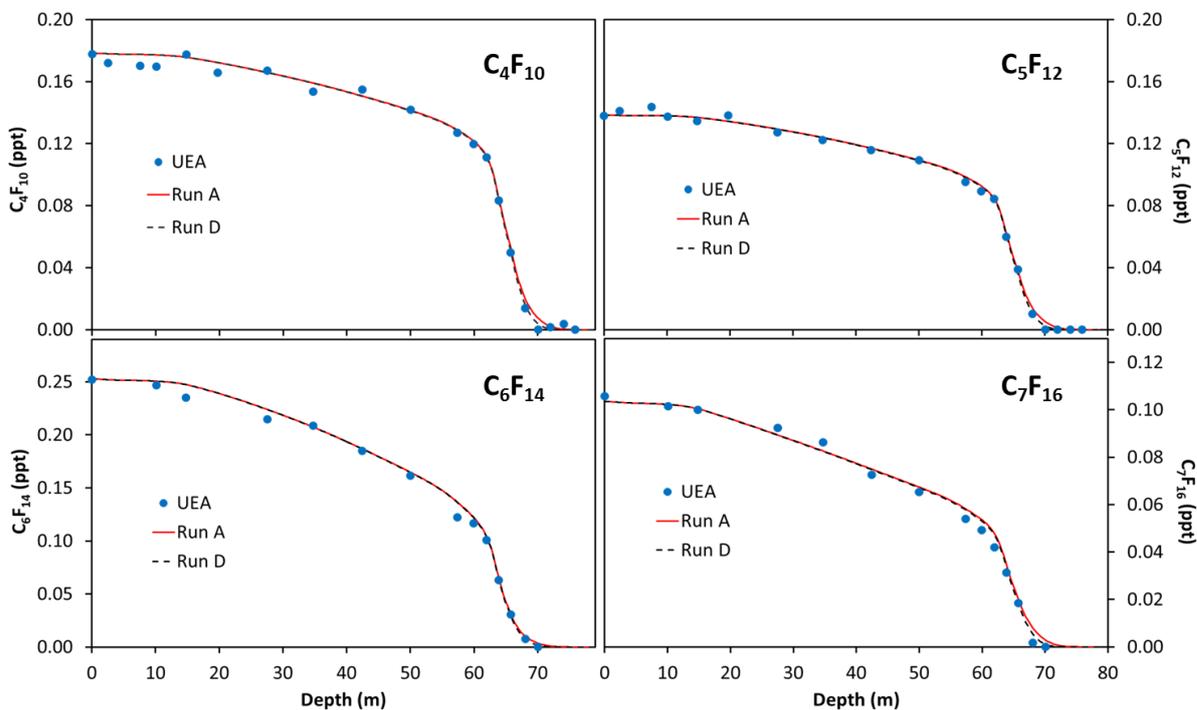


**Figure 4.8** Measured concentration-depth profiles of the higher PFCs from the firn air at NEEM (blue circles). Run A is output from the firn model based on input from an atmospheric model run (see Table 4.3). Panel A: C$_4$F$_{10}$, B: C$_5$F$_{12}$, C: C$_6$F$_{14}$, D: C$_7$F$_{16}$.

Though Run A fits the PFCs above $C_3F_8$ well, the fit generally appears to decline a little too early at depth. This suggests that emissions of these gases began at a later date than those of $C_2F_6$ and $C_3F_8$. Hence Run D was performed which is equivalent to Run A but extrapolates the emissions back to zero at 1970 rather than 1960. This run is seen to give a better fit at depth, especially for $C_5F_{12}$ and $C_6F_{14}$. $C_4F_{10}$ and $C_7F_{16}$ appear to possibly not have been emitted until even later.

Overall the remarkably good agreement between the model runs based on the measured mixing ratios at Cape Grim and the measurements in the firn suggests that the PFC signal is preserved in the firn and that the two datasets can be used together to give a consistent historical record of the atmospheric mixing ratios of the PFCs.

### 4.3.3    Global Annual PFC Emissions

Global annual emissions of the PFCs were derived using the 2-D atmospheric model introduced in Chapter 2. The emissions were constrained by fitting the model output at the latitude of Cape Grim to the measurements from Cape Grim.

The global annual emissions of the PFCs as derived from the model fit to the Cape Grim measurements are shown in Figures 4.9 – 4.12. Also shown are the bottom-up estimates reported by EDGAR and, where available, the model derived emissions of AGAGE (Mühle et al., 2010).

Annual emissions of $C_2F_6$ were about 1.7 Gg in 1978 and then increase slowly between 1978 and 1998 up to 2.1 Gg before increasing to 3.1 Gg in 2010 (Figure 4.9). This trend in emissions shows a good agreement with trend reported by AGAGE and EDGAR up to the mid-1990s. However both these records then show a steeper increase up to 2000 followed by a decline. The increase in emissions in the mid-1990s is presumably associated with increasing emissions from the electronics industry.

The difference in emissions trends between this work and AGAGE is a function of differences in the measurements (in addition to the apparent calibration offset) (Figure 4.1). It is believed that for $C_2F_6$ the AGAGE data is likely to be more accurate (J. Laube, personal communication).

Annual emissions of $C_3F_8$ increased from 0.15 Gg to 0.21 Gg between 1978 and 1990 (Figure 4.10). They then increased rapidly to 1.0 Gg by 2001 and have since declined to about 0.6 Gg in 2010. These emissions show a remarkable agreement with those reported by AGAGE. The emissions reported by EDGAR appear to only begin in the early 1990s with the rate of increase about a third of that derived from the two top down models. The emissions increase since the early 1990s is likely to be associated with the electronics industry. The decline since the early 2000s agrees well with reports that $C_3F_8$ has begun to be replaced by other gases for CVD chamber cleaning (its main use), such as $NF_3$ or $c-C_4F_8$, both of which have higher efficiencies and hence lead to lower PFC emissions (ISMI, 2005). However the emissions prior to the early 1990s are more difficult to explain. $C_3F_8$ has been reported to have no detectable natural source (Mühle et al., 2010) (though the firn profile from NEEM shown in Figure 4.10 suggests there may have been a small background mixing ratio). The mixing ratios prior to 1990 correlate well ($R^2=0.97$, n=8) with $CF_4$ mixing ratios prior to this time and so perhaps could be associated with the aluminium industry.
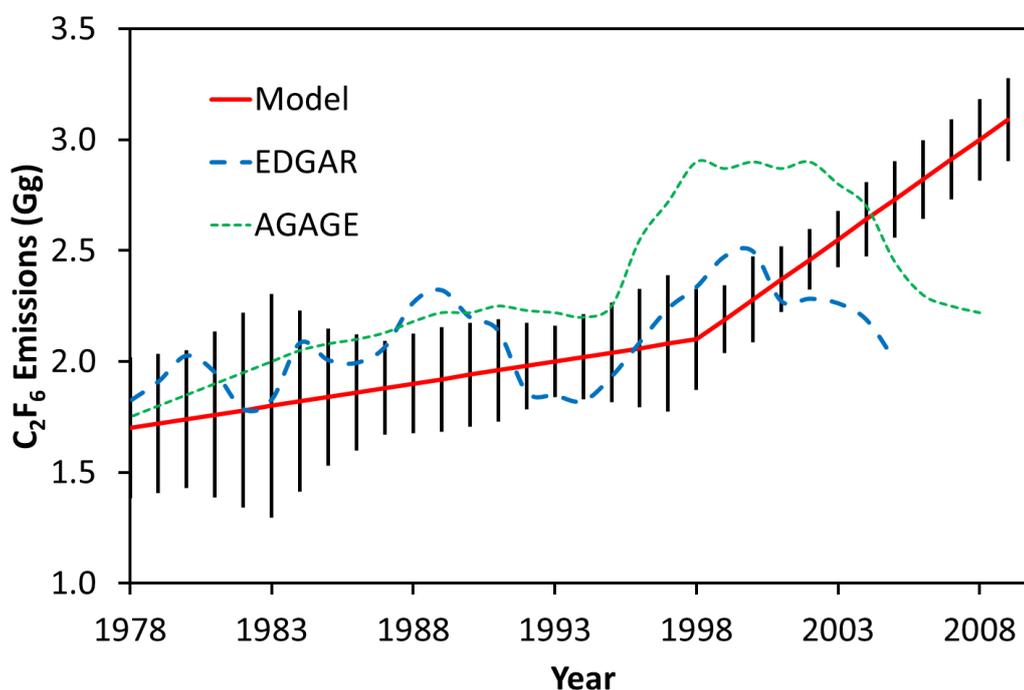


**Figure 4.9 $C_2F_6$:** Model derived annual emissions (Gg) (red line); annual emissions reported by EDGAR (blue dashed line); AGAGE model derived annual emissions (Mühle et al. (2010) (green dashed line). Annual emission uncertainties shown as black lines – see text for uncertainty calculations.

Annual emissions of c-$C_4F_8$ were about 0.9 Gg in 1978 rapidly increasing to 1.9 Gg in the mid-1980s before falling dramatically to 0.5 Gg in the mid-1990s and then rising again to about 1.6 Gg in 2010 (Figure 4.11). The most striking feature of the emissions history of c-$C_4F_8$ is the large emissions peak in the mid-1980s when annual emissions were higher even than those of $C_2F_6$. The high emissions in 1978 suggest that there must have been significant emissions prior to 1978 (see Table 4.4). The increase since the mid-1990s is probably associated with the electronics industry but the explanation for the emissions peak in the mid-1980s is unclear. The emissions reported by EDGAR begin in the late 1980s and are about 100 times lower than those derived from the modeling. This suggests that the use of c-$C_4F_8$ is not being reported by industry.
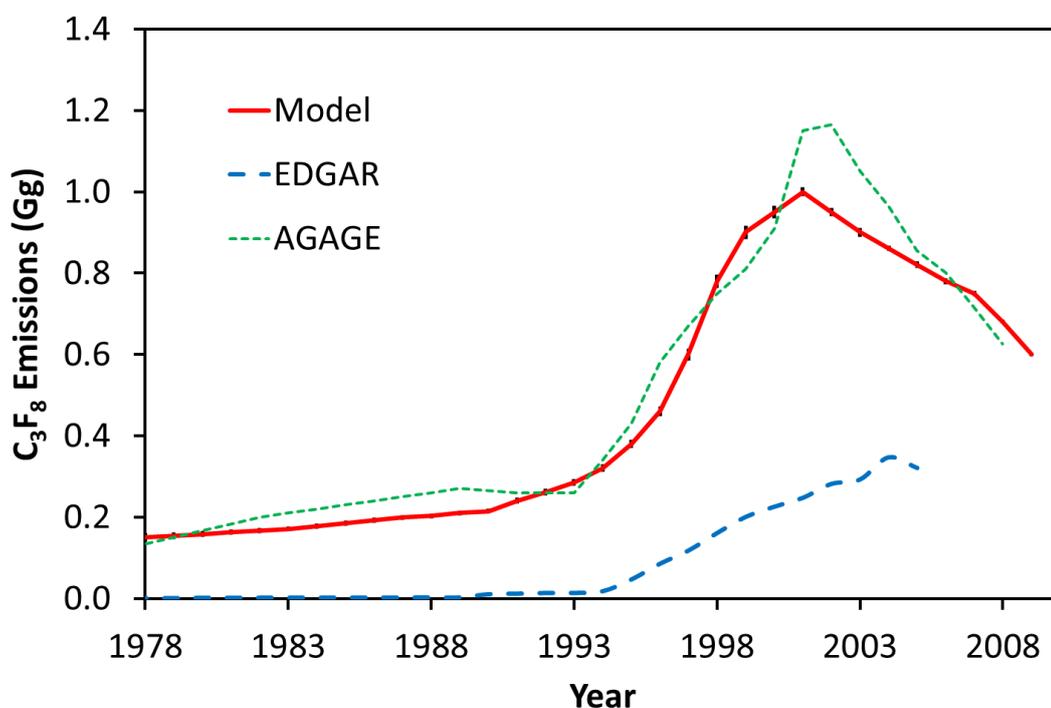


**Figure 4.10 $C_3F_8$:** Model derived annual emissions (Gg) (red line); annual emissions reported by EDGAR (blue dashed line); AGAGE model derived annual emissions (Mühle et al. (2010) (green dashed line). Annual emission uncertainties shown as black lines.

$C_4F_{10}$ and $C_5F_{12}$ have very similar atmospheric histories both in terms of the trend and the mixing ratios (Figure 4.12). The annual emissions of both gases increase steadily from 1978 to a peak in the mid-1990s before falling again to current values around 0.1 Gg. The emissions reported by EDGAR for $C_4F_{10}$ show a steady increase from 1978 to 2010 with

119

current emissions a factor of 10 lower than those derived from the modeling. The reported emissions for $C_5F_{12}$ are some four orders of magnitude smaller than those derived from the model (EDGAR, 2011). Clearly there are problems with the reporting of certain gases to EDGAR.
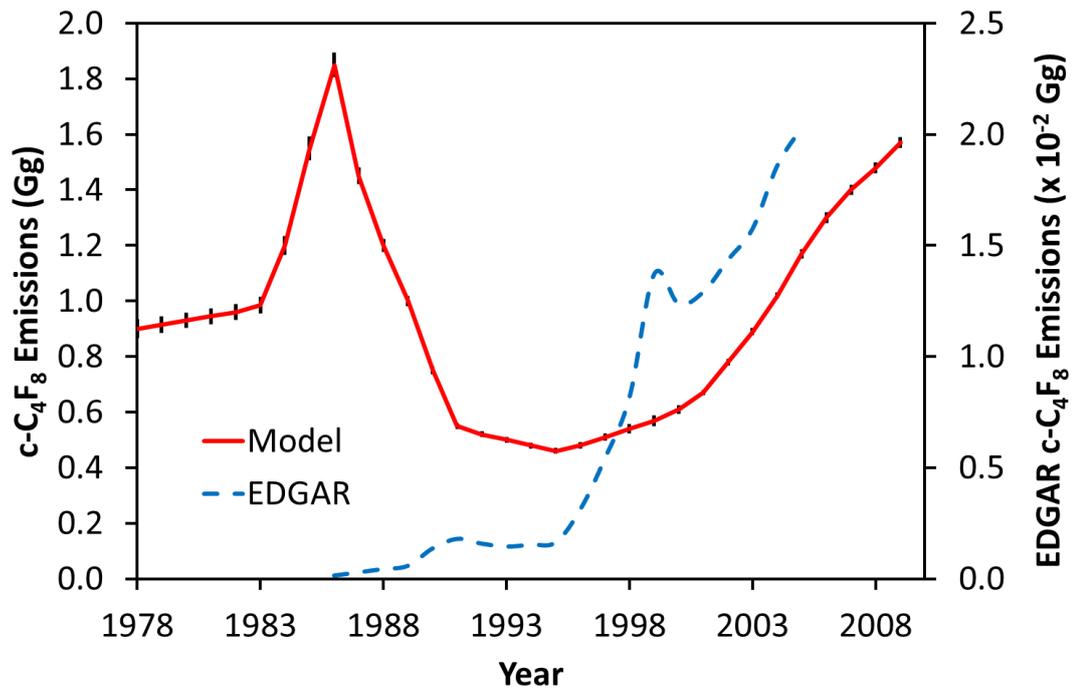


**Figure 4.11 c-$C_4F_8$:** Model derived annual emissions (Gg) (red line) and annual emissions reported by EDGAR (blue dashed line). Annual emission uncertainties shown as black lines.
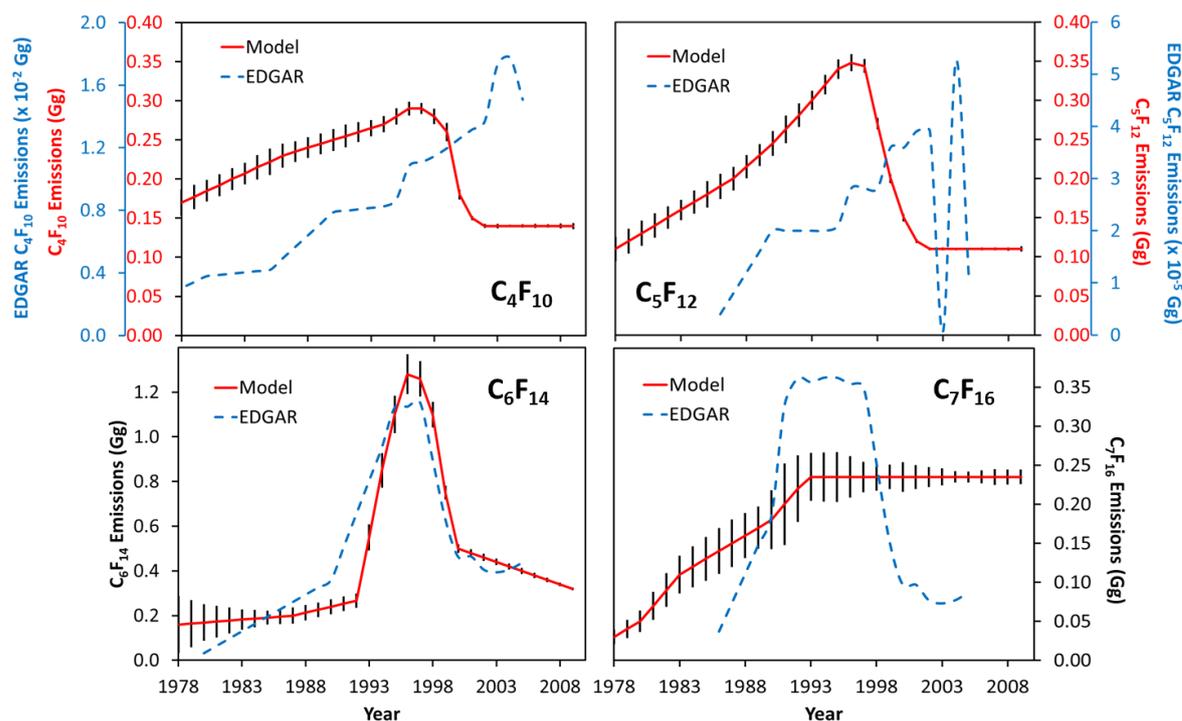
**Figure 4.12** Model derived annual emissions (Gg) (red line) and annual emissions reported by EDGAR (blue dashed line) of the higher PFCs ($C_4F_{10}$, $C_5F_{12}$, $C_6F_{14}$, $C_7F_{16}$). Annual emission uncertainties shown as black lines.

The model derived annual emissions of $C_6F_{14}$ (Figure 4.12) are about 0.2 Gg from 1978 up to the early 1990s. After this they increase five-fold within three years to about 1.3 Gg before declining again after 2001 back to about 0.35 Gg in 2010. The annual emissions reported by EDGAR agree very well with the model derived emissions.

Annual emissions of $C_7F_{16}$ (Figure 4.12) increased steadily from less than 0.05 Gg in 1978 up to about 0.25 Gg in the early 1990s and have remained fairly stable since this time. EDGAR report emissions of as similar magnitude but with a historical trend similar to that of the other minor PFCs ($C_4F_{10}$, $C_5F_{12}$, $C_6F_{14}$) with a peak in the mid-1990s and a decline more recently.

### 4.3.4   Discussion of Emissions Histories of the PFCs

The emissions of the majority of the PFCs reported here are declining having peaked in the mid-1990s. The only exceptions to this trend are $C_2F_6$ (although Mühle et al. (2010) report emissions to be in decline), c-$C_4F_8$ and $C_7F_{16}$. The most significant of these is c-$C_4F_8$ for which emissions are still increasing.

121

The reasons for the increase of the emissions of $C_2F_6$, $C_3F_8$ and c-$C_4F_8$ in the mid-1990s is presumably associated with their use in the electronics industry. The main use of these three gases is in CVD chamber cleaning with a secondary use in plasma etching. One reason for the increase in c-$C_4F_8$ in recent years could be that it is the most efficient PFC for CVD chamber cleaning with a 70 – 90% utilization efficiency (i.e. 10 – 30% of the gas used is lost) compared to 30 – 60% for $C_3F_8$ and 30% for $C_2F_6$ (ISMI, 2005). This leads to a 12 – 70% reduction in PFC emissions for $C_3F_8$ compared to a $C_2F_6$ baseline and a 50 – 85% reduction for c-$C_4F_8$. $NF_3$ is also used increasingly as a replacement gas for chamber cleaning (ISMI, 2005). Considering these replacements, and that the aluminium industry reports $C_2F_6$ emissions to be declining (IAI, 2005), it is surprising that Figure 4.9 shows annual emissions of $C_2F_6$ to still be rising and is perhaps a reason to put more credence in the results of Mühle et al. (2010) for this gas.

The decrease in $C_4F_{10}$, $C_5F_{12}$, and $C_7F_{16}$ since the mid-1990s can be attributed to their replacement as heat transfer fluids (HTFs) by other lower GWP alternatives such as segregated hydrofluoroethers (HFEs) (Tuma and Tousiganant, 2001). In addition to this there has probably been a continued improvement in the prevention of leakages when using PFCs in closed systems (EPA, 2008). The fact that $C_7F_{16}$ does not appear to have been replaced in a similar way could be because of its higher boiling point (80 – 85°C) making it more difficult to replace, though Tuma and Tousignant (2001) report the commercial availability of an HFE with a boiling point of 130°C ($C_3F_7CF(OC_2H_5)CF(CF_3)_2$) since 2000.


### 4.3.5   Future

The use of PFCs in the electronics industry looks set to continue to decline as the industry makes continued efforts to reduce emissions by improvements in technology and using low GWP replacements. The aluminium industry also continues to reduce PFC emissions per unit aluminium produced, however if there is a large increase in production this will lead to increased total PFC emissions. More concerning are reports that new production plants in China may be emitting PFCs continuously rather than just during periods affected by the primary anode effect (Rand, 2011).

Any reduction in emissions of the PFCs will not lead to a reduction in atmospheric mixing ratios but will only slow the growth rate, due to the atmospheric lifetimes of these species.

Therefore emissions and new uses must continue to be monitored and controlled since all emissions mark effectively a permanent change to atmospheric composition.

## 4.4 SF$_5$CF$_3$

### 4.4.1 Cape Grim Mixing Ratio Time Series

The historic atmospheric mixing ratios of SF$_5$CF$_3$ measured from the Cape Grim air archive are shown in Figure 4.13. The model fit to these measurements is also shown.

The mixing ratio at the beginning of the Cape Grim record, in 1978, is about 0.018 ppt. The mixing ratio is then seen to steadily increase with an average growth rate of 3.2 ppq a$^{-1}$ between 1978 and 1990 and of 7.6 ppq a$^{-1}$ between 1990 and 2000. After 2000 the growth rate begins to decrease and after 2005 it is indistinguishable from zero with a mixing ratio of 0.150 ppt.
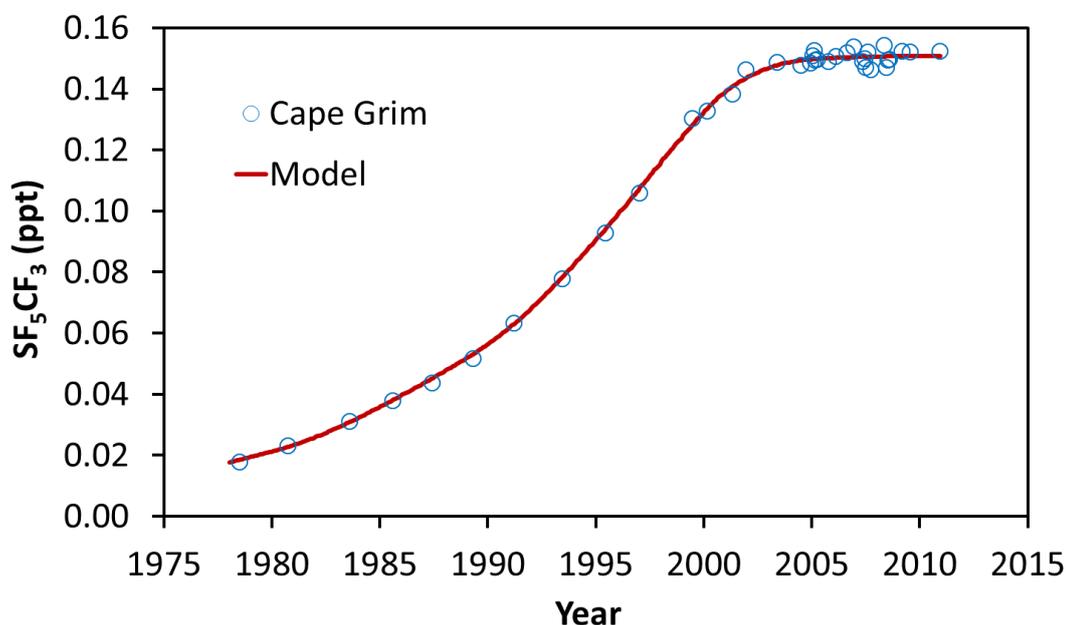


**Figure 4.13 SF$_5$CF$_3$:** Measured mixing ratios (ppt) from Cape Grim (blue circles) and modeled mixing ratios (red line).

### 4.4.2 SF$_5$CF$_3$ in NEEM Firn Air

The measured concentration-depth profile of SF$_5$CF$_3$ from firn air at NEEM is shown in Figure 4.14. The output from the atmospheric model scenario used to fit the Cape Grim measurements (Figure 4.13) was then used as input for the firn model. The output from this firn model run is shown as a red line in Figure 4.14. The mixing ratio prior to 1978 was extrapolated back to zero in 1958 with an exponential growth curve for the firn modeling. The measured mixing ratio is seen to fall to zero at depth confirming an entirely anthropogenic source for the gas (as reported by Sturges et al., 2000). The output of the firn model fits the profile well at depth but fits less well through the fast diffusion zone between 62 and 20 metres, overestimating mixing ratios slightly in the deeper part and underestimating them nearer the surface. This could be due to a changing emission distribution with time (the atmospheric modeling used a distribution with 100% of emissions in the northern hemisphere as described in Section 4.2.2).
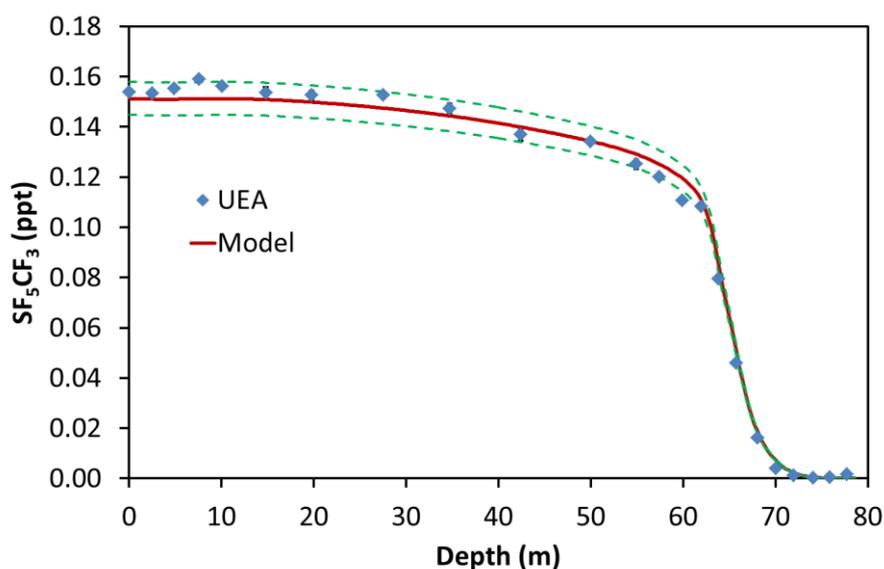


**Figure 4.14 SF$_5$CF$_3$:** Measured concentration-depth profile from the firn air at NEEM (blue diamonds). Output from the firn model based on input from the atmospheric model fit based to Cape Grim measurements (red line). Green dashed lines show uncertainty from atmospheric model fit and firn air measurements.

### 4.4.3 Global Annual Emissions and Source of SF$_5$CF$_3$

The global annual emissions of SF$_5$CF$_3$ derived from the model fit to the Cape Grim measurements are shown in Figure 4.15.
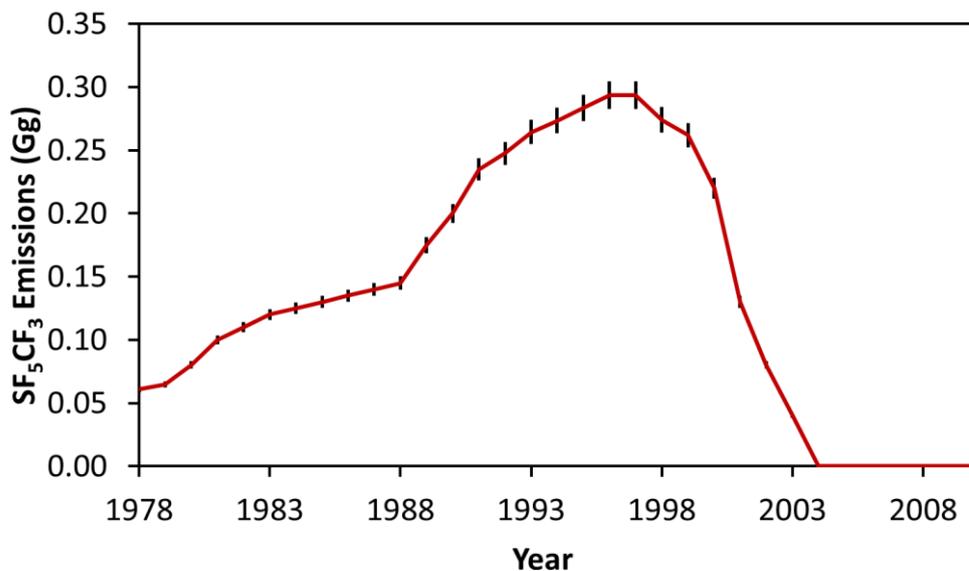
**Figure 4.15** Model derived annual emissions of $SF_5CF_3$ (Gg). Annual emission uncertainties shown as black lines.

The annual emissions of $SF_5CF_3$ are seen to increase steadily between 1978 and 1988 from 0.06 Gg to 0.14 Gg. There is then a more rapid increase to the mid-1990s to peak global emissions of about 0.3 Gg a$^{-1}$. After 1999 emissions decrease steeply to being indistinguishable from zero from 2004 and have remained so up to 2010 suggesting that emissions of $SF_5CF_3$ have ceased.

After $SF_5CF_3$ was first reported in the atmosphere by Sturges et al. (2000), a couple of groups worked on the suggestion put forward in that work that the source of the $SF_5CF_3$ could be as a breakdown product of $SF_6$ in high voltage equipment. Huang et al. (2005) showed that $SF_5CF_3$ could indeed be formed as a breakdown product of $SF_6$ under spark discharge conditions in the presence of HFC-23 and HFC-32. This suggestion was driven by the fact that $SF_6$ appeared at the time to have a very similar atmospheric history to $SF_5CF_3$. However Figure 4.16 shows that in recent years, as $SF_5CF_3$ emissions have decreased, the atmospheric trends of the two gases have begun to diverge. Hence it seems likely that the major source of $SF_5CF_3$ to the atmosphere was not linked to $SF_6$.
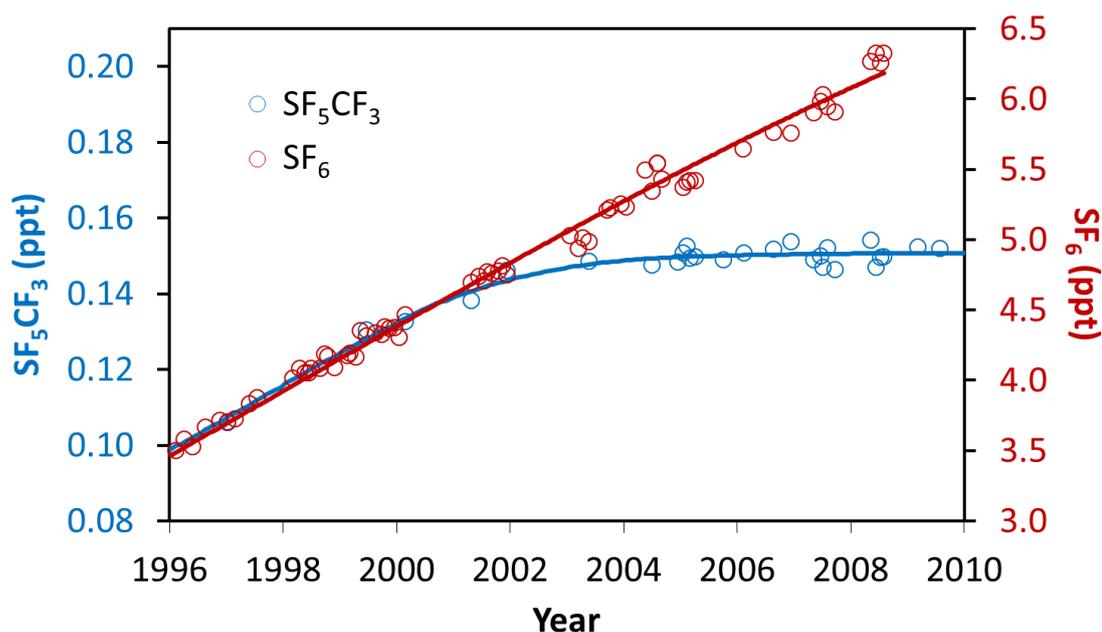
**Figure 4.16** Comparison of mixing ratios of $SF_5CF_3$ (blue-left axis) and $SF_6$ (red-right axis) between 1996 and 2010. Open circles are measured mixing ratios from the Cape Grim air archive. The blue line is the model fit in Figure 4.13, the red line is a third order polynomial fit.

Another suggested source of $SF_5CF_3$ emissions was the operations of the company 3M in making certain fluorochemicals, as suggested by Santoro (2000) in response to the original paper of Sturges et al. (2000). It was suggested that the gas was produced as a by-product during the manufacture of perfluorooctane sulfonyl fluoride (POSF) using the electrochemical fluorination (ECF) process.

The estimated trend in global production of POSF by 3M from 1970 to 2002 was reported by Paul et al. (2009) and is seen to closely resemble the model derived emissions trend (Figure 4.17). The timing of the close down of POSF production around 2002 coincides with the dramatic drop in emissions calculated by the model. Though POSF production supposedly ceased at the end of 2002, Paul et al. (2009) report that 3M was not able to completely close down production in 2002 without giving secondary users a time period to find alternatives. Additionally 3M introduced technologies to reduce emissions of POSF to air by about 40% around 1998 (Paul et al., 2009; Santoro, personal communication, 2009). Whether this would reduce $SF_5CF_3$ emissions is unclear but this time period does coincide with the beginning of the reduction of emissions calculated by the model but with no apparent reduction in POSF production (Paul et al., 2009).

126
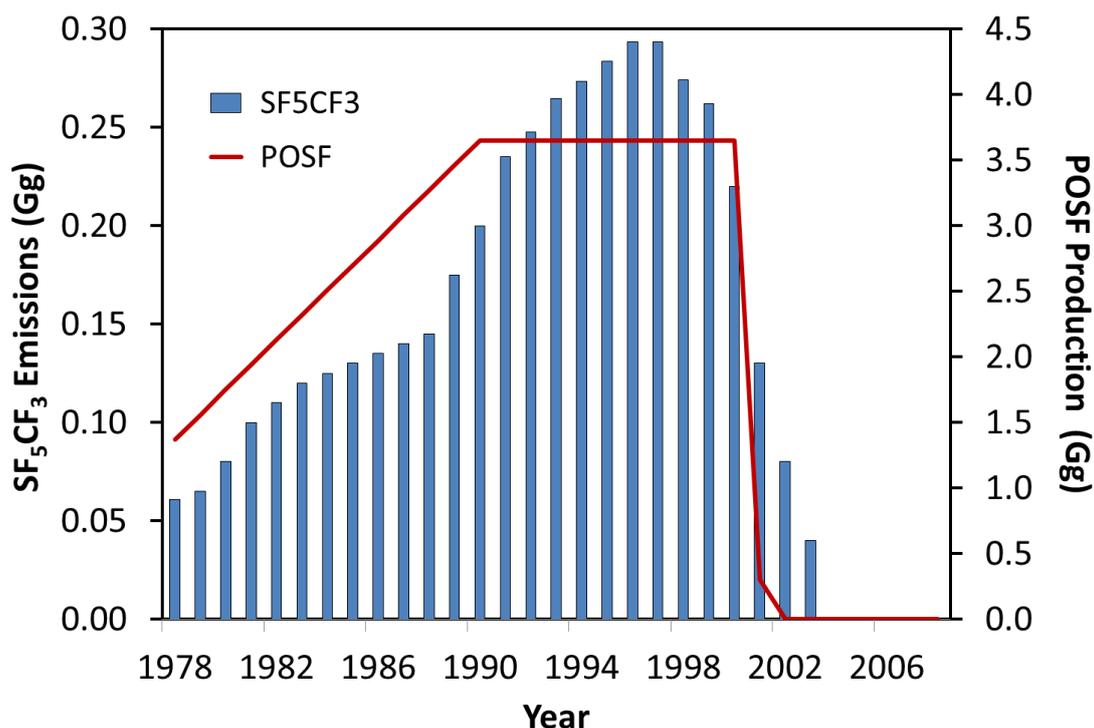
**Figure 4.17** Comparison of model derived annual $SF_5CF_3$ emissions (blue columns – left axis) with estimated annual POSF production by 3M (Paul et al., 2009) (red line – right axis).

If POSF production via the ECF process by 3M is assumed to have been the only source of $SF_5CF_3$ emissions then, using the production volume estimates of Paul et al. (2009) during maximum emissions, the annual $SF_5CF_3$ emissions can be divided by the POSF production volume and show that approximately 75 kg of $SF_5CF_3$ were produced per tonne of POSF produced before the introduction of emission abatement technology by 3M around 1998. Additionally if the sum of emissions of $SF_5CF_3$ up to 1998 is divided by the sum of 3M POSF production derived by Paul et al. (2009) (with POSF production linearly interpolated from 1970 estimates back to zero in 1958) then emissions of 62 kg of $SF_5CF_3$ per tonne of POSF produced are calculated.

### 4.4.4   The Future

Global production of POSF has reduced to about 1000 tonnes per year (Paul et al., 2009) and legislative restrictions on imports and use in Europe and the US may well reduce demand further. Although there is still production of POSF in south-east Asia, it seems that no $SF_5CF_3$ is being produced as a by-product. There are over 600 manufacturing steps during the POSF

production process by ECF (Paul et al., 2009). It is therefore perhaps not surprising that although there are plants still producing POSF they may have different manufacturing steps and hence avoid the production of $SF_5CF_3$. However it is also not inconceivable that another company will accidentally begin to produce $SF_5CF_3$ again and for this reason atmospheric concentrations must continue to be monitored so that such an event can be quickly recognized.

Another suggested use for $SF_5CF_3$ in the future has been in ocean tracer release experiments (e.g. Ho et al., 2008). However the predicted volume of use for these experiments is a few hundred kilograms over a decade which would not detectably add to the atmospheric budget.

## 4.5 HFC-227ea

### 4.5.1 Firn Derived Temporal Trend

The atmospheric trend of HFC-227ea at NEEM was reconstructed by Patricia Martinerie from the measured concentration-depth profile using an inverse modeling approach (Martinerie et al., 2009) (Figure 4.18). The upper and lower bounds of the trend derived from the firn are shown as green dashed lines in Figure 4.18 and were calculated as the maximum of the 2σ root mean square deviations of the reconstructed trend. The model output for the Arctic latitudes (i.e. NEEM) using the 'best fit' emissions scenario derived in Chapter 4.5.2 is shown as a red line.

The mixing ratio has increased exponentially from being indistinguishable from zero in the early 1990s to 0.53 ppt in the summer of 2008 when the firn air was taken. The modeled atmospheric trend shows a strong seasonal cycle at NEEM with growth of the mixing ratio during the winter months and fairly stable concentrations during the summer months. This trend is reversed, though of a smaller amplitude in modeled reconstructions for the southern hemisphere. This suggests that the cycle is caused by the seasonality of the OH radical, the major atmospheric sink for HFC-227ea (Zellner et al., 1994), which is at a maximum in the summer.
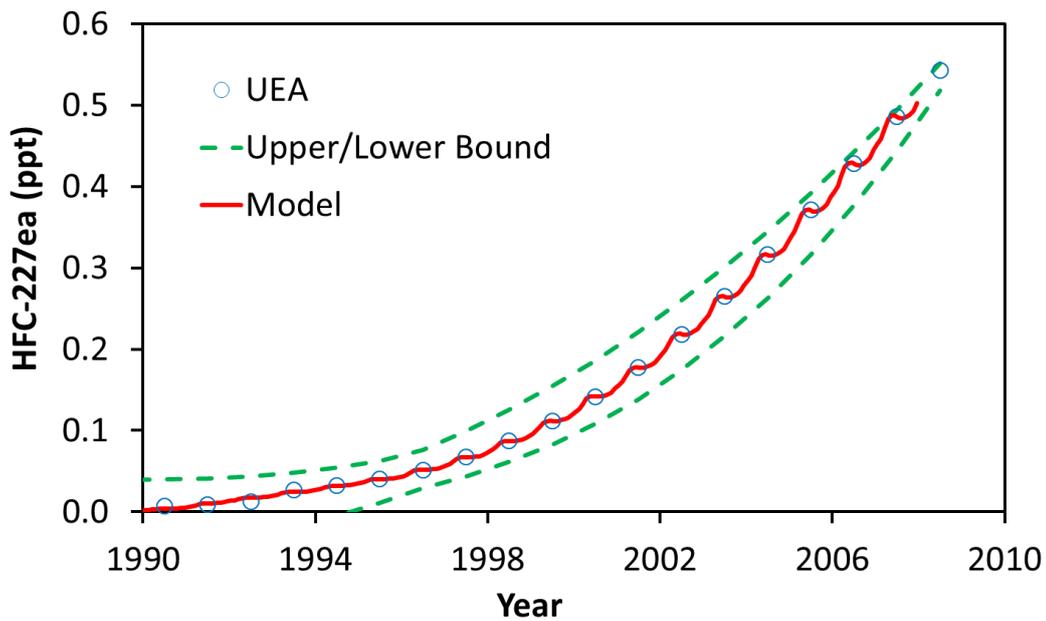
**Figure 4.18 HFC-227ea:** Temporal trend derived from inverse firn modeling at NEEM (blue circles) and the upper and lower bounds of this trend (green dashed lines) and model fit to the trend (red line).

### 4.5.2   Annual Emissions of HFC-227ea

Emissions were entered into the model starting from zero in 1989, around the time that the firn profile suggests that significant emissions began. However the lower uncertainty bound of the reconstruction in Figure 4.18 reaches zero in 1995 and so any emissions before this time are considered arbitrary, hence Figure 4.19 shows emissions only from 1995 – 2007. The emissions used to model the best estimate reconstruction increase steadily from zero in 1989 to the emissions needed to give the reconstructed mixing ratio in mid-1995 of 0.038 ppt.

The annual emissions increase from 0.35 Gg in 1995 to 2.33 Gg in 2007 and show a roughly linear increase in growth rate of about 0.11 Gg a$^{-1}$.
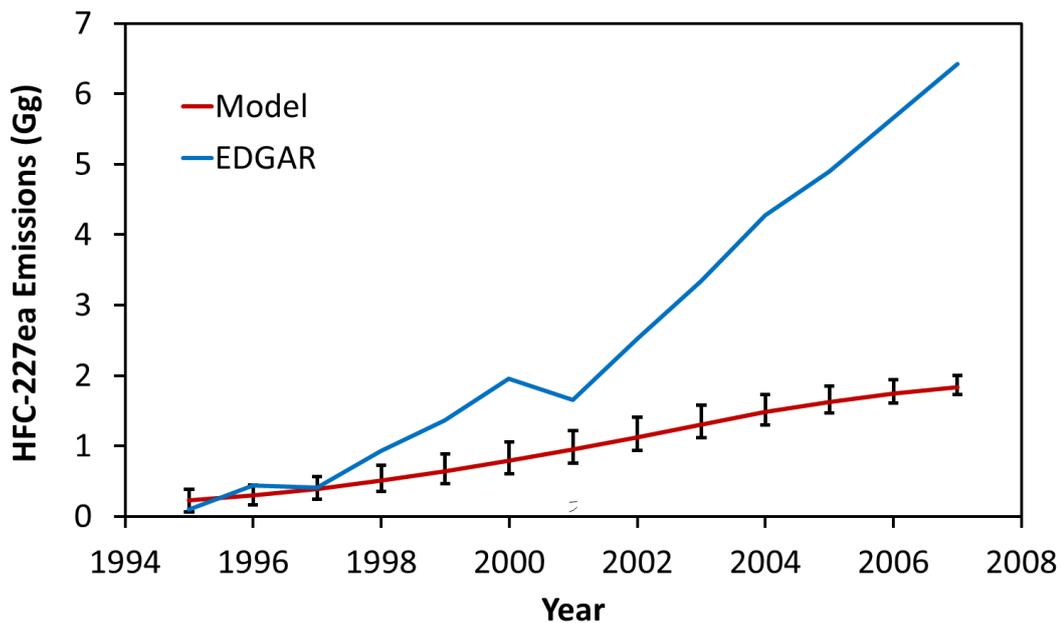
**Figure 4.19** Modeled HFC-227ea emissions 1995 – 2007 using NEEM concentrations derived from inverse firn modeling (red). Emissions from EDGAR emissions database (version 4.2, EDGAR Project Team, 2013) (blue). Emission uncertainties shown as black lines.

Emissions data for HFC-227ea are available from the EDGAR database (version 4.2, EDGAR Project Team, 2009) up to 2008. These are plotted in Figure 4.19 alongside the model derived emissions. It is seen that the emission estimates from EDGAR increase much more steeply than those derived from the model and that by 2007 emissions are estimated to be over three times those which are derived from the model.

Equation 4.1 can be used to check the validity of the modeled emissions for HFC-227ea. Since it has a relatively long lifetime compared to the period of study and is growing throughout this period, it can be assumed that there is little loss during the model run. Inputting cumulative emissions of 10.4 Gg, as the model derives, up to 2005 gives a mixing ratio of 0.35 ppt which is comparable to the firn derived measurement for the end of 2005 of 0.37 ppt. Using the emissions reported by EDGAR up to the end of 2005 in the same equation yields a tropospheric mixing ratio of 0.74 ppt which is considerably higher than the measured values for 2005.

The large discrepancy between the two sets of emissions estimates is probably due to the fact that there are no emission estimates available directly from industry because HFC-227ea is produced by fewer than four companies (IPCC/TEAP, 2005). The reasons for EDGAR

overestimating emissions could be that proposed switch over rates from CFCs and HCFCs to HFCs have been slower than expected, or that more alternative technologies have been used than expected.

### 4.5.3   The Future

Under the Kyoto Protocol HFCs were included in a 'basket of gases' marked for possible reduction from 1990 (or 1995 for HFCs) emission levels for Annex 1 countries. This means cuts of 8% for the EU, 7% for the US and 6% for Japan by the period 2008-2012 (UNFCCC, 1997).

The continued growth of HFC-227ea seems unlikely to be a major contributor to global warming even with a GWP of 3,220 (Forster and Ramaswamy, 2007). At a 2008 mixing ratio of 0.6 ppt this equates to cumulative emissions of about 14 Gg which is equivalent to 44 million tonnes of $CO_2$. Though the atmospheric mixing ratio is currently growing exponentially this seems unlikely to be the case for long. More not in kind technologies are being found to replace HFCs and legislation will likely be introduced to limit the production and use of these gases due to their high GWPs.

## 4.6     Emissions of Fluorinated Compounds Prior to 1978

In Sections 3, 4 and 5 of this chapter emissions of the nine compounds reported between 1978 and 2010 were derived from the measurements at Cape Grim. Some of the compounds have relatively high mixing ratios in 1978 which suggest that they must have had significant emissions prior to this time.

The emissions prior to the beginning of the Cape Grim record can be found by initialising the model with mixing ratios of zero and then releasing emissions, over a period of several years, until the 1978 Cape Grim mixing ratio is reached (Table 4.4). This method makes the assumption that there is no loss within the model domain over this period – a valid assumption considering the lifetimes of the PFCs and $SF_5CF_3$ are on the order of thousands of years (Table 4.1). These model derived values can be checked using Equation 5.1 which again assumes atmospheric losses to be zero – though this time the assumption is less valid since the likely period of release is a few decades.

$$m_i \quad = \quad \xi_i \cdot m_a \cdot \frac{M_i}{M_a} \qquad\qquad (E4.1)$$

where $m_i$, mass of species emitted; $\xi_i$, mixing ratio of species; $M_i$, molecular weight of species; $M_a$, molecular weight of air (28.97 g mol$^{-1}$), $m_a$, mass of atmosphere (5.1 x 10$^{18}$ kg). The emissions of the PFCs and SF$_5$CF$_3$ prior to 1978 calculated using Equation 4.1 are compared to those derived using the model in Table 4.4. A good agreement is seen between the two methods as expected with differences less than 10%.

Table 4.4 Model derived and calculated emissions of the PFCs and SF$_5$CF$_3$ prior to 1978.

| Compound | Emissions prior to 1978 (Gg) | |
|:---:|:---:|:---:|
| | Model Derived | Calculated |
| C$_2$F$_6$ | 20.6 | 20.2 |
| C$_3$F$_8$ | 1.60 | 1.59 |
| c-C$_4$F$_8$ | 11.9 | 12.3 |
| C$_4$F$_{10}$ | 0.78 | 0.75 |
| C$_5$F$_{12}$ | 0.90 | 0.91 |
| C$_6$F$_{14}$ | 0.74 | 0.71 |
| C$_7$F$_{16}$ | 1.00 | 1.09 |
| SF$_5$CF$_3$ | 0.63 | 0.63 |

## 4.7    Radiative Forcing Effects of Fluorinated Compounds

The radiative forcing capacity of a given greenhouse gas is the change in the amount of energy per unit area at the top of the atmosphere that the presence of that gas in the atmosphere causes and can be expressed as W m$^{-2}$ ppb$^{-1}$. The radiative forcing capacity (per ppb) of the nine gases studied in this chapter are given in Table 4.1. The total contribution of an atmospheric species to radiative forcing can be calculated by multiplying its atmospheric burden (kg) by its global warming potential (GWP) relative to CO$_2$. The cumulative

contribution of the fluorinated compounds reported in this work in terms of the equivalent in metric tonnes of $CO_2$ are shown in Figure 4.20. The cumulative contribution of each compound up to 2010 is shown in Table 4.5 as well as the contribution in 2010.

**Table 4.5** Model derived cumulative emissions and Million Metric Tonnes $CO_2$ Equivalent (MMTCE) of the fluorinated compounds reported herein.

| Compound | Cumulative Emissions to 2010 (Gg) | Cumulative MMTCE (Tg) | MMTCE (Tg) 2010 |
|---|---|---|---|
| $C_2F_6$ | 72 | 880 | 39 |
| $C_3F_8$ | 15 | 140 | 4.8 |
| c-$C_4F_8$ | 32 | 330 | 17 |
| $C_4F_{10}$ | 7 | 60 | 1.6 |
| $C_5F_{12}$ | 6 | 57 | 1.6 |
| $C_6F_{14}$ | 14 | 130 | 2.8 |
| $C_7F_{16}$ | 6 | 57 | 2.4 |
| $SF_5CF_3$ | 5 | 89 | 0 |
| HFC-227ea | 20 [a] | 45 | 5.9 [b] |

[a] Cumulative emissions only up to 2007. [b] Based on 2007 emissions

It is seen in Figure 4.20 that $C_2F_6$ is the largest contributor to MMTCE with over 50% of the total cumulative contribution and that a further 25% can be attributed to c-$C_4F_8$. The total rate of increase of MMTCE from the PFCs has not changed very much since 1995 and any decrease caused by the reduction in emissions of the higher PFCs is more than compensated for by the continued increase in emissions of c-$C_4F_8$ (with the caveat that $C_2F_6$ emissions may actually have been in decline). HFC-227ea emissions have grown rapidly since 1989 and continue to increase year on year.

Table 4.5 shows the emissions in 2010 of the compounds reported in this chapter to be equivalent to the emission of about 75 million tonnes of $CO_2$. This compares to roughly 30 billion tonnes of $CO_2$ estimated by the Carbon Dioxide Information Analysis Centre (CDIAC) to have been emitted in 2010 from fossil fuel and cement emissions (Marland et al., 2005), i.e. the emissions reported here are about 0.3% of $CO_2$ emissions. However it must be

remembered that not only does much of this $CO_2$ not remain in the atmosphere, with partitioning of about half of the annual emissions into the oceans and the biosphere (e.g. see Le Quéré et al., 2012), but that due to atmospheric lifetimes of several thousand years, any addition of PFCs to the atmosphere is effectively a permanent change to atmospheric composition.
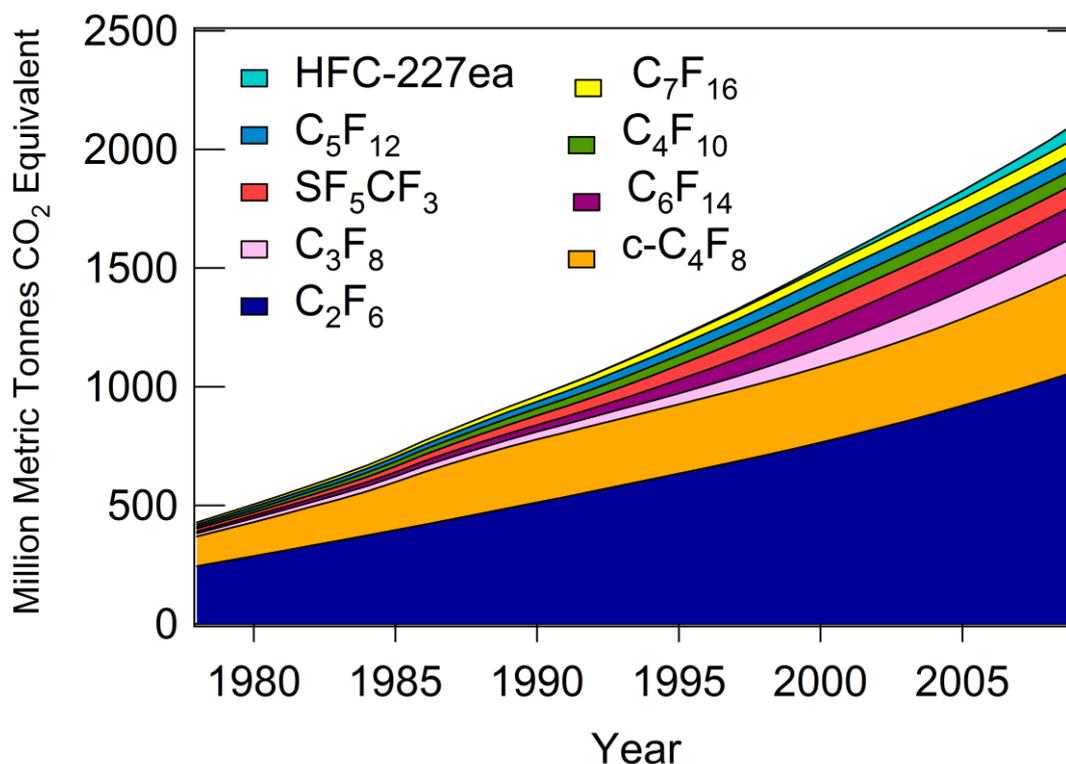


**Figure 4.20** Cumulative emissions of the fluorinated compounds reported in this chapter in terms of million metric tonnes $CO_2$ equivalent.

## 4.8 Conclusions from Atmospheric Modeling of Fully Fluorinated Gases

The work in this chapter has used a 2-D atmospheric model, constrained with measurements of background air from Cape Grim, to determine the global annual emissions of seven perfluorocarbons (PFCs) and $SF_5CF_3$ between 1978 and 2010. HFC-227ea annual emissions were constrained using measurements from Greenland firn air. The latitudinal distributions of the PFC emissions were constrained using firn air measurements from Greenland. The effects of the increasing mixing ratios of the fluorinated compounds on global radiative forcing are discussed. The main conclusions from this chapter are listed below.

(i)     The mixing ratios of all of the PFCs reported here have increased greatly between 1978 and 2011 and continue to increase. The greatest contribution to atmospheric mixing ratios of fluorinated compounds is from $C_2F_6$ followed by c-$C_4F_8$. The continued increase in mixing ratios is partly caused by their long lifetimes (on the order of thousands of years) so that once in the atmosphere they are effectively not removed.

(ii)    Emissions of $C_2F_6$ appear to currently be increasing form this work but this is disagreement with emissions reported by other top down work. Emissions of $C_3F_8$ are decreasing from a peak in the late 1990s.

(iii)   Emissions of c-$C_4F_8$ are currently increasing rapidly, possibly associated with increased use in the electronics industry as a replacement for $C_2F_6$ and $C_3F_8$.

(iv)    Emissions of the higher PFCs ($C_4F_{10} - C_7F_{16}$) peaked in the mid-1990s and have since decreased or remained stable.

(v)     Atmospheric mixing ratios of $SF_5CF_3$ have stabilised since the early 2000s implying that emissions have ceased.

(vi)    Emissions of $SF_5CF_3$ appear to have been related to production of perfluorooctane sulfonyl fluoride (POSF) by the company 3M, which has now ceased.

(vii)   Mixing ratios of HFC-227ea have rapidly increased in the atmosphere over the past 15 years. This has been caused by its increasing use as an HCFC replacement species.

# Chapter 5

# Firn Derived Alkane and Alkyl Nitrate Histories

# 5 Firn Derived Alkane and Alkyl Nitrate Histories

Chapter 5 describes the use measurements in firn air to derive atmospheric histories for the past 60 years of a series of alkanes and the alkyl nitrates in the Arctic. The atmospheric histories of the alkanes are then used in conjunction with information from the EDGAR database to derive emission histories of these compounds for the northern hemisphere. The changing ratios of the atmospheric mixing ratios of the alkyl nitrates to their parent hydrocarbons is then calculated and the implications discussed.

## 5.1 Introduction

The variation of the mixing ratio of the atmospheric species with depth in the firn will hereafter be referred to as the *firn profile*. The precise shape of a firn profile of a given molecule is dependent not only on the atmospheric history but also on the diffusivity profile of the firn and on the diffusivity coefficient of the molecule. In this chapter the atmospheric histories of the alkanes and alkyl nitrates will be reconstructed using a firn model to interpret the profiles. The firn model used for this study is a direct model developed at LGGE, Grenoble and is based on that described by Rommelaere et al. (1997) with further updates by Martinerie et al. (2009) and the model tuned for NEEM by Patricia Martinerie (Buizert et al., 2012).

The majority of the temporal information in a firn profile is found within the lowest part of the core with the top two-thirds or more of the core often covering only $10 - 20$ years and almost the top half covering only the previous year. This provides a high resolution view of these most recent years. The oldest air represented at NEEM has a mean age of about 70 years (i.e. from 1940) (Buizert et al., 2012). The NEEM samples were collected during the summer of 2008 at NEEM, Greenland (77.4°N, 51.0°W, Alt. 2484m). The air sampling and the measurements were performed by others, details of which are given in Chapter 2. Atmospheric histories of the alkanes and alkyl nitrates presented in this chapter have recently been reported from the North GRIP (NGRIP) firn site in the Arctic (Worton et al., 2012). The atmospheric histories derived from the NGRIP firn air are compared to the trends derived herein from NEEM firn air. The North GRIP firn data samples were collected during the summer of 2001 at NGRIP, Greenland (75.1°N, 42.4°W, Alt. 2960m).

Figure 5.1 shows an example firn depth profile from NEEM for the compound n-butane. Depth is shown on the x-axis and the measured mixing ratio of n-butane on the y-axis. An approximate date scale is shown on the top x-axis representing the mean age of air at these depths. These ages, derived from comparison to the in-put atmospheric scenario, are only rough estimates, both because of the age spread of air at a given depth and because of the different diffusion rates of different molecules, but give an idea of the disproportionate length of the x-axis given to recent air when firn profiles are viewed in this way. The first 30 – 40 metres of the profile represents the seasonal cycle of the molecule. The steep decline in the mixing ratio between 68 m and 60 m represents roughly the years 1980 – 2000. The section from the base of the firn (78.6 m) to 68 m represents roughly 1930 – 1980 (the mean age of the deepest measurement is interpreted from a comparison of the input to the firn model with the output).
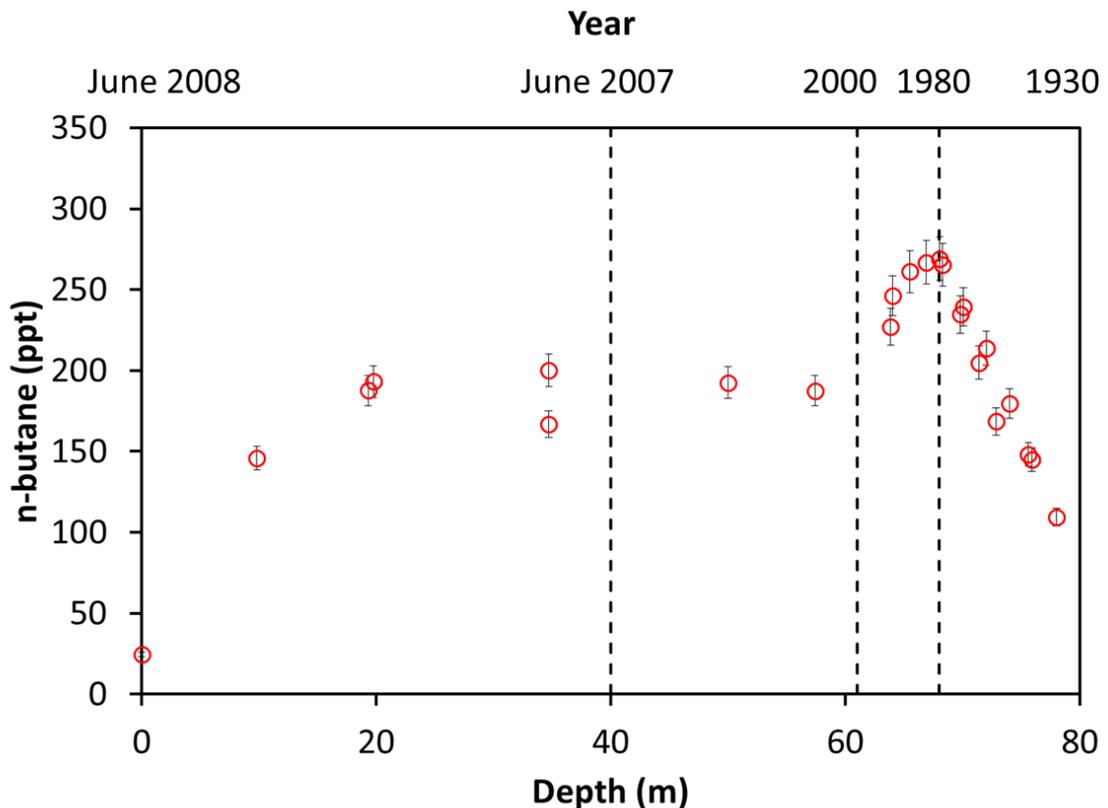


**Figure 5.1** Measurements of n-butane mixing ratios in the firn at NEEM against depth (bottom x-axis). Approximate mean ages of the air are also shown at given depths (top x-axis).

The firn measurements are used to derive an atmospheric history back to 1950, so the most recent year of data is of very little importance for the derivation of this trend but takes up roughly half of the x-axis. Hence an alternative way of presenting the data is shown in Figure 5.2. Here the x-axis is on a log scale and shows the height of the measurement from the base of the firn. This has two benefits: firstly it enlarges the region of interest (i.e. the deeper firn) making it easier to see how well the model fit compares to the firn measurements; secondly the age now increases from left to right on the plot, making it more easily comparable to atmospheric scenarios plotted as mixing ratio against time. The firn profiles shown hereafter in this chapter will therefore follow the form of Figure 5.2.

The atmospheric scenarios derived from the firn measurements shown in the following chapter are presented from 1950 to 2007. This start date is chosen because, although the earliest measurement represents a mean air age of about 1930, the compression of the data at depth means that the scenario derived for the earlier years from the measurements has more inherent uncertainty. The end date of 2007 is used because the samples were collected from NEEM in the summer of 2008 and so 2007 is the last year for which an annual mean of the atmospheric mixing ratios can be obtained.
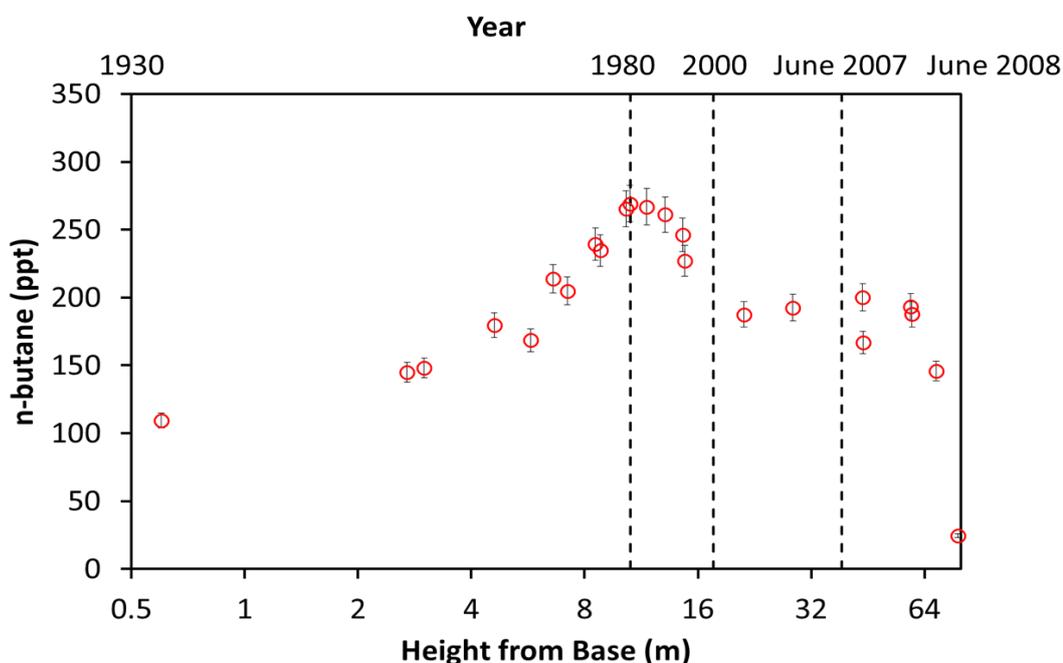


**Figure 5.2** Measurements of n-butane mixing ratios in the firn at NEEM against the height of the measurement from the base of the firn shown on a log scale (bottom x-axis). Approximate mean ages of the air are also shown at given depths (top x-axis).

## 5.2 Hydrocarbon Firn Profiles

### 5.2.1 NEEM

There were two sampling holes at NEEM, the EU hole and the US hole. Samples from both the EU hole and US hole were analysed by the INSTAAR laboratory, University of Colorado, Boulder and samples from the EU hole by the Max Planck Institute, Mainz (see Chapter 2.1 – 2.2 for further details). However only the data from INSTAAR for the US hole has been used for the firn modeling since this data set seems to have the least scatter and to generally agree better with the data from North GRIP.

### 5.2.2 Firn Profiles

Analysis of air extracted from firn can be used to derive atmospheric histories of the analysed species stretching back several decades. However the interpretation of the signal in the firn is complicated because the air at any given depth is representative of a mix of ages of air. Hence to deconvolute the atmospheric history from the measurements a firn model must be used.

The signal recorded in the firn (firn profile) is a function of the atmospheric history of the gas, the diffusion coefficient ($K_{diff}$) of the gas and the diffusion profile, or tortuosity, of the firn profile (i.e. how interconnected the air passages in the firn are). A firn model can be used to derive the atmospheric history of a gas because the three other parameters (firn profile, $K_{diff}$, and diffusion profile). The diffusion profile is initially constrained by the use of a series of reference gases, for which the atmospheric histories are already known.

The derived annual mixing ratios represent the annual average for that species in the atmosphere above the firn site. For species such as the butanes and pentanes which have short lifetimes in the summer and hence mixing ratios in the Arctic are close to zero (e.g. Swanson et al., 2003), the derived annual mixing ratio in the firn represents about half of the winter time peak.

Figure 5.3-A shows the firn profiles of the six alkanes reported here from NEEM firn air. atmospheric scenarios from 1950 to 2007 derived for ethane and propane from the firn measurements at NEEM. The red dashed lines through the measurements on the firn profiles are the best fit model output and correspond to the atmospheric scenarios shown in Figure 5.4.

The uncertainty ranges are presented as red solid lines, the calculation of these ranges is discussed in Section 5.3.
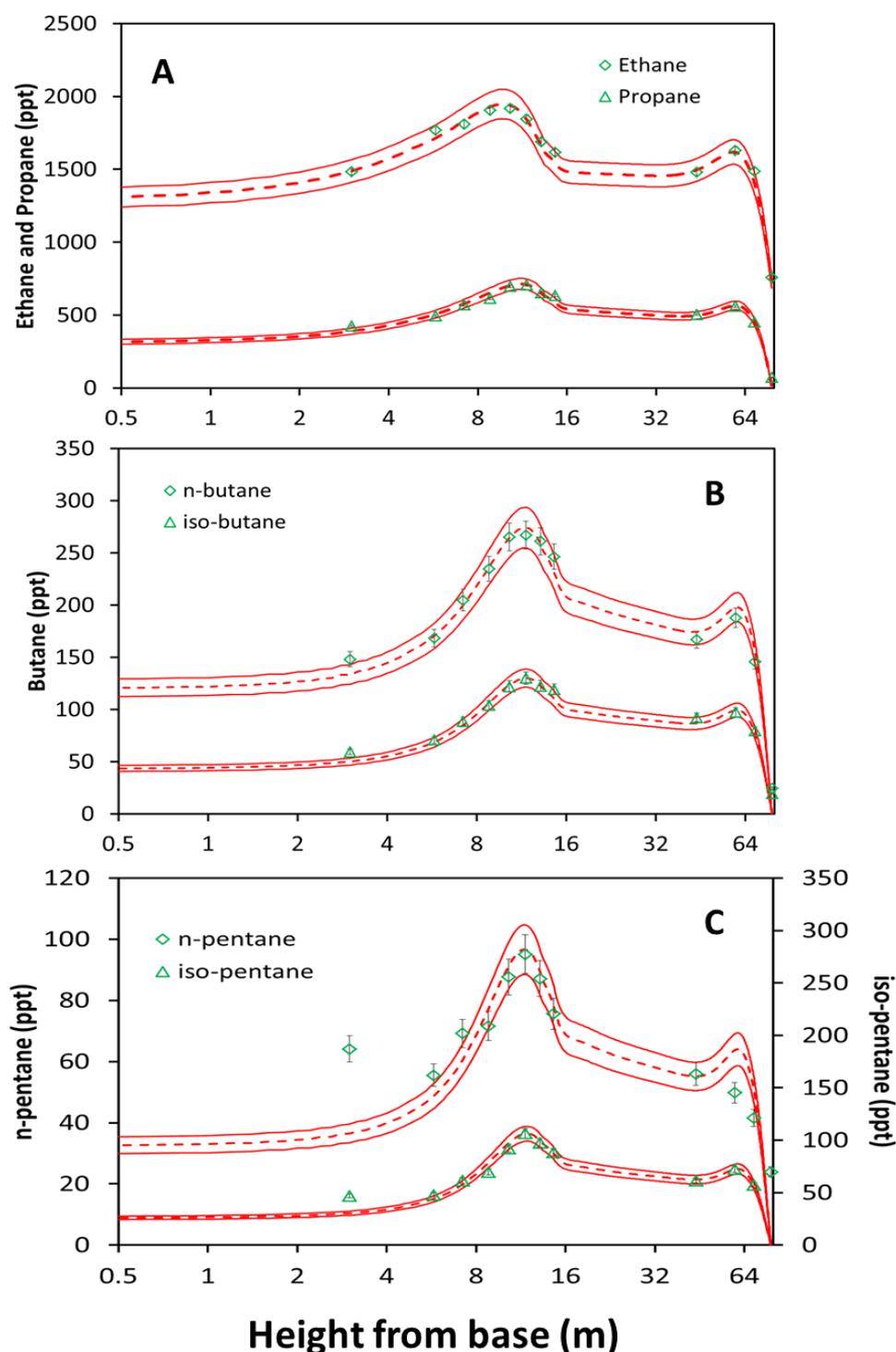


**Figure 5.3** The firn profiles of the six alkanes measured in firn air from NEEM (measurements in green). The 'best fit' model outputs from the firn model are shown as a red dashed line. The uncertainty ranges are shown as solid red lines. **A**: ethane and propane; **B**: n-butane and iso-butane; **C**: n-pentane and iso-pentane.
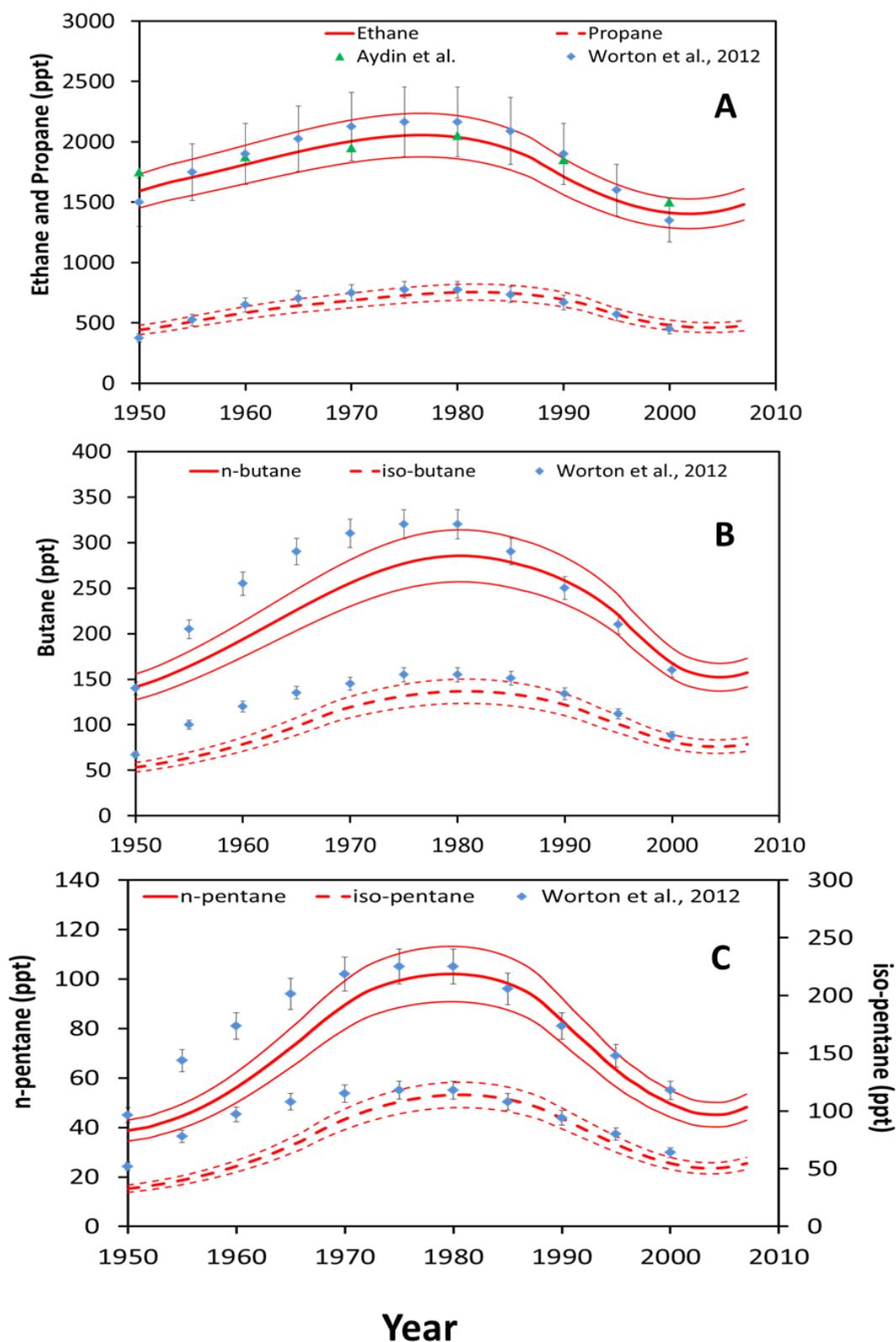
**Figure 5.4** The atmospheric histories of the six alkanes derived from the firn profiles for NEEM shown in Figure 5.3. Also shown are the trends derived from firn air from another Arctic site, NGRIP (Worton et al., 2012), and for ethane the trend derived from firn air from another Arctic site, Summit (Aydin et al., 2011). Uncertainty ranges, calculated as described in text, are shown as red solid/dashed lines. **A**: ethane and propane; **B**: n-butane and iso-butane; **C**: n-pentane and iso-pentane.

141

Figure 5.4 shows the atmospheric scenarios derived from the firn profiles of the six alkanes shown in Figure 5.3. They correspond to the atmospheric scenarios used to output the red dashed 'best fit' model lines in Figure 5.3. The calculation of the uncertainty ranges shown in Figure 5.4 is discussed in Section 5.3. Also shown in Figure 5.4 are the derived trends for the six alkanes from NGRIP firn air (Worton et al., 2012) and the ethane trend derived from firn air at the Greenland site Summit (Aydin et al., 2011).

All six profiles from NEEM display a peak about 11 m from the base of the firn. This depth corresponds to a peak in atmospheric mixing ratios in the late 1970s – early 1980s. Mixing ratios then decline to the early-2000s to levels similar to or below those in 1950 before beginning to increase again after this. Table 5.1 shows the magnitude of the increase of each alkane between 1950 and 1980 and of the subsequent decline. The percentage change between 1950 and the peak in 1980 generally increases with increasing carbon number (Table 5.1).

The trends from NGRIP (Worton et al., 2012) agree with those derived here within the uncertainties for all six alkanes from the late-1970s peak to 2000. They also agree with regards to the size of the increase from 1950 the late-1970s. However the Worton et al., (2012) trends tend to increase more rapidly in the early part of this period whereas the trends derived from the NEEM firn air increase more rapidly later in this period. The derived atmospheric scenario of ethane also agrees well with the trend derived from firn air at Summit, Greenland by Aydin et al. (2011). The agreement of trends from different sites provides a good indication that the observed trend is robust and the atmospheric signal of the alkanes is being preserved in the firn.

It is seen for the alkanes butane and pentane that mixing ratios at the surface are close to zero as expected during the summer time in the Arctic from measurements (Swanson et al., 2003) and runs with the 2-D model, whereas ethane and propane are still present at about 750 ppt and 80 ppt respectively at the surface, again consistent with measurements from Swanson et al. (2003).

**Table 5.1** Annual mean mixing ratio of alkanes derived from the Greenland firn site NEEM. Percentage increase from 1950 to the peak (around 1980).

| | Mean annual mixing ratio (ppt) | | | % increase 1950 – peak |
|---|---|---|---|---|
| | **1950** | **Peak (~1980)** | **2002** | |
| Ethane | 1600 | 2050 [a] | 1400 | 28 |
| Propane | 450 | 750 | 460 | 67 |
| n-butane | 140 | 285 | 152 | 105 |
| iso-butane | 53 | 137 | 77 | 160 |
| n-pentane | 39 | 102 | 45 | 160 |
| iso-pentane | 42 | 113 | 50 | 170 |

[a] Peak around 1970

For ethane an increase of about 28% is seen from the 1950 measurements to the peak, for propane concentrations increase by roughly 67%, for n-butane they increase by roughly 105%, for iso-butane and n-pentane they increase roughly 160% and for iso-pentane by roughly 170% (Table 5.1).

## 5.3 Firn Modeling Uncertainties

The measured firn profile of a particular atmospheric gas is a function of three parameters: the atmospheric history of that gas, the diffusion profile of the firn, and the diffusion coefficient of the gas. This assumes that the gas, once within the firn, is not subject to any post-depositional processes causing growth or decay of the recorded signal.

To consider the uncertainties in the atmospheric scenarios derived from the firn air measurements each of the separate parameters noted above are considered in turn.

### 5.3.1 Diffusion Profile

The diffusion profile of the US hole at NEEM was tuned for the firn model used by Patricia Martinerie and Emmauel Witrant at the Laboratoire de Glaciologie and Géophysique de l'Environnement, Grenoble (Martinerie et al., 2009; Buizert et al., 2012). The diffusion profile was defined using several reference gases for which the atmospheric histories (and

diffusion coefficients) are well known ($CO_2$, $CH_4$, $SF_6$, HFC-134a, CFC-11, CFC-12, CFC-113 and $CH_3CCl_3$), hence the diffusion profile can be constrained. The uncertainties in this diffusion profile are reduced by the use of several reference gases. A multi-model comparison of the diffusion profiles defined at the NEEM boreholes, using six different firn models, found that the firn diffusion profile for the NEEM boreholes defined by each different model were able to produce the measured firn profiles of each of the reference gases to within a 1-$\sigma$ normal distribution (Buizert et al., 2012). No estimate of the uncertainty associated with the calculated firn diffusion profile is available but the diffusivity profile established from the reference gases is simply scaled for another gas and hence any inherent uncertainty in this profile will be transferred to all derived atmospheric histories (Martinerie et al., 2009). So, the diffusion profile may lead to uncertainties in the absolute value of the gas at a particular age but the ratio of one gas to another is not affected by this uncertainty. An estimate of 5% was used for the uncertainty in the firn diffusion profile.

## 5.3.2   Diffusion Coefficients

The diffusion coefficients of the gases used in the firn modeling were calculated using the method of Fuller et al. (1966) based on the molecular structure of the molecules. This method of calculating diffusion coefficients has a stated average error of 4.3% for a wide range of different species (Fuller et al., 1966). Figure 5.5 shows the effect on the firn profile of running the model with the 'best fit' atmospheric scenario and changing the diffusion coefficients of n-butane and of 2-butyl nitrate by 5% and 10%. It is seen that for n-butane changing the diffusion coefficient by 10% leads to a difference in the modeled firn profile of <2.5% compared to the base case and for 2-butyl nitrate of <3%. A value of 3% is used for all species as a conservative estimate of the uncertainty that can be attributed to the diffusion coefficient.
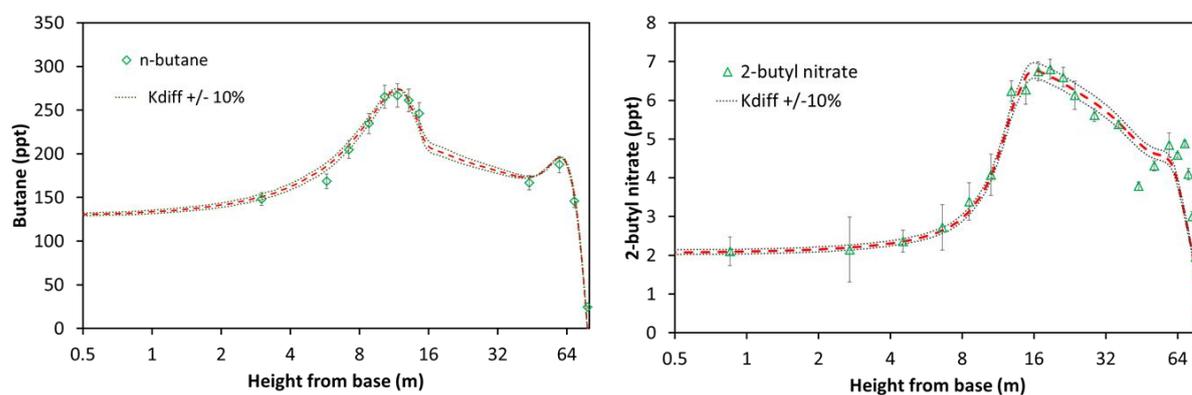
**Figure 5.5** Showing the effect on the model output of changing the diffusion coefficient ($K_{diff}$) by 10% in the firn model for n-butane and 2-butyl nitrate.

### 5.3.3 Measurement Uncertainties

The air samples were analysed for the alkanes at the INSTAAR laboratory in Boulder, Colorado with the measurements provided by D. Helmig. Each dataset has a defined uncertainty in the calibration and in the measurement precision. These are shown on each data point in Figure 5.3 as error bars.

### 5.3.4 Model-Measurement Agreement

The uncertainties in the model fits to the measured firn profiles for all species were derived by linear regression of the measurement points against the model output at that depth (Figure 5.6). A number of apparent outliers were removed from some of the compounds before this correlation. Measurement points between 0 and 35 m depth were excluded as they represent only the previous year's seasonal cycle and are subject to greater uncertainty, with a large number of data points with significant scatter. Furthermore, the firn profiles of the butanes and pentanes are a very similar shape, as would be expected for species that are likely to have the same sources and do have the same sinks. The measurements of the butanes and pentanes below 35 m were correlated against each other with those lying more than 2-σ away from the linear regression line considered to be outliers and excluded from the model-measurement correlations shown in Figure 5.6.
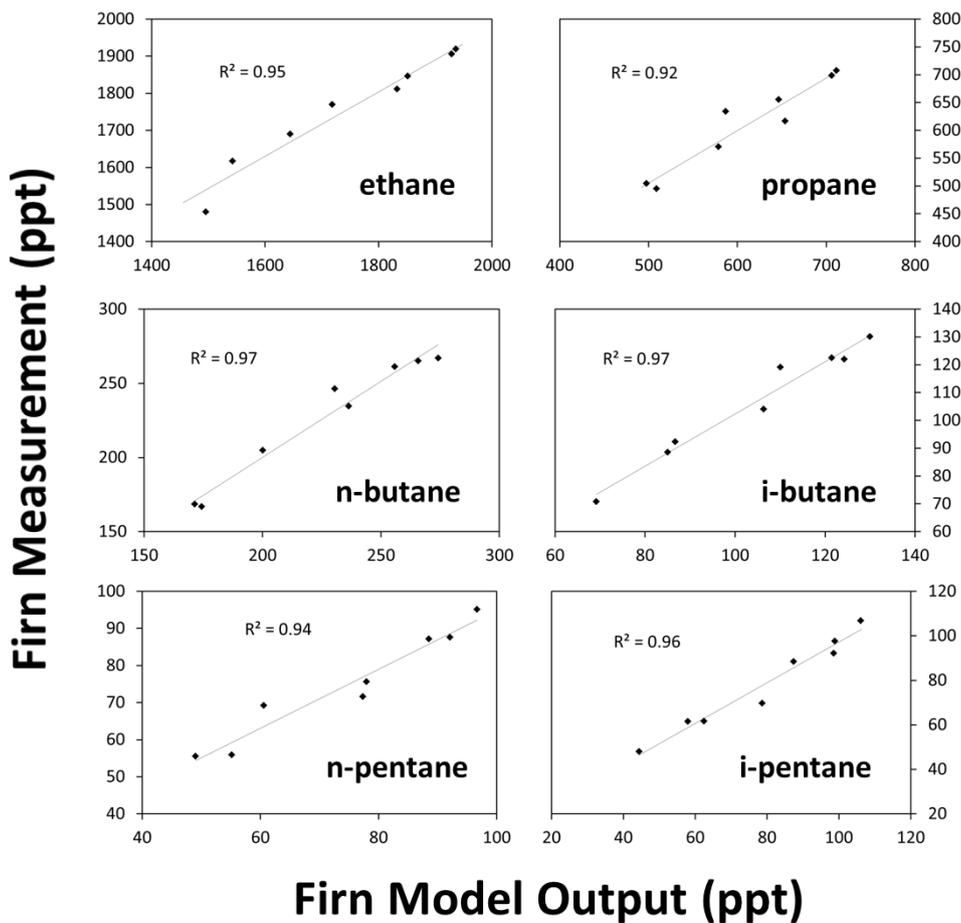
**Figure 5.6** Correlation of firn model output with measurements from the firn for six hydrocarbons.

Figure 5.6 shows that the correlations between the measurements and the model output show a variance of <8% for all six hydrocarbons.

The total uncertainty in the model fits to the firn measurements in Figure 5.3 are calculated as the square root of the sum of the squares of the uncertainties in the precision and calibration of the measurements and the variance of the model-measurement correlation in Figure 5.6. These total uncertainties for the firn profile fits are shown in Table 5.2.

The uncertainty envelopes on the atmospheric scenarios in Figure 5.4 are calculated by combining the total uncertainty in the model fits to the firn profiles (Table 5.2) with the uncertainties in $K_{diff}$ and a 5% uncertainty associated with the firn diffusion profile using the

square root of the sum of the squares to give a total error on the atmospheric scenario for each year.

**Table 5.2** Uncertainties considered for uncertainty ranges on Model fits to firn profiles in Figure 5.3.

| Alkane | Precision Uncertainty, % | Calibration Uncertainty, % | Model-Measurement Correlation, % | Total Uncertainty, % |
|---|---|---|---|---|
| Ethane | 1 | 1 | 5 | 5.2 |
| Propane | 1 | 1 | 8 | 8.1 |
| n-butane | 4 | 3 | 3 | 5.8 |
| iso-butane | 4 | 2 | 3 | 5.4 |
| n-pentane | 6 | 3 | 6 | 9 |
| iso-pentane | 3 | 3 | 4 | 5.8 |

## 5.4 Hydrocarbon Derived Emissions

This section demonstrates the ability of the 2-D atmospheric model to recreate observed alkane mixing ratios. The model is then used to derive northern hemisphere emissions of the alkanes using the atmospheric histories derived in Section 5.2.

### 5.4.1 Atmospheric Modeling of the Alkanes

The main sink for the alkanes in the troposphere is reaction with OH. Their atmospheric lifetimes vary globally with latitude and season. This is because concentrations of the OH radical are dependent on local radiation due to the photochemical nature of its production from the photolysis of ozone. The alkanes also react with atomic chlorine with reaction rates greater than those for reaction with OH but this is not thought to be an important sink for the alkanes globally because of the low mixing ratios of atomic chlorine in the majority of the troposphere – though estimates are still poorly constrained (e.g. von Glasow and Crutzen, 2007; Saiz Lopez and von Glasow, 2012). However the reaction is likely to be important in certain situations, such as during ozone depletion events in the Arctic springtime when high chlorine mixing ratios are observed (e.g. Jobson et al., 1994; Ramacher et al., 1999).

The rate constants used in the model for the reactions of the butanes and pentanes with OH are shown in Table 5.3. They are taken from Atkinson and Arey (2003) (except for that of iso-pentane, from Wilson et al. (2006)) and fit the three parameter expression $k = A.T^n.e^{-B/T}$,

where $k$ is the rate constant, $A$ is the pre-exponential factor, $T$ is the temperature, and $B$ is equal to $E_a / R$, the activation energy.

The lifetimes of n-butane and n-pentane for each latitudinal band and each month were calculated using the 2-D model by labelling the emissions from each band and then dividing the total atmospheric burden of each labelled species by the emissions (Figures 5.7 and 5.8) as shown in Equation 2.3. It is seen that the modeled lifetimes of butanes and pentanes emitted in the tropics are on the order of a few days whereas in the Arctic, during the winter, they can be several weeks. These lifetimes agree well with the range of reported values from the literature, e.g. for n-butane, 5.5 days for summer ($[OH] = 1 \times 10^6$ molecules cm$^{-3}$) and 59 days for winter ($[OH] = 1 \times 10^5$ molecules cm$^{-3}$) (Swanson et al. 2003).

**Table 5.3** Reaction rates of the butanes and pentanes with OH and modeled minimum (August) and maximum (March) lifetimes between 66.4°N and 90°N.

| Alkane | $k_{OH}$ (x10$^{-17}$ cm$^3$ molec$^{-1}$ s$^{-1}$) | $\tau_{OH}$ winter (days)[a] | $\tau_{OH}$ summer (days)[a] |
|---|---|---|---|
| n-butane | $1.81\ T^2\ e^{(114/T)}$ [b] | 61 | 7 |
| iso-butane | $1.17\ T^2\ e^{(213/T)}$ [b] | 62 | 7 |
| n-pentane | $2.52\ T^2\ e^{(158/T)}$ [b] | 51 | 4 |
| iso-pentane | $254\ T^{1.267}\ e^{(15.7/T)}$ [c] | 52 | 4 |

[a] Lifetimes between 66.4°N and 90°N, January (winter) and July (summer)
[b] Atkinson and Arey (2003)
[c] Wilson et al. (2006)
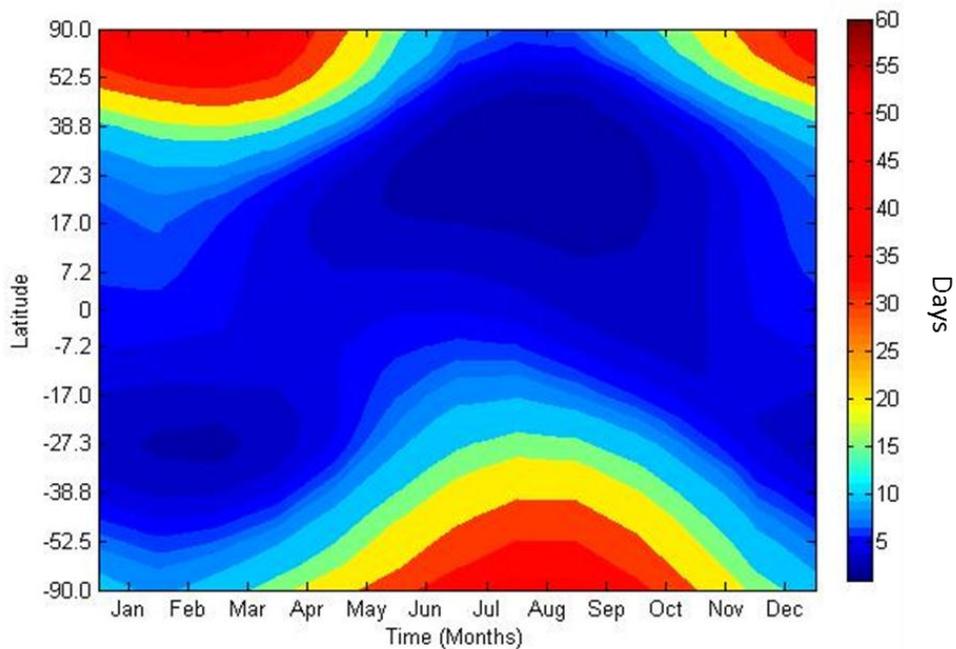
**Figure 5.7** Modeled lifetime (days) of n-butane by latitude and month.
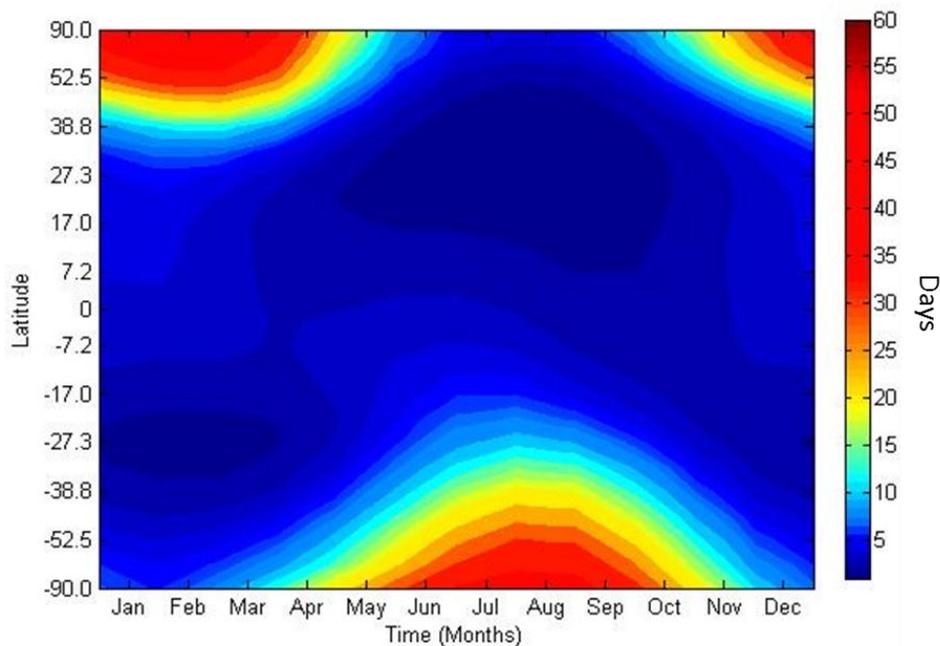


**Figure 5.8** Modeled lifetime (days) of n-pentane by latitude and month.

In order to validate the behaviour of butane and pentane within the atmospheric model measured mixing ratios from three Arctic sites, monitored by NOAA (Helmig et al., 2011), are compared with model output. The Arctic sites used are Alert, Canada (ALT), Barrow,

149

Alaska (BRW) and Summit, Greenland (SUM). The use of three measurement sites for validation also allows an inter-comparison between the measurements at these three Arctic sites, one of which is at the altitude of the Greenland ice sheet.

Latitudinal mixing in the troposphere is fairly rapid, on the order of two to three weeks, and hence leads to similar mixing ratios at a given latitude, particularly during the winter when the lifetimes of the butanes and pentanes are on the order of weeks. This similarity is observed in measurements from Barrow (71.3°N, 156.6°W, Alt. 11m) and Alert (82.5°N, 62.5°W, Alt. 200m) for the period mid-2005 to mid-2010. Figure 5.9 shows a linear correlation of monthly means of the measurements for the two sites from 2009. This correlation gives an R-squared value of 0.88 and a gradient of 0.95. The good correlation suggests that the two Arctic sites have similar sources and the gradient being close to 1 suggests that they are receiving air that has had a similar amount of photochemical processing.
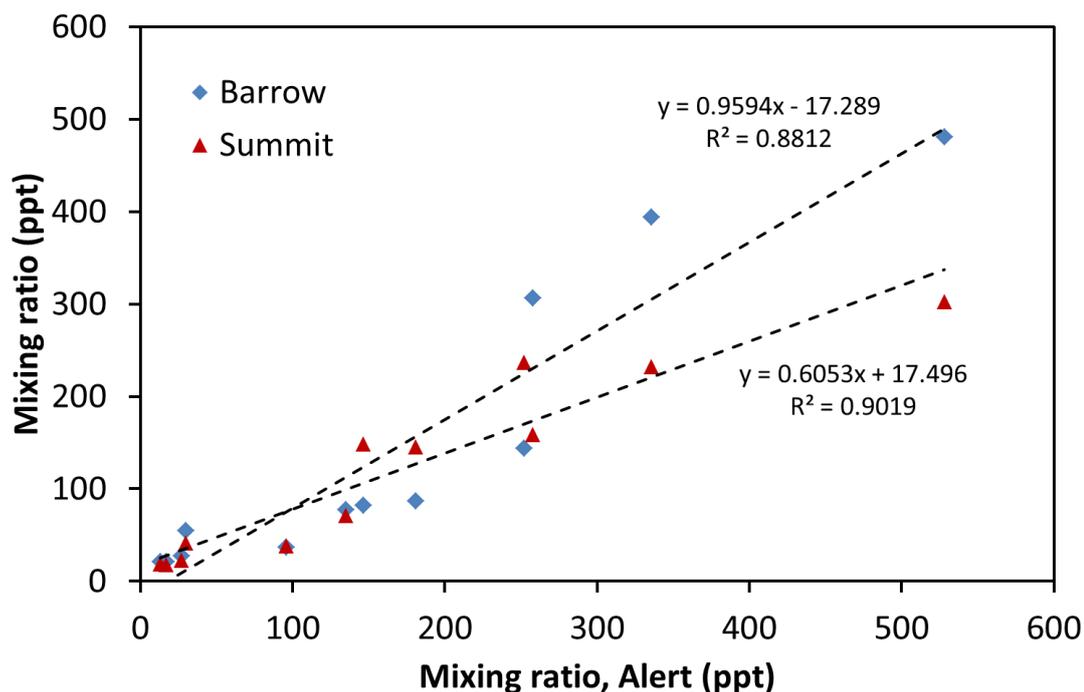


**Figure 5.9** Correlation of monthly means of n-butane data from Barrow (blue diamonds) and Summit (red triangles) against Alert.

Sites at high altitude on the Greenland ice sheet can be influenced by either boundary layer air or free tropospheric air. Swanson et al. (2003) state that the similarities of seasonal alkane profiles at Barrow and Summit (72.58°N, 38.48°W, Alt. 3238m) suggest that Summit can generally be assumed to be "representative of a surface site". A comparison of the Summit data against the Alert data for monthly means during 2009 (Figure 5.9) shows a strong correlation with an R-squared value of 0.90. The gradient of 0.61 confirms the difference in processing of the air received at the two sites. Summit is receiving more aged air with lower mixing ratios of alkanes.

### 5.4.2   Latitudinal Distribution of Alkane Emissions

The latitudinal distribution of emissions used for the alkane modeling is more important to get right than those used for the long lived gases in chapters 4 and 5 because of the short lifetimes of the alkanes. A small emission of alkane from high northern latitudes can have the same effect on Arctic mixing ratios as a large emission from Asia. Similarly the location of emissions of the hydrocarbons is important for the modeled mixing ratios of alkyl nitrates in the Arctic.

The major source of non-methane alkane emissions to the atmosphere is anthropogenic, accounting for more than 98% of emissions of butanes and pentanes, 90% of propane and 75% of ethane (Pozzer et al., 2010). For propane, butane and pentane these emissions come mainly from fossil fuel combustion and evaporative emissions from transport and hence are associated with the major areas of population. Ethane emissions are associated with the production and distribution of natural gas and so may have less of a direct association with major population areas.

In the 2-D atmospheric model the northern hemisphere emissions have been split in to the four regions, North America, Europe, Russia and Asia. These are shown in Figure 5.10. It should be noted that although the North America region appears to have a similar latitudinal distribution to Russia, the majority of the emissions come from the United States, which is at a similar latitude to southern Europe. The specific latitudinal distributions of each region used for the modeling are shown in Figure 5.11.
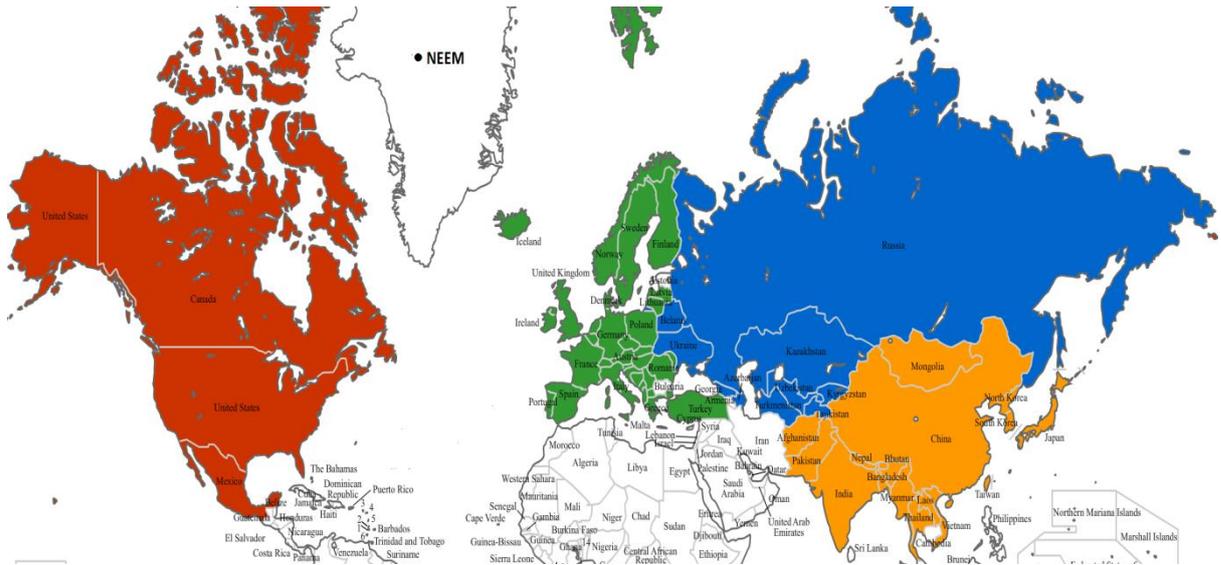
**Figure 5.10** Map showing the four anthropogenic emission regions used in the model. North America (red), Europe (green), Russia (blue), Asia (orange). Also shown is the location of the NEEM site in Greenland.
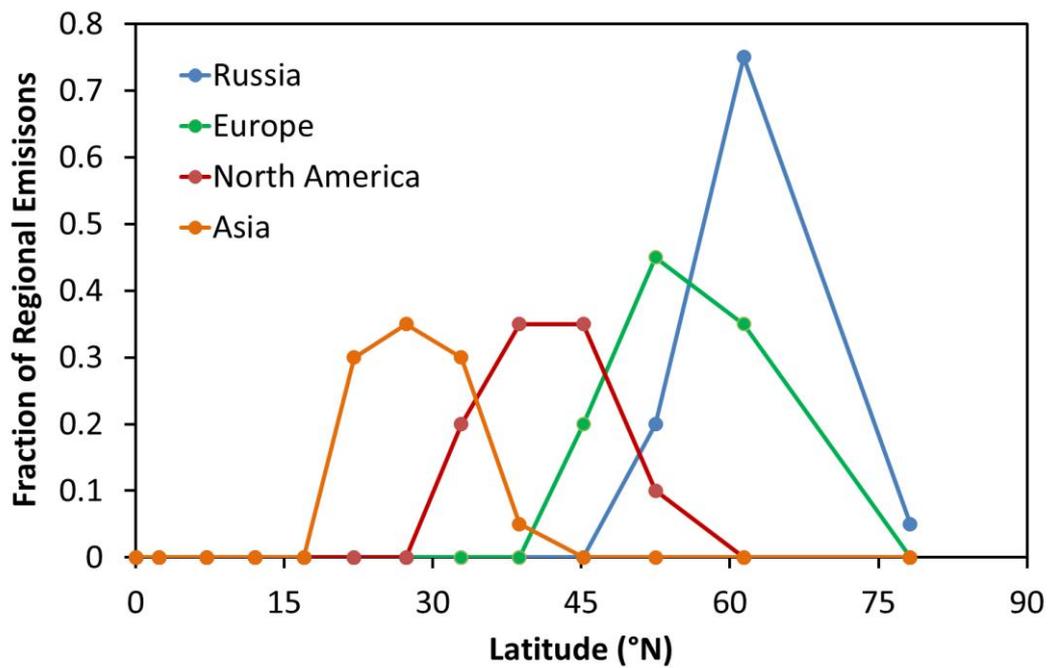


**Figure 5.11** Latitudinal distribution used in the 2-D model for each of the four emission regions shown in Figure 5.10.

Four northern hemisphere emission regions were defined in the model (North America, Europe, Asia and Russia) as described in Chapter 2. The changing emissions distribution with

152

time with respect to each of these regions was inferred from linear fits to the NMVOC emissions reported by EDGAR for the period 1970 – 2008 (Figure 5.12). It is seen that Asian emissions increase from roughly 30 percent of northern hemisphere NMVOC emissions to 60 percent in this period while the contributions from the other three regions all decrease. Using the EDGAR database in this way means that the derived emissions for each region are not independent of EDGAR in relative terms but are independent in terms of the magnitude of the emissions.
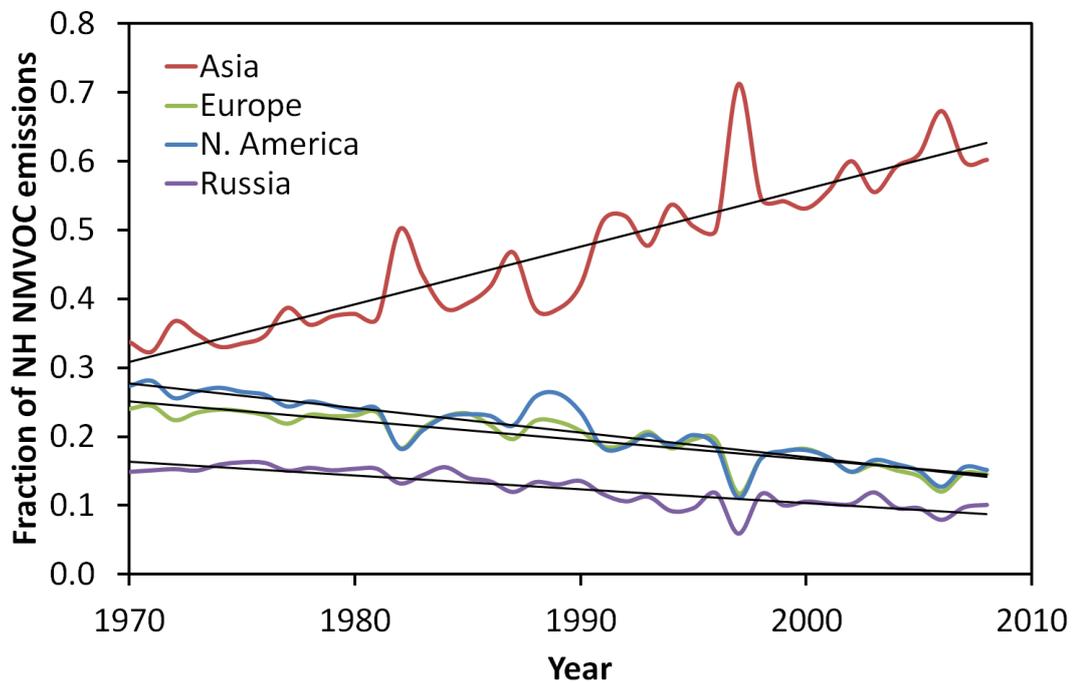


**Figure 5.12** Fraction of total northern hemisphere NMVOC emissions (EDGAR v4.2) for each of the four regions used in the atmospheric modeling. The black lines are linear fits to each data set that were used to scale the total northern hemisphere emissions for each region.
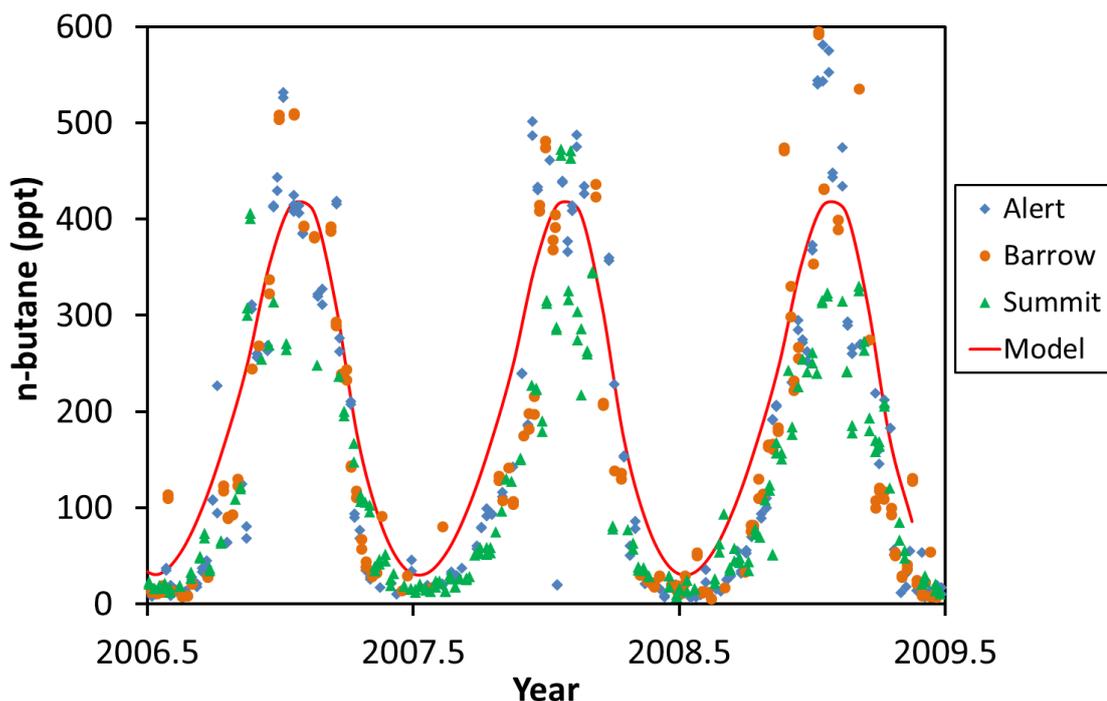
**Figure 5.13** Comparison of observed n-butane mixing ratios at three Arctic sites: Alert, Barrow and Summit (blue diamonds, orange circles, green triangles) (Helmig et al., 2011) and modeled n-butane mixing ratios in the Arctic (red line).

Figure 5.13 shows measurements of n-butane between mid-2005 to mid-2010 from the three Arctic sites: Alert, Barrow and Summit (Helmig et al., 2011). The measurements display clear seasonal cycles with summer minima and winter maxima. The winter maxima are around 400 – 500 ppt and the summer minima are 0 – 15 ppt. It is seen that the observed peak mixing ratios at Summit (a.s.l. 3238 m) are often, but not always, lower than those at Alert and Barrow. This reinforces the theory that Summit is at times receiving the same boundary layer air as is being received at Alert and Barrow and at other times receiving air from the free troposphere which has had a longer processing time.

The northern hemisphere n-butane emissions used to produce the Arctic mixing ratios displayed in Figure 5.13 were fixed so that the modeled annual peak roughly matched that of the measurements. The seasonality of the model output can then be compared to that of the measurements.

The model output for the Arctic is shown as a red line in Figure 5.13. It is seen that the model is capable of recreating the observed seasonality of n-butane to a large extent. However the increase of mixing ratios after the summer minimum appears to begin a little too soon.

154

### 5.4.3 Derivation of Historic Alkane Emission Trends

The 2-D atmospheric model was used to derive global annual emissions of the alkanes constrained by the atmospheric histories derived from firn air measurements from NEEM (Section 5.2). The model was run in the same way as for the long lived species with an annually repeating fixed OH field (the only sink for the alkanes) which gives a global lifetime for methyl chloroform of 6.1 years with respect to reaction with OH (Montzka and Reimann, 2011). The alkane emissions were adjusted using an iterative approach to fit the model output for the Arctic latitude band to the atmospheric histories derived from the firn measurements.

The model run started in 1970 because of the availability of the changing regional emissions distribution from EDGAR (Figure 5.12). The alkane emissions were assumed to show no seasonality as suggested in previous work (Jobson et al., 1994; Poisson et al., 2000). Non-anthropogenic emissions were taken from Pozzer et al. (2010) and assumed to be constant through time. These were 2.8 Tg $a^{-1}$ and 0.9 Tg $a^{-1}$ from biomass burning for ethane and propane respectively, and 0.5 Tg $a^{-1}$ and 0.3 Tg $a^{-1}$ from the oceans. The emissions of the butanes and pentanes were assumed to be 100% anthropogenic (Pozzer et al., 2010). The emissions for each hydrocarbon were then adjusted so that the annually averaged mixing ratios of the model output for the grid box representing the Arctic matched the atmospheric histories derived from the firn measurements in Section 5.2.

Figure 5.14 shows the total northern hemisphere emissions for the six alkanes: ethane, propane, n-butane, iso-butane, n-pentane and iso-pentane derived in this way. Figure 5.XX then shows the emissions of each alkane for each of the four northern hemisphere regions: North America, Europe, Asia and Russia.
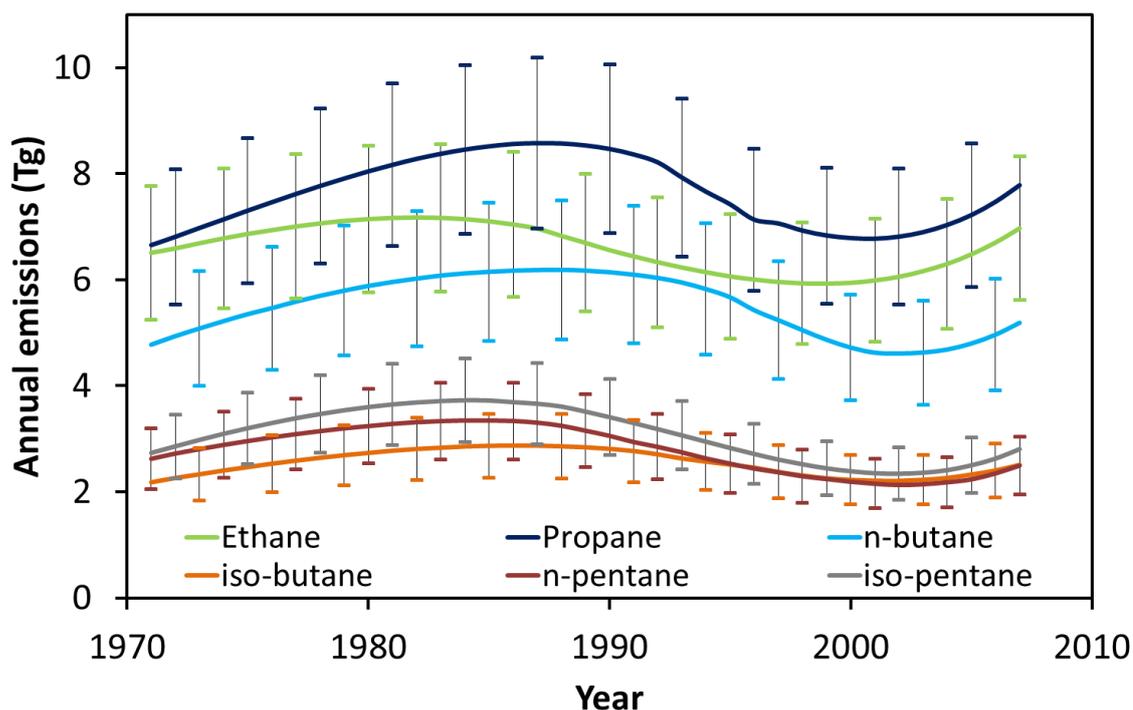
**Figure 5.14.** Total northern hemisphere emissions of six alkanes: ethane, propane, n-butane, iso-butane, n-pentane and iso-pentane derived from atmospheric modeling constrained by NEEM firn air measurements. Uncertainty ranges shown are based on uncertainties in the atmospheric histories derived from the firn, the model transport, and the reaction rates of methyl chloroform with OH and the alkanes with OH, see text.

Figure 5.14 shows that the amount of the alkanes emitted in the northern hemisphere does not change very much between 1970 and 2007, with emissions only varying by about 10% from the levels in 1970. However Figure 5.15 shows that this trend in total northern hemisphere emissions is caused by the increase in emissions from Asia counteracting the large decreases in emissions from North America, Europe and Russia. Asian emissions of all the alkanes roughly doubled between 1970 and 2007, while those of the other three regions fell by about 40% to the early 2000s but have stabilised since this time.

The apparent large increase in emissions from Asia during the 2000s seems unlikely to be real. It is a function of the Arctic mixing ratios (Figure 5.4) stopping their decline and then beginning to increase during this period. Because the fraction of northern hemisphere NMVOC emissions are decreasing in the other three regions during this period (Figure 5.12) any increase in the Arctic mixing ratio calculates a large increase from Asia. As discussed earlier the emissions calculated in this work are based on the assumption that [OH] has not changed significantly during the past 40 years (e.g. Montzka et al., 2011). However it seems

more likely that the increase in Arctic mixing ratios during this period is brought about changes to the sink, i.e. OH. If this were the case then the large increase in Asian emissions in the 2000s would disappear. This possibility is discussed further in Chapter 6.
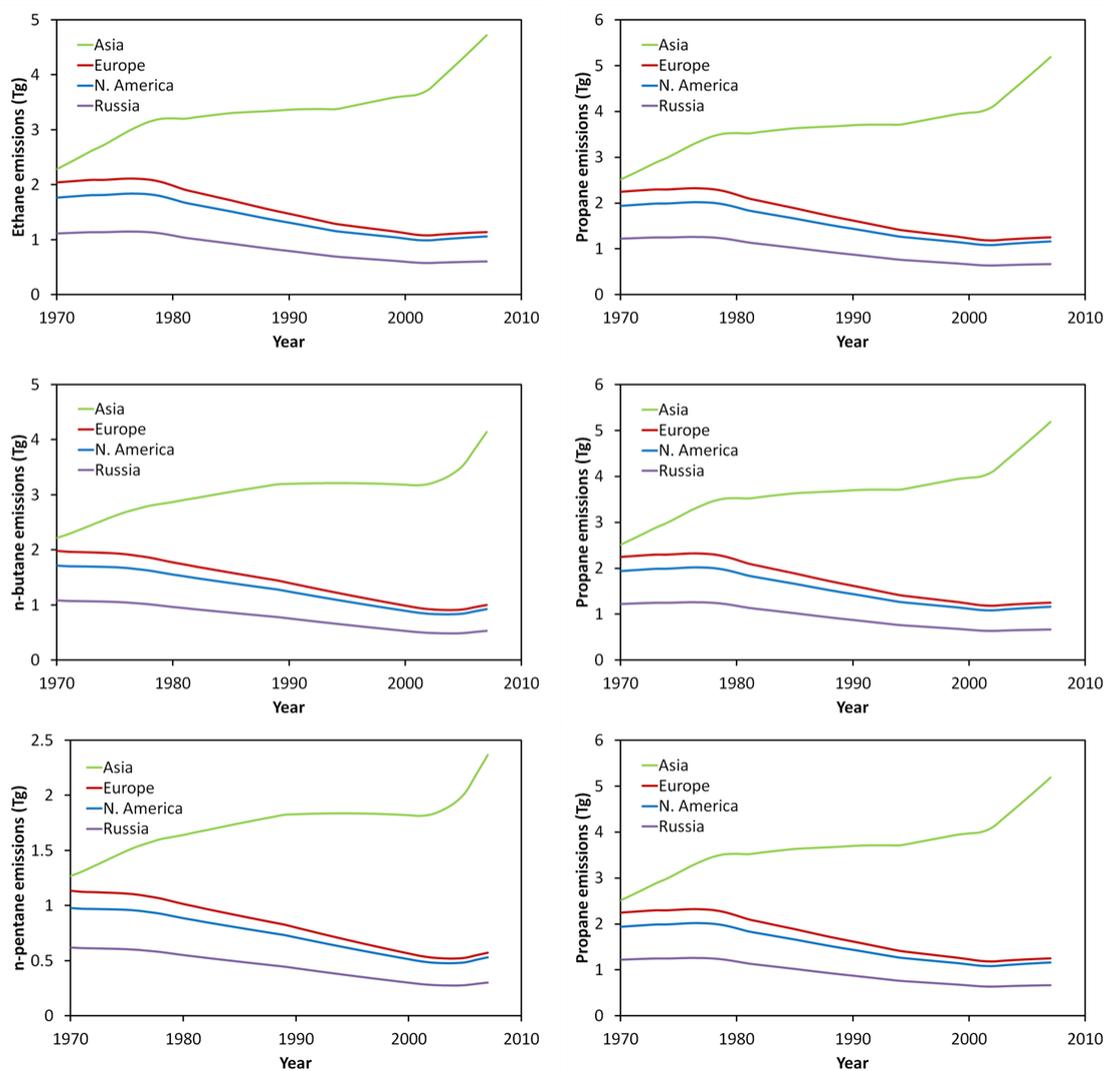


**Figure 5.15** Northern hemisphere alkane emissions by region for the period 1970-2007. Uncertainties associated with the modeled emissions are as for Figure 5.14, i.e. ~ 20% assuming constant OH for the whole model run.

### 5.4.4    Uncertainties in the Alkane Emissions

The emissions of the alkanes shown in Figures 5.14 and 5.15 were derived by fitting the output from the atmospheric model to the derived atmospheric histories (Figure 5.4). The uncertainties shown in Figures 5.14 and 5.15 were calculated based on the uncertainties in the derived atmospheric histories (Figure 5.4), uncertainties in the model transport, taken to be

5% based on tracer experiments recreating northern hemisphere mixing ratios for species with northern hemisphere emissions (Hough, 1989), uncertainties in the reaction rate of methyl chloroform with OH – 15% (Sander et al., 2011) (the global lifetime of methyl chloroform with respect to reaction with OH is used to define the OH field), and uncertainties in the reaction rates of the alkanes with OH – ethane 7%, propane 5%, butanes and pentanes 10% (Atkinson and Arey, 2003). These uncertainties were combined using the square root of the sum of the squares to give a total uncertainty for the emissions which is roughly 20% for all the alkanes.

## 5.5 Hydrocarbon Emission Trends Discussion

### 5.5.1 Comparison to Arctic Measurements

One of the most striking features of the firn air records of the hydrocarbons is the rapid decline in atmospheric mixing ratios since the early 1980s. This has now been observed for many anthropogenically produced hydrocarbons (e.g. Aydin et al., 2011, Worton et al., 2012) associated with oil and gas production and road transport. A contemporaneous decline has been observed for CO (emissions of which are also associated with fossil fuel combustion) in firn air from NEEM (Petrenko et al., 2012).

To validate this trend observed in the firn it would be useful to have a long term trend of atmospheric observations in the Arctic. Such a trend exists with measurements made at the Zeppelin Observatory, Svalbard between 1989 and 1999 (Solberg et al., 1996; Eneroth et al., 2007). This is during the period of declining mixing ratios derived from the Greenland firn air. Figure 5.16 shows the observed trends at Zeppelin for ethane, propane, n-butane and n-pentane and the output of the 2-D atmospheric model for the box representing the Arctic using the emissions derived in Section 5.4.
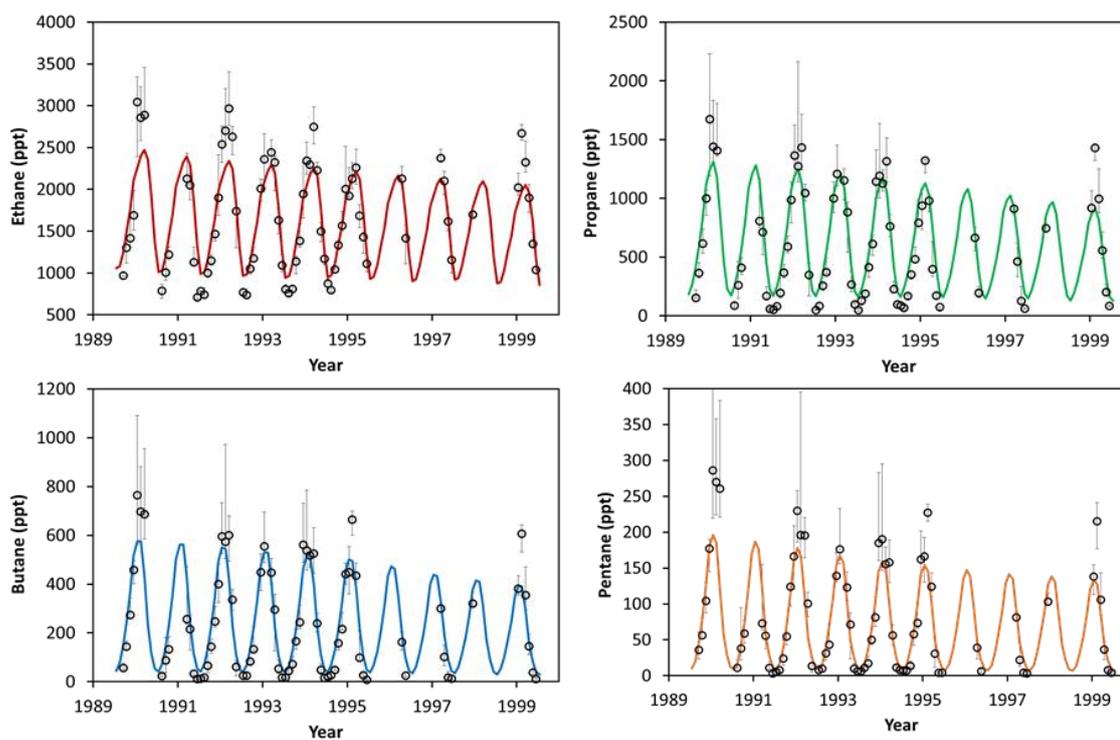
**Figure 5.16** Monthly means of measured mixing ratios of ethane, propane, n-butane and n-pentane at Zeppelin Observatory, Svalbard from 1989 to 1999 (from D. Worton, Solberg et al., 1996). Solid lines are model output using the emissions derived from the Greenland firn air in Section 5.3.

It is seen that the winter time measured mixing ratios of the alkanes shown in Figure 5.16 decline during the record. The model output agrees very well with the measured mixing ratios both in terms of the overall declining trend and in terms of the seasonality of the measurements in the Arctic.

## 5.5.2   Comparison to Bottom-up Emission Estimates

Bottom-up emission estimates of alkane emissions have been made in the past. The estimates of northern hemisphere emissions of the alkanes reported from RETRO (Schultz and Rast, 2007) are shown in Figure 5.17.

159
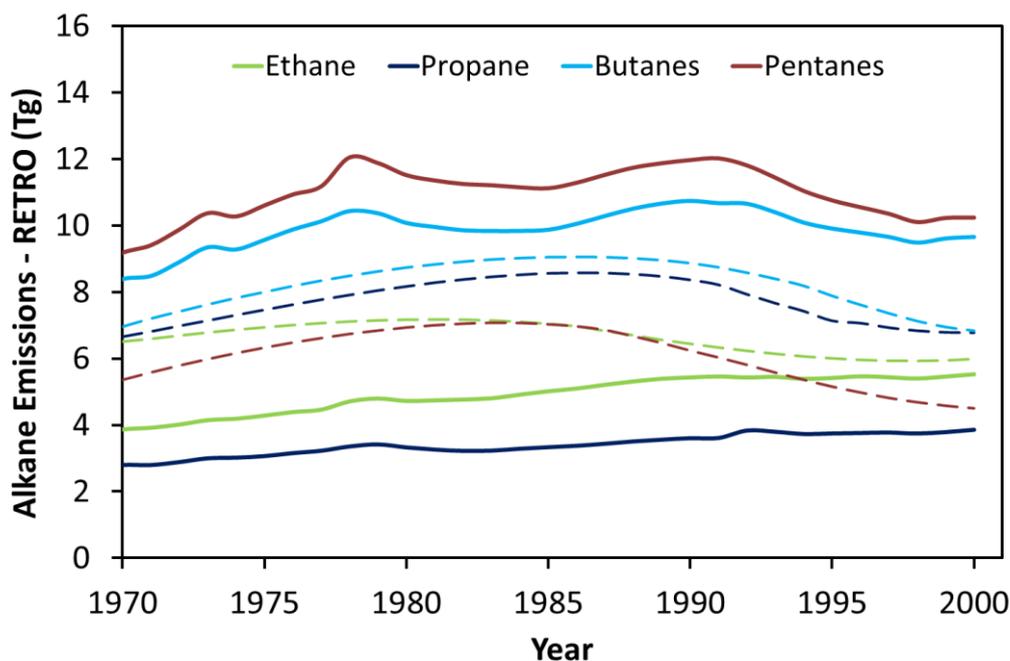
**Figure 5.17** Northern hemisphere annual emission estimates (anthropogenic) of the four alkanes: ethane, propane, butane and pentane from the RETRO project (Worton, 2012; Schultz and Rast, 2007) – solid lines. Also shown are the northern hemisphere anthropogenic annual emission estimates derived from the firn modeling (Figure 5.14) – dashed lines.

It is seen in Figure 5.17 that bottom-up emission estimates show total northern hemisphere alkane emissions not to have varied greatly between 1970 and 2000, in qualitative agreement with the trends derived using the 2-D model (Figure 5.14). However the annual emission estimates from RETRO shown in Figure 5.17 do not show the decline from the late 1970s to the early 2000s that is seen in Figure 5.14. The estimated annual emissions for the butanes from RETRO (9 – 10 Tg) are similar to those derived by the modeling (7 – 8 Tg). Those for the pentanes from RETRO (10 – 12 Tg) are much higher than those from the modeling (~ 6 Tg). While those for ethane and propane from RETRO (4 – 5 & 3 – 4 Tg respectively) are lower than those derived from the modeling (~6 & 7 – 8 Tg respectively). The discrepancy between the propane emissions and the pentane emissions is particularly large. These comparisons are shown in Table 5.4, in which global anthropogenic emission estimates from EDGAR are also given, these can be expected to be reasonably close to northern hemisphere anthropogenic emission estimates since the majority of anthropogenic emissions are in the northern hemisphere.

160

**Table 5.4** Annual emissions derived using the 2-D atmospheric model (uncertainty shown in brackets) and bottom-up estimates from RETRO (Schultz and Rast, 2007) and EDGAR v2.0 (Olivier et al., 1996) and 3.2, fast track (van Aardenne et al., 2005) for year 2000. Model derived emissions and RETRO are just northern hemisphere, EDGAR are global estimates.

| | Northern Hemisphere | | Global Emissions (Tg) |
| Alkane | Annual Emissions, 2000 (Tg) | | |
| | This Work | RETRO | EDGAR, year 2000 |
| --- | --- | --- | --- |
| Ethane | 6.8 (5.5 – 8.1) | 9.6 | 9.2 [a] |
| Propane | 6.8 (5.5 – 8.1) | 3.8 | 10.5 [a] |
| Butanes | 6.0 (4.7 – 7.3) | 5.5 | 14.1 [b] |
| Pentanes | 4.5 (3.5 – 5.5) | 10.2 | 12.3 [b] |

[a] EDGAR v3.2, fast track
[b] EDGAR v2.0

### 5.5.3 Emissions Controls

Figure 5.18, taken from Wallington et al. (2006), shows the emission limits on the emissions of road transport in Europe during the period 1985 to 2010. It is seen that since 1985 emission limits of hydrocarbons and $NO_x$ from gasoline vehicles have fallen by around 99%, while for diesel vehicles $NO_x$ emissions have fallen by almost 90%. Hence even though road vehicle traffic has roughly doubled during this period in both the U.K. (e.g. National Statistics, 2012) and the U.S. (e.g. Federal Highway Administration, 2013), emissions would be expected to have decreased significantly. Considering these decreases one might expect emissions to have fallen even further than observed, however it seems likely that the majority of vehicular emissions of hydrocarbons and $NO_x$ now come from a small number of 'high emitters', engines that have not been properly maintained and so do not conform to the emission limits (Zhang et al., 1995, 1996; Wallington et al., 2006).
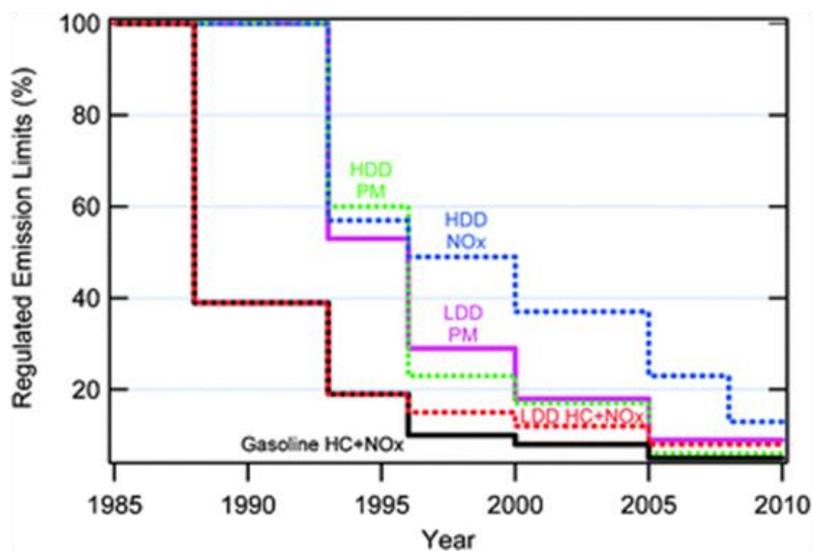
**Figure 5.18** Regulated emission levels *vs* time for European vehicles, normalized to 1985 levels (Wallington et al., 2006).

### 5.5.4   Historic OH Changes

The obvious conclusion to be drawn from the decline in atmospheric mixing ratios of the alkanes observed in the Arctic is that northern hemisphere emissions have declined. However the argument has also been proposed that at least a part of the decline could be caused by changes in the mean concentration of the OH radical in the northern hemisphere. CO is the main sink of the OH radical in the unpolluted atmosphere, accounting for roughly 70% of the OH sink (Wayne, 2006). Hence as CO emissions have decreased (Petrenko et al., 2013), so OH may be expected to have increased which would depress the growth rate of methane and would also depress the atmospheric mixing ratios of other species whose main sink was reaction with the OH radical. Using methyl chloroform (see Section 2.4.5.2 for further details) it has been estimated that northern hemisphere [OH] may have increased by up to 30% between 1979 and 1990 (Prinn et al., 2001). However later work using the same methyl chloroform methodology has suggested that there has been little change to global [OH] in recent years (e.g. Montzka et al., 2011).

If northern hemisphere [OH] varied significantly during the twentieth century then this must be taken into account in the derivation of the alkane emissions using the 2-D atmospheric model. The [OH] field in the model, fixed to give a global lifetime of methyl chloroform with respect to reaction with OH of 6.1 years (Montzka and Reimann et al., 2011), is annually repeating, i.e. there is no inter-annual variability in [OH]. It is recognised that the derived

162

'emission trends' of the alkanes are actually a function of both alkane emissions and northern hemisphere atmospheric OH concentrations. If [OH] has increased between 1980 and 2000 (i.e. when the alkane mixing ratios decrease) that this could explain at least a part of the observed trend in the mixing ratios.

## 5.6 Alkane Source Regions to the Arctic

Another question that can be explored with the 2-D model is 'what is the contribution of each of the four anthropogenic emission regions defined in the model to the observed alkane mixing ratios in the Arctic?' In Section 5.4.3 the historical trend of alkane emissions from each region was derived from measurements in Arctic firn air. However it has also been noted earlier that the relative contribution of each region to mixing ratios observed in the Arctic does not correspond to the relative magnitudes of the emission from each region. This is because of the different distances of each region from the Arctic (as a first order assumption).

The transport time of an air mass from each source region to the Arctic is different and hence the amount of photochemical processing (i.e. the amount of exposure to the sink, OH) of air masses arriving in the Arctic originating from these regions is different. A more processed air mass will have lost a greater proportion of the initial amount of alkane.

This question was investigated using the 2-D model by labelling the n-butane emissions from each region, i.e. treating n-butane from each region as distinct species. In this way, the contribution of each region to the total n-butane mixing ratios in the Arctic can be examined.

**Table 5.5** Relative contributions of the four northern hemisphere source regions to modeled n-butane and 2-butyl nitrate mixing ratios in the Arctic for year 2000.

| Source region | % contribution to total n-butane Arctic mixing ratio year 2000 |
|---|---|
| Russia | 37 |
| Europe | 48 |
| North America | 12 |
| Asia | 4 |

Table 5.5 shows the mean percentage contribution of each of the four regions to the total modeled n-butane mixing ratio in the Arctic during December to February for year 2000. The percentage contributions from Russia and Europe are seen to account for the majority of the modeled Arctic mixing ratios at roughly 40% and 50% respectively. The contribution from North America is roughly 10% while that from Asia is just 4%. Model runs for the period 1970–2008 show that these numbers varied very little over this time.

These regional contributions agree well with a multi-model assessment of transport of pollution to the Arctic by Shindell et al. (2008). Using a 'CO-like' tracer with a lifetime of 50 days, similar to that of butane and pentane in the winter, they concluded that for such a pollutant, "During all seasons, the Arctic surface level is most sensitive to European emissions". In the months December to February they ascribe ~70% of the observed Arctic mixing ratio of the tracer to Europe, ~30% to North America and ~15% to south and east Asia. These are somewhat larger than the figures in Table 5.5. However this is because Shindell et al. did not include Russia as a source region in their simulation because, "its total emissions of most pollutants are comparatively small". While it is seen in Figure 5.XX that emissions of the alkanes in Russia are roughly half of those in Europe and North America, Table 5.5 suggests that the effect that these emissions have on Arctic mixing ratios is very significant. Stohl et al. (2007) also note that the majority of emissions to the Arctic of gaseous pollutants and aerosol with lifetimes less than a few weeks must come from northern Eurasia. This is because in order for isentropic transport to occur the air masses must have the same low potential temperature as the air already trapped in the Arctic (Klonecki et al., 2003). Klonecki et al., also suggest that, at least during the TOPSE campaign, there is a barrier in the lower troposphere around 60° in the winter, mixing ratios of anthropogenic pollutants north of which tend to have been influenced by northern Eurasian emissions and south of which are more likely to have been influenced by North American emissions.

## 5.7   Alkyl Nitrate Firn Profiles

The firn profiles of the alkyl nitrates 2-propyl nitrate, 2-butyl nitrate, 2+3 pentyl nitrates and 3-methyl-2-butyl nitrate are presented in this section. 2-pentyl nitrate and 3-pentyl nitrate are presented together because they co-elute on the chromatogram and the individual contribution of each to the signal cannot be accurately determined. The firn profiles of methyl and ethyl nitrate are presented and discussed separately in Section 5.7.3.

The alkyl nitrate samples from NEEM were taken from the EU hole and were analysed at UEA by Chris Hogan (see Chapter 2.1 − 2.2 for further details).

### 5.7.1  C3 – C5 Alkyl nitrates

Figure 5.19 shows the firn profiles for 2-propyl nitrate, 2-butyl nitrate, 2+3-pentyl nitrates and 3-methyl-2-butyl nitrate. The firn model output, using the atmospheric scenarios shown in Figure 5.20 is presented as a dashed line. The uncertainty envelopes (red solid lines) were calculated by combining the uncertainty in the calibration and precision of the measurements and the variance in the correlation between the measurements and the model output (Figure 5.21), as described for the alkanes in Section 5.3.

The atmospheric histories determined from the firn measurements are shown in Figure 5.20. Also shown are the trends of the alkyl nitrates recently reported by Worton et al. (2012) in firn air from NGRIP, Greenland. The uncertainty envelopes (red dashed lines) are calculated by considering the uncertainty in the model fit to the measurements (Figure 5.21), and the uncertainties in the diffusion coefficients and in the diffusion profile, as described for the alkanes in Section 5.3.
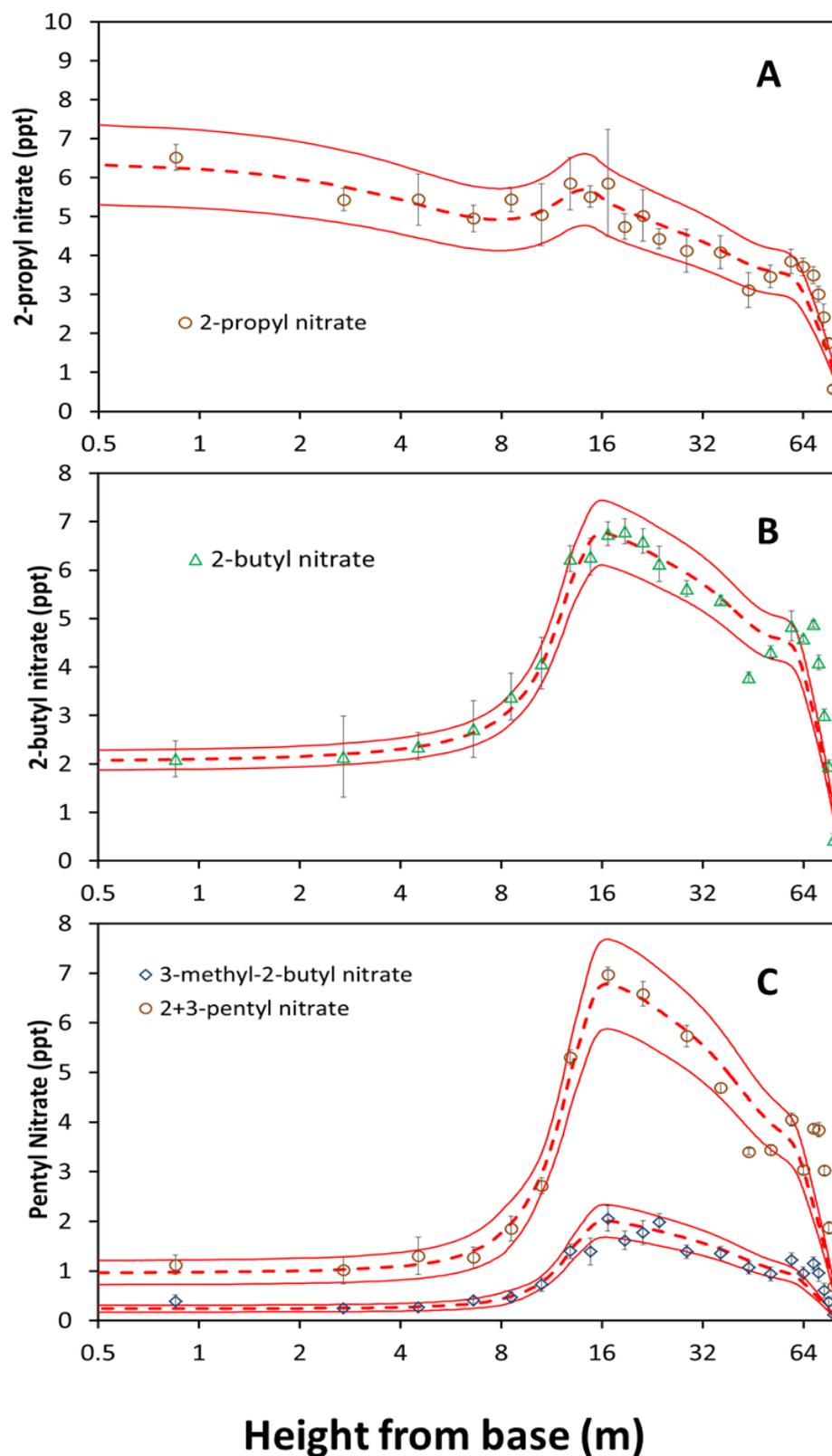
**Figure 5.19** The firn profiles of 2-propyl nitrate (**A**), 2-butyl nitrate (**B**), 2+3-pentyl nitrates (**C**) and 3-methyl-2-butyl nitrate (**C**) measured in firn air from NEEM. The 'best fit' model outputs from the firn model are shown as red dashed lines. The uncertainty ranges are shown as solid red lines.
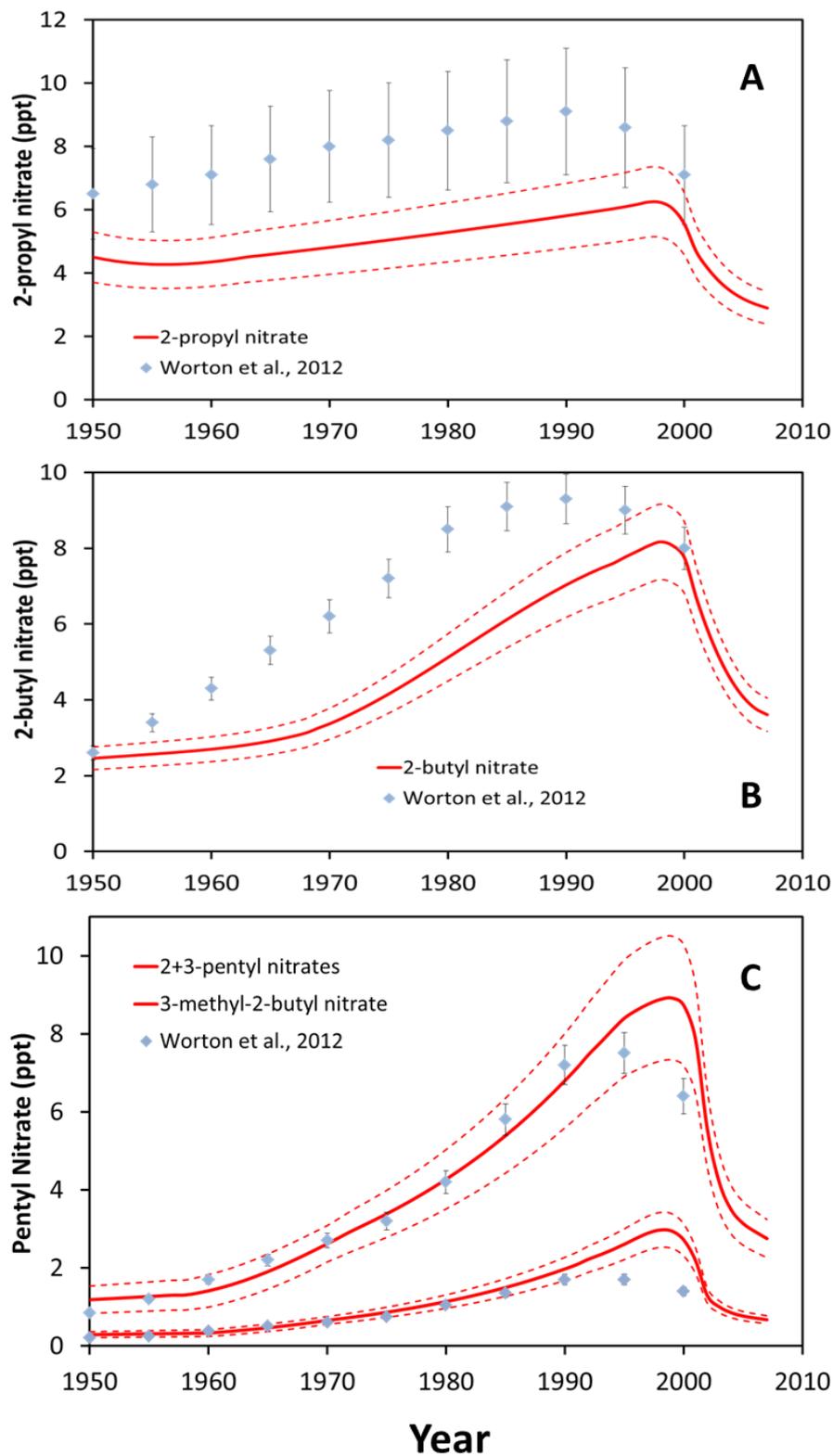
**Figure 5.20** The atmospheric histories of four alkyl nitrates derived from the firn profiles for NEEM shown in Figure 5.19. Also shown are the trends derived from firn air from another Arctic site, NGRIP (Worton et al., 2012). Uncertainty ranges, calculated as described in text, are shown as red dashed lines. **A**: 2-propyl nitrate; **B**: 2-butyl nitrate; **C**: 2+3-pentyl nitrates and 3-methyl-2-butyl nitrate.

The atmospheric scenarios of all four alkyl nitrates shown in Figures 5.20 increase from 1950 to a peak in the late-1990s. They then rapidly decrease back to roughly 1950 levels for the butyl and pentyl nitrates and below 1950 levels for 2-propyl nitrate. The relative size of the increase from 1950 to the mid-1990s peak appears to increase with increasing carbon number (Table 5.6). 2-propyl nitrate increases by a factor of roughly 1.4 between 1950 and the peak, 2-butyl nitrate increases by roughly a factor of 3, and 2+3 pentyl nitrates and 3-methyl-2-butyl nitrate increase by a factor of 7 – 10.

**Table 5.6** Annual mean mixing ratio of alkyl nitrates derived from NEEM firn air. Percentage increase from 1950 to the peak (around 1998).

| Alkyl nitrate | Mean annual mixing ratio (ppt) | | | % increase 1950 – Peak |
|---|---|---|---|---|
| | 1950 | Peak | 2007 | |
| 2-propyl | 4.5 | 6.2 | 2.7 | 38 |
| 2-butyl | 2.5 | 8.2 | 3.4 | 230 |
| 2+3-pentyl | 1.2 | 8.9 | 2.5 | 640 |
| 3-methyl-2-butyl | 0.3 | 3.0 | 0.6 | 900 |

The NEEM firn profile for 2-propyl nitrate displays a growth near the base of the firn. In contrast the butyl and pentyl nitrate profiles display a large increase in mixing ratios from the base of the firn to the peak in the mid-1990s. These differences suggest that there may be some growth of 2-propyl nitrate at depth in firn unrelated to the atmospheric mixing ratios at the time at which the air was trapped in the firn. This is believed to be the case for methyl and ethyl nitrate and is discussed further in Section 5.7.2.

For this reason only the butyl and pentyl nitrates are discussed from this point with reference to their photochemical production and preservation of the atmospheric signal in the firn. However the fact that the growth of mixing ratios at depth in the firn appears to decrease with increasing carbon number suggests that it could be an incremental effect and that perhaps there may also some minimal growth of 2-butyl nitrate at depth in the firn. However the fact that mixing ratios continue to decrease with depth throughout the firn profile for the butyl and pentyl nitrates suggest that this effect is negligible.
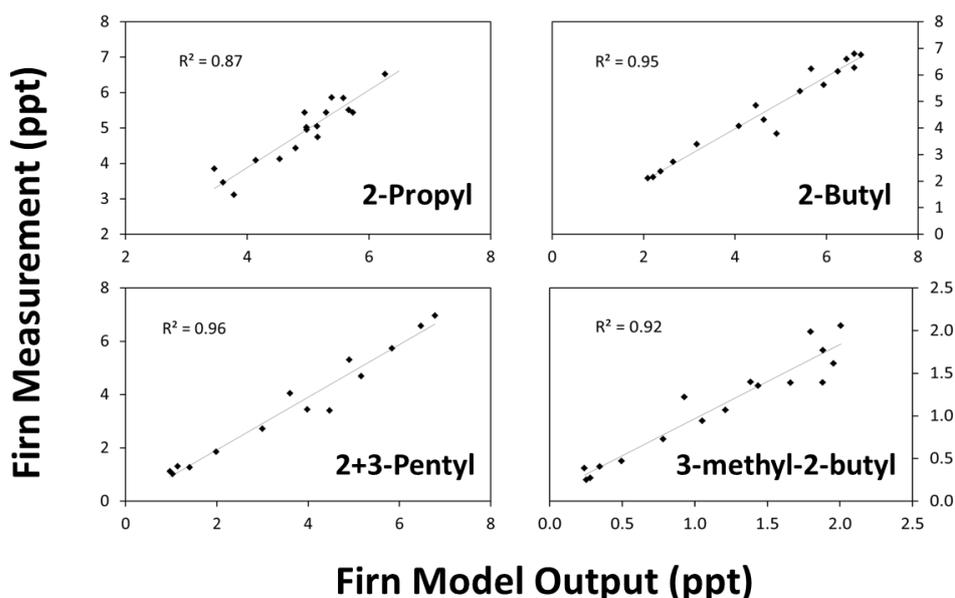
**Figure 5.21** Correlation of firn model output with measurements from the firn for four alkyl nitrates.

### 5.7.2 Methyl and Ethyl Nitrate

The firn profiles of methyl and ethyl nitrate at both NEEM and NGRIP (Worton et al., 2012) show steep increases in measured mixing ratios at depth, methyl nitrate by a factor of $7 - 8$ from present day concentrations and ethyl nitrate by a factor of $4 - 5$. This would suggest that the atmospheric mixing ratios of both species were significantly higher in the past. This is in contrast to the results of the C3 − C5 nitrates. The observed increase of methyl and ethyl nitrates at depth has also previously been reported in another set of firn measurements at the northern hemisphere site Devon Island (McIntyre, 2001), whereas concentrations of both were seen to be relatively constant with depth in firn from two southern hemisphere sites, Dronning Maud Land and Dome Concordia (Worton, 2005). It was proposed by McIntyre (2001) and Worton et al. (2012) that this increase at depth was as a result of in-situ growth within the firn, the source of which is presently unexplained. McIntyre (2001) reports strong correlations for the C1 − C3 alkyl nitrates with the mainly marine derived species methyl bromide ($CH_3Br$) which displays a similar steep growth toward the lock in depth. Worton et al. (2012) report a strong correlation for methyl and ethyl nitrate with methyl iodide.

Worton (2005) suggests that "the presence of OH concentrations on the order of $10^6$ molecules cm$^{-3}$ in sunlit firn (Beyersdorf et al., 2004)" and in-situ production of $NO_x$ from the photolysis of nitrate in the snowpack (Dibb et al., 2002; Honrath et al., 1999) could "provide the necessary components for alkyl nitrate production" within the snowpack. Additionally Swanson et al. (2002) observe elevated levels of alkyl nitrates (as well as methyl bromide, methyl iodide, ethene and propene) in the surface firn at Summit, Greenland in the summer to a depth of between $0 - 1.5$ m, generally about 50% greater than measured atmospheric mixing ratios and those measured below 1.5 m. However photochemistry near the surface of the firn does not seem to be a mechanism that should affect the deep firn and lead to the observed profiles of methyl and ethyl nitrate. A process occurring at the base of the firn is required to explain the observed perturbation at depth.

However, while there is a factor of $5 - 6$ difference between the observed concentrations of methyl and ethyl nitrate near the lock in zone at North GRIP and Devon Island, the observed concentrations at North GRIP and NEEM are similar. The deepest measured mixing ratios of methyl nitrate are 46 and 38 ppt for North GRIP and NEEM respectively, while for ethyl nitrate they are 15 and 17 ppt respectively. This surprising similarity presents the possibility that the records may in fact be a true representation of the atmospheric histories of the two species. For this reason firn modeling for the two species was performed and the derived atmospheric scenarios are shown in Figure 5.22. (Atmospheric scenarios for methyl and ethyl nitrate were not presented in Worton et al. (2012)).
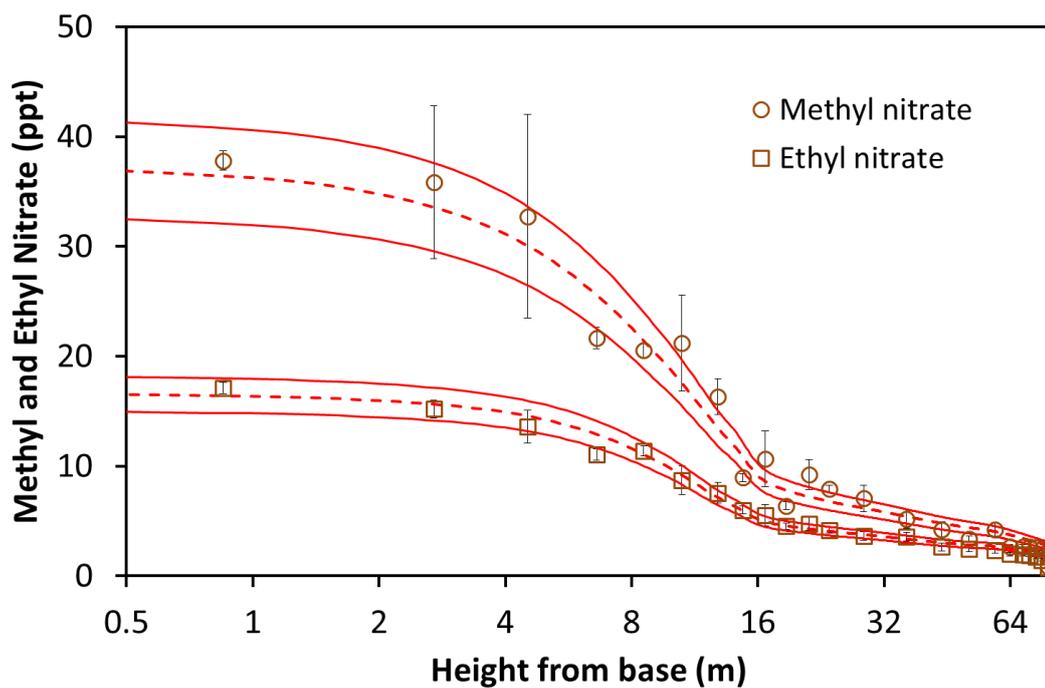
**Figure 5.22** The firn profiles methyl and ethyl nitrate measured in firn air from NEEM (measurements in brown). The 'best fit' model outputs from the firn model are shown as a red dashed line. The uncertainty ranges are shown as solid red lines.
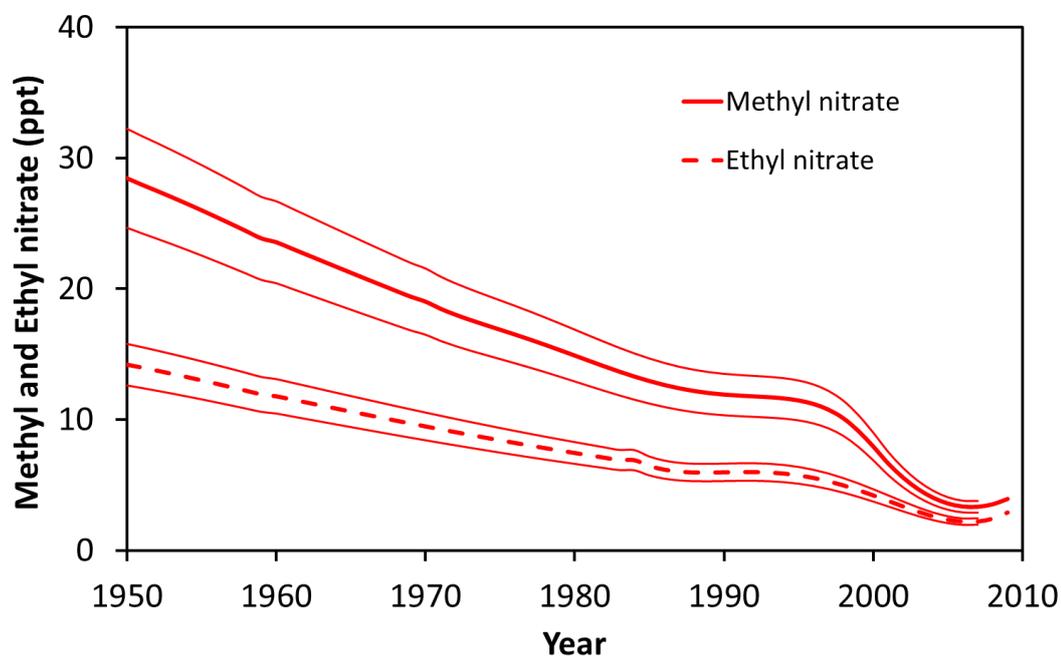


**Figure 5.23** The atmospheric histories of methyl and ethyl nitrate derived from the firn profiles for NEEM shown in Figure 5.22. Uncertainty ranges, calculated as described in text, are shown as red solid lines.
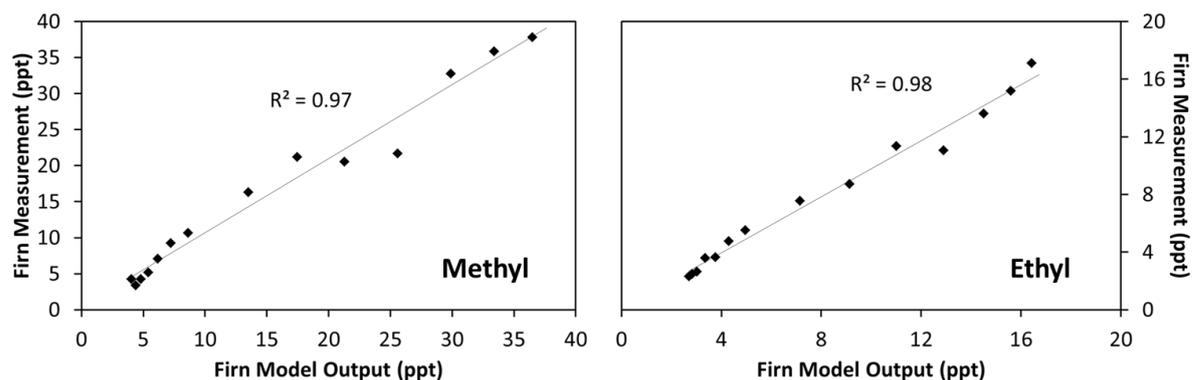
**Figure 5.24** Correlation of firn model output with measurements from the firn for methyl and ethyl nitrate.

The atmospheric history of methyl nitrate shown in Figure 5.23 begins around 30 ppt in 1950 and then declines steadily to a mixing ratio of about 15 ppt in 1990. The decrease stops for a few years and then begins again in the mid-late 1990s falling to about 5 ppt. Ethyl nitrate displays a similar trend beginning at around 15 − 20 ppt in 1950, falling steadily to mixing ratios of about 2 − 3 ppt with a brief plateau in the early 1990s. The mixing ratios of methyl and ethyl nitrate derived for the year 1998 (about 12 and 6 ppt respectively) are somewhat higher than the mean annual mixing ratios measured by Swanson et al. (2003) at Summit in 1998, 4.0 and 4.2 ppt respectively. This would again suggest that the mixing ratios observed in the firn may be being influenced by growth within the firn in addition to the atmospheric signal.

Whether the trend could represent a true atmospheric history of these species is considered below.

There are several reasons to expect that the behaviour of photo-chemically produced methyl and ethyl nitrate may be different to the higher alkyl nitrates. Firstly, methane and ethane are present year round at all latitudes because of their slow reaction rates with OH with methane having a seasonal amplitude of only 25% (Swanson et al., 2003), this is in contrast to the >C2 alkanes for which mixing ratios in the Arctic fall to near zero in the summer because of their short lifetimes (Swanson et al., 2003). Consequently there is likely to be in-situ production of methyl and ethyl nitrates in the Arctic in the summer. This has been confirmed by observations of methyl nitrate mixing ratios in the Arctic, which show little intra-annual variability (Swanson et al. 2003).

Secondly the main loss process of methyl and ethyl nitrate is by photolysis whereas for the >C2 alkyl nitrates it is by reaction with OH. Consequently while changes in [OH] affect both the production rate of the peroxy radical and the loss rate of the alkyl nitrate for the >C2 nitrates, for methyl and ethyl nitrate only the production rate of the peroxy radical is affected. Also changes to photolysis will affect the loss rate of methyl and ethyl nitrate but not the higher alkyl nitrates.

Thirdly, the <C4 nitrates have been reported to have possible direct emission sources from the oceans (e.g. Atlas et al., 1993; Chuck et al., 2002; Blake et al., 2003; Dahl et al., 2005), and from biomass burning (e.g. Friedli et al., 2001; Simpson et al., 2002).

Fourthly, the methyl peroxy radical is present at much higher mixing ratios than the peroxy radicals of the other alkanes (e.g. Madronich and Calvert, 1990), which affect the chemistry with $NO_x$ and with other peroxy radicals.

Finally, methyl nitrate can be produced in the atmosphere by the alternative pathway $RO + NO_2$ (Reaction 1.10) in highly polluted environments ($NO_2 > \sim 40$ ppb) (e.g. Archibald et al., 2007).

However none of these differences seem to give a reason for methyl and ethyl nitrate to have been present in the atmosphere at higher mixing ratios in the middle of the twentieth century than at its close. The observed trend in methyl nitrate mixing ratios with time would require either a decrease in the sources (i.e. atmospheric methane mixing ratios or those of the OH radical) or a large increase in the sinks (i.e. the photolysis rate or OH) in the past. Atmospheric methane has increased by roughly 60% since 1950 (e.g. Etheridge et al., 1998; Dlugokencky et al., 2012). The OH radical has almost certainly not increased by a factor of 5 − 6 in this time frame. It seems unlikely that $NO_x$ was much higher in 1950 (e.g. EDGAR v4.2) as would be required to have increased production via the $RO + NO_2$ pathway. Therefore the only possible reason for higher mixing ratios of methyl nitrate in the past would seem to be a reduced loss rate to photolysis.

Photolysis in the troposphere is dependent on two parameters, the incident solar flux and the attenuation of that flux, as shown in Section 2.3. The solar flux at the top of the atmosphere does not vary greatly over such a relatively short time period, though there was a reported increase of the solar constant by roughly 2 $Wm^{-2}$ during the $20^{th}$ century (Lean et al., 2005). Hence the only reason for reduced photolysis would appear to be increased attenuation of the

solar flux in Earth's atmosphere. This could be caused by greater amounts of black and organic carbon in the troposphere. Ice core records from North GRIP show that the black carbon being deposited on the ice sheet from northern hemisphere industrial emissions peaked around 1910 and remained high until a large decrease around 1950 (McConnell et al., 2007). The effects of carbonaceous aerosol on photolysis has been studied in Asia (Tang et al., 2003) China and the US, Mexico City (Li et al., 2011) and has been shown to reduce photolysis values by up to 40%. It may be expected that a large proportion of the carbonaceous aerosol would be fairly short lived in the atmosphere, however its effect on secondary pollutants could be high since it likely has been co-emitted and so will be entrained in the same air masses as these pollutants.

Consequently it appears that the growth at depth cannot be explained by atmospheric processes alone and that processes within the snowpack must be considered the cause. The similarities of the records at the two sites, NEEM and North GRIP may just be a coincidence perhaps brought about by similarities in the conditions at the two sites.

### 5.7.3   Atmospheric Modeling of Alkyl Nitrates

The 2-D model was run with a fixed $NO_x$ field taken from results of a full chemistry run with model by Hough and Johnson (1990). This allows the simulation of alkyl nitrate production, transport and loss following alkane oxidation in the model.

The main sinks for the alkyl nitrates in the troposphere are reaction with OH and photolysis. For the <C3 alkyl nitrates photolysis is the most important sink whereas for the >C3 alkyl nitrates the main sink is reaction with OH. The reaction with chlorine atoms may also play a role in some circumstances as it does with the alkanes.

The reaction rates of the alkyl nitrates with OH are taken from Atkinson and Arey (2003) and shown in Table 5.7. The temperature dependent absorption cross sections used for the calculation of the photolysis rates of 2-butyl nitrate are based on data from IUPAC (Atkinson et al. 2006) and those for the pentyl nitrates are based on a least squares fit to the data from Roberts and Fajer (1989) of the form $\sigma = e(a\lambda^2 + b\lambda + c)$, where $\sigma$ is the absorption cross section and $\lambda$ is the wavelength. The photolysis rates for $48.6 - 56.4°N$ for the middle of July using these data are shown in Table 5.7.

**Table 5.7** Reaction rates of C4 – C5 alkyl nitrates with OH, modeled photolysis rates at 48.6 – 56.4°N and peak summer and winter lifetimes at 66.4 - 90°N with respect to reaction with OH.

| Alkyl Nitrate | $k_{OH}$ (x10$^{12}$ cm$^3$ molec$^{-1}$ s$^{-1}$) (298K) [a] | $j$ (x10$^7$ s$^{-1}$) | Winter OH lifetimes (days) | Summer OH lifetimes (days) |
|---|---|---|---|---|
| 2C4 | 0.86 | 3.58 [c] | 80 | 15 |
| 2+3C5 | 1.35 [b] | 26 [c] | 69 | 12 |
| 3M2C4 | 1.7 | 26 [d] | 64 | 8 |

[a] Atkinson and Arey (2003).
[b] A combination of $k_{OH}$ 2-pentyl (1.0x10$^{12}$) and 3-pentyl (1.7x10$^{12}$) nitrates.
[c] Based on the absorption cross sections from Atkinson et al. (2006) (2C4) and Roberts and Fajer (1989) (2+3C5). Rates were calculated using the photolysis stream used in the 2-D model. Values are winter means for 48.6 – 56.4°N.
[d] No data available, used that of 2-pentyl nitrate.

The lifetimes of the butyl and pentyl nitrates were calculated for each latitudinal band and each month (Figures 5.25 and 5.26) by emitting labelled emissions (i.e. considering emissions from each latitude as a different species) directly into each latitudinal band, and dividing the emissions by the total atmospheric burden. It is seen that the lifetimes of the C4 – C5 alkyl nitrates in the tropics are on the order of 10 – 15 days for 2-butyl nitrate and 5 – 10 days for 2-pentyl nitrate. In the Arctic, during the winter, the lifetimes can be several weeks and in the summer about 10 days. The modeled high latitude summer lifetimes and the tropical lifetimes show a good agreement with those reported by Clemitshaw et al. (1997); the modeled high latitude winter lifetimes are rather shorter than those reported.
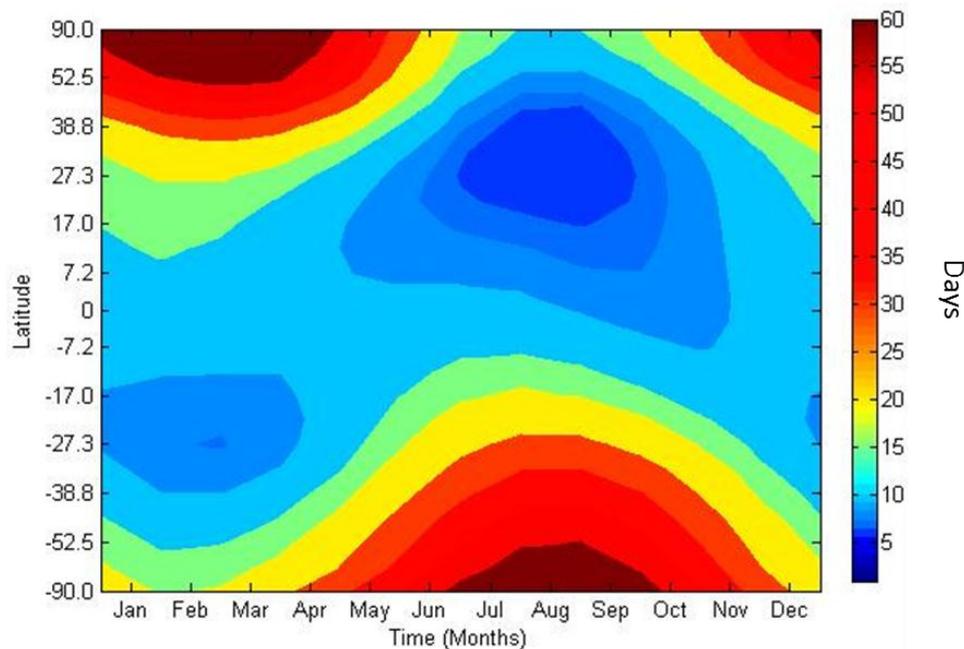
**Figure 5.25** Modeled lifetime (days) of 2-butyl nitrate by latitude and month.
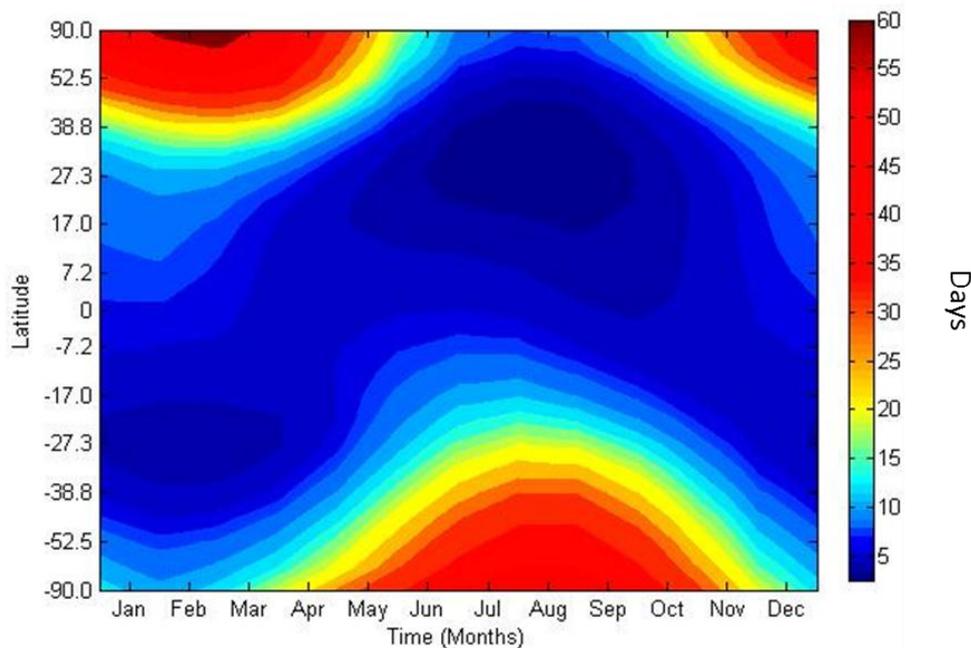


**Figure 5.26** Modeled lifetime (days) of 2-pentyl nitrate by latitude and month.

To validate the alkyl nitrate chemistry in the chemical mechanism of the model, measurements of alkyl nitrates in the Arctic are compared to the model output. Few such measurement datasets exist. Figure 5.27 shows monthly means from a year's measurements of 2-butyl nitrate at Summit during the year 1997 - 1998 by Swanson et al. (2003) compared to

176

the model output for the same year for 2-butyl nitrate. Also shown is the model output for n-butane for comparison to the alkyl nitrate.
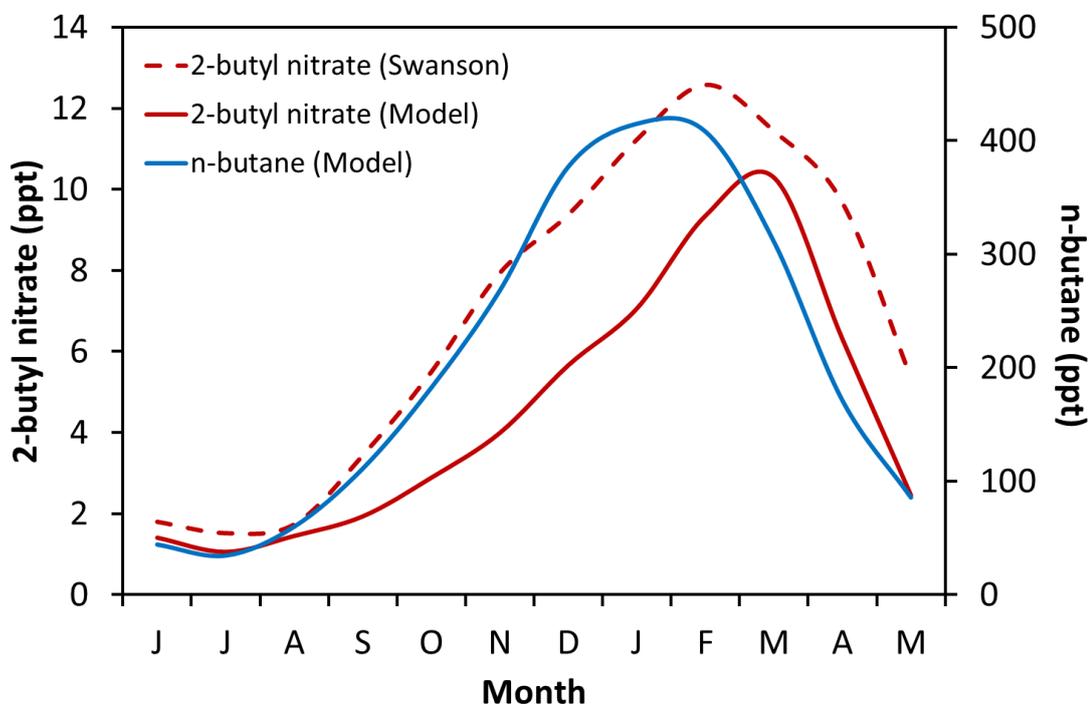


**Figure 5.27** Seasonal cycle of modeled Arctic mixing ratios of n-butane (blue solid, right axis) and 2- butyl nitrate (red solid, left axis). Measured 2-butyl nitrate by Swanson et al. (2003) at Summit, Greenland, from 1997 – 1998 (red dash, left axis).

Figure 5.22 shows the model output for a year for the 2-butyl nitrate mixing ratios in the Arctic. It is seen that the 2-butyl nitrate in the Arctic follows a similar trend to that of n-butane, though with a slightly later peak. The model is seen to recreate both the measured seasonality of the alkyl nitrate, and the peak mixing ratio, reasonably well. The model shows the seasonal cycle of 2-butyl nitrate mixing ratios lagging those of the parent alkane by about a month with n-butane peaking in February and 2-butyl peaking in March. This is in reasonable agreement with the observations of Swanson et al. (2003) at Summit though they see both n-butane (not shown in Figure 5.25) and 2-butyl nitrate peaking a few weeks earlier. The modeled peak concentrations of 2-butyl nitrate (~10.5 ppt) are a little lower than observed by Swanson et al. (2003) (~13 ppt), whereas the modeled n-butane mixing ratios are slightly higher (450 ppt) compared to the observations (about 420 ppt). The modeled

minimum mixing ratio again agrees well with the observations both in timing (July) and in magnitude, 1 ppt and ~1.5 ppt respectively.

## 5.8   Alkyl Nitrate Source Regions to the Arctic

The butyl and pentyl nitrates are assumed to have insignificant emission sources and to be almost entirely secondary oxidation products of butane and pentane. In considering the question of what has caused the observed historical trends in the alkyl nitrates it must be established where the majority of production of the alkyl nitrates is taking place.

The measurements of the alkyl nitrates in the firn air from Greenland are representative of the annual means of the mixing ratios in the Arctic. There seems to be three main possibilities as to where the alkyl nitrates were produced:

(i)      The alkyl nitrates are mainly formed in-situ in the Arctic by the reaction of transported alkanes and $NO_x$ that has been transported by reservoir species.

(ii)     The alkyl nitrates are largely formed close to the source regions of the alkanes and $NO_x$ and are subsequently transported to the Arctic.

(iii)    The alkyl nitrates are formed during transport of air masses from source regions to the Arctic.

These possibilities are explored in the following sections.

### 5.8.1   In-situ Production of Alkyl Nitrates in the Arctic

The 2-D atmospheric model was used to investigate this question. The model was run with the 2-butyl nitrate produced within the model box representing the Arctic labelled separately to the 2-butyl nitrate produced in the rest of the model domain. This allowed an investigation of the changing regions of production of the alkyl nitrates within the model throughout the year.

178
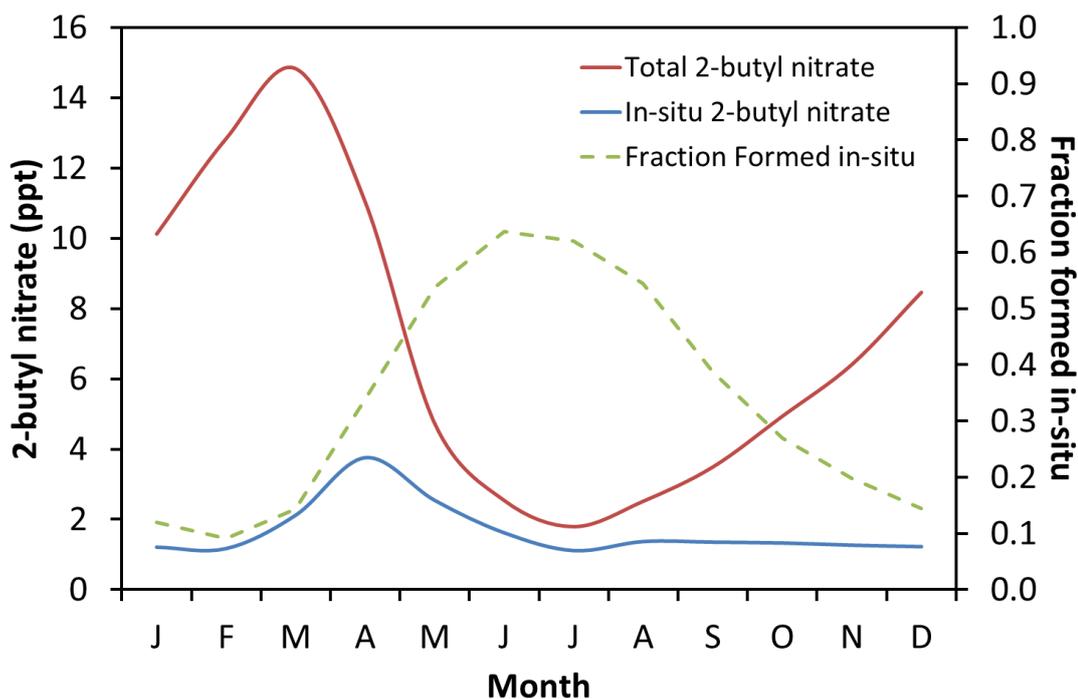
**Figure 5.28**  A comparison of the modeled contribution of 2-butyl nitrate produced in-situ (right axis) to the total 2-butyl nitrate (left axis) modeled in the Arctic.

In Figure 5.28 it is seen that during the winter months the contribution of 2-butyl nitrate formed in-situ in the Arctic to the total modeled mixing ratio is around 10%, whereas in the summer it peaks at about 65%. The absolute contribution of 2-butyl nitrate produced in the Arctic remains fairly constant through the year with the exception of a peak during the months March to May, it is the contribution from air transported from outside the Arctic for which large changes are seen.

The reason for the low in-situ alkyl nitrate production in the winter in the Arctic is the absence of sunlight. This leads to very low mixing ratios of the two precursors to the alkyl nitrate, the peroxy radical and the NO radical. The lack of sunlight prevents the photochemical production of OH and so, even though there is a high n-butane mixing ratio, very few peroxy radicals are produced by n-butane oxidation. NO and $NO_2$ exist in a state of equilibrium which is dependent on the very fast inter-conversion of the two species. In the Arctic winter time this equilibrium is skewed completely toward $NO_2$ because the conversion pathway back to NO via photolysis does not exist. The $NO_2$ is lost (mainly by $N_2O_5$ hydrolysis in the winter (Stroud et al., 2003)) thus removing $NO_x$ from the system leading to

very low observed mixing ratios of both NO and $NO_2$ in the Arctic winter (e.g. Beine et al., 2002).

During the months March to May it is seen that mixing ratios of the alkyl nitrate produced in-situ in the Arctic increase by a factor of 3 – 4. The explanation for this is presumably a peak in the production of alkyl peroxy radicals. This is brought about by the return of sunlight increasing mixing ratios of the OH radical (and atomic chlorine during ozone depletion events, though this mechanism is not present in the model). The large amount of n-butane present during the winter is then rapidly oxidised to alkyl peroxy radicals which react with the NO, now also present, to form the alkyl nitrate. The mixing ratios of NO and OH will peak in mid-summer, with the peak in photolysis, but in-situ production of alkyl nitrates is low because mixing ratios of the pre-cursor alkanes ($\geq$C3) are very low.

The reason that the contribution from in-situ production is high relative to that from production outside of the Arctic during the summer is that alkyl nitrates have a lifetime on the order of a few days in the summer (see Table 5.7). So alkyl nitrates produced in more southerly regions are rapidly lost, due to reaction with OH and photolysis, before they can be transported to the Arctic.

So in summary, during the winter months, during which alkyl nitrate mixing ratios peak and hence which contribute most to the annual averages observed in the firn, the alkyl nitrates present in the Arctic are almost entirely from transport of air from regions outside of the Arctic in which there is still sunlight to drive production of OH and hence create peroxy radicals and to allow photolysis of $NO_2$ to NO. The lifetimes of both n-butane and 2-butyl nitrate are on the order of 2 months during northern hemisphere winter and so both have time to be transported to the Arctic from the source regions.

### 5.8.2   Source Region Production of Alkyl Nitrates

Having determined that the most important contribution to the observed annual mean mixing ratios of the alkyl nitrates is from production in regions outside of the Arctic, the next question is what is the contribution of each of the four anthropogenic emission regions defined in the model? In Section 5.6 it was shown that the majority of the observed alkane mixing ratios in the winter time in the Arctic could be attributed to emissions from Europe

and Russia. It would be expected, since the alkyl nitrates are oxidation products of the alkanes, that the source regions would be similar.

This question was investigated using the 2-D model by labelling the n-butane emissions from each region as in Section 5.6 and also the 2-butyl nitrate which was formed from these labelled emissions. In this way, the contribution of each region to the total 2-butyl nitrate mixing ratios was examined.

**Table 5.8** Relative contributions of the four northern hemisphere source regions to modeled 2-butyl nitrate mixing ratios in the Arctic for year 2000.

| n-butane source region | % contribution to total 2-butyl nitrate Arctic mixing ratio year 2000 |
| --- | --- |
| Russia | 26 |
| Europe | 44 |
| North America | 19 |
| Asia | 11 |

Table 5.8 shows the mean percentage contribution of each of the four regions to the modeled total 2-butyl nitrate mixing ratio in the Arctic during December to February for year 2000. It is seen that Europe, as with n-butane, is still the region with the greatest effect on Arctic mixing ratios, Russia has a lower effect on alkyl nitrate mixing ratios (~30%) than on n-butane mixing ratios (~40%), North America has a significantly greater influence on 2-butyl nitrate (~20%) to n-butane mixing ratios (~10%) and the influence of Asia increases throughout the record more significantly than it does for n-butane, from roughly 5% in 1970 to 13% in 2008.

## 5.9   Comparison of Alkyl Nitrates with Hydrocarbons

Long term atmospheric histories of both the alkanes and the alkyl nitrates at the NEEM site have been derived so far in this chapter. The alkanes all have reasonably similar atmospheric histories to each other and the C4 – C5 alkyl nitrates also have similar histories to each other. In this Section the trends of the alkanes are compared to those of the alkyl nitrates.

It is seen in Figure 5.29, in which the atmospheric histories of butane and 2-butyl nitrate are plotted together, that although both species increase to a peak from 1950 mixing ratios and

then decline again, the timing of the peak is different for the alkyl nitrate and the alkane. This relationship has been shown to hold for the >C2 alkanes and associated alkyl nitrates in Section 5.2 and 5.7. This suggests that atmospheric alkyl nitrate mixing ratios are not directly related to atmospheric hydrocarbon mixing ratios. The difference in the timing of the peak of the parent hydrocarbon and daughter alkyl nitrate has been noted before at North GRIP by Worton et al. (2012), in which it was interpreted as representing a change in northern hemisphere $NO_x$ atmospheric mixing ratios and by inference $NO_x$ emissions.

Since alkyl nitrates are formed from the reaction of alkyl peroxy radicals (formed from reaction of alkanes with OH) with $NO_x$ it seems reasonable to say that if the alkyl nitrate mixing ratios are not varying linearly with their parent hydrocarbon (when both have the same sink, reaction with OH) that this must be caused by changes in either atmospheric OH or $NO_x$ concentrations.
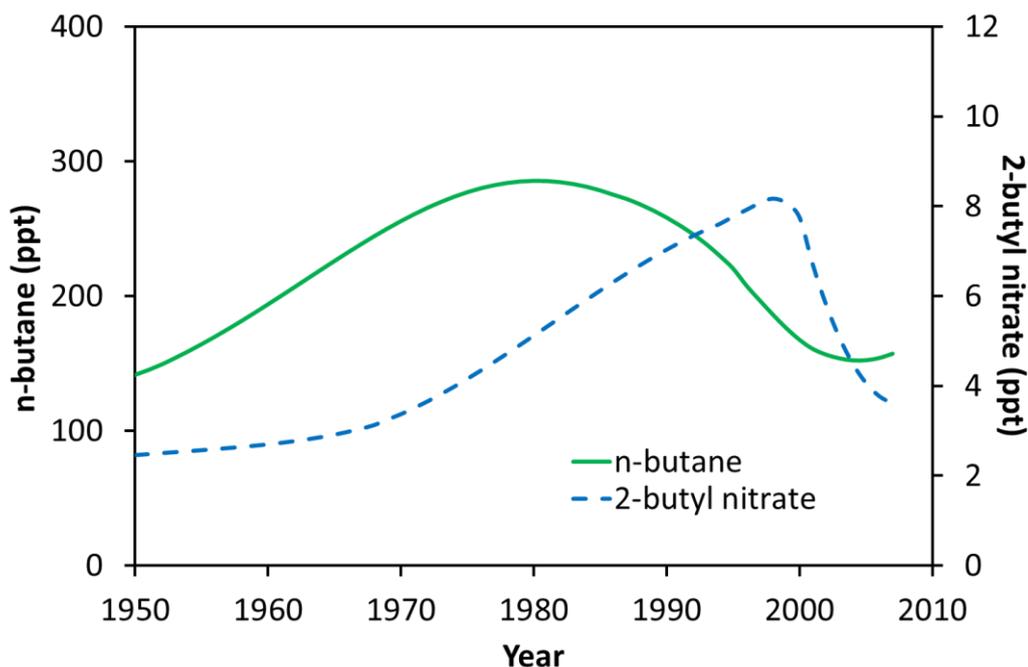


**Figure 5.29** Comparison of the atmospheric histories of the annual mean Arctic mixing ratios of n-butane and 2-butyl nitrate at NEEM.

A time series of the ratios of each parent-daughter pair of alkanes and alkyl nitrates can be plotted using the atmospheric histories of each derived in Sections 5.2 and 5.7. Plotting these ratios effectively de-trends the data removing the effect of the change in the mixing ratios of the alkane, leaving just the other effects, i.e. changing atmospheric [NO] or [OH]. These are

shown in Figure 5.30 for the three pairs: n-butane and 2-butyl nitrate, n-pentane and 2+3-pentyl nitrate and iso-pentane and 3-methyl-2-butyl nitrate.
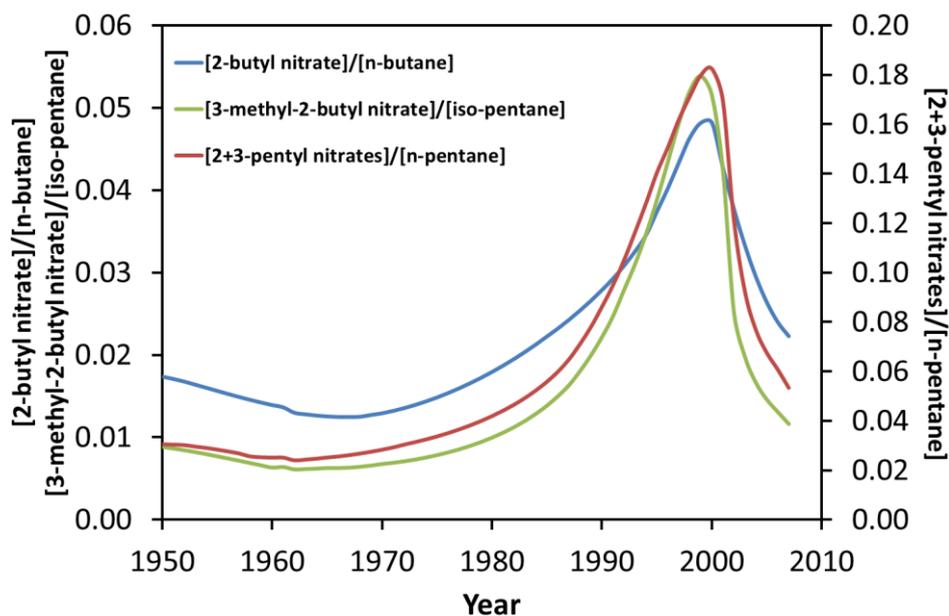


**Figure 5.30** Ratios of the three alkane-alkyl nitrate pairs: n-butane and 2-butyl nitrate, n-pentane and 2+3-pentyl nitrate, and iso-pentane and 3-methyl-2-butyl nitrate derived from NEEM firn air.

In Figure 5.30 it is seen that the ratios of the three alkane-alkyl nitrate pairs remain fairly stable up to about 1975, after which all three begin to increase up to a peak in the late-1990s and then decreases again to roughly pre-1975 values. These changes are shown in Table 5.9. It is seen that the ratio [2-butyl nitrate]/[n-butane] increases by about a factor of 3 between 1975 and the peak, whereas those of [2+3-pentyl nitrates]/[n-pentane] and [3-methyl-2-butyl nitrate]/[iso-pentane] increase by roughly a factor of 5 – 7.

**Table 5.9** Annual mean ratio of alkyl nitrates to parent alkanes derived from NEEM firn air. Percentage increase from 1975 to the peak (late-1990s).

| Ratio | 1975 | Peak | 2007 | % increase 1975 –peak |
|---|---|---|---|---|
| [2-butyl nitrate]/[n-butane] | 0.015 | 0.048 | 0.022 | 220 |
| [2+3-pentyl nitrates]/[n-pentane] | 0.034 | 0.18 | 0.053 | 430 |
| [3-methyl-2-butyl nitrate]/[iso-pentane] | 0.008 | 0.053 | 0.012 | 560 |

## 5.10 Conclusions from Firn Modeling

In this chapter a forward firn model was used to derive atmospheric histories of six alkanes and six alkyl nitrates from measurements in firn air from the NEEM site, Greenland. The 2-D atmospheric model was used to derive northern hemisphere emissions of the six alkanes. Some general conclusions from this chapter are listed below.

(i)  The alkanes all have similar atmospheric histories with mixing ratios increasing from 1950 to a peak around 1980 (except for ethane which peaks around 1970) and subsequently falling back to roughly 1950 levels by 2008.

(ii)  The relative size of the change from 1950 to the peak increases with increasing carbon number.

(iii)  The majority (>80%) of the measured n-butane mixing ratios in the Arctic in winter-time originate in either Europe or Russia (rather than North America or Asia). About 70% of the measured 2-butyl nitrate mixing ratios in the Arctic in winter-time are produced from n-butane originating in Europe or Russia.

(iv)  Emissions of all of the alkanes from Europe, North America and Russia roughly halved between 1970 and 2000 (assuming mean annual OH concentrations have not changed during this period). However total northern hemisphere emissions have changed little during this period because of increasing emissions from Asia.

(v) The atmospheric histories of the butyl and pentyl nitrates look similar with low mixing ratios from 1950 – 1970 which then increase rapidly several fold to a peak in the late-1990s before rapidly declining to 2008. 2-propyl nitrate has a peak in the late-1990s but also appears to increase again in the early part of the record.

(vi) The relative size of the increase of mixing ratios from 1970 to the peak in the late-1990s increases with increasing carbon number for the propyl – pentyl nitrates.

(vii) The measured mixing ratios of methyl and ethyl nitrate increase with depth in the firn suggesting that atmospheric mixing ratios have steadily decreased with time. This seems unlikely and the measurements are attributed to post-depositional processes. However it cannot be discounted that the trends are real and the chemistry is not fully understood.

(viii) The atmospheric histories of the alkanes and the alkyl nitrates do not show contemporaneous peaks. Since the butyl and pentyl nitrates are assumed to be almost entirely secondary oxidation products of the butanes and pentanes, the observed histories suggest that one of the other species involved in alkyl nitrate formation (or destruction), i.e. $NO_x$ or OH, have changed significantly during this period and are largely controlling the atmospheric alkyl nitrate mixing ratios.

# Chapter 6

# Historical Trends of OH and NO$_x$ in the Atmosphere

# 6 Historical Trends of OH and NO$_x$ in the Atmosphere

This chapter will use the atmospheric histories of the alkanes and alkyl nitrates derived in Chapter 5 to derive trends in atmospheric concentrations of the OH radical and NO$_x$ over the past sixty years.

First a steady state analysis of the alkane-alkyl nitrate system is explored in order to consider the behaviour of the system in background air. A series of studies using a box model examine the dependencies of alkyl nitrate mixing ratios and the [alkyl nitrate]/[alkane] ratio on OH and NO concentrations and on the [NO]/[HO$_2$] ratio in the system at steady state.

The alkane-alkyl nitrate system is then explored in terms of production of the alkyl nitrates within a pollution plume. A series of studies using a box model, representing a Lagrangian study of an air mass, again examine the dependencies of alkyl nitrate mixing ratios and the [alkyl nitrate]/[alkane] ratio on OH and NO concentrations as well as considering the role of aldehydes in the air mass and production of methyl nitrate via the alternative RO$_2$ + NO$_2$ pathway.

The atmospheric histories of the hydrocarbons derived in Chapter 5 are used in a photochemical clock to determine the photochemical age of the air that is being measured in the Arctic. The atmospheric histories of the alkyl nitrates are then used in an alternative photochemical clock. From these studies a historical trend in the photochemical age of air at NEEM is determined and interpreted as a semi-quantitative historical trend in concentrations of the OH radical in the northern hemisphere. This trend is compared to other studies and to the trend in the growth rate of atmospheric methane to see if the [OH] trend is evident in the records of other atmospheric species.

Finally the [OH] trend is combined with the atmospheric histories of the alkanes and the alkyl nitrates and with the understanding of the alkane-alkyl nitrate system derived from the box modeling studies in this chapter to examine the relative contributions of changes in [OH] and changes in [NO$_x$] to the observed alkane and alkyl nitrate trends. From this analysis a qualitative historical trend in northern hemisphere atmospheric NO$_x$ concentrations is derived.

## 6.1 Alkyl Nitrate Production in Background Air

6.1.1 Steady State Analysis

In the background atmosphere the photochemical production and loss of the alkyl nitrates can be thought of as a system in steady state. This photochemical production is described by Reactions 6.1 – 6.5.

$$RH + OH \xrightarrow{\alpha_1, O_2} RO_2 \qquad\qquad k_1 \qquad\qquad\qquad (R6.1)$$

$$RO_2 + NO \xrightarrow{\alpha_3} RONO_2 \qquad\qquad k_3 \qquad\qquad\qquad (R6.2a)$$

$$\xrightarrow{1-\alpha_3} RO + NO_2 \qquad\qquad k_3 \qquad\qquad\qquad (R6.2b)$$

$$RO_2 + HO_2 \rightarrow ROOH \qquad\qquad k_4 \qquad\qquad\qquad (R6.3)$$

$$RONO_2 + h\nu \rightarrow products \qquad\qquad j_6 \qquad\qquad\qquad (R6.4)$$

$$RONO_2 + OH \rightarrow products \qquad\qquad k_7 \qquad\qquad\qquad (R6.5)$$
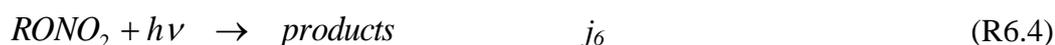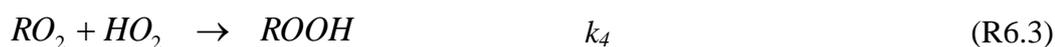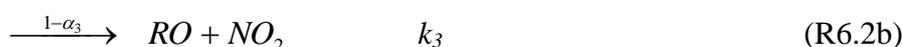
Using Equations 6.1 – 6.6 an expression can be derived to describe the system shown in Reactions 6.1 – 6.5 in terms of the observed ratio of the alkyl nitrate to the parent hydrocarbon (Equation 6.7). This steady state analysis is shown below. The assumption is made that $k_3$ [NO] and $k_4$ [HO$_2$] $\gg k_5$ [R'O$_2$], where R'O$_2$ here represents all other organic peroxy radicals. It is also assumed that $k_7$ [OH] $> j_6$, this is the case for the >C3 alkyl nitrates.

$$\frac{d[RH]}{dt} = -k_1[RH][OH] \qquad\qquad\qquad (E6.1)$$

$$\frac{d[RO_2]}{dt} = k_1\alpha_1[RH][OH] - (k_3[RO_2][NO] + k_4[RO_2][HO_2]) = 0 \qquad (E6.2)$$

$$\frac{d[RONO_2]}{dt} = k_3\alpha_3[RO_2][NO] - k_7[RONO_2][OH] = 0 \qquad\qquad (E6.3)$$

Rearranging Equation 6.2,

$$[RO_2] = \left( \frac{k_1\alpha_1[RH][OH]}{k_3[NO]+k_4[HO_2]} \right) \qquad \text{(E6.4)}$$

Substituting Equation 6.4 into Equation 6.3 to remove [RO$_2$],

$$k_7[RONO_2][OH] = k_3\alpha_3[NO]\left( \frac{k_1\alpha_1[RH][OH]}{k_3[NO]+k_4[HO_2]} \right) \qquad \text{(E6.5)}$$

$$[RONO_2] = \frac{k_3\alpha_3[NO]}{k_7[OH]}\left( \frac{k_1\alpha_1[RH][OH]}{k_3[NO]+k_4[HO_2]} \right) \qquad \text{(E6.6)}$$

$$\frac{[RONO_2]}{[RH]} = \frac{k_1\alpha_1k_3\alpha_3[NO]}{k_7(k_3[NO]+k_4[HO_2])} \qquad \text{(E6.7)}$$

Equation 6.7 shows that at steady state, and presuming the hydrocarbon to be constant, the mixing ratio of the alkyl nitrate is dependent on the atmospheric mixing ratios of NO and HO$_2$.

Using Equation 6.7 and the atmospheric histories of the alkanes and the alkyl nitrates derived from the firn measurements, an attempt can be made to quantify past changes in the NO and HO$_2$ in the atmosphere of the northern hemisphere. The equation can be rearranged to give Equation 6.8 in which the terms on the right hand side are all constants except for the ratio of the hydrocarbon to the alkyl nitrate.

$$\frac{[NO]}{[HO_2]} = \frac{k_4k_7}{k_3(k_1\alpha_1k_3\alpha_3 \dfrac{[RH]}{[RONO_2]} - k_7)} \qquad \text{(E6.8)}$$

A time series of the ratio [NO]/[HO$_2$] can be plotted by using the derived histories of the alkanes and alkyl nitrates. This is shown in Figure 6.1. The rate constants and branching ratios used for the calculations are shown in Table 6.1. A similar method was adopted in Worton et al. (2012) except that in that work [HO$_2$] was assumed to be constant with time and the changes were interpreted as reflecting changes in northern hemisphere NO$_x$ mixing ratios and, by implication, emissions. However there seems to be no reason that atmospheric HO$_2$ mixing ratios may not have changed; the main source of the HO$_2$ radical is the oxidation of CO, emissions of which in Europe, North America and Russia are thought to have roughly halved since 1980 (EDGAR v4.2).

**Table 6.1** Rate constants and branching ratios used in the calculations of the [NO]/[HO$_2$] ratio (Figure 6.1).

| Alkyl nitrate | Rate constants (x10$^{12}$ cm$^3$ molecule$^{-1}$ s$^{-1}$) (298K) | | | | Branching ratios [c] | |
|---|---|---|---|---|---|---|
| | $k_1$ [a] | $k_3$ [b] | $k_4$ [b] | $k_7$ [a] | $\alpha_1$ | $\alpha_3$ |
| **2-butyl** | 2.36 | 5.0 | 1.42 | 0.86 | 0.873 | 0.09 |
| **2+3 pentyl** | 3.80 | 3.5 | 1.60 | 1.47 | 0.917 | 0.130 |
| **3-methyl-2-butyl** | 3.65 | 3.5 | 1.60 | 1.7 | 0.297 | 0.141 |

[a] Values are for 298K from Atkinson and Arey (2003)
[b] Values from recommended fits to measured data (Jenkin et al., 1997)
[c] Values from Master Chemical Mechanism (MCM) v3.2 (mcm.leeds.ac.uk/MCM) in 2012

Figure 6.1 shows the [NO]/[HO$_2$] ratio derived from three alkane-alkyl nitrate pairs at NEEM. There is a good agreement between the trends calculated at the two sites. There is also a good agreement between the two pairs derived from the pentanes at NEEM. However the absolute values of [NO]/[HO$_2$] calculated from n-butane and 2-butyl nitrate are different to those from the pentanes. The [NO]/[HO$_2$] ratio calculated from the n-butane–2-butyl nitrate pair begins around 0.2 and remains around this value until about 1975 at which time it begins to increase up to a maximum value of about 0.8 in the late-1990s. The ratio then declines back to pre-1975 values by 2007. The [NO]/[HO$_2$] ratio derived in this way from n-pentane–2+3-pentyl nitrate and iso-pentane–3-methyl-2-butyl nitrate pairs begins around 0.5 between 1950 and

1975 and then increases up to a peak of 6.5 – 7 in the late-1990s before decreasing back to around 0.3 by 2007.
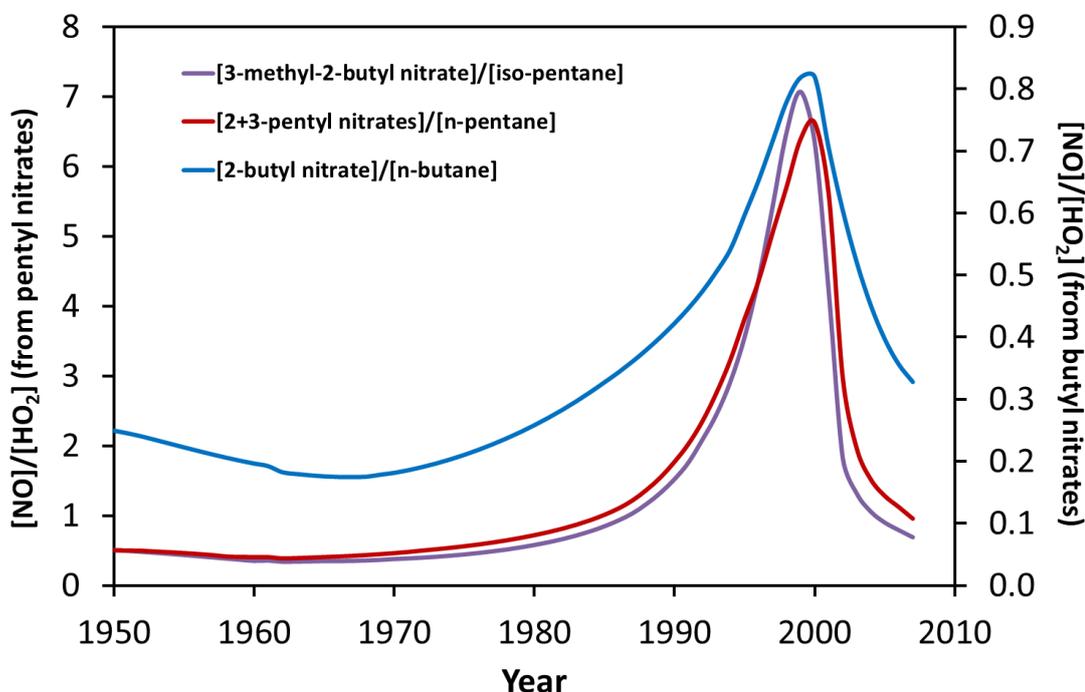


**Figure 6.1** Ratio of atmospheric $[NO]/[HO_2]$ calculated from firn derived atmospheric histories of three alkane-alkyl nitrate pairs ([n-butane]/[2-butyl nitrate], [n-pentane]/[2+3-pentyl nitrate] and [iso-pentane]/[3-methyl-2-butyl nitrate]) at NEEM.

Table 6.2 shows the percentage increase of the $[NO]/[HO_2]$ ratio calculated for each pair at each site. It is seen that the ratio calculated from 2-butyl nitrate increases by a factor of 4 between 1975 and the late-1990s, whereas that calculated from the pentyl nitrates increases by a factor of 13 to 14. This large difference between the change in the ratio calculated from the butyl nitrates and the pentyl nitrates, coupled with the good agreement between the two sites for each pair, suggests that there is something else happening rather than just a change in the $[NO]/[HO_2]$ ratio, something which affects the different pentyl nitrates in a similar manner but affects the butyl and pentyl nitrates differently.

**Table 6.2** The atmospheric [NO]/[HO$_2$] ratio calculated using Equation 6.8 using three alkane-alkyl nitrate pairs derived from NEEM firn air. Percentage increase from 1975 to the peak.

| Alkyl nitrate | [NO]/[HO$_2$] Pre-1975 | Peak | % increase 1975 – peak |
|---|---|---|---|
| *NEEM* | | | |
| 2-butyl nitrate | 0.2 | 0.8 | 300 |
| 2+3-pentyl nitrates | 0.5 | 6.6 | 1200 |
| 3-methyl-2-butyl nitrate | 0.5 | 7.0 | 1300 |

### 6.1.2    Changes to Northern Hemisphere NO Mixing Ratios

The apparent changes to the atmospheric [NO]/[HO$_2$] ratio between 1950 – 2007 suggest that either atmospheric [NO] has changed or [HO$_2$] has changed or perhaps both. The following section will examine possible reasons for these changes to the atmospheric composition of the northern hemisphere.

The main source of atmospheric NO$_x$ in the northern hemisphere is anthropogenic emissions from fossil fuel combustion (Olivier et al., 2001). The main sink of NO$_x$ in the atmosphere is reaction of NO$_2$ with OH, leading to HNO$_3$, much of which is lost from the atmosphere via wet deposition (e.g. Seinfeld and Pandis, 2006). Possible changes to atmospheric [OH] in the northern hemisphere were discussed in Section 5.5.4. These suggested a possible increase in [OH] between 1979 and 1990. However this would lead to more formation of HNO$_3$ and hence reduce atmospheric NO$_x$, reducing the [NO]/[HO$_2$] ratio, whereas the measurements show the ratio to have increased during this period (Figure 6.1), so we can assume any changes in [OH] to not be having a significant effect on atmospheric [NO]. Therefore it can be assumed that any changes to atmospheric NO$_x$ are likely caused by changes in the source, i.e. anthropogenic emissions.
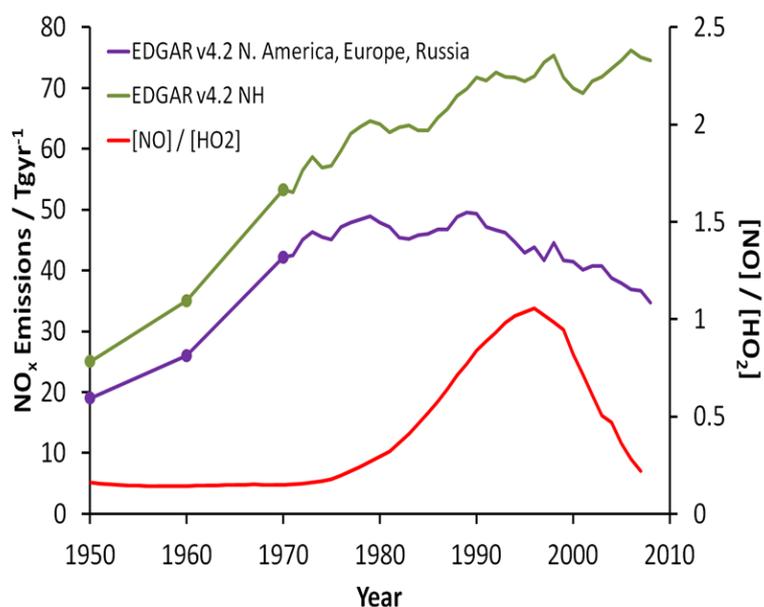
**Figure 6.2** Total northern hemisphere $NO_x$ emissions and $NO_x$ emissions from North America, Europe and Russia between 1950 and 2007 (EDGAR v4.2) and the calculated $[NO]/[HO_2]$ ratio.

Figure 6.2 shows the total northern hemisphere NO emissions and the NO emissions from Europe, North America and Russia, for the period 1950 – 2007 taken from the EDGAR database (EDGAR v4.2). The latter is shown since it is considered that Asia (the other main northern hemisphere anthropogenic source) is unlikely to contribute greatly to Arctic mixing ratios particularly in the early part of the record (see Section 5.6). Also shown in Figure 6.2 is the $[NO]/[HO_2]$ ratio derived using 2-butyl nitrate. A comparison of the two emission trends and the derived ratio shows that neither trend appears to be directly correlated to the ratio. The trend for the whole northern hemisphere shows emissions increasing throughout the record with a slow down in the growth rate after 1980. The trend for North America, Europe and Russia shows emissions increasing up to the mid-1970s, remaining fairly stable until about 1990 and then slowly decreasing after this time. The lack of correlation is particularly evident for the period 1950 to 1975 during which time there is no change in the $[NO]/[HO_2]$ ratio but NO emissions more than double. Therefore it appears that changes in NO emissions are not the sole cause of the observed changes in the atmospheric $[NO]/[HO_2]$ ratio, though they may still be contributing to it.

### 6.1.3 Changes to Northern Hemisphere HO$_2$ Mixing Ratios

The main source of the HO$_2$ radical in the background troposphere is the oxidation of CO by the OH radical. The main sinks are reaction with other HO$_2$ radicals, with other peroxy radicals and with NO. Both the sources and sinks may have changed in the past. Figure 6.3 shows the atmospheric CO trend derived by Petrenko et al. (2012) from firn air at NEEM for the period 1950 – 2007. It is seen that atmospheric [CO] in the Arctic displays a very similar trend to those derived for the alkanes, with growth from 1950 to a peak in the late 1970s and a decline after this time to mixing ratios below those observed in 1950. This similarity is unsurprising since the major source of both CO and the alkanes is the combustion of fossil fuels. This decrease in CO mixing ratios would lead to a decrease in CO oxidation and hence could be expected to lead to a reduction in atmospheric HO$_2$ mixing ratios. This would explain why the [NO]/[HO$_2$] ratio begins to increase in the late 1970s (Figure 6.1) at the same time that the alkane and CO mixing ratios begin to decline. However it would not explain the subsequent decline in the ratio after the late-1990s, or why there was no concomitant increase in the ratio associated with lower CO mixing ratios prior to 1980.
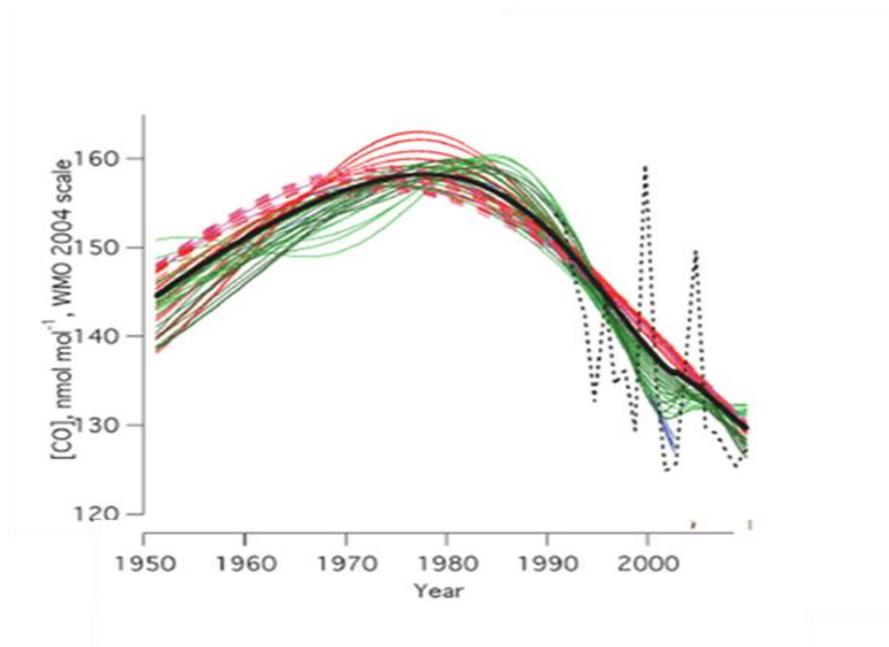


**Figure 6.3** Atmospheric [CO] trend derived from firn air at NEEM (Petrenko et al. 2012). The solid black line is the average of all the considered atmospheric scenarios.

Hence it seems that it may just be a co-incidence that the ratio begins to change as CO mixing ratios begin to fall, or it could be that there are other phenomena affecting the [NO]/[HO$_2$]

ratio at other times. Or it could be that this change is important but does not represent the whole story.

### 6.1.4 Alkyl nitrate Production Efficiency in Background Air

A box model was developed to investigate the alkyl nitrate chemistry in the absence of transport and mixing. The chemical mechanism is described in Section 2.8. For model runs representing the chemistry of the background atmosphere, the model can be run using fixed parameters simulating a steady state. For runs simulating Lagrangian transport of a polluted air mass, the chemistry must be allowed to vary.

For model runs investigating the formation of 2-butyl nitrate in the background atmosphere initial concentrations of all species were fixed to typical winter time values. The $[NO]/[HO_2]$ ratio was varied between runs by varying $[NO]_0$ and the model was run to steady state at a range of ratios.

The reaction rates used for the peroxy radicals ($RO_2$) with the NO and $HO_2$ radicals are based on work by Jenkin et al. (1997) (Figure 6.4). The reaction rates with NO are based on the general rate coefficient $4.1x10^{-12}.\exp(180/T)$ $f$, where $f = 1$ for C1 and C2 peroxy radicals and then for C $\geq$ 3, $f = \exp(-0.17(n-1))$, where n = carbon number. The reaction rates with $HO_2$ are given by $3.0x10^{-13}.\exp(1250/T)$ $[1-\exp(-0.34n)]$. Both of these expressions are empirically derived from measurements by various groups, references within Jenkin et al. (1997).

The steady state mixing ratios of 2-butyl nitrate achieved using these runs are shown in Figure 6.5.
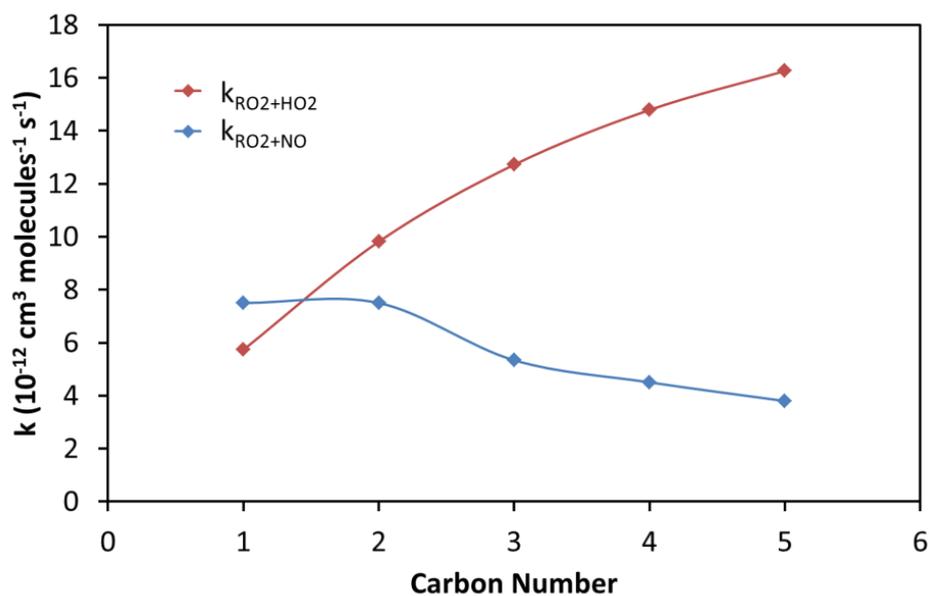
**Figure 6.4** Reaction rates of the alkyl peroxy radicals with the NO and HO$_2$ radicals used in the modeling. Rates are calculated from empirical expressions derived by Jenkin et al. (1997).
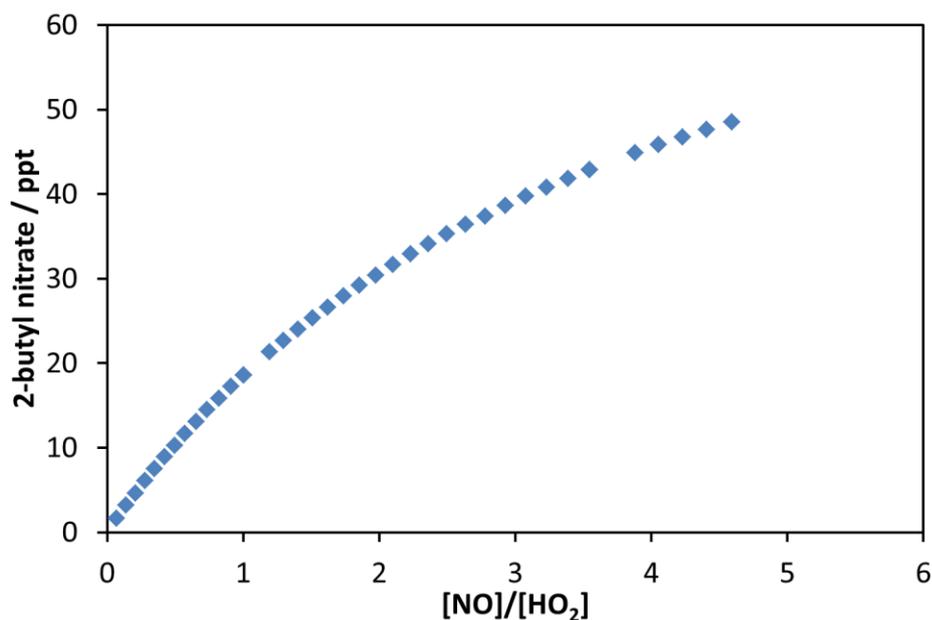


**Figure 6.5** Steady state mixing ratio of 2-butyl nitrate produced in the box model with a fixed n-butane mixing ratio at various ratios of [NO]/[HO$_2$]

It is seen in Figure 6.5 that as the [NO]/[HO$_2$] ratio increases so does the steady state mixing ratio of 2-butyl nitrate. This is because the percentage of the 2-butyl peroxy radical that reacts

with NO (Reaction 6.2a), rather than with $HO_2$ (Reaction 6.3), increases as the amount of NO relative to $HO_2$ increases.

The amount of the alkyl peroxy radical that reacts with NO can be defined as the ***production efficiency*** of the alkyl nitrate (P.E.$_{AN}$). This concept is shown in Figure 6.6 in which the percentage of the alkyl peroxy radicals reacting with NO for a given $[NO]/[HO_2]$ ratio is shown. The steady state mixing ratio of the alkyl nitrate tends towards a maximum value at higher $[NO]/[HO_2]$ ratios as the production efficiency approaches 100%. It is seen that the production efficiency of 2-butyl nitrate is 50% when the $[NO]/[HO_2]$ ratio is roughly 3. This can be understood by looking at the rate constants $k_{NO}$ and $k_{HO2}$ for the reactions with the 2-butyl peroxy radical ($2C4O_2$), $k_{HO2} / k_{NO} = 3.04$ (see Figure 6.5). Therefore $k_{NO}[2C4O_2][NO]$ (the loss of the peroxy radical to reaction with NO) will equal $k_{HO2}[2C4O_2][HO_2]$ (the loss to $HO_2$) when $[NO]/[HO_2]$ is equal to 3.04. This can be expressed in terms of Equation 6.9.

$$P.E._{AN} \quad = \quad \frac{k_3[NO]}{k_4[HO_2] + k_3[NO]} \qquad\qquad (E6.9)$$

It is also seen in Figure 6.6 that the production efficiency at a given $[NO]/[HO_2]$ ratio decreases with increasing carbon number. This is easily related to Figure 6.4 that shows the reaction rates with NO and $HO_2$ for the alkyl peroxy radicals. As the carbon number increases, the reaction rate with NO decreases while that with $HO_2$ increases. Hence the relative amount of the peroxy radical reacting with NO at a given $[NO]/[HO_2]$ ratio will decrease with increasing carbon number.
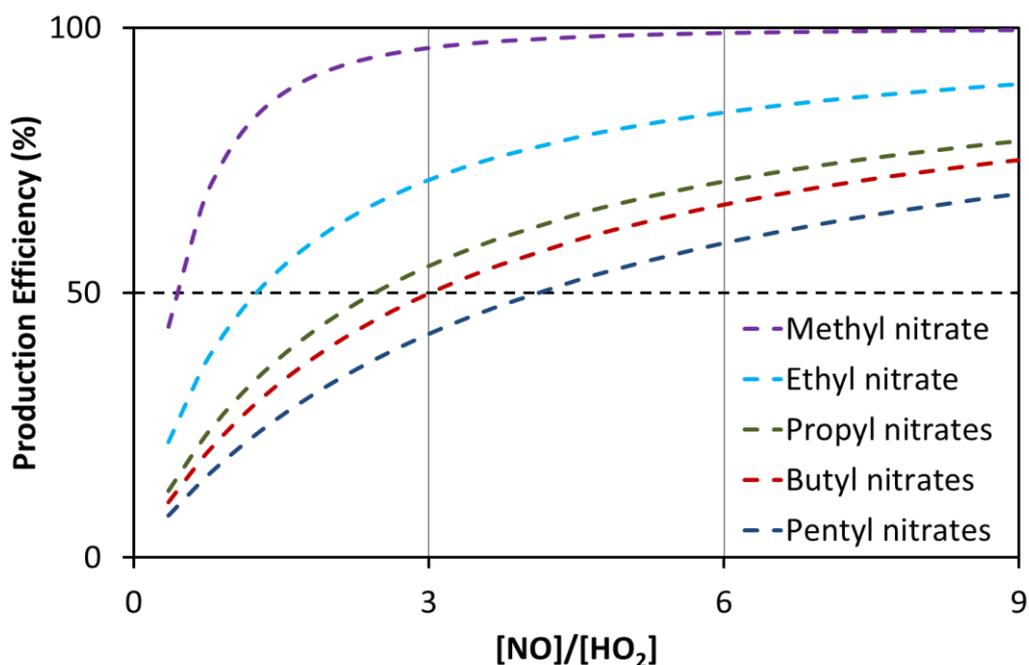
**Figure 6.6** Production efficiency of the C1 – C5 alkyl nitrates for varying atmospheric $[NO]/[HO_2]$.

The typical winter time $[NO]/[HO_2]$ ratio in the mid-high latitude northern hemisphere background atmosphere varies between about 1 and 5. Typical $[HO_2]$ values are about $1 \times 10^8$ molecules $cm^{-3}$, while typical $[NO]$ values are on the order of 10 ppt or $2.5 \times 10^8$ molecules $cm^{-3}$. From Figure 6.6 it can be seen that this corresponds to a production efficiency for butyl nitrates varying between 25% and 60%. Hence the production of 2-butyl nitrate in the background atmosphere is not occurring at 100% efficiency and is variable with changing $[NO]/[HO_2]$ ratios.

### 6.1.5 The Effect of Photolysis on $[RONO_2]/[RH]$

So far the effect of the photolysis sink of the alkyl nitrates has been largely ignored. This is because it is believed that it will have a negligible effect on the butyl and pentyl nitrates with the dominant sink begin reaction with OH (e.g. Worton et al., 2012). In this section the effect of changing the relative magnitudes of the OH sink and photolysis sink on the steady state $[RONO_2]/[RH]$ ratio is considered.

The $[RONO_2]/[RH]$ ratio at steady state in the absence of photolysis is given by Equation 6.10.

$$\frac{[RONO_2]}{[RH]} = \frac{k_1 \alpha_1 k_3 \alpha_3 [NO][OH]}{k_7 (k_3 [NO] + k_4 [HO_2])[OH]} \quad\quad\quad \text{(E6.10)}$$

Assuming that alkyl nitrate production efficiency is 100% (i.e. $k_3$[NO] $>>$ $k_4$[HO$_2$]) and including the photolysis sink, Equation 6.10 can be written as Equation 6.11.

$$\frac{[RONO_2]}{[RH]} = \frac{[OH]k_1 \beta}{([OH]k_7 + j_6)} \qu\quad\quad\quad \text{(E6.11)}$$

Or, assuming $j_6 << k_7$[OH],

$$\left(\frac{[RONO_2]}{[RH]}\right)_{SS} = \frac{k_1 \beta}{k_7} \qu\quad\quad\quad \text{(E6.12)}$$

Where $\beta = \alpha_1 \alpha_3$. It is seen from Equation 6.12 that each alkyl nitrate-alkane pair has a maximum theoretical ratio of ([RONO$_2$]/[RH])$_{ss}$) which is reached at steady state. These steady state ratios can be calculated using Equation 6.12 and are shown in Table 6.3 for each alkyl nitrate-alkane pair. These ratios are a maximum value as they assume 100% production efficiency of the alkyl nitrate and ignore the photolysis loss.

**Table 6.3** The rate constants for hydrocarbon oxidation ($k_1$), alkyl nitrate oxidation ($k_7$) and the rate of photolysis ($j_6$) of alkyl nitrates. Also, β (the product of the branching ratios for alkyl nitrate formation) and the steady state [alkyl nitrate]/[alkane] ratio ($[RONO_2]$ / $[RH])_{ss}$.

| Alkyl nitrate | Rate Constant (298 K) (x10$^{-12}$ cm$^3$ molecule$^{-1}$ s$^{-1}$) | | $j_6{}^a$ (x10$^7$ s$^{-1}$) | β | ([RONO$_2$] / [RH]) $_{ss}$ |
| --- | --- | --- | --- | --- | --- |
| | $k_1$ | $k_7$ | | | |
| Methyl | 0.0064 | 0.023 | 0.78 | 0.001 | (8.35 – 27.8) x10$^{-5\,c}$ |
| Ethyl | 0.248 | 0.18 | 0.68 | 0.009 | 0.01 |
| 2-propyl | 1.09 | 0.29 | 0.27 | 0.031 | 0.12 |
| 2-butyl | 2.36 | 0.86 | 3.58 | 0.079 | 0.22 |
| 2+3-pentyl | 3.80 | 1.35 | 26 | 0.119 | 0.34 |
| 3-methyl-2-butyl | 3.65 | 1.70 | 26 $^b$ | 0.042 | 0.09 |

[a] Based on the absorption cross sections from Atkinson et al. (2006), except 2+3-pentyl nitrate from Roberts and Fajer (1989). Rates were calculated using the photolysis stream in the 2-D atmospheric model. Values are for 48.6 – 56.4°N. Annual means for C1 – C2 nitrates, winter means for C3 – C5 nitrates.
[b] No data available, used that of 2-pentyl nitrate.
[c] Based on the two reported branching ratios of 0.001 (MCM) and <0.0003 (Flocke et al., 1998).

If the photolysis sink of the alkyl nitrates is ignored then the steady state ratio $[RONO_2]/[RH]$ towards which the system is tending is defined by the reaction rate of the alkane ($k_1$) and the alkyl nitrate ($k_7$) with OH and of the branching ratios for the formation of the peroxy radical ($\alpha_1$) and the alkyl nitrate ($\alpha_3$) (Equation 6.12). Changing [OH] will affect the rate at which the system tends towards this steady state but not the value of $[RONO_2]/[RH]$.

If the photolysis sink of the alkyl nitrates is considered in the steady state analysis (Equation 6.11), then the steady state ratio $[RONO_2]/[RH]$ will be affected. If photolysis is not insignificant compared to $k_7$[OH], then changing [OH] will affect $([RONO_2]/[RH])_{ss}$, i.e. an increase to [OH] will not only increase the rate at which the system tends towards steady state but also the absolute value of $([RONO_2]/[RH])_{ss}$. This is demonstrated in Figure 6.7 using $j_6$ values from Table 6.3 and a range of [OH] values.
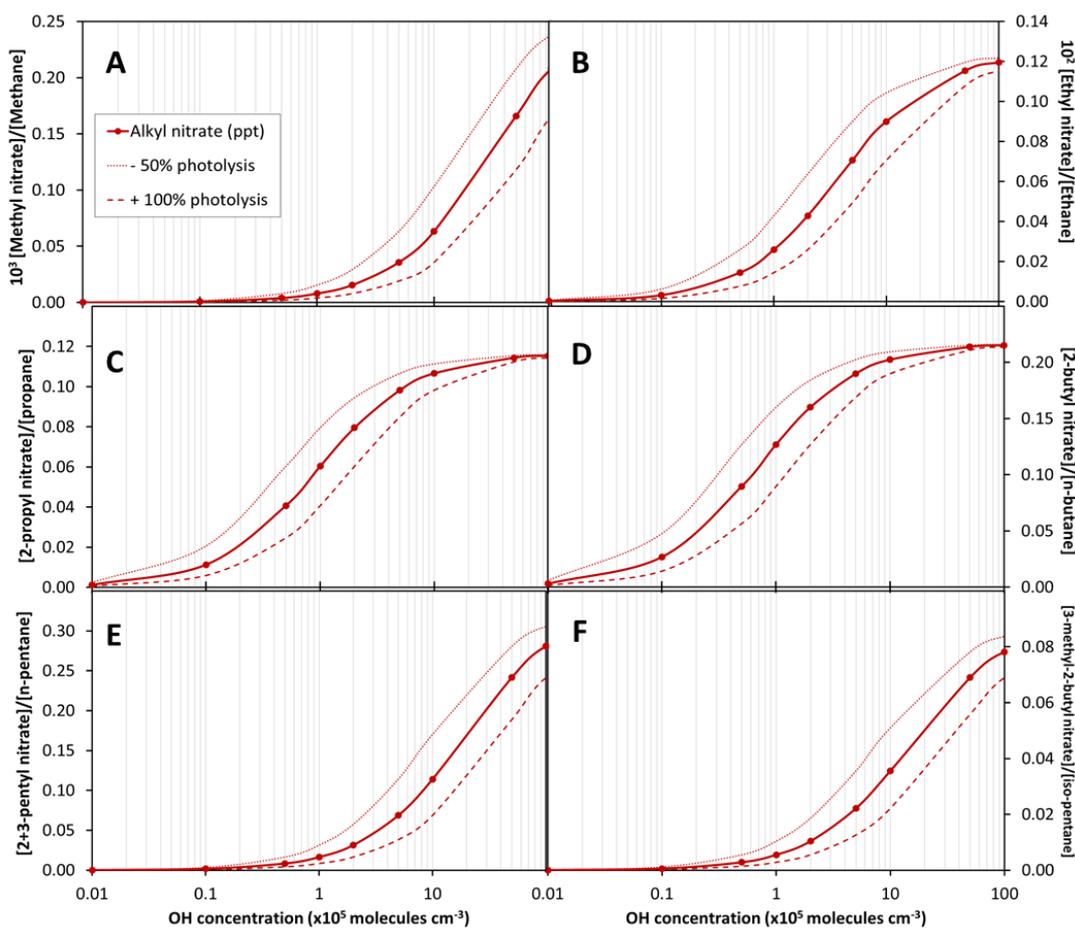
**Figure 6.7** Variation of the steady state [alkyl nitrate]/[alkane] with [OH] between $1 \times 10^3$ molecules cm$^{-3}$ and $1 \times 10^7$ molecules cm$^{-3}$ calculated using Equation 6.11. Dashed line: Photolysis sink increased by a factor of two; dotted line: photolysis sink decreased by a factor of two.

The lines shown in Figure 6.7 are very sensitive to the photolysis rates used. The photolysis rates shown in Table 6.3 were calculated in the 2-D atmospheric model using absorption cross sections from Atkinson et al. (2006). The photolysis rates used were annual means for methyl and ethyl nitrate (since they are present in the Arctic year round – Swanson et al., 2003) and winter means for propyl, butyl and pentyl nitrates. It should be noted that the photolysis rates calculated for the pentyl nitrates in the model are rather high compared to other values from the literature (e.g. Worton et al., 2007).

It is seen in Figure 6.7 that at low OH concentrations the steady state [alkyl nitrate]/[alkane] ratio is very low. The steady state of the system then begins to increase as OH is increased and reaches a maximum at higher [OH] as photolysis becomes insignificant. It appears that in the region of the OH concentration we might expect in the winter mid-high latitudes ($\sim 1 \times 10^5$

$- 1 \times 10^6$) that the photolysis sink could be having an effect on limiting the steady state [alkyl-nitrate]/[alkane] ratio towards which the system is tending. It should be noted that these are the maximum steady state values which the system can reach but that whether the system does reach this value is dependent on [OH], photolysis and the transport time.

## 6.2 Alkyl Nitrate Production in Polluted Air Masses

If the emission of hydrocarbons and $NO_x$ from urban environments are considered as point sources then an air mass emanating from these sources can be thought of as a pollution plume. These plumes can have different chemistry to the background atmosphere (e.g. Sillman, 1999) because of the very high initial mixing ratios of hydrocarbons and $NO_x$. In the short term these plumes can behave as semi-coherent air masses (i.e. there is little mixing) and hence some species, such as $NO_x$, can effectively be 'used up' from a system that begins with a finite amount. Over time, mixing will incorporate the constituents of the air mass into the background atmosphere.

### 6.2.1 Box Model Runs

A box model was used to investigate the effect of changes to initial hydrocarbon and NO concentrations on alkyl nitrate production in an air mass. The n-butane, 2-butyl nitrate system was used for this analysis.

In Section 6.2.1.1 runs are shown in which the effects of changing each of the three relevant parameters for 2-butyl nitrate formation ([n-butane]$_0$, [NO]$_0$ and [OH]$_0$) separately on the evolution of the 2-butyl nitrate concentration are explored. The point at which the system becomes $NO_x$ saturated is explored.

In Section 6.2.1.2 more of the chemistry is variable to investigate the effects of the alkyl nitrate precursors on each other. The ratio of the initial total hydrocarbon in the atmosphere to NO is varied between runs. The parameter $\Sigma HC$ represents the total hydrocarbon burden in the atmosphere. It follows the same oxidation pathway as n-butane and acts to suppress [OH], to convert NO to $NO_2$ and to form aldehydes, the importance of which will be shown in Section 6.2.2. Hence varying $\Sigma HC_0/NO_0$ will affect the evolution of 2-butyl nitrate not only by varying

NO and n-butane (which is scaled to $\Sigma$HC) but also by controlling [OH]. These controls and feedbacks are explored in Section 6.2.1.2.

Table 6.4 shows the parameters used in the model runs and which of these were varied in Sections 6.2.1.1 and 6.2.1.2.

**Table 6.4** Fixed parameters used in box model runs

| Parameter | Initial Mixing Ratio | Fixed Runs | Variable Runs |
|---|---|---|---|
| CO | 400 ppb | Fixed | Fixed |
| $CH_4$ | 1700 ppb | Fixed | Fixed |
| $O_2$ | 20% | Fixed | Fixed |
| $H_2O$ | 1% | Fixed | Fixed |
| $O_3$ | 25 ppb | Fixed | Fixed |
| OH | 16 ppq[a] | Varied between runs | Variable |
| $HO_2$ | 4 ppt | Fixed | Variable |
| HCHO | 20 ppb | Fixed | Variable |
| $\Sigma$HC | 320 ppb | Fixed | Variable |
| n-butane | 600 ppt[a] | Varied between runs | Variable |
| NO | 400 ppt[a] | Varied between runs | Variable |
| $NO_2$ | 4 ppb | Fixed | Variable |

[a] When fixed during runs in Section 6.2.1.1

### 6.2.1.1 Fixed Parameter Runs

Figure 6.8 shows the effect on the alkyl nitrate mixing ratio of varying the initial n-butane mixing ratio. It is seen that, for a given set of fixed initial conditions, the mixing ratio of the alkyl nitrate varies proportionally to the initial mixing ratio of the parent alkane. The corollary of this, as is also shown in Figure 6.8 is that the ratio [2-butyl nitrate]/[n-butane] is independent of the initial mixing ratio of the parent alkane.
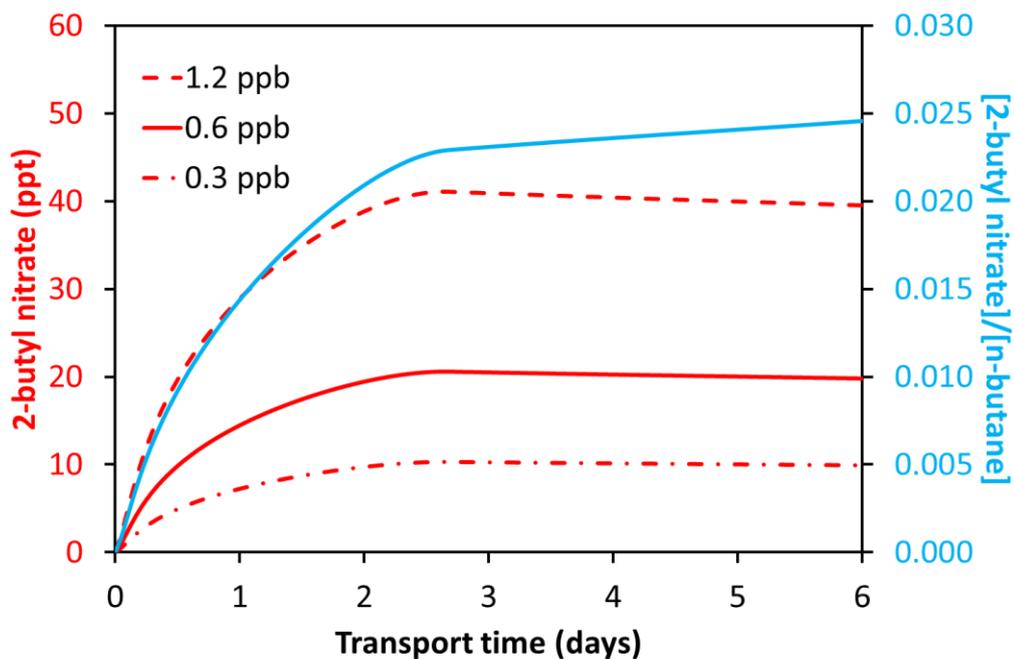
**Figure 6.8** Three model runs, using the initial conditions in Table 6.4, in which the initial n-butane mixing ratio was varied.

Panel A of Figure 6.9 shows how the mixing ratio of the alkyl nitrates after six days varies with increasing NO mixing ratios. It is seen that for [NO] mixing ratios above roughly 100 ppt any further increase in [NO] has little effect on the formation of the alkyl nitrate. The system can be said to be NO saturated with respect to the formation of a given alkyl nitrate above this point. Panel B of Figure 6.9 shows how the mixing ratio after six days varies as a fraction of the mixing ratio at NO saturation. It is seen that the NO saturation point increases with increasing carbon number.
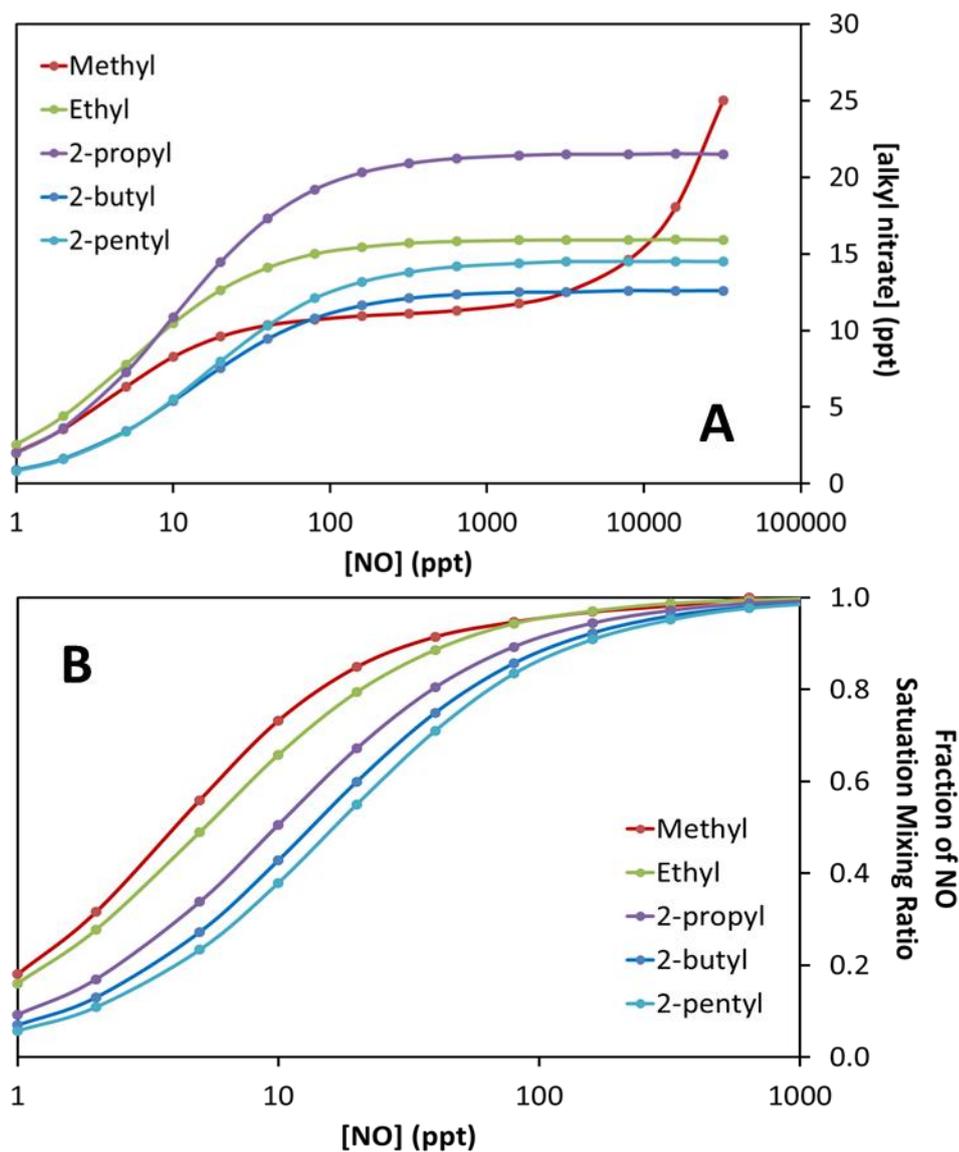
**Figure 6.9** Showing the effect of [NO] on the modeled alkyl nitrate mixing ratios after six days. Panel A shows absolute alkyl nitrate mixing ratios. Panel B shows alkyl nitrate mixing ratios as a fraction of the mixing ratio at NO saturation. Note [NO] is plotted on a log scale.

Panel A of Figure 6.9 shows that whereas the other four alkyl nitrates appear to reach a limit above which an increase in NO makes no difference to the mixing ratios of the alkyl nitrate, methyl nitrate mixing ratios are seen to rapidly increase again with increasing NO above roughly 10 ppb. This can be explained by formation via the alkoxy radical (RO + NO$_2$ – Reaction 1.10) becoming important for methyl nitrate at very high NO concentrations. [NO$_2$] was kept equal to [NO] in the model runs shown in Figure 6.9. So the formation of methyl nitrate reaches NO saturation at roughly 20 ppt but then increases again above 20 ppb as formation via the alkoxy radical plus NO$_2$ becomes important. For the other alkyl nitrates

[NO$_x$] increases have no effect on their mixing ratios above about 100 ppt (for the range of NO mixing ratios shown).

The observed NO$_x$ saturation occurs because, as NO$_x$ mixing ratios increase, it is the oxidation of the hydrocarbon which becomes the rate determining step in the formation of the alkyl nitrate. This is because $k_3$ [NO][RO$_2$] becomes greater than $k_1$ [RH][OH]. From model runs varying [OH] and [alkane] (not shown) this point appears to be independent of both of these parameters and to depend only on [NO] (and [NO$_2$] for methyl nitrate).

This demonstration of peroxy radicals experiencing NO$_x$ saturated and unsaturated regimes has been described previously for peroxy radicals by Kleinman (1991, 1994).
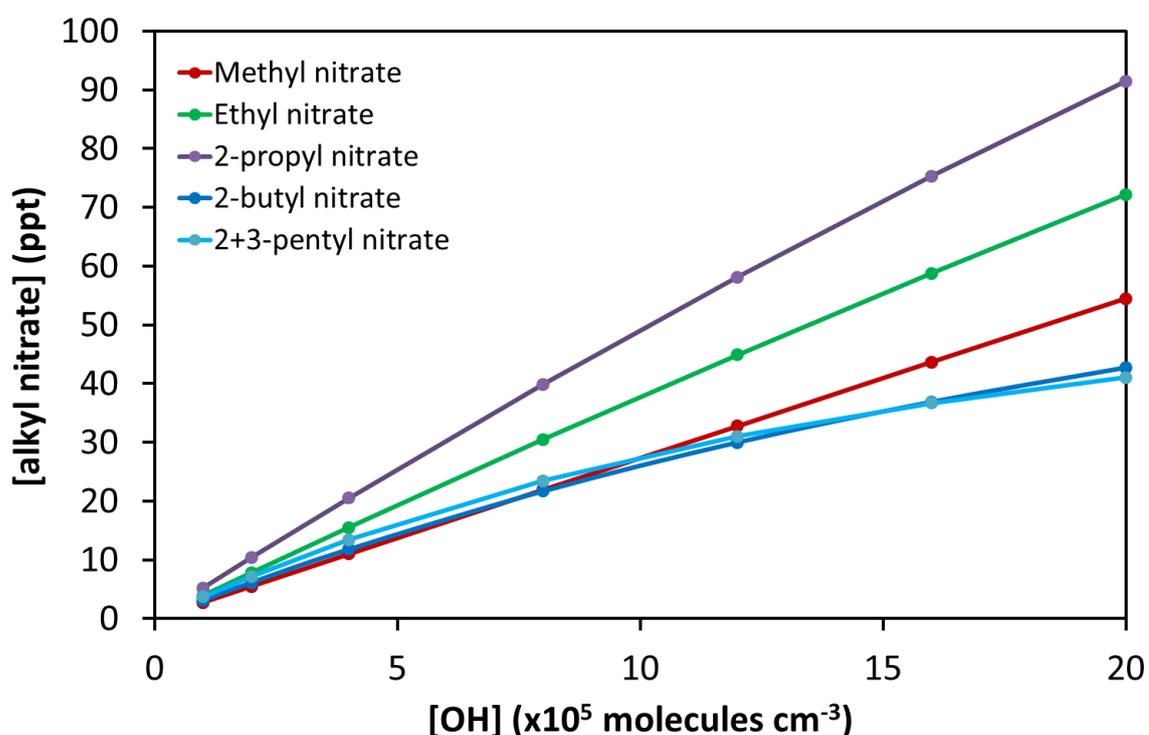


**Figure 6.10** The effect of increasing [OH] on alkyl nitrate mixing ratios after six days. [NO] = 400 ppt, i.e. above the NO saturation point.

Figure 6.10 shows the variation of the alkyl nitrate mixing ratio after six days when NO is above the saturation point. It is seen that the mixing ratios of the alkyl nitrates after six days increase roughly proportionally to the OH concentration.

For methyl and ethyl nitrate the mixing ratio after six days appears to be directly proportional to the OH concentration, whereas for the higher nitrates this proportionality appears to decrease with increasing [OH]. It should also be noted that the gradient of the proportionality will begin to increase again for methyl nitrate as $NO_2$ increases above about 20 ppb.

### 6.2.1.2 Variable Parameter Runs

The kinds of run performed using the one-box model in the previous section displayed the dependence of the rate of production of the alkyl nitrate on different variables. However changing only one of these variables is unrealistic since the chemistry of each of them is linked to the others. In the following section model runs are performed in which most of the species are variable and hence the effect of species on each other can be examined.

A series of six runs were performed. CO, $CH_4$, $H_2O$ and $O_2$ are fixed parameters with the values shown in Tables 6.4. OH, $O_3$, $NO_2$ and HCHO are all variable with initial mixing ratios as shown in Table 6.4. The same initial n-butane mixing ratios were used for each run. The initial total hydrocarbon ($\Sigma HC$) and NO mixing ratios for each run are shown in Table 6.5. These were chosen to simulate the initial mixing ratios observed in pollution plumes from urban environments.

**Table 6.5** Six model runs. Initial total hydrocarbon ($\Sigma HC$) and NO mixing ratios and the consequent 2-butyl nitrate mixing ratio and [2-butyl nitrate]/[n-butane] ratio after six days.

| Model Run | Initial mixing ratios (ppb) | | $\Sigma HC$/NO initial ratio | 2-butyl nitrate (ppt) | [2-butyl nitrate]/ [n-butane] |
|:---:|:---:|:---:|:---:|:---:|:---:|
| | *ΣHC* | *NO* | | *6 days* | *6 days* |
| A1 | 1600 | 80 | 20 | 14.3 | 0.014 |
| A2 | 800 | 40 | 20 | 13.8 | 0.015 |
| A3 | 400 | 20 | 20 | 13.0 | 0.015 |
| B1 | 800 | 80 | 10 | 21.1 | 0.023 |
| B2 | 400 | 40 | 10 | 19.8 | 0.025 |
| C2 | 200 | 40 | 5 | 28.2 | 0.046 |

Table 6.5 shows the modeled mixing ratios of 2-butyl nitrate and the ratio of [2-butyl nitrate]/[n-butane] after six days. Figure 6.11 displays the evolution with time of the 2-butyl nitrate mixing ratio, the NO mixing ratio and the OH concentration. Note that there is no diurnal variation included in the model. Runs A, in which the initial $\Sigma$HC/NO ratio is 20, are coloured blue, Runs B in which the initial $\Sigma$HC/NO ratio is 10 are coloured red and Run C, in which the initial $\Sigma$HC/NO ratio is 5 is green.
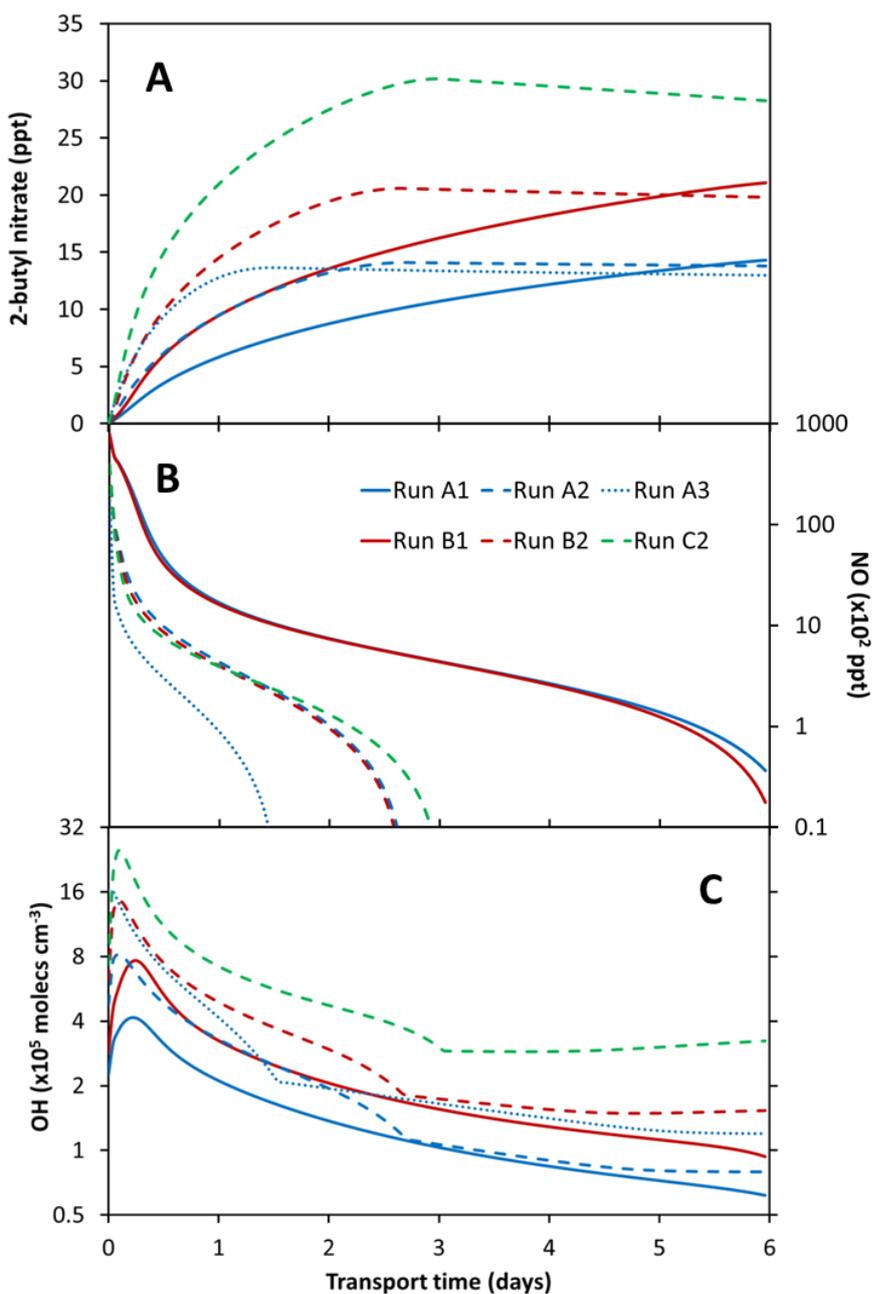


**Figure 6.11** Evolution of 2-butyl nitrate, NO and OH mixing ratios for the six model runs detailed in Table 6.5.

In Panel A of Figure 6.11 it is seen that the mixing ratio of 2-butyl nitrate at day 6 appears to be largely dependent on the initial $\Sigma HC/NO$ ratio, the blue lines are all about 12 ppt, the red lines are about 20 ppt and the green line about 30 ppt. In fact it appears that the mixing ratios for each group of scenarios cross at the end of day 5. So although the evolution of the 2-butyl nitrate mixing ratio is different for each different scenario, with [2-butyl nitrate] falling at day 6 for Runs A2, A3, B2 and C2 but still rising for A1 and B1, the final value is similar for scenarios with the same initial $\Sigma HC/NO$ ratio.

Panel B of Figure 6.11 shows the variation of the mixing ratios of the NO radical with time for the six model runs. It is seen that NO falls rapidly initially in all runs. For Run 3, with an initial NO mixing ratio of 20 ppb, the NO mixing ratio falls to below 10 ppt during the second day. For Runs 2, with an initial NO mixing ratio of 40 ppb, NO falls to below 10 ppt during the third day and for Runs 1, with initial mixing ratios of 80 ppb, mixing ratios remain above 100 ppt until the sixth day. So the time at which the NO is 'used up' in the air mass is largely dependent on the initial NO mixing ratio.

Panel C of Figure 6.11 shows the variation in concentration of the OH radical during the six model runs. All Runs show an initial rapid increase from an initial concentration of $2 \times 10^5$ molecules $cm^{-3}$ followed by a more steady decline during the following days. In Run C2 the OH concentration begins to gradually increase again after day 3 and in Run B2 it begins to increase after day 5. Looking at Runs A2, B2 and C2 it is seen that when the initial NO mixing ratio is the same that the OH concentration appears to be inversely proportional to the initial total hydrocarbon mixing ratio (i.e. [OH] in C2 = 2[OH] in B2 = 4[OH] in A2, whereas $\Sigma HC$ in A2 = 2$\Sigma HC$ in B2 = 4 $\Sigma HC$ in C2). However comparing Runs A2 & B1 and A3 & B2, which have initial total hydrocarbon mixing ratios of 800 ppb and 400 ppb respectively, it is seen that the B runs, which have higher initial NO mixing ratios, both have slightly higher final OH mixing ratios.

It is seen that the OH mixing ratios of Runs 2 and 3 have a point at which the OH decrease slows significantly (e.g. at 3 days for Run C2). This is seen to be associated with the time at which the NO falls to near zero for each run, hence it is not seen for Runs 1. It is presumably due to the end of the suppression of OH mixing ratios by the reaction of OH with $NO_2$ to give $HNO_3$. The falling of NO to near zero is also evident in the evolution of the mixing ratios of 2-butyl nitrate in panel A, in which a comparison to panel B shows that production of 2-butyl nitrate stops for each run when the NO falls to near zero.
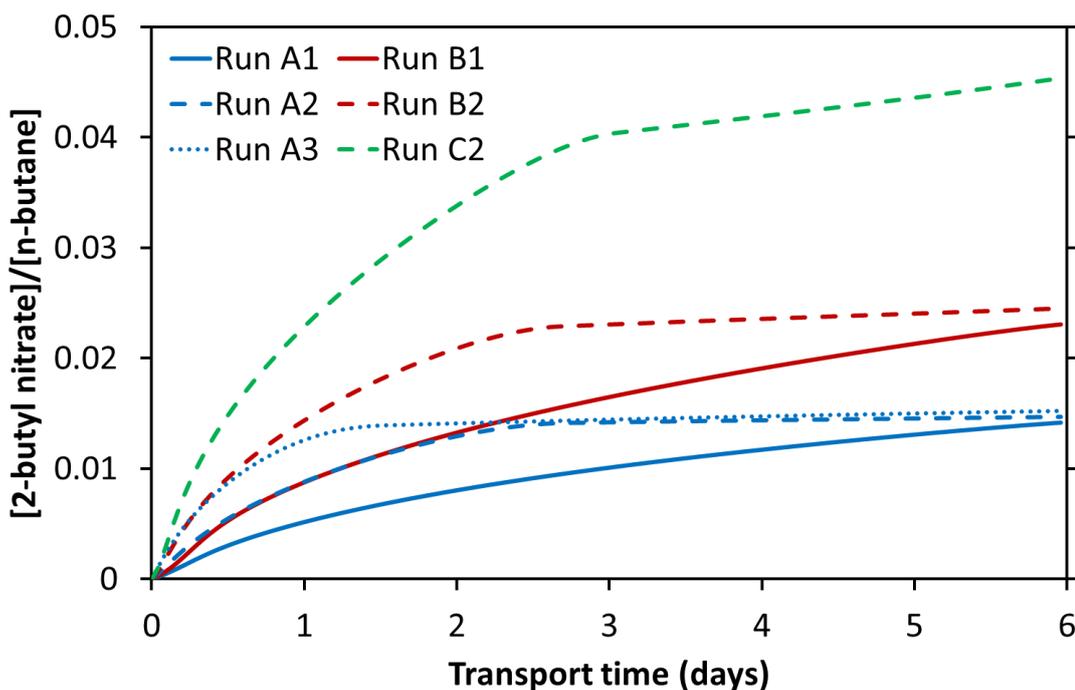
**Figure 6.12** The modeled [2-butyl nitrate]/[n-butane] ratio for the six scenarios in Table 6.5.

Figure 6.12 shows the evolution with time of the [2-butyl nitrate]/[n-butane] ratio for the six model runs defined in Table 6.5. It is seen, similarly to the total 2-butyl nitrate mixing ratio (Figure 6.11-A), that the ratio at the end of day 6 is largely dependent on the initial ΣHC/NO ratio. In fact the only real difference between these two plots is that the [2-butyl nitrate]/[n-butane] ratio continues to rise even when there is no more alkyl nitrate production. This is because the alkyl nitrate has a longer lifetime than the alkane. One interesting point to note is that the evolution of the ratio in Figure 6.12 is seen to begin almost identically for scenarios with the same initial total hydrocarbon (Runs A2 & B1 and B2 & C3). The point at which they diverge is also seen in the OH concentrations for these runs (Figure 6.11-C), which begin similarly but diverge at this point. It appears to be related to the beginning of the steep decline in NO mixing ratios (Figure 6.11-B).

The idea that air masses can 'use up' the $NO_x$ is seen in ozone chemistry in which close to source air masses are seen to be $NO_x$ saturated while downwind the same air masses have become $NO_x$ limited (e.g. Sillman, 1999 and references therein). The concept has also been proposed in relation to observations of alkyl nitrate chemistry by Reeves et al. (2007) during Lagrangian experiments on outflow from the east coast of North America.

This concept demonstrates a second way in which $NO_x$ levels can limit alkyl nitrate production in addition to that shown in Section 6.2.1.1.

## 6.2.2 The Effect of Formaldehyde on Alkyl nitrate Production

The effect of formaldehyde on the formation of ozone is well documented. An increase in the HCHO mixing ratio has been shown in chamber experiments to lead to more rapid conversion of NO to $NO_2$ and lead to a greater rate of ozone production (e.g. Finlayson-Pitts et al., 1977). It can be expected therefore that an increase in the initial formaldehyde mixing ratio in an air mass may also lead to a greater rate of alkyl nitrate production. This possibility is explored in this section.

Formaldehyde (HCHO) is present in the atmosphere both due to photochemical production as a part of the oxidation chain of hydrocarbons but also as direct emissions from transport and industry (e.g. Parrish et al., 2012).

The reactions formaldehyde undergoes in the atmosphere, and some of the subsequent chemistry, are shown in Reactions 6.6 to 6.16.

$$HCHO + OH \quad \rightarrow \quad HCO + H_2O \tag{R6.6}$$

$$HCHO + h\nu \quad \xrightarrow{\phi} \quad H + HCO \tag{R6.7a}$$

$$\xrightarrow{(1-\phi)} \quad H_2 + CO \tag{R6.7b}$$

$$HCO + O_2 \quad \rightarrow \quad CO + HO_2 \tag{R6.8}$$

$$H + O_2 + M \quad \rightarrow \quad HO_2 + M \tag{R6.9}$$

Net photolysis: $\quad HCHO + \phi 2O_2 + h\nu \quad \rightarrow \quad \phi 2HO_2 + (1-\phi)H_2 + CO \tag{R6.10}$

Net OH reaction: $\quad HCHO + OH + O_2 \quad \rightarrow \quad CO + HO_2 + H_2O \tag{R6.11}$
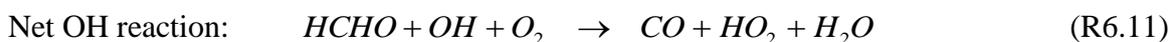
where $\varphi$ is the quantum yield for Reaction 6.7. The reaction of formaldehyde with OH (Reaction 6.6) leads to no net change in $HO_x$ as OH is converted to $HO_2$. It is seen that the photolysis of a molecule of formaldehyde can lead to the production of two molecules of $HO_2$ via Reaction 6.7a, or to no $HO_2$ production via Reaction 6.7b. Given that $\varphi$ is roughly 0.5 (Atkinson et al., 2006), the net result of the photolysis of a molecule of formaldehyde is to produce one molecule of $HO_2$. This leads to an increase in the total $HO_x$ in the system. The $HO_2$ formed in these reactions can convert an NO radical to $NO_2$ (converting the $HO_2$ back to OH) (Reaction 6.12) which is then photolysed producing $O(^3P)$ (Reaction 6.13) which reacts with $O_2$ to produce ozone (Reaction 6.14).

$$HO_2 + NO \quad \rightarrow \quad NO_2 + OH \tag{R6.12}$$

$$NO_2 + h\nu \quad \rightarrow \quad NO + O(^3P) \tag{R6.13}$$

$$O(^3P) + O_2 \quad \xrightarrow{\quad M \quad} \quad O_3 \tag{R6.14}$$

Net photolysis: $\quad HCHO + 2O_2 + h\nu \quad \rightarrow \quad O_3 + OH + \frac{1}{2}H_2 + CO \tag{R6.15}$

Net OH reaction: $\quad HCHO + 2O_2 + h\nu \quad \rightarrow \quad O_3 + H_2O + CO \tag{R6.16}$
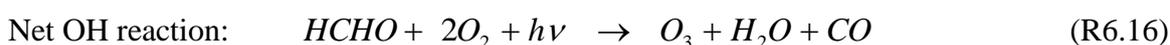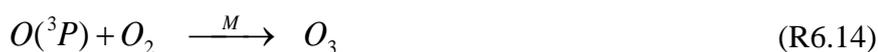
It is seen that both loss pathways of formaldehyde yield one ozone molecule (Reactions 6.15 and 6.16) but only the photolysis pathway increases the total $HO_x$ in the system.

The chemistry shown above interestingly suggests that the presence of formaldehyde should tend to keep the $HO_x$ in an air mass above a certain minimum level. If OH were to become low, then the photolysis sink of formaldehyde would become more important and this would increase the $HO_x$ again acting as a negative feedback on decreasing $HO_x$.

The formaldehyde chemistry was examined using the box model. The model was run with variable chemistry with initial conditions as used for Run C2 in Table 6.5, with an initial $\Sigma HC/NOx$ ratio of 5. Twelve different runs were performed to examine the effect of the

different atmospheric loss processes of HCHO on the formation of 2-butyl nitrate by switching on only one of the sinks at a time.
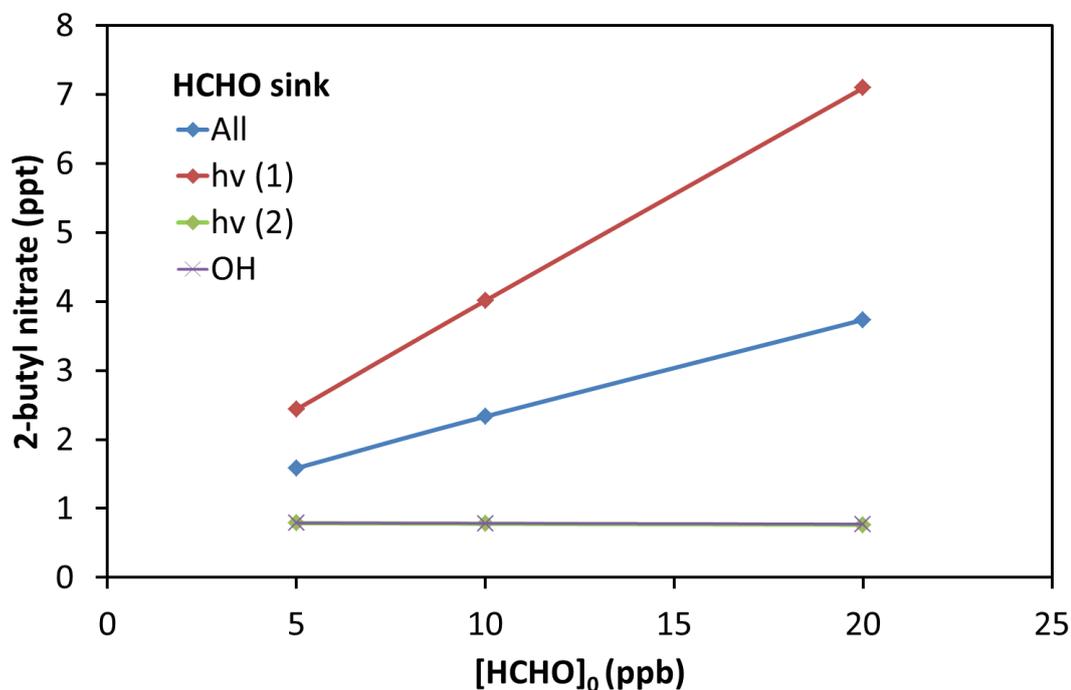


**Figure 6.13** Showing the effect of each of the sinks of HCHO in the atmosphere on 2-butyl nitrate mixing ratios after six days in the box model.

Figure 6.13 shows the effect of the different sinks of formaldehyde on 2-butyl nitrate mixing ratios after six days.

The run in which all loss processes were switched on ('All') (with $\varphi = 0.5$) shows that the final 2-butyl nitrate mixing ratio increases linearly with increasing $[HCHO]_0$.

The run 'hv(1)', in which only Reaction 6.7a was switched on shows a similar but more pronounced effect on 2-butyl nitrate mixing ratios of increasing $[HCHO]_0$. This is as predicted above and shows that Reaction 6.7a is the only HCHO reaction important in increasing alkyl nitrate mixing ratios because it is the only reaction to add $HO_x$ to the system. It also once again shows the large effect of increasing [OH] on final alkyl nitrate mixing ratios assuming that there is enough $NO_x$ available.

The two runs with each of the other loss processes switched on ('hv(2)' and 'OH') (Reactions 6.7b and 6.6) show that 2-butyl nitrate mixing ratios decrease slightly with increasing $[HCHO]_0$. This slight decrease can possibly be explained by a slight shift in the $NO/NO_2$ equilibrium caused by conversion of NO to $NO_2$ by the formaldehyde reactions, reducing the amount of NO available for alkyl nitrate formation. However this should not occur for Reaction 6.7b since no $HO_2$ is formed to react with NO.

The evolution with time of the 2-butyl nitrate mixing ratio, $[NO]/[NO_2]$ and the OH concentration for model runs with various initial mixing ratios of formaldehyde (5, 10 and 20 ppb) are shown in Figure 6.14. These initial mixing ratios were chosen based on reported values from urban environments. The rest of the initial conditions are as for Run B2 (Table 6.5), with an initial ΣHC/NOx ratio of 8, $\varphi$ was assumed to be 0.5.

It is seen in Panel A of Figure 6.14 that 2-butyl nitrate mixing ratios increase at a faster rate with higher initial [HCHO]. This can be explained by panel C which shows that the OH concentration in the air mass appears to vary almost linearly with initial HCHO. This in turn can be explained by Reaction 6.10 which shows that there is a net production of $HO_x$ from the photolysis of HCHO. Panel B shows that in the runs with higher initial HCHO there is a lower $NO/NO_2$ ratio. This is because the loss of formaldehyde converts one molecule of NO to $NO_2$ both by photolysis (assuming that $\varphi = 0.5$) and reaction with OH. However the effect of this lower $NO/NO_2$ ratio (as well as slightly lower absolute NO mixing ratios – not shown) does not affect the production of 2-butyl nitrate as much as the increase in OH concentration, hence higher initial HCHO still leads to higher 2-butyl nitrate.

Recent work by Parrish et al. (2012) in Houston suggests that direct emissions of formaldehyde from road vehicles accounts for only 4% of atmospheric HCHO in the region and that by far the greatest source of formaldehyde is the rapid oxidation of alkenes emitted both from road vehicles and industry. However this study is possibly skewed by the large amount of industry in Houston. They also conclude that only 24% of HCHO associated with vehicle emissions are direct emissions with the rest again mainly attributed to oxidation of highly reactive alkenes.

An historic trend of atmospheric HCHO is not available and so it is not known how atmospheric mixing ratios may have varied during the period of study. Whether or not catalytic converters have had the same effect on vehicular HCHO emissions as on many other

hydrocarbon emissions (i.e. whether the trend is similar to those derived for the alkanes in Chapter 5) is unclear.
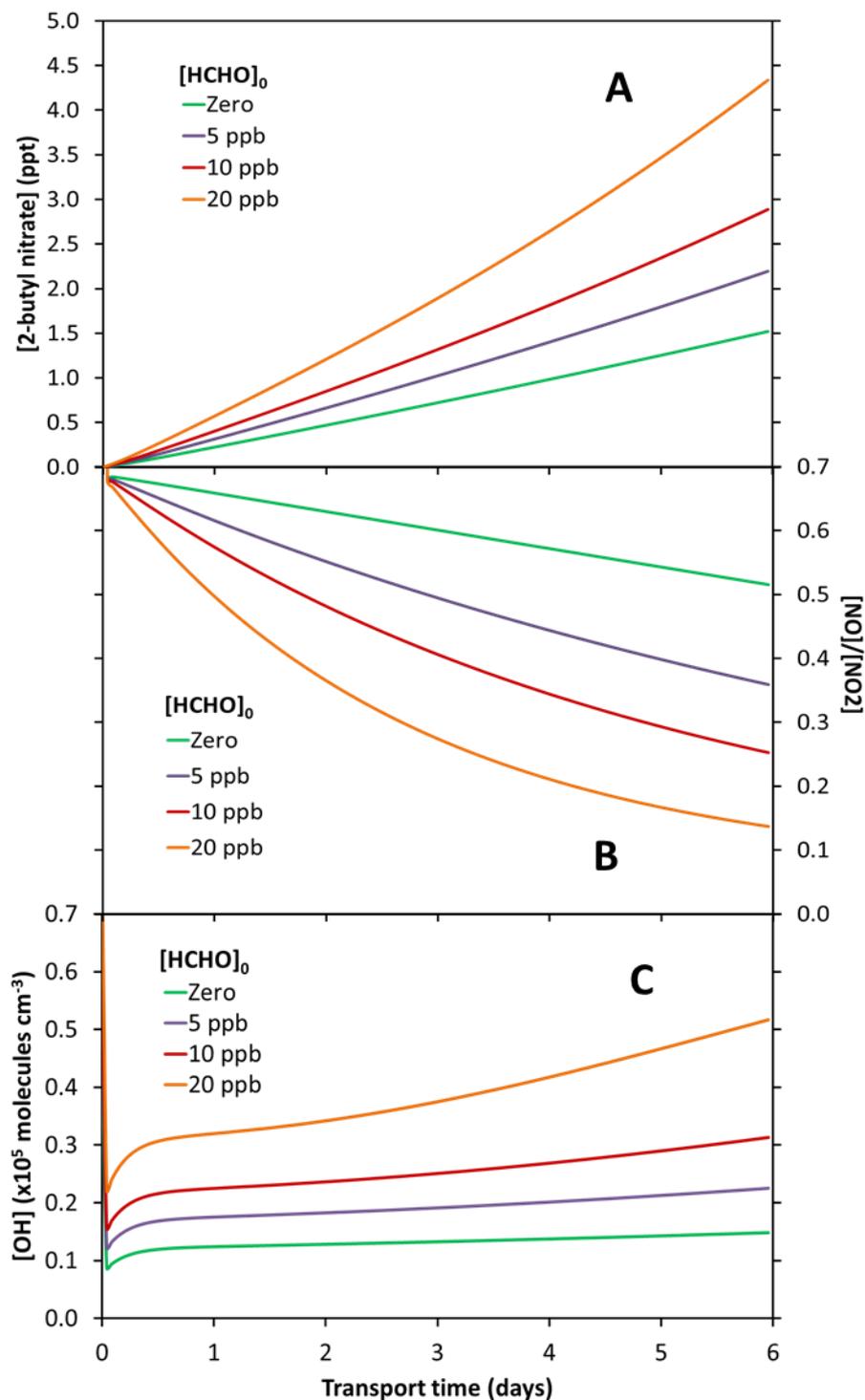


**Figure 6.14** Showing the effect of changing the initial formaldehyde mixing ratio used for model run B2 Table 7.5. Panel A, 2-butyl nitrate mixing ratio (ppt); B, $[NO]/[NO_2]$ ratio; C, OH concentration.

### 6.2.3 RO + NO$_2$

So far in this work it has been assumed that the sole formation mechanism of the alkyl nitrates is by the reaction of the alkyl peroxy radical with the NO radical (Reaction 6.2a). However it has been suggested that in highly polluted environments, the reaction of the alkoxy radical with the NO$_2$ radical (Reaction 1.10) may be important for formation of the C1 – C2 alkyl nitrates (Flocke et al., 1998; Simpson et al., 2006; Archibald et al., 2007).

$$RO_2 + NO \xrightarrow{\alpha_3} RONO_2 \qquad\qquad k_3 \qquad\qquad\qquad (R6.2a)$$

$$\xrightarrow{(1-\alpha_3)} RO + NO_2 \qquad\qquad k_3 \qquad\qquad\qquad (R6.2b)$$

$$RO + NO_2 \rightarrow RONO_2 \qquad\qquad k_8 \qquad\qquad\qquad (R6.17)$$

$$RO + O_2 \rightarrow RCHO + HO_2 \qquad\qquad k_9 \qquad\qquad\qquad (R6.18)$$
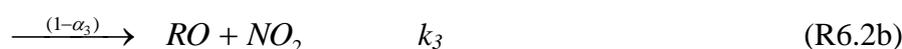
Using a steady state analysis, the relative influence of the two reaction pathways (Reaction 6.2a and Reaction 6.17) can be determined. The rate equations for the formation of the alkyl nitrate via each pathway are shown in Equations 6.13 and 6.14.

$$\frac{d[RONO_2]}{dt} = k_3[RO_2][NO]\alpha_3 \qquad\qquad\qquad (E6.13)$$

$$\frac{d[RONO_2]}{dt} = k_8[RO][NO_2] \qquad\qquad\qquad (E6.14)$$

Equation 6.15 gives the rate equation for [RO], then, assuming [RO] to be at steady state, Equation 6.16 gives an expression for [RO].

$$\frac{d[RO]}{dt} = k_3(1-\alpha_3)[RO_2][NO] - [RO]\left(k_9[O_2] + k_8[NO_2]\right) = 0 \qquad (E6.15)$$

$$[RO] = \frac{k_3(1-\alpha_3)[RO_2][NO]}{k_9[O_2]+k_8[NO_2]} \tag{E6.16}$$

Since $k_9[O_2] \gg k_8[NO_2]$ when $[NO_2] < 500$ ppb,

$$[RO] = \frac{k_3(1-\alpha_3)[RO_2][NO]}{k_9[O_2]} \tag{E6.17}$$

Substituting Equation 6.17 into Equation 6.14,

$$\frac{d[RONO_2]}{dt} = \frac{k_8 k_3(1-\alpha_3)[RO_2][NO][NO_2]}{k_9[O_2]} \tag{E6.18}$$

Then equating Equation 6.13 and Equation 6.18 to show when the formation from Reaction 6.2a (via the peroxy radical) is equal to that from Reaction 6.17 (via the alkoxy radical), and rearranging for $[NO_2]$ (Equation 6.20),

$$\frac{k_8 k_3(1-\alpha_3)[RO_2][NO][NO_2]}{k_9[O_2]} = k_3[RO_2][NO]\alpha_3 \tag{E6.19}$$

$$[NO_2] = \frac{k_9[O_2]\alpha_3}{k_8(1-\alpha_3)} \tag{E6.20}$$

Equation 6.20 gives an expression to calculate at what $[NO_2]$ the production of the alkyl nitrate from the $RO+NO_2$ route is equal to that from the $RO_2+NO$ route. It is seen that for a given alkyl nitrate this point is dependent only on the branching ratio, $\alpha_3$, and the ratio of the rate constants $k_9$ and $k_8$ (assuming the $O_2$ mixing ratio is constant). Table 6.6 shows the relevant rate constants for the C1 – C5 nitrates and the $NO_2$ mixing ratio at which this point of equality is reached. A value of $5.25 \times 10^{18}$ was assumed for the $O_2$ mixing ratio. Figure 6.16

shows the contribution of Reaction 6.17 as a percentage of the total alkyl nitrate produced for a range of values of $NO_2$.

**Table 6.6** Rate constants and branching ratios used for steady state analysis shown in Figure 6.16. Also shown is the $NO_2$ mixing ratio at which 50% of the alkyl nitrate is formed via Reaction 6.17.

| Alkyl nitrate | Rate constant ($\times 10^{-12}$ cm$^3$ molecule$^{-1}$ s$^{-1}$) | | $\alpha_3$ | [$NO_2$] (ppb) |
|:---:|:---:|:---:|:---:|:---:|
| | $k_9$ [a] | $k_8$ [a] | | |
| Methyl | 0.0019 | 15 | 0.001[b] | 27 |
| Ethyl | 0.0081 | 28 | 0.009 | 550 |
| 2-propyl | 0.0070 | 34 | 0.042 | 1900 |
| 2-butyl | 0.0077 | 33 | 0.09 | 4800 |
| 2-pentyl | - [c] | - [c] | 0.129 | - |

[a] From Atkinson et al., 2006
[b] $\alpha_3$ of methyl nitrate given as 0.001 in MCM (MCM, 2013) and <0.0003 in Flocke et al., (1998)
[c] No data available

In Figure 6.15 it is seen that for methyl nitrate a significant amount of the production occurs via the alkoxy radical even at $NO_2$ mixing ratios of only a few parts per billion. Two lines are shown for methyl nitrate as the branching ratio, $\alpha_3$, of Reaction $k_3$ is poorly constrained, given as 0.001 in the MCM in 2013 but Flocke et al. (1998) derived a value of $\leq 0.0003$. Flocke et al. (1998) and Simpson et al. (2006) have both noted levels of methyl nitrate (Flocke et al. mention ethyl nitrate too) in polluted areas that appeared to be too high to be explained by the reaction of the peroxy radical with NO (or by a natural marine source) and have postulated the alkoxy pathway as a possibly important alternative formation route. Archibald et al. (2007) reported a model run which suggested that the formation of methyl nitrate via the two production routes would be equal at $NO_x$ values of 37 ppb. It is unclear from the paper whether they mean the $NO_x$ mixing ratio or $NO_2$ mixing ratio but either would suggest a value of a similar magnitude to that shown in Table 6.6.
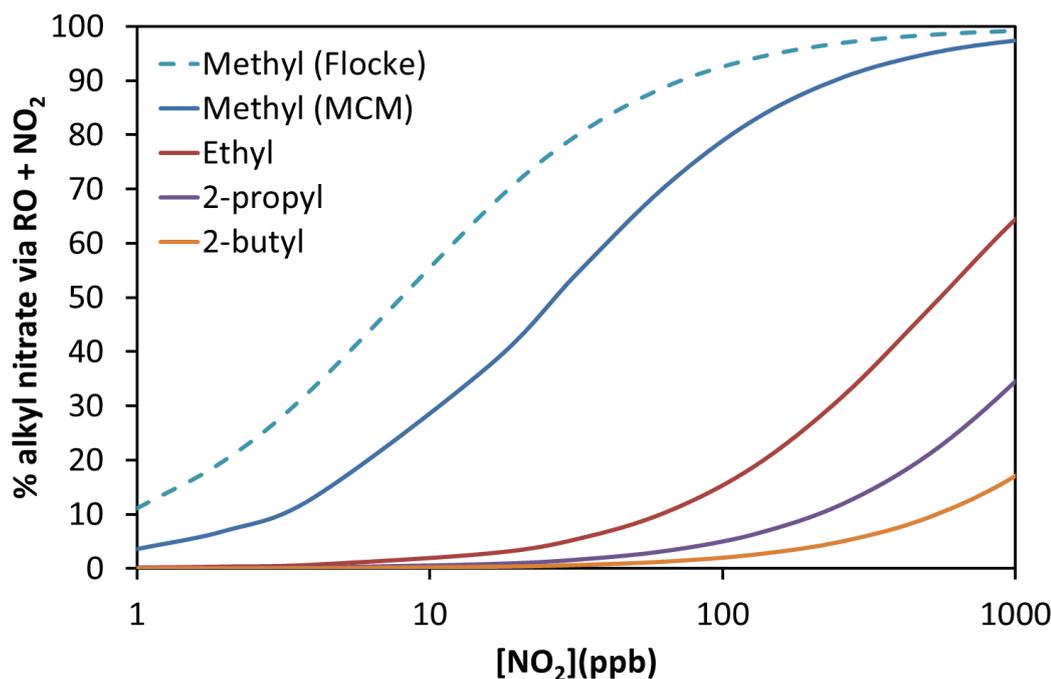
**Figure 6.15** The contribution of the formation of the alkyl nitrate via the alkoxy radical as a percentage of the total alkyl nitrate for a range of values of $NO_2$.

### 6.2.4   Summary of Box Model Studies

The findings of the investigations with the one-box model are summarised below. The dependencies described are first order dependencies, i.e. the most important, changes in other factors may also have effects but to a lesser extent.

(i)     The ratio of an alkyl nitrate to its parent alkane is independent of the initial mixing ratio of that alkane.

(ii)    The production rate of an alkyl nitrate is roughly linearly proportional to the OH concentration.

(iii)   There are two ways in which $NO_x$ mixing ratios can limit alkyl nitrate production: either through air masses being NO limited with respect to the formation of a given alkyl nitrate (see (v)) or by the $NO_x$ in an air mass being 'used up' (see (vi)).

(iv)    Alkyl nitrate production becomes $NO_x$ saturated above a given NO mixing ratio. This limit increases with increasing carbon number.

(v)     The time taken for an air mass to 'use up' all the initial $NO_x$ is dependent mainly on the initial $NO_x$ mixing ratio.

(vi)     The OH concentration of an air mass is governed by both the initial $\Sigma$HC and the initial $NO_x$ mixing ratios but mainly by $\Sigma$HC.

(vii)    Greater initial emissions of formaldehyde lead to higher [OH] in the air mass because of photolysis of formaldehyde. This leads to a greater production rate of alkyl nitrates.

(viii)   Formaldehyde may act as a buffer to the lower limit of the amount of $HO_x$ in a system by producing more $HO_x$, via photolysis, when [OH] is low.

(ix)     At high [$NO_2$] (> 27 ppb), methyl nitrate production is dominated by the reaction of the alkoxy radical with $NO_2$.


## 6.3   An Historic Northern Hemisphere OH Trend

The OH radical is the main sink in the atmosphere for the majority of trace gases. It is present in the atmosphere at mean global concentrations of roughly $1 \times 10^6$ molecules cm$^{-3}$ (e.g. Stone et al., 2012). However how the concentrations of the OH radical have changed in the past remains a large uncertainty in atmospheric chemistry and is key to being able to understand how atmospheric composition has changed in the past and how it might change in the future in response to a changing climate. In this Section an historical trend of the OH radical is derived using the atmospheric histories inferred from the firn air measurements in Chapter 5.


### 6.3.1   Photochemical Clock: Hydrocarbon Pairs

The ratio of an alkyl nitrate to its parent alkane in an air mass is dependent on the amount of processing which the air mass has undergone. This processing is dependent on both the transport time between the source and the Arctic and the mean OH concentration during transport.

Two co-emitted species with the same chemical loss mechanism but different reaction rates can be used as a ***photochemical clock*** if the initial and final ratios of the two species to each other are known (e.g. Roberts et al., 1984; Parrish et al., 1992). However if only the final ratio is known this method cannot be used. Bertman et al. (1995) developed a photochemical clock that uses two sequential first order reactions. This overcomes the need to know the initial

emission ratio of the two species. Both of these methods are described in more detail below and applied to the firn measurements from NEEM.

These photochemical clocks, as suggested by the name, provide information on [OH] (the photochemistry) and the transport time ($t$). These two variables cannot be separated by using the methods described below because they both represent chemical processing. A hydrocarbon in an air mass which has twice the OH concentration of a second air mass will undergo the same amount of processing as a hydrocarbon in the second air mass but in half the time, i.e. how processed an air mass can be said to be is the product of the loss rate and the transport time.

The mean transport time of a 'mean air mass' (i.e. the combination of air from each of the four defined regions of anthropogenic emissions) to the Arctic can be derived from examining measurements of pairs of hydrocarbons in the firn air that have different reaction rates with the OH radical. This method relies on knowing the initial ratio at which the pair of hydrocarbons were emitted.

The continuity equation for a hydrocarbon, $X$ (Equation 6.21), can be combined with the equation for a second hydrocarbon, $Y$, to give Equation 6.22.

$$[X]_t \quad = \quad [X]_0 \, e^{(-k_X [OH] t)} \tag{E6.21}$$

$$[X]_t / [Y]_t \quad = \quad [X]_0 / [Y]_0 \, e^{-(k_X - k_Y)[OH] t} \tag{E6.22}$$

$$\ln([X]_t / [Y]_t) \quad = \quad \ln([X]_0 / [Y]_0) - (k_X - k_Y)[OH] t \tag{E6.23}$$

$$\ln\left(\frac{[X_t][Y_0]}{[Y_t][X_0]}\right) \quad = \quad -(k_X - k_Y)[OH] t \tag{E6.24}$$

where $k_x$ is the reaction rate coefficient of the reaction of hydrocarbon $X$ with OH and $k_y$ that of hydrocarbon $Y$ with OH. Having rearranged Equation 6.23 to the form y = mx + c in Equation 6.24, a series of hydrocarbon pairs can be plotted to give the gradient as [OH]$t$.

### 6.3.2   Alkane Emission Ratios

To use Equation 6.24 to calculate the photochemical age [OH]$t$, both the final and initial ratios of the alkane pairs need to be known. The final ratio ($[X]_t/[Y]_t$) can be taken from the atmospheric histories derived from the NEEM firn air measurements in Section 5.2. However the initial ratio ($[X]_0/[Y]_0$) is not known. However, this ratio is equivalent to the emission ratio for two isomers and hence we can use the emissions modeling in Section 5.4 to derive an estimate of the initial emission ratios. (When comparing butanes to pentane, the emission ratio must be adjusted based on the ratio of the molecular weights to give $[Y_0]/[X_0]$.) The emissions ratios calculated in the 2-D model in this way are shown in Table 6.7. Also shown in Table 6.7 is the difference between the OH reaction rate coefficients of the hydrocarbon pairs. If $k_X - k_Y$ is positive, it is expected that the ratio ($[X]/[Y]$) will decrease with time, whereas if it is negative the ratio should increase.

The emission ratios of short chain alkanes in fuel tend to remain fairly similar due to a similar composition of fuel being burned and is also likely to be true of the butanes and pentanes as they have the same emission source (fossil fuel combustion and evaporation). This is particularly true of two isomers of the same compound such as n- and iso-butane. Goldan et al. (2000) reported the n-butane/i-butane ratio in the urban plume of Nashville to be roughly 2.0. This is close to the estimate from the 2-D model using the year 2000 emissions in Europe of 2.12.

**Table 6.7** The initial mixing ratios (derived from the emission ratios from Chapter 5) for year 2000, measured ratios in the firn air for year 2000, and comparison of reaction rates of pairs of butane and pentane isomers.

| X / Y | Derived initial ratio $(X_0/Y_0)$ | Arctic measured ratio $(X_t/Y_t)$ | $k_X - k_Y$ $(\times 10^{12}$ cm$^3$ molecules$^{-1}$ s$^{-1})$ 298K |
|---|---|---|---|
| n-butane/iso-butane | 2.12 | 2.06 | 0.24 |
| n-pentane/iso-pentane | 0.92 | 0.91 | 0.15 |
| n-butane/n-pentane | 2.67 | 3.38 | -1.44 |
| n-butane/iso-pentane | 2.45 | 3.06 | -1.29 |
| iso-butane/iso-pentane | 1.16 | 1.49 | -1.53 |
| iso-butane/n-pentane | 1.26 | 1.64 | -1.68 |
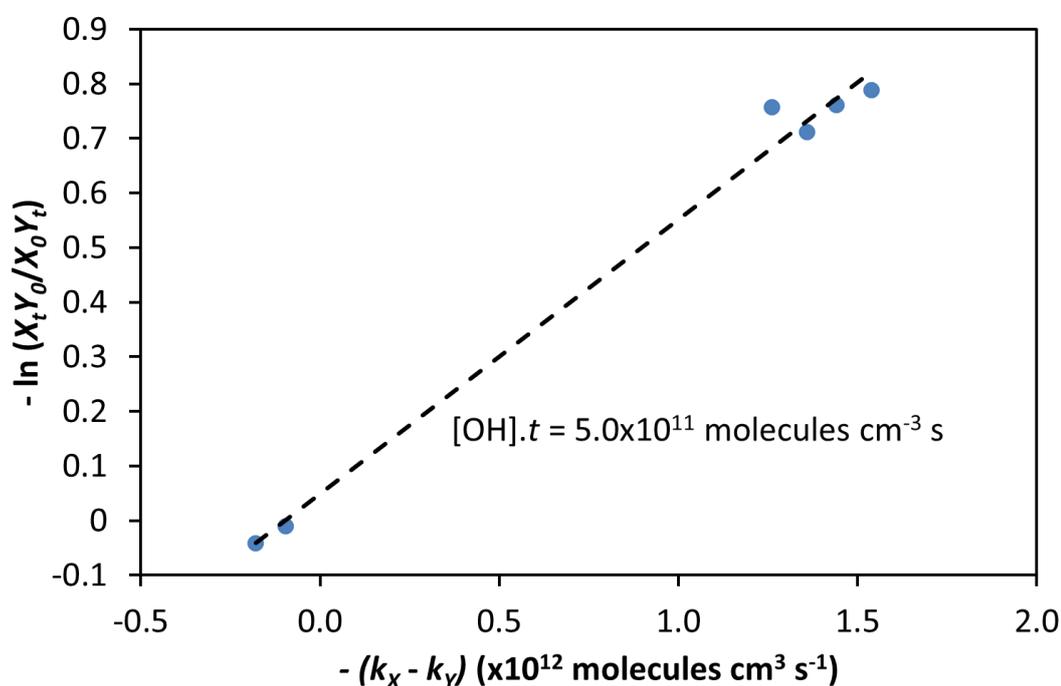


**Figure 6.16** Plot to determine the photochemical age (i.e. the product of mean transport time and mean OH concentration) of a mean air mass received in the Arctic. Using Equation 6.24 and the hydrocarbon pairs shown in Table 6.7 for year 2000. All data used are shown in Table 6.7. The gradient is equal to the mean OH concentration (molecules cm$^{-3}$) during transport multiplied by the mean transport time (s).

Figure 6.16 shows that the mean transport time (s), multiplied by the mean OH concentration during transport (molecules cm$^{-3}$), gives a value of $5.0 \times 10^{11}$ molecules cm$^{-3}$ s. With the measurements available it is not possible to split this value into the constituent OH concentration and transport time. However it is possible to calculate the range which these two values could take. These are shown in Table 6.7 for a typical range of OH concentrations (e.g. Spivakovsky et al. 2000). By using real world studies, such as that of Stohl et al. (2007) following a biomass burning plume from eastern Europe to the Arctic, it is be seen that transport times from northern Eurasia can be very rapid, on the order of $3 - 4$ days. While it is also possible that air masses can arrive at the Arctic by a more circuitous route it seems likely that the mean transport time is at the lower end of that shown in Table 6.8 and hence the mean [OH] during transport would be on the order of $5 \times 10^5$ molecules cm$^{-3}$. This is in between the reported mean summer time and winter time OH concentrations in the northern hemisphere of roughly $1 \times 10^6$ and $1 \times 10^5$ molecules cm$^{-3}$ respectively (e.g. Spivakovsky et al. 2000).

**Table 6.8** Mean OH concentration and mean transport time of air masses transported to the Arctic in winter based on the [OH].$t$ value of $5.0 \times 10^{11}$ molecules cm$^{-3}$ s for year 2000 calculated in Figure 6.17.

| Mean [OH] (molecules cm$^{-3}$) | Mean transport time (days) |
|---|---|
| $1 \times 10^5$ | 58 |
| $2 \times 10^5$ | 29 |
| $5 \times 10^5$ | 12 |
| $1 \times 10^6$ | 5.8 |

If mean transport time, $t$, is assumed to remain the same inter-annually (i.e. the atmospheric transport patterns remain similar and the contributions from the source regions do not change significantly), and emission ratios are assumed to remain constant, then a comparison of the changing measured Arctic ratio of pairs of hydrocarbons through time should be a record of changing OH concentrations in the transported air masses.

In relation to inter-annual variability of the mean transport time to the Arctic, Kahl et al. (1999) suggest that there is decadal scale (4 – 14 years) variability in transport patterns of pollutants from the northern hemisphere to the Greenland ice sheet based on three climate teleconnection indices (North Atlantic Oscillation, Southern Oscillation index, and Pacific/North America Oscillation), however note no overall long term trend. Additionally Hirdman et al. (2010) note that only a very small part of the long term Arctic trends in black carbon and sulfate aerosol can possible be explained by changes in transport from source regions (which they identify as being northern Eurasia).

By plotting the types of graph shown in Figure 6.16 above, a time series of values for [OH].*t* can be obtained. This is shown in Figure 6.17 for the period 1950 – 2008.
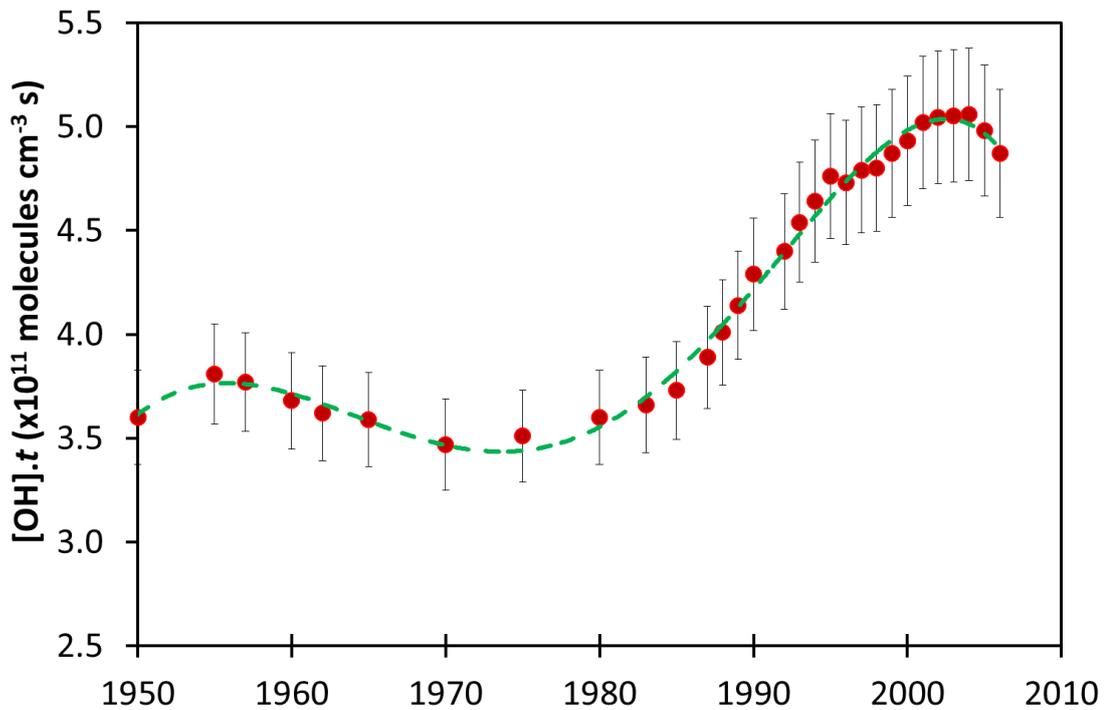


**Figure 6.17** Time series of the value [OH].*t* calculated using Equation 6.24 with the six hydrocarbon pairs shown in Table 6.7. Green dashed line is a sixth order polynomial fit. Uncertainties are calculated as described in the text.

It is seen in Figure 6.17 that the [OH].*t* value appears to display a self-consistent trend during the period of study. From 1970 to the early 2000s the [OH].*t* value (and hence the mean OH concentration if the transport time, *t*, is assumed to be constant with time) increased steadily,

almost doubling during this period. After the early-2000s the value begins to decline again. Prior to 1970 it appears that the OH concentration may have been a little higher than during the 1970s but this is not significant within the uncertainties.

### 6.3.2.1 Uncertainties in the [OH].t trend

The uncertainties in the trend in the photochemical age, [OH].$t$, derived from the atmospheric histories of the alkanes come from three terms, the initial ratio $[X]_0/[Y]_0$ (or emission ratio), the final ratio $[X]_t/[Y]_t$, and the $(k_x - k_y)$ term.

It is assumed that the emission ratios do not change through the period of study.

The uncertainties derived from the atmospheric histories presented in Section 5.2 are shown in Figure 6.17. For each data point used in the plot to calculate the gradient (see Figure 6.16) the uncertainties from the two atmospheric histories were combined using the square root of the sum of the squares. The uncertainty for each [OH].$t$ value was then calculated as the square root of the sum of the squares of each six data points, divided by n-1.

The emission ratios used are calculated in the 2-D atmospheric model and the derived emissions are a function of the transport in the model, the OH concentrations, the atmospheric histories and the reaction rates of both the alkanes with OH and methyl chloroform with OH (which defines the mean annual OH). These uncertainties are discussed in Section 5.4 in which the emissions of the alkanes are derived from the atmospheric histories.

Figure 6.17 shows the [OH].$t$ trend derived using two different sensitivity runs in which the emission ratios of the butanes to each other and the pentanes to each other are kept the same, but the emission ratios of the butanes to the pentanes are increased / decreased by 20%. It is seen that the absolute changes to [OH].$t$ remain the same when changing the emission ratios, an increase of roughly $1.6 \times 10^{11}$ molecules cm$^{-3}$ s between 1970 and 2000. However the relative change is affected. For the scenario using the emissions derived from the 2-D model, the relative change in [OH].$t$ between 1970 and 2000 is roughly 45%. For the scenario in which the butane/pentane emission ratios are increased by 20%, the relative change in [OH].$t$ increases to 65%, while for the scenario in which the butane/pentane emission ratios are decreased by 20%, the relative change in [OH].$t$ decreases to 35%.
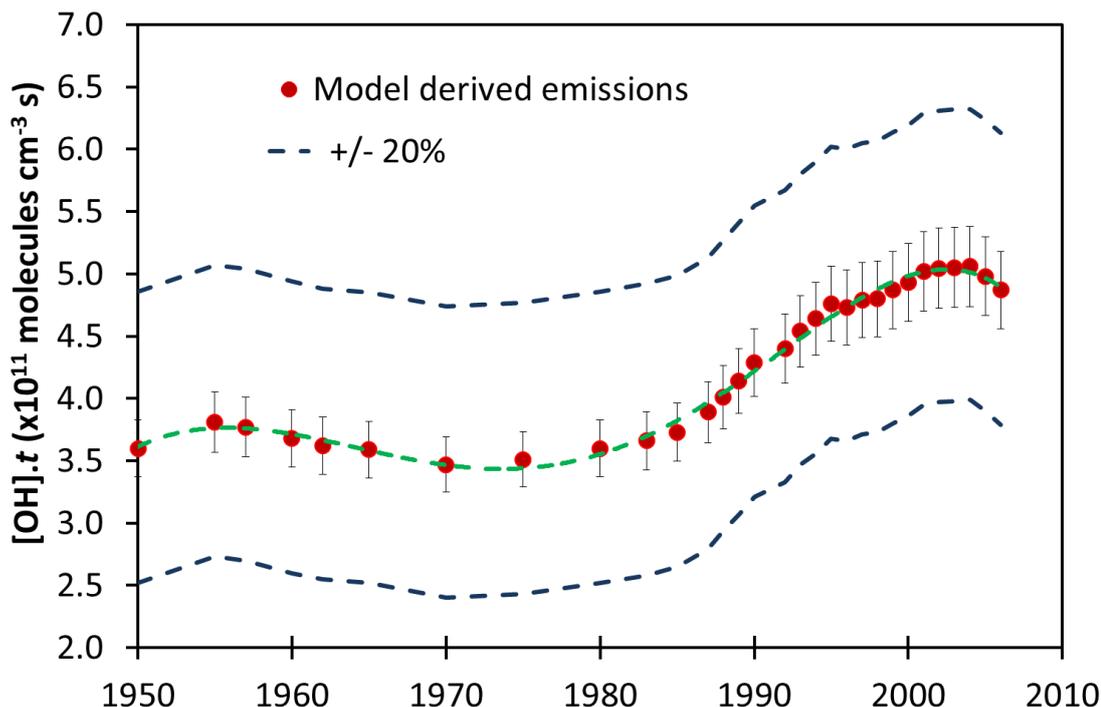
**Figure 6.18** Sensitivity runs for [OH].$t$. 'Model derived emissions' taken from Figure 6.17. '+/-20%' runs butane/pentane ratios increased or decreased by 20%.

From this analysis it is seen that the emission ratios, probably the greatest uncertainty in the work, do not affect the conclusion that [OH].$t$ has increased between 1970 and 2000 (still assuming that the ratios do not change with time). However they do affect the size of that increase.

### 6.3.3   Photochemical Clock: Alkyl nitrate - Alkane Ratios

Another way to calculate the value [OH].$t$ is by using a sequence of first order reactions such as the alkyl nitrate-alkane system. The benefit of this is that there is no need to know the initial ratio of the reactants in order to use the equation. This method was first proposed by Bertman et al. (1995). Equation 6.25 shows the rate equation for the alkyl nitrate (RONO$_2$), with formation from oxidation of the hydrocarbon (RH) and loss to the sinks. β represents the product of the two branching ratios $\alpha_1$ and $\alpha_3$ (see Reactions 6.1 and 6.2), $k_A$ and $k_B$ are pseudo first order rate constants with $k_A = k_1[OH]$ and $k_B = (k_7[OH] + j_6)$ (see Reactions 6.1, 6.4 and 6.5).

$$\frac{d[RONO_2]}{dt} = \beta k_A[RH] - k_B[RONO_2] \qquad \text{(E6.25)}$$

Integrating Equation 6.25 gives Equation 6.26 and this can be simplified by assuming that the initial alkyl nitrate-hydrocarbon ratio is zero, i.e. there is no alkyl nitrate. This yields Equation 6.27 – this derivation is from Bertman et al. (1995).

$$\frac{[RONO_2]}{[RH]} = \frac{\beta k_A}{(k_B - k_A)}\left(1 - e^{(k_A - k_B)t}\right) + \frac{[RONO_2]_0}{[RH]_0}e^{(k_A - k_B)t} \qquad \text{(E6.26)}$$

$$\frac{[RONO_2]}{[RH]} = \frac{\beta k_A}{(k_B - k_A)}\left(1 - e^{(k_A - k_B)t}\right) \qquad \text{(E6.27)}$$

Equation 6.27 can then be expanded to Equation 6.28 (making the assumption that the loss to OH is greater than that to photolysis and hence $k_B = k_7[OH]$) and then rearranged to Equation 6.29 in order to make it of the form y = mx + c with the gradient as [OH].$t$.

$$\frac{[RONO_2]}{[RH]} = \frac{\beta k_1[OH]}{[OH](k_7 - k_1)}\left(1 - e^{(k_1 - k_7)[OH]t}\right) \qquad \text{(E6.28)}$$

$$\ln\left(1 - \frac{[RONO_2]}{[RH]}\frac{(k_7 - k_1)}{\beta k_1}\right) = (k_1 - k_7)[OH]t \qquad \text{(E6.29)}$$

where $k_1$ and $k_7$ are from Reactions 6.1 and 6.5. Using Equation 6.29, a graph can be plotted using the three alkyl nitrate-alkane pairs, n-butane and 2-butyl nitrate, n-pentane and 2+3-pentyl nitrate and iso-pentane and 3-methyl-2-butyl nitrate, of which the gradient is [OH].$t$. This is shown in Figure 6.19 for year 2000.
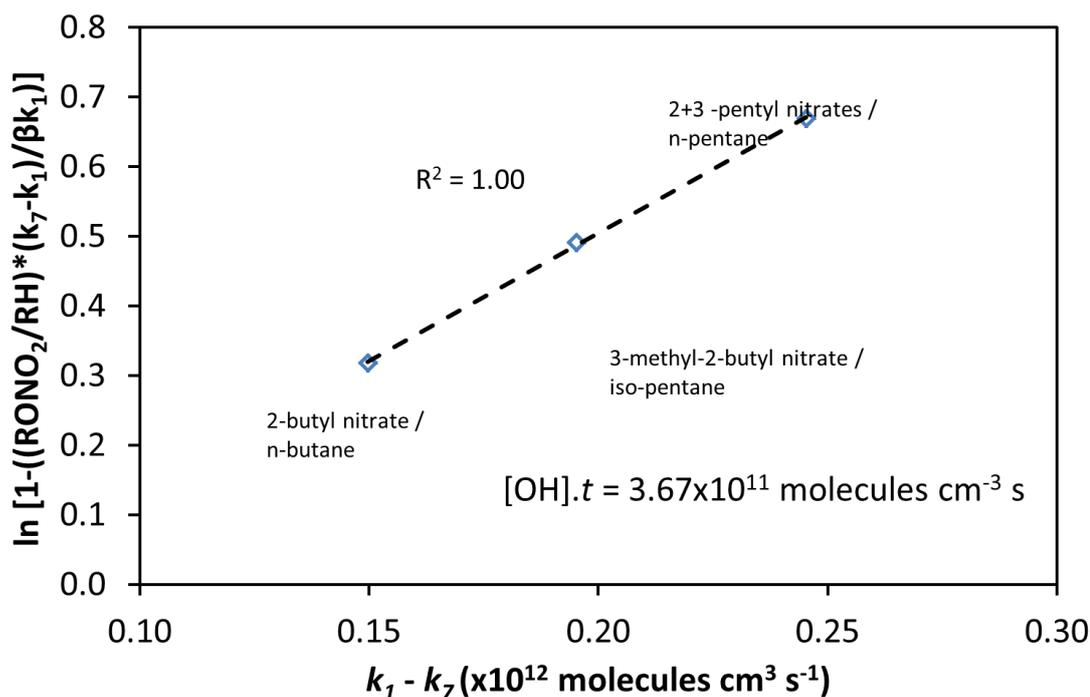
**Figure 6.19** Calculation of the value [OH].$t$ for year 2000 using Equation 6.29 with the three alkyl nitrate-alkane pairs: n-butane and 2-butyl nitrate, n-pentane and 2+3-pentyl nitrate and iso-pentane and 3-methyl-2-butyl nitrate.

Figure 6.19 shows a correlation between the values calculated from the three alkyl nitrate-alkane pairs for year 2000 with an R-squared value of 1.00.

A time series of the gradients calculated for different years can then be produced, making the same assumptions as made in the previous section for the time series plot of [OH].$t$ (i.e. that mean transport time and the contributions from source regions have not changed significantly, though now there need be no assumption of constant emission ratios). This is shown in Figure 6.20 for the period 1950 – 2008.
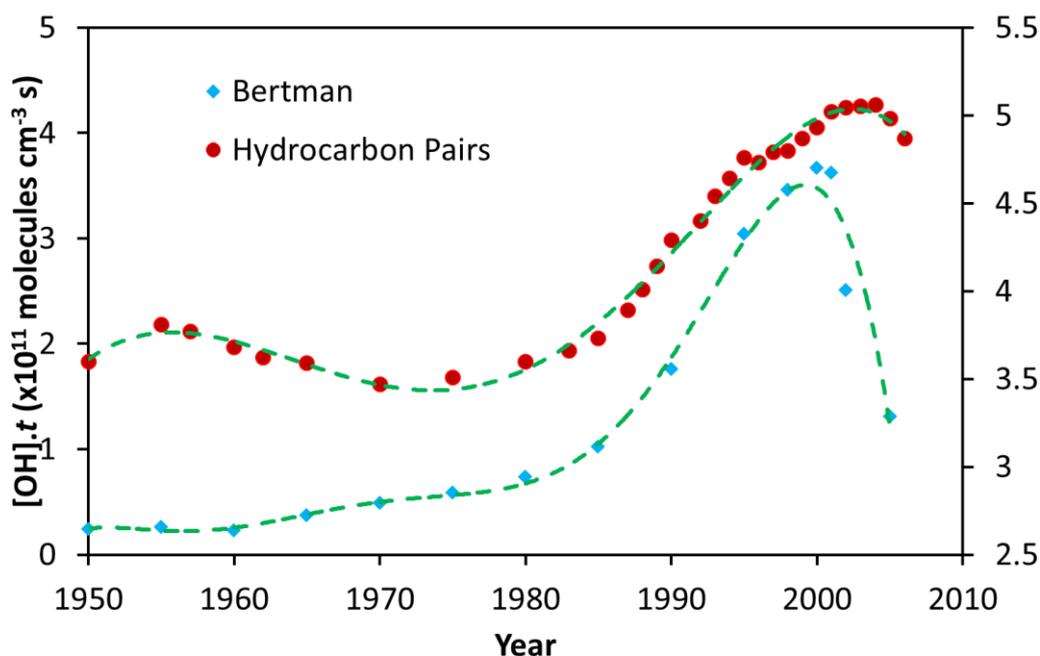
**Figure 6.20** A comparison of the [OH].*t* trend derived using alkyl nitrate-alkane pairs (Equation 6.29) – left hand axis and using hydrocarbon pairs (Equation 6.24) – right hand axis (Figure 6.17).

It is seen in Figure 6.20 that the time series of [OH].*t* derived from the alkyl nitrate-alkane pairs is below $0.5 \times 10^{11}$ molecules cm$^{-3}$ s between 1950 and 1975 before rising to about $3.7 \times 10^{11}$ molecules cm$^{-3}$ s in 2000 and then declining back to roughly $1.3 \times 10^{11}$ molecules cm$^{-3}$ s by 2005. The peaks and troughs of this trend show a similar timing to those derived using the hydrocarbon pairs. However the relative change between the peaks and troughs is much greater for the trend derived from the alkyl nitrate-alkane pairs.

The shape and amplitude of the [OH].*t* trend calculated from the alkyl nitrate-alkane pairs is not surprising since it is a function of the mean of the alkyl nitrate-alkane ratios shown in Figure 6.1. However the reason for the difference in amplitude of the [OH].*t* trend calculated by the two methods shown in Figure 6.20 must be explained. The Bertman equation assumes production of the alkyl nitrates in an excess of NO$_x$ so that the system is never NO$_x$ limited. It will be seen later in this chapter that is unlikely to be the case for transport to the Arctic. At this time the photolysis sink has also been ignored and there is an assumption of there being no initial alkyl nitrate mixing ratios.

For these reasons, when the [OH].$t$ trend is discussed further below, it is the trend derived using the hydrocarbon pairs (Figure 6.17) which is shown rather than that using the Bertman equation.

### 6.3.4 The Atmospheric Methane Growth Rate

Having derived an historic OH trend (assuming mean transport, $t$, not to have changed) using two semi-independent methods in the previous two sections, further corroborating evidence is presented below using measurements of atmospheric methane.

The mixing ratio of methane can be expected to be sensitive to the OH concentration since reaction with OH is the main loss process of methane in the troposphere. Methane displays a clear seasonality with loss during the summer, when [OH] is high and growth during the winter when [OH] is low. Any change in the mean annual mixing ratio of atmospheric methane can be assumed to be representative of a change to either the source, i.e. emissions, or to the loss process, i.e. a change in the concentration of the OH radical. So, assuming constant emissions, an increase in the methane growth rate would represent decreasing [OH] and vice versa. Though methane is not at steady state in the atmosphere and northern hemisphere (and global) emissions are increasing (e.g. EDGAR v4.2), the effect of changing concentrations of the OH radical might still be seen in the methane growth rate.

Figure 6.21 shows a comparison of the time series of the value [OH].$t$ (Figure 6.17) and the growth rate of atmospheric methane mixing ratios ($d[CH_4]/dt$). The methane mixing ratios used were global means taken from Etheridge et al. (1998) for the period 1945 – 1984, and the measured mixing ratios at Mauna Loa, Hawaii (Dlugokencky et al., 2012) for the period 1985 – 2008. The growth rate was calculated by first fitting a polynomial to the methane mixing ratio and then calculating the derivative of the polynomial fit. This polynomial fit smooths out some of the intra-annual variability as well as some of the short-term inter-annual variability giving a record comparable to that derived from measurements in the firn.
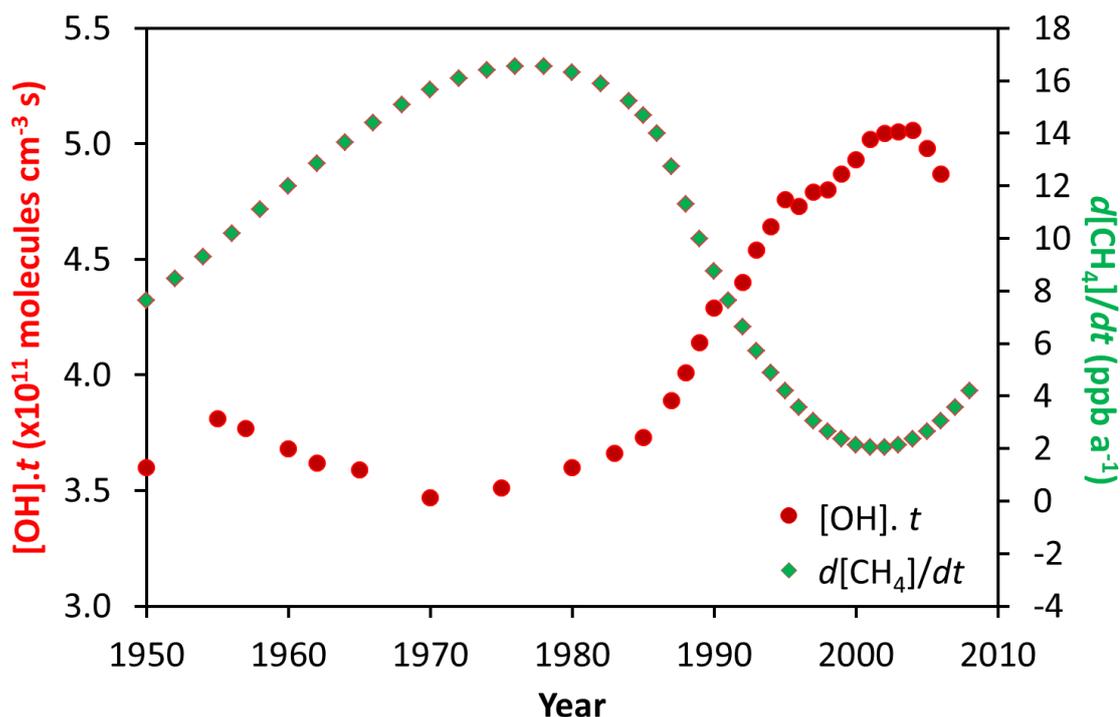
**Figure 6.21** Comparison of the growth rate of atmospheric methane mixing ratios to the value [OH].*t* shown in Figure 6.17. Methane growth rate: 1945 – 1984, the derivative of a fourth order polynomial fit to the global mean mixing ratio reported in Etheridge et al. (1998); 1985 – 2008, the derivative of a third order polynomial fit to measured methane mixing ratios at Mauna Loa, Hawaii (NOAA).

It is seen in Figure 6.21 that the growth rate of the atmospheric methane mixing ratio ($d$[CH$_4$]/$dt$) appears to be anti-correlated with the derived value [OH].$t$. If [OH].$t$ is assumed to be representative of OH concentrations then it is seen that this relationship is as predicted above – increasing OH concentrations lead to a decrease in $d$[CH$_4$]/$dt$ and vice-versa. Assuming that these two parameters, [OH] and $d$[CH$_4$]/$dt$ are directly linked to each other the question arises which is the independent variable. The OH radical is the main sink for CH$_4$ but CH$_4$ is also a significant sink for OH. However from Figure 6.21 it can be argued that it must be the changing OH that is controlling $d$[CH$_4$]/$dt$ rather than the other way around because $d$[CH$_4$]/$dt$ is always positive. Hence if $d$[CH$_4$]/$dt$ was controlling OH, there should just be an attenuation on a background of constantly falling OH. It appears from Figure 6.21 that there is a relatively constant growth rate of roughly 6 – 8 ppb yr$^{-1}$, presumably caused by rising emissions, which is being attenuated by changes to the sink, OH.

Figure 6.22 shows the correlation of $d[CH_4]/dt$ with the [OH].$t$ trend derived using hydrocarbon pairs. The earlier methane growth rate data (from Etheridge et al. 1998) is available bi-annually, the data from Mauna Loa is available annually.
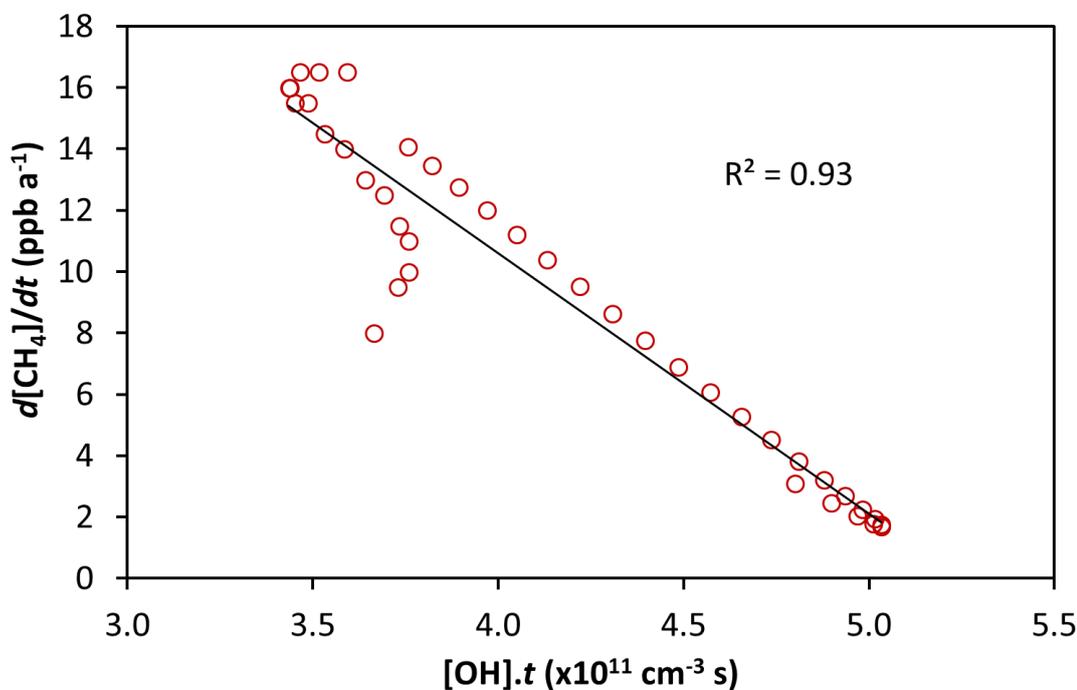


**Figure 6.22** Correlation of [OH].$t$ derived from hydrocarbon pairs with the atmospheric methane growth rate between 1950 and 2007.

It is seen in Figure 6.22 that there is a strong anti-correlation between the [OH].$t$ values derived using the hydrocarbon pairs and the annual growth rate of methane mixing ratios in the atmosphere. When [OH].$t$ values are high, the methane growth rate is low, because more methane is being oxidised in the atmosphere, [OH].$t$ values are low the methane growth rate is high because less of the methane being emitted to the atmosphere is being lost. The R-squared value is 0.93 for the period 1950 – 2007. This rises to 0.99 for the period 1970 – 2007. The less good agreement during the period 1950 – 1970 could be caused by emissions changing in a different way to during the later period or simply by the fact that the there is a greater uncertainty in the [OH].$t$ values during this period.

The contribution of changes in the sources and sinks to $d[CH_4]/dt$ cannot be established from Figure 6.21, but it seems very unlikely that the observed strong correlation throughout the record between $[OH].t$ and $d[CH_4]/dt$ is mere coincidence. Assuming that the decadal variation in $d[CH_4]/dt$ is being caused by changes in $[OH]$ it can also be said that the sources of methane (i.e. $E_{CH4} + C_{CH4}$) have been growing fairly constantly during this period because the decadal variation of $d[CH_4]/dt$ is superimposed on a mean $d[CH_4]/dt$ value of about 8 ppb $a^{-1}$.

One of the implications of this negative correlation between $[OH]$ and the atmospheric methane growth rate is that if $[OH]$ continues to fall from the peak in the early-2000s, the atmospheric methane burden will begin to rapidly increase again, as indeed has been seen in recent years (e.g. Dlugokencky et al., 2012).

At a simple level the steady state mixing ratio of methane in the atmosphere is a balance of the sources (i.e. emissions) and the sinks (i.e. the concentration of the OH radical). I.e. $[CH_4]$ = Emissions / $k[OH]$. The methane mixing ratio in 2000 can be considered as being at steady state, i.e. the growth rate is zero, in 1970 the system is not at steady state, $[CH_4]$ is growing, so the 1970 mixing ratio represents a minimum estimate of the steady state mixing ratio. Northern hemisphere $[CH_4]$ in 1970 was roughly 1400 ppb, in 2000 it was roughly 1780 ppb, an increase of 27%. Bottom-up emission estimates suggest that global methane emissions increased by roughly 45 − 60% during this same time period (EDGAR v4.2, Stern and Kaufmann, 1996). If $[OH]$ had remained constant during this period then $CH_4$ mixing ratios should also have increased by 50 − 60%. In order to recreate this $[OH]$ would need to have increased by 20 − 25%. Conversely if $[OH]$ has increased by 45% as suggested by Figure 6.17, global $CH_4$ emissions would have to have risen by about 80% during this period.

There have been several explanations proposed to account for the recent trend in atmospheric methane. These have generally focused on possible changes to emissions (partly because is widely believed that the OH sink has not varied greatly over the past few decades based on methyl chloroform work (e.g. Montzka et al., 2011) − see Section 6.3.5 below). Changes to methane emissions from agriculture (Kai et al., 2011), natural wetlands (e.g. Pison et al., 2013) or a combination of both (e.g. Bousquet et al., 2006; Kirschke et al., 2013) have been examined.

The link between mean OH concentrations and the growth rate of methane in the atmosphere has been examined by Rigby et al. (2008). Although the time scales over which they

considered the methane growth rate are very short, they conclude that observed changes in methane growth rates at sites from both hemispheres are likely caused by changes to mean global [OH] (backed up by an extension of the Prinn et al. methyl chloroform record which appears to show a slight decrease from 2004 – 2007 (though increases from 1997 – 2004)) and not by emissions. Other studies have sought to explain the slow-down in growth rate, e.g. Dlugokencky et al. (1998) suggest that the slow-down of the methane growth rate from 1984 – 1996 can be accounted for by assuming constant [OH] and methane emissions and that the system has just been tending towards a steady state.

### 6.3.5   Comparison of [OH].$t$ Trend to Methyl Chloroform Derived [OH] Trend

Making the assumption that the mean transport time, $t$, has not changed, then the trend shown in Figure 6.17 represents the changing mean OH concentration to which air masses reaching the Arctic have been exposed, i.e. a trend in mid-high latitude northern hemisphere annual mean [OH].

The agreement between the [OH] trend derived from the two semi-independent methods using the firn measurements, and a third line of corroborating evidence, using the change in the growth rate of atmospheric methane, is remarkable and strengthens the case that this is a robust result.

A northern hemisphere trend in the concentration of the OH radical has previously been reported by Prinn et al. (2001) for the period 1979 – 2001. This trend was calculated using the changing growth rate of methyl chloroform ($CH_3CCl_3$) in the atmosphere using background air measurements from five AGAGE stations. $CH_3CCl_3$ has a global lifetime of 6.1 years with respect to reaction with OH. The other minor sinks of atmospheric $CH_3CCl_3$ are thought to be well constrained. If the emissions are known then the changes in the growth rate can be used to provide a constraint on the sink (i.e concentrations of the OH radical).

A comparison between the trend in northern hemisphere [OH] from Prinn et al. (2001) and that derived from the hydrocarbon pairs (Figure 6.17) is shown in Figure 6.23. Using the same method, Prinn et al. (2005) and then Rigby et al. (2008) extended the [OH] record up to 2007 but only presented global averages. This is surprising given the spread of AGAGE measurement sites available and that the 2001 paper showed significant differences between

the derived northern and southern hemisphere [OH] trends. For this reason the trends derived in these subsequent papers are not presented for comparison in Figure 6.23.
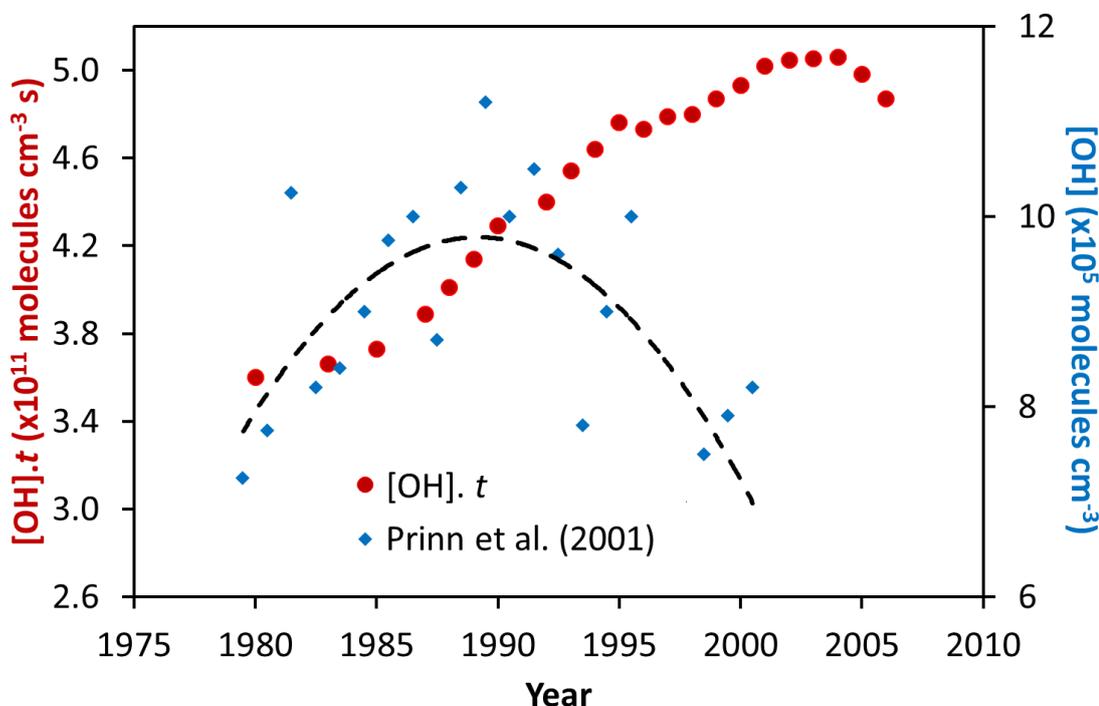


**Figure 6.23** A comparison of annual mean [OH].*t* values calculated using hydrocarbon pairs (Figure 6.17) and annual mean northern hemisphere [OH] calculated by Prinn et al. (2001) calculated using the growth rate of methyl chloroform. A second order polynomial fit to the Prinn data is also shown (black dashed line), as used in Prinn et al. (2001).

It is seen in Figure 6.23 that the trend in northern hemisphere [OH] derived by Prinn et al. (2001) increases from an annual mean of about $7 \times 10^5$ to $10 - 11 \times 10^5$ molecules cm$^{-3}$ between 1979 and about 1990. It then decreases back to about $7 \times 10^5$ molecules cm$^{-3}$ by 2001. A second order polynomial is fitted to the data in Figure 6.23 as in Prinn et al. (2001).

The increase of [OH] derived by Prinn et al. during the period 1979 – 1991 shows a good agreement with the values of [OH].*t* derived using the hydrocarbon pairs. However the decline in [OH] begins earlier than that of [OH].*t* and the decline is more steep.

The scatter in the Prinn dataset (assuming it to be 'real') serves to demonstrate once again the smoothing effect of the firn. The firn does not resolve inter-annual variability but it also does

not resolve short scale intra-annual variability and this effect becomes more pronounced with depth as the resolution of the firn decreases.
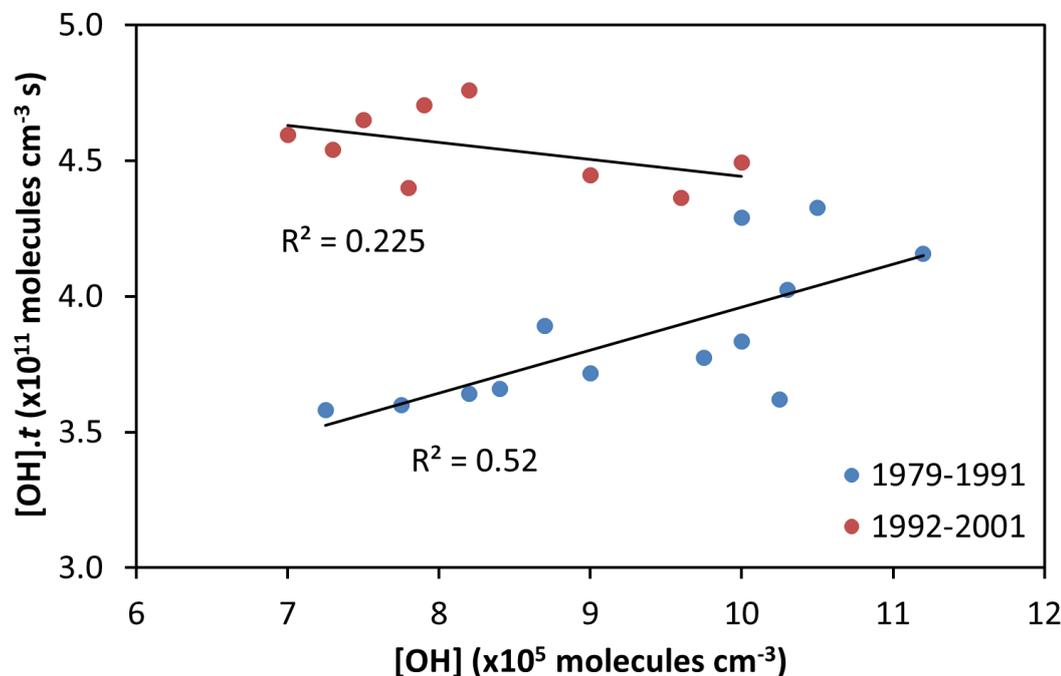


**Figure 6.24** Correlation of [OH].$t$ derived from hydrocarbon pairs (Figure 6.17) with annual mean [OH] derived by Prinn et al. (2001) for the periods 1979 – 1991 and 1992 – 2001. A linear fit is applied to each period.

Figure 6.24 shows a correlation between the two data sets seen in Figure 6.23. It is seen that the data between 1979 and 1991 show a correlation with an R-squared value of 0.52. However the period 1992 – 2001 shows no correlation.

Emissions (and hence atmospheric mixing ratios) of methyl chloroform decreased rapidly after 1992 because of regulation under the Montreal Protocol (Prinn et al., 2001). It is noted that the decline in the [OH] values calculated by Prinn et al. began after 1991 and it must be questioned how reliable the values of [OH] mixing ratios calculated from a species with such rapidly changing atmospheric mixing ratios are. The point was noted by Krol and Lelieveld (2003) that the [OH] trend derived using the Prinn et al. method is very sensitive to the assumed emissions. Measurements by Krol et al. (2003) during aircraft flights over central Europe suggested that there were still significant emissions of methyl chloroform into the late

1990s and that a shift in the timing of emissions based on their observations would reduce the magnitude of the [OH] decrease reported by Prinn et al. (2001) after 1991. The emissions used by Prinn et al. were further questioned by Wennberg et al. (2004) who suggested that the polar oceans may have acted as a sink for methyl chloroform when atmospheric mixing ratios were increasing but may have become a source as atmospheric mixing ratios began to fall after 1991.

Finally, using the good agreement between the dataset [OH].$t$ derived from the firn measurements and the [OH] trend derived by Prinn et al. (2001) for the period 1979 – 1991, an estimate can be made of the mean transport time. This calculates a mean transport time from the source regions to the Arctic of about 5 days. This agrees well with the study of Stohl et al. (2007) who, as discussed above, followed a biomass burning plume from north-eastern Europe to the Arctic taking 3 – 4 days.

The results from this section raise the question: what is causing the apparent trend in the [OH] radical in the northern hemisphere. This is explored further in the following section.

## 6.4 Separating the Effects of OH and NO$_x$ on Observed Alkyl Nitrate Mixing Ratios

In this chapter it has been seen that the alkyl nitrate mixing ratios expected to be produced from a system are dependent on both the OH and the NO concentrations. In the following section the measurements from the firn are used to try to examine how much of the changes in the observed mixing ratios can be attributed to changing [OH] and how much to changing [NO].
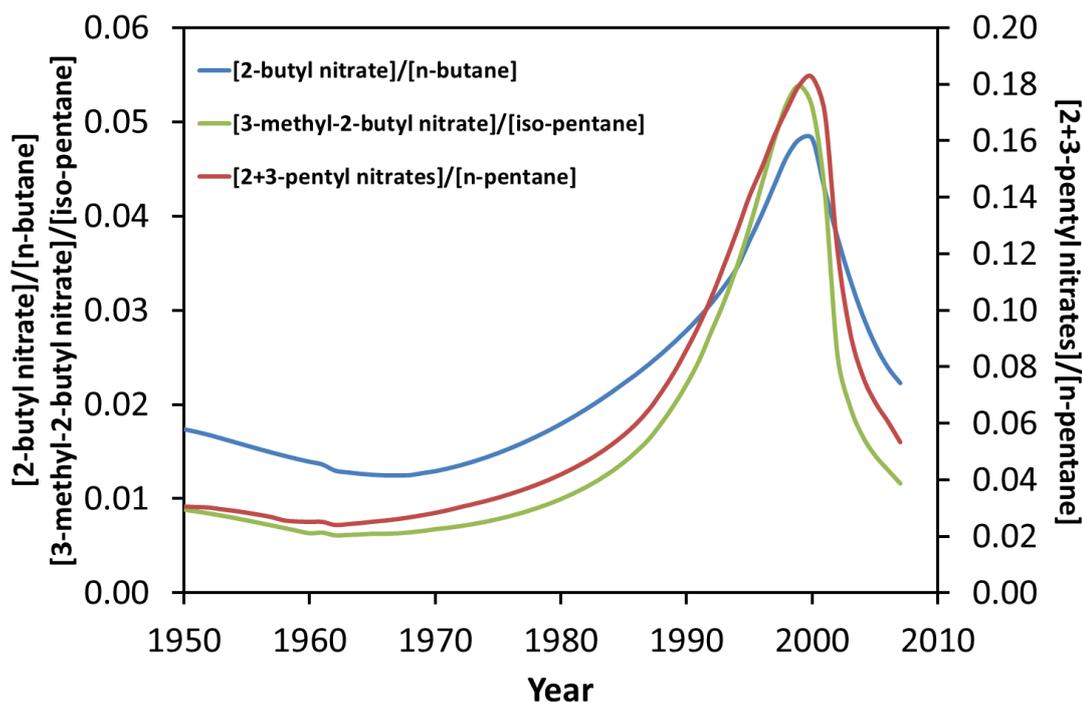
**Figure 6.25** Ratios of the three alkane-alkyl nitrate pairs: n-butane and 2-butyl nitrate, n-pentane and 2+3-pentyl nitrate, and iso-pentane and 3-methyl-2-butyl nitrate derived from NEEM firn air.

The different percentage increases in the [alkyl nitrate]/[alkane] ratios from 1975 to the peak in the late-1990s (Figure 6.25) by each pair can be explained using the values of the steady state mixing ratios for each alkyl nitrate given in Table 6.3 (calculated using Equation 6.12). It would be expected that, if the system is assumed to be NO saturated, and so the rate of production of the alkyl nitrate is dependent on the rate of oxidation of the hydrocarbon, that as the reaction rate $k_1$ increases the system will tend towards steady state more quickly. This assumes [OH].$t$ is the same for each pair. This indeed is seen and is shown in Figure 6.26 which plots the fraction of the steady state [alkyl nitrate]/[alkane] ratio reached at the mid-1990s peak, against the reaction rate $k_1$. It is seen that the pentyl nitrates reach about 0.4 of the steady state [alkyl nitrate]/[alkane] ratio, 2-butyl nitrate 0.18 and 2-propyl nitrate 0.09. This could explain why the higher nitrates appear to show a greater response to changing OH concentrations. It is not possible to compare ethyl and methyl nitrate in Figure 6.26 because they are also produced during the summer months and hence the mean [OH] to which they are exposed is greater than that to which the propyl, butyl and pentyl nitrates are exposed.
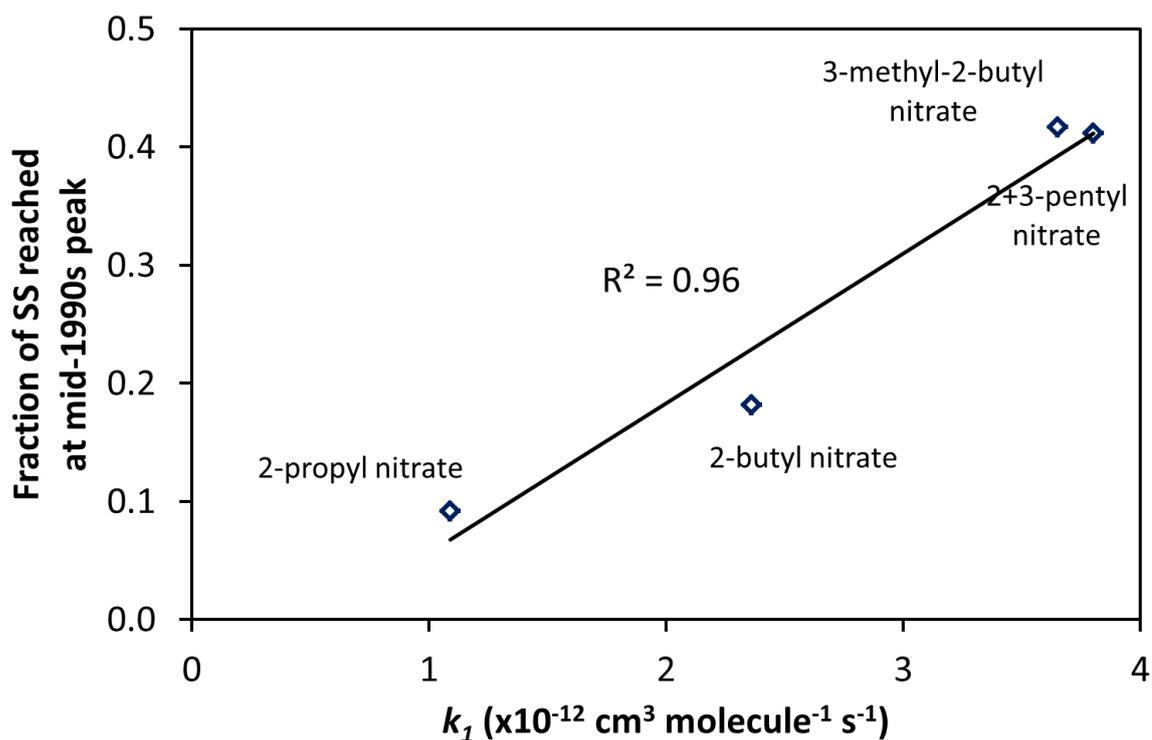
**Figure 6.26** The fraction of the steady state [alkyl nitrate]/[alkane] ratio (see Table 6.3) reached at the mid-1990s peak for the C3 – C5 nitrates.

Figure 6.27 shows correlation plots of the [alkyl nitrate]/[alkane] ratios with $[OH].t$ for the butyl and pentyl nitrates for three periods: 1950 – 1969, 1970 – 1999 and 2000 – 2006, i.e. the two periods of relatively stable OH either side of the rapid growth in [OH] between 1970 and 2000. It should be noted that the range of the x and y-axes are different for each plot. Figure 6.28 shows the same correlation plot for [2+3-pentyl nitrate]/[n-pentane] for the whole period 1950 – 2006 so the gradients can easily be compared.
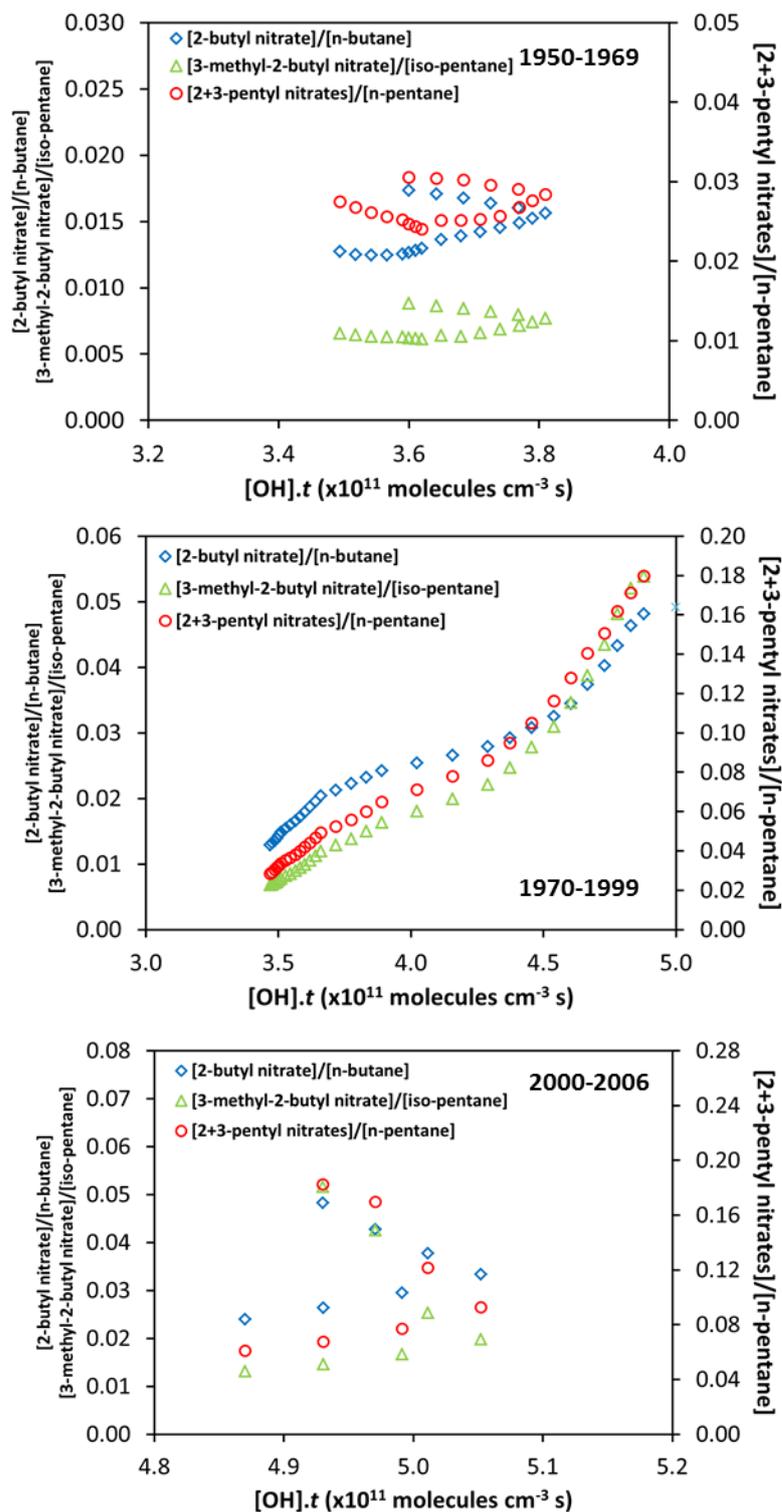
**Figure 6.27** Correlation of [alkyl nitrate]/[alkane] ratios with [OH].*t* (Figure 6.17) for the three periods 1950 – 1969, 1970 – 1999 and 2000 – 2006. Note the different scales for the x and y axes in the different panels.
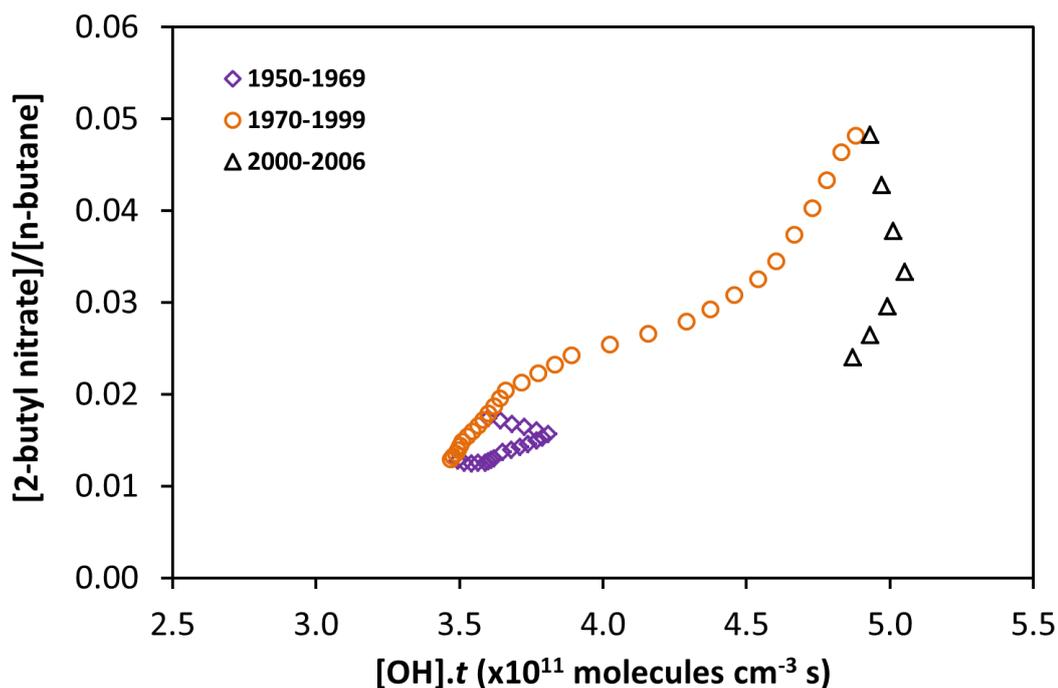
**Figure 6.28** Correlation of [2-butyl nitrate]/[n-butane] with [OH].*t* (Figure 6.17) for the period 1950 – 2006.

It was shown in Figure 6.8 that the variation of the [alkyl nitrate]/[alkane] ratio is independent of the alkane mixing ratio. Hence any variation in the ratio can be assumed to be caused by changing [OH] and [NO]. From what is known from Chapters 5 and 6 about the derived [OH] trend (Figure 6.17) and the reported NO emissions trend (Figure 6.2, EDGAR v4.2, HYDE), it is seen that the time periods covered by the three plots in Figure 6.27 broadly represent three regimes. In the first, 1950 – 1969, [OH].*t* is relatively stable while NO emissions are rising, in the second, 1970 – 1999, [OH].*t* is rising while NO emissions are fairly stable, and in the third, 2000 – 2006, both [OH].*t* and NO emissions are falling.

It was shown in Figure 6.10 that there is a roughly linear relationship in the change in the steady state mixing ratio of the alkyl nitrate (and hence the [alkyl nitrate]/[alkane] ratio), i.e. if [OH] doubles then the maximum response from the ratio should be a doubling. Anything in excess of this gradient could be assumed to be a response to changing [NO]. As already stated, it is not immediately clear whether this [NO] limitation would be caused by [NO] mixing ratios being below the NO saturation point (Figure 6.9) or by NO being 'used up' in the air mass and preventing further production of the alkyl nitrate.

240

## 6.5   Conclusions and Implications for Atmospheric Chemistry

This section summarises the findings from this chapter and the implications of these for wider atmospheric chemistry.

### 6.5.1   Conclusions

- *In the background atmosphere, production of alkyl nitrates is dependent on the atmospheric $[NO]/[HO_2]$ ratio.*

- *Assuming constant $NO_x$, the alkyl nitrate-alkane ratio at a given point in time is linearly dependent on $[OH]$.*

- *Below a certain $[OH]$ mixing ratio the rate of change of an alkyl nitrate is dominated by the photolysis sink. This point appears to increase with decreasing carbon number.*

- *Given fixed conditions, changes to the initial formaldehyde mixing ratio of an air mass have a roughly linear effect on the OH concentration (because photolysis of a molecule of formaldehyde produces a molecule of $HO_2$) and therefore a roughly linear effect on the rate of net production of alkyl nitrate in that air mass.*

- *At a certain NO mixing ratio production of alkyl nitrates becomes NO saturated, i.e. the rate determining step becomes the oxidation of the alkane rather than the reaction of the peroxy radical with NO.*

- *Above a certain $NO_x$ mixing ratio alkyl nitrates begin to be formed by the reaction of the alkoxy radical with $NO_2$. This effect only becomes important in very polluted air masses and then only for methyl nitrate.*

- *The NO saturation point with regard to alkyl nitrate formation increases with increasing carbon number.*

- *Mid-high latitude northern hemisphere mean atmospheric OH concentrations appear to have varied by roughly 45% during the period 1970 – 2000, assuming a constant mean transport time of air masses from source regions to the Arctic during this period.*

- *Changes in the atmospheric growth rate of methane during the period 1950 – 2006 are strongly correlated with the northern hemisphere [OH] trend derived in this work.*

- *Assuming mean [OH] concentrations as calculated by Prinn et al. (2001) for the period 1979 – 1991, then the mean transport time for an air mass to the Arctic from the source regions of pollution, based on using hydrocarbon pairs as a photochemical clock, is roughly 5 days.*

- *The regions that contribute most to modeled alkane and alkyl nitrate mixing ratios in the Arctic are Europe and Russia.*

### 6.5.2   Implications for Atmospheric Chemistry

The northern hemisphere atmospheric lifetime of all atmospheric species whose main loss process is reaction with OH may have varied by up to 45% between 1970 and 2000. However for longer lived species the lifetime would also be dependent on the [OH] trend in the southern hemisphere which may have varied differently.

Variation in the atmospheric methane growth rate on a decadal time scale during the period 1950 – 2008 appear to have been driven by changes in northern hemisphere [OH] (superimposed on a fairly constant growth rate attributable to increasing $CH_4$ sources). These variations in the methane sink suggest that historic top-down derived methane emission trends which have assumed a constant OH burden will have derived a trend which is actually a function of both emissions and changing [OH] (although this depends to some extent on the southern hemisphere trend in [OH]). This is also the case for top-down derived emission trends of all species for which reaction with OH is a sink, such as the alkane emissions derived in Chapter 5.

If northern hemisphere atmospheric [OH] declines, as it appears to have done since the early 2000s, then methane concentrations can be expected to rise again from the plateau of the early 2000s, as has indeed been observed in recent years (e.g. Dlugokencky et al., 2012).

The observed trend in [OH] could be explained by changes to the total hydrocarbon (caused by changing emissions, as suggested by the firn data presented in Chapter 5) and CO (Petrenko et al., 2012) and $NO_x$ (e.g. Lawrence and Crutzen, 1999) burdens in the northern hemisphere atmosphere.

In Section 6.2.1.2 it was shown that an air mass with a high initial $\Sigma HC/NO_x$ ratio produced lower alkyl nitrate mixing ratios than an air mass with a low initial $\Sigma HC/NO_x$ ratio. It was also shown that the OH concentration in the air mass is inversely proportional to the initial $\Sigma HC$ mixing ratio. It has also been shown that higher OH concentrations will lead to higher alkyl nitrate mixing ratios.

From the work in this chapter, using the alkanes and alkyl nitrates, a qualitative history of mid-high northern hemisphere [OH] and [$NO_x$] can be proposed. The [OH] trend shown in Figure 6.17 suggests that [OH] was relatively stable between 1950 and 1970, increased between 1975 and the early-2000s and has decreased since this time. The increase in [OH] after 1975 may be partly attributable to a reduction in emissions of hydrocarbons and CO. While hydrocarbon emissions may not have decreased as much as suggested by the derived alkane atmospheric histories in Chapter 5 (since these are seen to also be influenced by the increased [OH]), the EDGAR v4.2 database shows total NMVOC emissions from North America, Europe and Russia decreasing between 1975 and 2000 by roughly a third. It could also be that the reactivity of the total NMVOC mix has declined. The fall in [OH] subsequent to the early-2000s can perhaps be attributed to the facts that, firstly the decline in hydrocarbons has, if not stopped completely, then at least slowed significantly, and $NO_x$ emissions are falling. $NO_x$ has been shown to be linked to [OH] by production of ozone which subsequently forms OH radicals (e.g. Lawrence and Crutzen, 1999). The effect of falling atmospheric $NO_x$ on ozone has been observed at mid-latitude northern hemisphere sites, e.g. at Hohenpiessenberg, Germany (Parrish et al., 2012).

The description of possible changes to northern hemisphere atmospheric composition given above, based on the observations of long term trends of alkanes and alkyl nitrates from firn air from NEEM, requires much more work to be fully described. The trend in [OH] has been

determined semi-quantitatively (assuming a non-changing mean transport time). The effect of changing the total hydrocarbon burden on atmospheric [OH] has been demonstrated qualitatively in the box model. The effect of changing $NO_x$ on [OH], has been the subject of numerous studies over the past decades and a full investigation of how this system works is beyond the scope of this thesis.

# Chapter 7

# Conclusions and Future Research Directions

# 7 Conclusions and Future Research Directions

In this section the major conclusions from each results chapter are presented, followed by a synthesis of the conclusions and finally a suggestion of future research directions based on the findings from this work.

The first two results chapters use an established technique to derive global annual emissions of long lived ozone depleting and greenhouse gases. The final two chapters use historic atmospheric measurements from firn air, in conjunction with a box model and a 2-D atmospheric model to investigate the historic composition of the northern hemisphere atmosphere. These chapters have yielded some unexpected and exciting results. The original hypothesis of the work using contemporaneous alkyl nitrate and alkane measurements from the Greenland firn, was that this would enable an historic trend of northern hemisphere $NO_x$ emissions to be derived. This has not been possible except for a very broadly qualitative history. However a far more important result has arisen. An historic trend of mean annual mid-high latitude northern hemisphere [OH] has been derived. This trend has implications for our understanding of atmospheric chemistry in the past, present and future that extend far beyond the scope of this thesis. The implications and possible future directions of this work are discussed in Sections 3 and 4 of this chapter.

## 7.1 Long Lived Gases

### 7.1.1 Halons

- *The atmospheric mixing ratios of H-1202, H-1211 and H-2402 are all declining and are likely to continue to do so due to the cessation of all halon production in 2010. H-1301 mixing ratios are still growing.*

*Chapter 3.3*

- o The total contribution of the halons to tropospheric bromine at Cape Grim peaked at 8.1 ppt in 2007 – 2008 and has since declined to 7.9 ppt in mid-2011.
- o H-1301 is likely to become the main halon contributing to tropospheric bromine by 2025.

- o The total contribution to tropospheric bromine from the halons in 2060 is predicted to be about 3.0 ppt, 38% of that in 2010.

- *Emissions of all of the halons have declined since peaking in the late-1980s to mid-1990s but the decline has slowed in recent years with no significant changes in emissions of H-1301 and H-2402 between 2006 and 2010.*

    *Chapter 3.4*

- *Emissions of H-1202 are continuing even though H-1211 production has supposedly ceased suggesting either that H-1211 production has not ceased, that there is an alternative source of H-1202, that there is an existing bank of H-1202 which is being used up or that H-1211 stocks are contaminated with H-1202.*

    *Chapter 3.5*

- *Alternative atmospheric lifetimes for the halons based on recently reported new stratospheric lifetimes imply alternative values for the remaining banks and have implications for the predicted future decrease of halons in the atmosphere.*

    *Chapter 3.8*

    - o Lifetimes are calculated as 15 years for H-1211, 82 years for H-1301, 17 years for H-2402 and 2.6 years for H-1202.
    - o For H-1301 this alternative lifetime implies that the 2010 bank is 48 Gg, 13% larger than estimated by HTOC. This would delay the predicted decline in tropospheric bromine. For H-1211 this alternative lifetime implies a 2010 bank of 24 Gg, 63% smaller than estimated by HTOC. With estimated current emission rates, a bank of this size would be rapidly exhausted, quickening the predicted decline in tropospheric bromine.

### 7.1.2 Fully Fluorinated Gases

- *The atmospheric mixing ratios of all the PFCs reported herein have increased greatly since the late 1970s.*

    *Chapter 4.3.1*

- *Emissions of the majority of the PFCs reported herein are falling. However atmospheric mixing ratios continue to increase because of their long atmospheric lifetimes (>2,500 years).*

*Chapter 4.3*

   o It is unclear whether emissions of $C_2F_6$ are rising or falling.
   o Emissions of c-$C_4F_8$ are rising rapidly, probably associated with its use as a more efficient replacement for $C_2F_6$ and $C_3F_8$ in chemical vapour deposition (CVD) chamber cleaning in the electronics industry.
   o Emissions of the higher PFCs ($C_4F_{10}$, $C_5F_{12}$, $C_6F_{14}$ and $C_7F_{16}$) all peaked in the mid-1990s and have since fallen, with the exception of $C_7F_{16}$.

- *The total rate of increase of the contribution of the PFCs reported herein to atmospheric radiative forcing has remained steady for the past decade.*

*Chapter 4.7*

- *Emissions of the greenhouse gas SF$_5$CF$_3$ appear to have ceased in the mid-2000s. The emission source seems to have been related to perfluorooctanesulfonyl fluoride (POSF) production by the company 3M.*

*Chapter 4.4*

- *There has been a rapid increase of the atmospheric mixing ratio of the CFC replacement gas HFC-227ea since 1995.*

*Chapter 4.5*

## 7.2 Hydrocarbon-NO$_x$ Chemistry

### 7.2.1 Alkanes

- *Measurements from firn air at NEEM show the trend in mean annual mixing ratios of six alkanes (ethane, propane, n-butane, iso-butane, n-pentane, iso-pentane) in the Arctic from 2008 back to at least 1950.*

*Chapter 5.2*

- o All alkanes display a similar trend in mixing ratios with an increase between 1950 – ~1980 (ethane ~25%, propane ~60%, n-butane ~80%, iso-butane ~115%, n-pentane ~160%, iso-pentane ~210%) followed by a decrease back to slightly below 1950 levels.

- o The firn measurements suggest the decline in Arctic alkane mixing ratios stopped in the early-2000s and began to increase again up to 2008.

- *Northern hemisphere emissions histories of the six alkanes, derived using a 2-D atmospheric model in conjunction with the firn measurements, and changing emission distributions derived from EDGAR v4.2, show emissions from Europe, North America and Russia roughly halving between 1970 and 2008, whereas those from Asia roughly doubled over the same period. This conclusion assumes that there have been no long-term trends in OH during this period.*

*Chapter 5.3*

- o The decline in emissions from Europe, North America and Russia is presumably driven by ever stricter emission controls on road transport. The increase in Asia is driven by the rapid industrialisation and population growth and increasing affluence of south-east Asia, particularly China.
- o However a part of the observed emissions trend may be accounted for by changing [OH]. The [OH] trend derived in this work would greatly reduce the rate of decline of emissions since 1975. This would give a much better agreement between the derived emissions and reported bottom-up emissions.

### 7.2.2 Alkyl Nitrates

- *Measurements from firn air at NEEM show the trend in mean annual mixing ratios of six alkyl nitrates (methyl, ethyl, 2-propyl, 2-butyl, 2+3-pentyl and 3-methyl-2-butyl nitrate) in the Arctic from 2008 back to at least 1950.*

*Chapter 5.7*

o The Arctic mixing ratios of the butyl and pentyl nitrates increased slowly between 1950 and 1970 before increasing rapidly up to the late 1990s (2-butyl nitrate ~230%, 2+3-pentyl nitrate ~640%, 3-methyl-2-butyl nitrate ~900%) and subsequently falling back to roughly 1970 levels.

o The Arctic mixing ratios of methyl and ethyl nitrate appear to decline throughout the record with mixing ratios in 2008 less than 20% of those in 1950. It is unclear whether this represents a real atmospheric trend or is caused by processes occurring within the firn.

- ***In background air, the amount of alkyl nitrate production from alkyl peroxy radicals is controlled by the [NO]/[HO$_2$] ratio. The amount of the peroxy radical being converted to the alkyl nitrate has been termed the production efficiency.***

*Chapter 6.1*

o In background air, with an [NO]/[HO$_2$] ratio of ~3, alkyl nitrates are not being produced at 100% efficiency and hence a change in the [NO]/[HO$_2$] ratio will significantly change the amount of alkyl nitrate produced per peroxy radical.

- ***Alkyl nitrate production in an air mass becomes NO$_x$ saturated at a given NO$_x$ mixing ratio which appears to increase with increasing carbon number.***

*Chapter 6.2.1.2*

- ***The photochemical formation pathway RO + NO$_2$ can become important in polluted air masses for methyl nitrate (and to a lesser extent ethyl nitrate).***

*Chapter 7.2.3*

o The importance of the RO + NO$_2$ pathway compared to RO$_2$ + NO is entirely dependent on the branching ratio ($\alpha_3$) of the RO$_2$ + NO reaction pathway. The smaller $\alpha_3$ is, the more important the RO + NO$_2$ pathway is.

- o At 10 ppb of $NO_2$ the $RO + NO_2$ pathway accounts for 30 – 60% of methyl nitrate production. At 100 ppb it accounts for 85 – 95% of methyl nitrate production and almost 20% of ethyl nitrate production.

- ***The rate of alkyl nitrate production in a polluted air mass is proportional to the OH concentration in that air mass.***

    *Chapter 7.2.1.1*

- ***An increase in the initial aldehyde mixing ratio of a polluted air mass increase the rate of alkyl nitrate production by increasing the $HO_x$ in the system via the photolysis reaction: $HCHO + h\nu \longrightarrow HCO + H \longrightarrow 2HO_2$.***

    *Chapter 7.2.2*

## 7.2.3   Northern Hemisphere [OH] trend

- ***A derived time series of northern hemisphere mean annual photochemical processing of air masses reaching the Arctic suggests an increase in atmospheric OH concentrations between 1970 and 2000, with concentrations increasing by roughly 45%, and a subsequent decline of about 5% to 2005.***

    *Chapter 6.4*

    - o The time series was derived by two semi-independent photochemical clock methods from firn measurements using hydrocarbon pairs and alkyl nitrate-alkane pairs.

    - o The trend is also anti-correlated with the growth rate of atmospheric methane and the period 1979 – 1991 agrees well with the trend reported by Prinn et al. (2001).

    - o Using the OH concentrations reported by Prinn et al. (2001) for 1979 – 1991, suggests a mean transport time of pollutants from source regions to the Arctic on the order of 5 days.

250

## 7.3 Implications for Global Atmospheric Chemistry

- *If concentrations of the OH radical in the northern hemisphere continue to fall, as they appear to have done since the early 2000s (suggested by both the hydrocarbon and the alkyl nitrate atmospheric histories derived from the firn air, assuming the mean transport time from the sources to have remained constant), possibly caused by falling $NO_x$ emissions, the lifetimes of many greenhouse gases will increase. This will accelerate global warming and climate change.*

  *Chapter 6*

  o The growth rate of atmospheric methane has been shown to correlate with the derived [OH] trend. This correlation can be taken as a proxy for all greenhouse gases whose major sink is reaction with OH.

- *Emissions of the halons have fallen from a peak in the mid-1990s and if they continue to decline as predicted, the contribution to stratospheric bromine will also decline aiding the recovery of the stratospheric ozone layer.*

  *Chapter 3*

- *The total growth rate of the fully fluorinated compounds, in terms of million metric tonnes of $CO_2$ equivalent, reported in this work is falling. However any decrease in emissions will not reduce atmospheric mixing ratios, just slow the growth rate, because of the extremely long lifetime of the gases. Hence the emissions to date and any future emissions must be considered a permanent change to the radiative forcing capacity of the atmosphere.*

  *Chapter 4*

## 7.4   Future Research Directions

This thesis, particularly the final chapter, has thrown up many new questions the answers of which were beyond the remit of this thesis but which could provide fruitful avenues for further research.

### 7.4.1   Long Lived Gases

The work on the long lifetime gases requires continued monitoring of these gases. As emissions of halons continue to decline and those of $SF_5CF_3$ have apparently ceased it is important to periodically monitor these gases to ensure that global production has not restarted. This is particularly the case for $SF_5CF_3$ since its long lifetime and high radiative efficiency means that any emission is effectively a permanent change to atmospheric composition.

Questions remain about the lifetimes of the halons, which affect the future atmospheric fate both in terms of the sizes of the remaining banks and the residence time in the atmosphere. There is also still a question as to the source of H-1202.

The continued emission of the PFCs must also be monitored, particularly in light of the possibility that PFC emissions from aluminium smelting may begin to rise again in the near future as new Chinese plants have been reported to emit PFCs during standard production time rather than just during 'anode effects'. Again, the long lifetimes of these gases means that continual monitoring is important to ensure that any rapid increase caused by an industrial process can quickly be recognised and alternative methods sought.

The emission of CFC replacements such as HFCs has rapidly increased and must continue to be monitored since many of these have been found to be effective greenhouse gases.

In addition to the monitoring of known trace gases in the atmosphere, work must continue to identify new trace gases in the atmosphere, to identify their sources and to assess their impact in terms of ozone depleting potential or global warming potential, so that agreements such as the Montreal Protocol can continue to be effective.

### 7.4.2 Modeling

In this work a 2-D atmospheric chemical transport model, constrained by atmospheric measurements was used to derive annual emissions. The method of fitting the model output to the measurements which were used to constrain the emissions was to fit to a rough mean of the measurements. This approach has been used historically in much published work on the emissions of long lived gases. However it is clear that a more mathematical approach to fitting the model output to the atmospheric measurements would be appropriate and would provide a mathematically valid 'best fit' scenario. Such a curve fitting approach could look to reduce the errors associated with the fit to each data point, i.e. a least squares type approach to a curve fitted by a commonly available statistical package such as R. This is the direction in which the work should be taken in the future.

The emissions modeling work presented here naturally leads on to more detailed inverse modeling approach in which measurements from several sites are used to constrain the location of emissions of a gas on a regional scale. It was shown in this work how this can be done to a certain extent using the 2-D model with just atmospheric trends from different hemispheres. However the future of this this work continues to develop at smaller scales using 3-D regional models to provide much better constraints on emission sources.

This work has suggested that changes in [OH] in polluted air masses are far more important in determining mixing ratios of alkyl nitrates than changes in $NO_x$. The historic [OH] variation derived in this work would be straightforward to implement in the model by using a fixed OH field. This work would help to confirm whether it is the 2-D nature of the model that is limiting its ability to recreate the observed alkyl nitrate trends. It seems likely to be a combination of the two factors, since the homogeneity of the atmosphere assumed in the model will mean that $NO_x$ is never present at the mixing ratios which are observed in pollution plumes.

Hence future work in this direction would ideally use a 3-D model to investigate the problem. This model could be run with a fixed OH field and a variable field.

### 7.4.3 Historic Emission Trends and Atmospheric Lifetimes

In Chapter 5 historic trends of alkane emissions were derived, however, as was noted in the chapter, these were derived using the 2-D model with a non-varying OH field and that in fact

the emission trends derived are actually a function of both emissions and the loss process, i.e. reaction with OH. The 2-D model should be used with a parameterized OH field that varies as suggested in Chapter 6. That running a model with OH varying as derived in Chapter 6 would give better results is further strengthened by the improved agreement of the top-down emission estimates with bottom-up emission estimates that would result from this.

Furthermore, the [OH] trend derived in Chapter 6 suggests that emission histories of all species which have reaction with OH as a sink that have assumed non-varying annual [OH] should be re-evaluated. In particular work on the atmospheric trend of methane which does not appear to be related directly to emissions.

In addition, this work suggests that reports such as those of the WMO and the IPCC which report atmospheric lifetimes should ensure that these are either given with reference to a specific mean OH concentration or be given as a range based on the observed changes in [OH]. However for gases with mainly northern hemisphere emissions but with lifetimes of several years, the southern hemisphere [OH] trend will be almost as important which, as suggested by Prinn et al. (2001) may be quite different to the northern hemisphere trend.

### 7.4.4   The Historic Oxidative Capacity and Composition of the Atmosphere

The first question to address is the validity of the presented OH trend, particularly in light of the general agreement of chemistry-climate models that there has been very little variation in global mean [OH] during the past century (e.g. Naik et al., 2013). This question is strongly linked to the question of what exactly the presented OH trend represents, i.e. is it only valid for winter time pollution plumes from Europe/Russia, or is it representative of a wider northern hemisphere trend (as would be suggested by a correlation with the global methane growth rate).

To confirm the observed OH trend in the Arctic, firn derived records of other trace gases with well established emission histories could be investigated. To explore whether the trend is representative of a wider northern hemisphere trend more long term records of secondary oxidation products should be studied, e.g. ozone. Further work using a suite of gases measured at various global stations, such as the use of methyl chloroform and other species in Montzka et al. (2011), must continue to be used and improved upon.

The derived [OH] trend poses the obvious question, what has led to this trend? There are some brief suggestions at the end of Chapter 6 that the increase from 1975 – 2000 was caused by a combination of the reduction in both the total NMVOC burden and the reactivity of that burden and that the decrease since 2000 may be related to reduced $NO_x$ emissions. However these are just suggestions and much more detailed work needs to be done to understand this trend. Though much work has been done and continues to be done in this area of research, having an historical trend of [OH] with which to work should make progress in this field more productive especially on a long timescale.

In addition the apparent relationship of [OH] to the methane growth rate suggests that if we understand the source of the [OH] changes then this could provide a control on the growth of methane in the atmosphere. A confirmation of this link and work to examine how this could be controlled could play a key role in providing a temporary respite from increasing global temperatures caused by the predicted growth of methane in the atmosphere. Depending on how [OH] was controlled, this could be a much safer and more viable alternative to many of the geo-engineering solutions to climate change proposed. This is because whereas many such solutions will effectively treat the Earth as a laboratory and try to push the atmosphere to states the effects of which are unknown, increasing [OH], perhaps by increasing $NO_x$ emissions, is an experiment which the atmosphere has already been through during the 1990s, when the methane growth rate was close to zero.

### 7.4.5   Alkyl Nitrates

The alkyl nitrate data from NEEM and North GRIP has yielded many results in this thesis, however one of the original aims of this work was to use the 2-D atmospheric model to recreate the observed trends of the alkyl nitrates and in so doing to derive an historic trend of northern hemisphere $NO_x$ emissions. Based on the work presented in this thesis it seems that this may not be possible, partly because this work has suggested that alkyl nitrate formation in polluted environments is most likely currently in a $NO_x$ saturated state. So the original hypothesis, that changing alkyl nitrate mixing ratios reflect changing $NO_x$ emissions, only holds in certain environments. However it is possible that further analysis of the data could yield a more quantitative history of $NO_x$ in polluted air masses based on the relative responses of the various alkyl nitrates to changes in [OH]. For example though butyl and pentyl nitrates appear to be in a $NO_x$ saturated regime, it may be that they are close to not being so and that

further analysis of the data would reveal this. If data from higher nitrates were available it may be that these have higher $NO_x$ saturation limits and so could provide a constraint on the amount of $NO_x$ in air masses. The use of a model to examine this problem, if it could be shown that the model was responding in the way predicted by the chemistry, would make it possible to derive a quantitative emissions trend from this data.

A large amount of alkyl nitrate data is now available including data on short timescales from a range of urban and rural environments. This can be used in conjunction with the understanding developed in this work to examine whether the relationships proposed in this work hold for different timescales and different regions. If they do then alkyl nitrates could be used as a valuable tool in these environments to help understand the chemistry that is occurring.

# Thesis Publications (to date)

## Chapter 4

Newland, M. J., C. E. Reeves, D. E. Oram, J. C. Laube, W. T. Sturges, C. Hogan, P. Begley, P. J. Fraser, Southern hemispheric halon trends and global emissions, 1978-2011, *Atmos. Chem. Phys.*, **13**, 5551-5565, 2013

## Chapter 5

### *Section 5.3*

Laube, J. C., C. Hogan, M. J. Newland, F. S. Mani, P. J. Fraser, C. A. M. Brenninkmeijer, P. Martinerie, D. E. Oram, T. Röckmann, J. Schwander, E. Witrant, G. P. Mills, C. E. Reeves, and W. T. Sturges, Distributions, long term trends and emissions of four perfluorocarbons in remote parts of the atmosphere and firn air, *Atmos. Chem. Phys.*, **12**, 4081-4090, 2012

Oram, D. E., F. S. Mani, J. C. Laube, M. J. Newland, C. E. Reeves, W. T. Sturges, S. A. Penkett, C. A. M. Brenninkmeijer, T. Röckmann, and P. J. Fraser, Long-term tropospheric trend of octafluorocyclobutane (c-$C_4F_8$ or PFC-318), *Atmos. Chem. Phys.*, **12**, 261-269, 2012

### *Section 5.4*

Sturges, W. T., D. E. Oram, J. C. Laube, C. E. Reeves, M. J. Newland, C. Hogan, P. Martinerie, E. Witrant, C. A. M. Brenninkmeijer, T. J. Schuck, and P. J. Fraser, Emissions halted of the potent greenhouse gas $SF_5CF_3$, *Atmos. Chem. Phys.*, **12**, 3653-3658, 2012

### *Section 5.5*

Laube, J. C., P. Martinerie, E. Witrant, T. Blunier, J. Schwander, C. A. M. Brenninkmeijer, T. J. Schuck, M. Bolder, T. Röckmann, C. van der Veen, H. Bönisch, A. Engel, G. P. Mills, M. J. Newland, D. E. Oram, C. E. Reeves, and W. T. Sturges, Accelerating growth of HFC-227ea (1,1,1,2,3,3,3-heptafluoropropane) in the atmosphere, *Atmos. Chem. Phys.*, **10**, 5903-5910, 2010

## Chapter 6

### *Section 6.7*

Worton, D. R., W. T. Sturges, C. E. Reeves, M. J. Newland, S. A. Penkett, E. Atlas, V. Stroud, K. Johnson, N. Schmidbauer, S. Solberg, J. Schwander, J-M. Barnola, Evidence from firn air for recent decreases in non-methane hydrocarbons and a 20th century increase in nitrogen oxides in the northern hemisphere, *Atmos. Env.*, **54**, 592-602, 2012

# References

3M Website. What is 3M doing? 3M's Phase out and New Technologies. Retrieved 17/05/2010 http://solutions.3m.com/wps/portal/3M/en_US/PFOS/PFOA/Information/Action/#phaseout

AGAGE: (http://agage.eas.gatech.edu/data.htm), Accessed $6^{th}$ August 2012

Andreae, M. O. and P. Merlet, (2001) Emission of trace gases and aerosols from biomass burning, Global Biogeochem. Cy., 15, 955–966.

Archibald, A. T., M. A. H. Kahn, L. A. Watson, K. C. Clemitshaw, S. R. Utembe, M. E. Jenkin, and D. E. Shallcross, (2007) Comment on 'Long-term atmospheric measurements of $C_1$-$C_5$ alkyl nitrates in the Pearl River Delta region of southeast China' by Simpson et al., Atmos. Environ., 34, 7369-7370

Atkinson, R., Baulch, D. L., Cox, R. A., Hampson, R. F., Kerr, J. A., Rossi, M. J., and Troe, J. (1997) Evaluated kinetic, photochemical and heterogeneous data for atmospheric chemistry, Supplement V – IUPAC Subcommittee on Gas Kinetic Data Evaluation for Atmospheric Chemistry, J. Phys. Chem. Ref. Data, 26, 521–1011

Atkinson, R., and J. Arey (2003), Atmospheric degradation of volatile organic compounds, Chem. Rev., 103, 4605– 4638.

Atkinson, R., D. L. Baulch, R. A. Cox, J. N. Crowley, R. F. Hampson, R. G. Haynes, M. E. Jenkin, M. J. Rossi, and J. Troe (2004) Evaluated kinetic and photochemical data for atmospheric chemistry: Volume I - Gas phase reactions of Ox, HOx, NOx and SOx species, Atmos. Chem. Phys., 4, 1461-1738

Atkinson, R., D. L. Baulch, R. A. Cox, J. N. Crowley, R. F. Hampson, R. G. Hynes, M. E. Jenkin, M. J. Rossi, J. Troe, and IUPAC Subcommittee (2006). Evaluated kinetic and photochemical data for atmospheric chemistry: Volume II – gas phase reactions of organic species. Atmos. Chem. Phys., 6, 3625–4055

Atkinson, R., D. Baulch, R. Cox, J. Crowley, R. Hampson, R. Hynes, M. Jenkin, M. Rossi, J. Troe, and T. Wallington (2008) Evaluated Kinetic and Photochemical data for Atmospheric Chemistry : Volume IV - Gas-phase Reactions of Organic Halogen Species, Atmos. Chem. Phys., 8, 4141-4496

Atlas, E., W. Pollock, J. Greenberg, L. Heidt, and A. M. Thompson. (1993) Alkyl nitrates, nonmethane hydrocarbons, and halocarbon gases over the equatorial Pacific Ocean during SAGA3, J. Geophys. Res., 98 (D9), 16933-16947

Aydin, M., K. R. Verhulst, E. S. Saltzman, M. O. battle, S. A. Montzka, D. R. Blake, Q. Tang, and M. J. Prather (2011) Recent decreases in fossil-fuel emissions of ethane and methane derived from firn air, Nature, 476, 198-201

Baker A. K., F. Slemr, and C. A. M. Brenninkmeijer (2010) Analysis of non-methane hydrocarbons in air samples collected aboard the CARIBIC passenger aircraft, Atmos. Meas. Tech., 3, 311-321

Barnett, J. J. and M. Corney (1985) A middle atmosphere temperature reference model from satellite observations, Adv. Space. Res., 5, 125-134

Barnett, J. J., and M. Corney. (1986) Middle atmosphere reference model derived from satellite data, in Middle Atmosphere Program Handbook 16, edited by K. Labitzke, J. J. Barnett, and D. Edwards,pp. 47-85, SCOSTEP Secretariat, Univ. of Illinois, Urbana

Barrie, L. A., (1986) Arctic air pollution: An overview of current knowledge, Atmos. Environ., 20, 643-663

Bates, D. R., and M. Nicolet (1950) The photochemistry of atmospheric water vapour, J. Geophys. Res., 55, 301

Battle, M., M. Bender, T. Sowers, P. P. Tans, J. H. Butler, J. W. Elkins, J. T. Ellis, T. Conway, N. Zhang, P. Lang, and A. D. Clarke (1996) Atmospheric gas concentrations over the past century measured in air from firn at the South Pole, Nature, 383, 231– 235

Beine, H.J., R. E. Honrath, F. Dominé, W. R. Simpson, and J. D. Fuentes, (2002) $NO_x$ during background and ozone depletion periods at Alert: Fluxes above the snow surface, J. Geophys. Res., 107, 10.1029/2002JD002082

Bertman, S. B., J. M. Roberts, D. D. Parrish, M. P. Buhr, P. D. Goldan, W. C. Kuster, F. C. Fehsenfeld, S. A. Montzka, and H. Westberg, (1995) Evolution of alkyl nitrates with air mass age. J. Geophys. Res. 100, 22805-22813

Beyersdorf, A., N. Blake, A. Swanson, S. Meinardi, J. E. Dibb, D. R. Blake, and F. Rowland (2004) Comparison of spring and summer OH concentrations in the snowpack at Summit, Greenland (Poster) AGU Conference, San Francisco, USA

Beyersdorf, A. J., D. R. Blake, A. Swanson, S. Meinardi, F. S. Rowland, D. Davis (2010) Abundances and variability of tropospheric volatile organic compounds at the South Pole and other Antarctic locations, Atmos. Environ., 44, 4565-4574

Blake, N. J., D. R. Blake, A. L. Swanson, E. Atlas, F. Flocke, and F. S. Rowland (2003), Latitudinal, vertical, and seasonal variations of C1-C4 alkyl nitrates in the troposphere over the Pacific Ocean during PEM Tropics A and B: Oceanic and continental sources, J. Geophys. Res.,108(D2), art. no. -8242,

Bousquet, P., P. Ciais, J. B. Miller, E. J. Dlugokencky, D. A. Haglustaine, C. Prigent, G. R. Van Der Werf, P. Peylin, E. -G. Brunke, C. Carouge, R. L. Langenfelds, J. Lathière, F. Papa, M. Ramonet, M. Schmidt, L. P. Steele, S. C. Tyler, and J. White (2006) Contribution of anthropogenic and natural sources to atmospheric methane variability, Nature, 443, 439-443

Broadgate,W. J., (1995) Non-methane hydrocarbons in the marine environment Ph.D. Thesis, University of East Anglia, Norwich

Broadgate,W. J., Liss, P. S., and Penkett, S. A. (1997) Seasonal emissions of isoprene and other reactive hydrocarbon gases from the ocean, Geophys. Res. Lett., 24, 2675–2678

Buizert, C., P. Martinerie, V. V. Petrenko, J. P. Severinghaus, C. M. Trudinger, E. Witrant, J. L. Rosen, A. J. Orsi, M. Rubino, D. M. Etheridge, L. P. Steele, C. Hogan, J. C. Laube, W. T. Sturges, V. A. Levchenko, A. M. Smith, I. Levin, T. J. Conway, E. J. Dlugokencky, P. M. Lang, K. Kawamura, T. M. Jenk, J. W. C. White, T. Sowers, J. Schwander, and T. Blunier (2012) Gas transport in firn: multiple-tracer characterisation and model intercomparison for NEEM, Northern Greenland, Atmos. Chem. Phys., 12, 4259-4277

Burkholder, J. B., R. R. Wilson, T. Gierczak, R. Talukdar, S. A. McKeen, J. L. Orlando, G. L. Vaghijiani, and A. R. Ravishankara (1991) Atmospheric fate of $CBrF_3$, $CBr_2F_2$, and $CBrF_2CBrF_2$, J. Geophys. Res., 96, 5025-5043

Butler, J. H., Battle, M., Bender, M. L., Montzka, S. A., Clarke, A. D., Saltzman, E. S., Sucher, C. M., Severinghaus, J. P., and Elkins, J. W. (1999), A record of atmospheric halocarbons during the twentieth century from polar firn air, Nature, 399, 749-755

Buys, Z., (2009) Atmospheric Sources, Destruction Processes and Tropospheric Trends of the Very Long-Lived "Super Greenhouse Gases" $CF_4$, $C_2F_6$, $NF_3$, $SF_6$ and $SF_5CF_3$. MSc. Dissertation, School of Environmental Sciences, University of East Anglia, Norwich, U.K.

Carrier, W., C. S. Jamieson and R. I. Kaiser (2007) Mechanistic Studies on the Formation of Trifluoromethyl Sulfur Pentafluoride, $SF_5CF_3$ – a Greenhouse Gas. Inorg. Chem., 46, 1332-1336

Chapman, S., (1930) A theory of upper atmospheric ozone, Q.J.R. Meteorol. Soc., 3, 103-125

Chen N. H., and D. F. Othmer (1962) New generalized equation for gas diffusion coefficient, J. Chem. Eng. Data, 7, 37-41

Chim, R.Y.L., R. A. Kennedy, and R. P. Tuckett (2003) The vacuum-UV absorption spectrum of SF5CF3; implications for its lifetime in the earth's atmosphere. Chem. Phys. Lett. 369, 697–703.

Chim, R. Y. L., R. A. Kennedy, R. P. Tuckett, W. Zhou, G. K. Jarvis, D. J. Collins, and P. A. Hatherly (2001) Fragmentation of energy-selected SF5CF3 + probed by threshold photoelectron photoion coincidence spectroscopy: bond dissociation energy of SF5– CF3 and its atmospheric implication. J. Phys. Chem. A 105, 8403–8412.

Chuck, A. L., Turner, S. M., and Liss, P. S. (2002). Direct evidence for a marine source of C1 and C2 alkyl nitrates. Science, 297, 1151-1154

Cicerone, R. J., (1979) Atmospheric carbon tetrafluoride: A nearly inert gas, Science, 206, 59-61

Clemitshaw, K.C., Williams, J., Rattigan, O.V., Shallcross, D.E., Law, K.S., Cox, R.A., (1997) Gas phase ultraviolet absorption cross sections and atmospheric lifetimes of several C2-C5 alkyl nitrates. J. Photochem. Photobiol. a- Chemistry, 102, 117-126.

Conway, T. J., P. P. Tans, L. S. Waterman, K. W. Thoning, D. R. Kitzis, K. A. Masarie, and N. Zhang (1994) Evidence for interannual variability of the carbon cycle from the National Oceanic and Atmospheric Administration/Climate Monitoring and Diagnostics Laboratory Global Air Sampling Network, J. Geophys. Res., 99 (D11), 22831-22855

Crutzen, P. J., (1970) The influence of nitrogen oxides on the atmospheric ozone content, Q. J. Roy. Meteorol. Soc., 96, 320

Cunnold D., P. J. Fraser, R. F. Weiss, R. G. Prinn, D. Hartley, P. G. Simmonds, B. R. Miller, F. N. Aleya, and A. J. Crawford (1994) Global trends and annual releases of $CCl_3F$ and $CCl_2F_2$ estimated from ALE/GAGE and other measurements from July 1978 to June 1991, J. Geophys. Res., 99, 1107-1126

Curtis, A. R. and Sweetenham, W. P.: 1987, FACSIMILE/CHEKMAT Users Manual, AERE Report-R12805, H.M. Stationery Office, London.

Dahl, E. E., S. A. Yvon-Lewis, and E. S. Saltzman (2005), Saturation anomalies of alkyl nitrates in the tropical Pacific Ocean, Geophys. Res. Lett., 32, L20817, doi:10.1029/2005GL023896.

Dahl, E. E., Yvon-Lewis, S. A., and Saltzman, E. S. (2007). Alkyl nitrate (C 1-C3) depth profiles in the tropical Pacific Ocean. J. Geophys. Res., 112(C1), 1-11. doi: 10.1029/2006JC003471.

Daniel, J. S., Velders, G. J. M. (Coordinating Lead Authors), Douglass, A. R., Forster, P. M. D., Hauglustaine, D. A., Isaksen, I. S. A., Kuijpers, L. J. M., McCulloch, A., Wallington, T. J., Ashford, P., Montzka, S. A., Newman, P. A., and Waugh, D. W.: Scientific Assessment of Ozone Depletion: 2010, Global Ozone Research and Monitoring Project, Report No. 52, 516 pp., Chapter 5, Halocarbon scenarios, ozone depletion potentials, and global warming potentials, World Meteorological Organization, Geneva, Switzerland, 2011.

Deeds D. A., M. K. Vollmer, J. T. Kulongoski, B. R. Miller, J. Mühle, C. M. Harth, J. A. Izbicki, D. R. Hilton, and R. F. Weiss (2008) Evidence for crustal degassing of $CF_4$ and $SF_6$ in Mojave Desert groundwaters, Geochim Cosmochim Ac, 72, 999-1013

De Gouw, J.A., J. B. Gilman, A. Borbon, C. Warneke, W.C. Kuster, P. D. Goldan, J.S. Holloway, J. Peischl, T. B. Ryerson, D. D. Parrish, D. R. Gentner, A. H. Goldstein, and R. A. Harley (2012) Increasing atmospheric burden of ethanol in the United States, Geophys. Res. Lett., 39, art. no. L15803

DeMore, W. B., S. P. Sander, C. J. Howard, A. R. Ravishankara, D. M. Golden, C. E. Kolb, R.F. Hampson, M. J. Kurylo, and M. J. Molina (1997) Chemical kinetics and photochemical data for use in stratospheric modelling, Evaluation number 12, JPL Publ., 97-4, 266

Denman, K.L., G. Brasseur, A. Chidthaisong, P. Ciais, P.M. Cox, R.E. Dickinson, D. Hauglustaine, C. Heinze, E. Holland, D. Jacob, U. Lohmann, S Ramachandran, P.L. da Silva Dias, S.C. Wofsy and X. Zhang (2007) Couplings Between Changes in the Climate System and Biogeochemistry. In: Climate Change 2007: The Physical Science Basis. Contribution of Working Group I to the Fourth Assessment Report of the Intergovernmental Panel on Climate Change [Solomon, S., D. Qin, M. Manning, Z. Chen, M. Marquis, K.B. Averyt, M.Tignor and H.L. Miller (eds.)]. Cambridge University Press, Cambridge, United Kingdom and New York, NY, USA.

Derwent, R. G., (1996) The Influence of Human Activities on the Distribution of Hydroxyl Radicals in the Troposphere, Phil. Trans. R. Soc. Lond. A354, 501-531

Dibb, J. E., M. Arsenault, M. C. Peterson, and R. E. Honrath (2002) Fast nitrogen oxide photochemistry in Summit, Greenland snow, Atmos. Environ. 36, 2501-2511

Dickerson, R. R., S. Kondragunta, G. Stenchikov, K. L. Civerolo, B. G. Doddridge, and B. N. Holben (1997) The impact of aerosols on solar ultraviolet radiation and photochemical smog, Science, 278, 827-830

Dlugokencky, E. J., K. A. Masarie, P. M. Lang, and P. P. Tans (1998) Continuing decline in the growth rate of the atmospheric methane burden, Nature, 393, 447-450

Dlugokencky, E. J., P. M. Lang, A. M. Crotwell, and K. A. Masarie (2012) Atmospheric Methane Dry Air Mole Fractions from the NOAA ESRL Carbon Cycle Cooperative Global Air Sampling Network, 1983-2011, Version: 2012-09-24, Path: ftp://ftp.cmdl.noaa.gov/ccg/ch4/flask/event/

Douglass, A. R., R. S. Stolarski, M. R. Schoeberl, C. H. Jackman, M. L. Gupta, P. A. Newman, J. E. Nielsen, and E. L. Fleming (2008) Relationship of loss, mean age of air and the relationship of CFCs to stratospheric circulation and implications for atmospheric lifetimes, J. Geophys. Res., 113, D14, doi:10.1029/2007JD009575

Douglass, A., and V. Fioletov (Coordinating Lead Authors), S. Godin-Beekman, R. Müller, R. S. Stolarski, A. Webb, A. Arola, J. B. Burkholder, J. P. Burrows, M. P. Chipperfield, R. Cordero, C. David, P. N. den Outer, S. B. Diaz, L. E. Flynn, M. Hegglin, J. R. Herman, P. Huck, S. Janjai, I. M. Janosi, J. W. Krzyscin, Y. Liu, J. Logan, K. Matthes, R. L. McKenzie, N. J. Muthama, I. Petropoavlovskikh, M. Pitts, S. Ramachandran, M. Rex, R. J. Salawitch, B. -M. Sinnhuber, J. Staehelin, S. Strahan, K. Tourpali, J. Valverde-Canossa, C. Vigouroux (2011) Scientific Assessment of Ozone Depletion: 2010, Global Ozone Research and Monitoring Project, Report No. 52, 516 pp., Chapter 2, Stratospheric Ozone and Surface Ultraviolet Radiation, World Meteorological Organization, Geneva, Switzerland, 2011.

Emmons, L. K., S. Walters, P. G. Hess, J. -F. Lamarque, G. G. Pfister, D. Fillmore, C. Granier, A. Guenther, D. Kinnison, T. Laepple, J. Orlando, X. Tie, G. Tyndall, C. Wiedinmyer, S. L. Baughcum, and S. Kloster (2010) Description and evaluation of the Model for Ozone and Related chemical Tracers, version 4 (MOZART-4), Geosci. Model Dev., 3. 43-67

Eneroth, K., K. Holme, T. Berg, N. Schmidbauer, and S. Solberg (2007) Springtime depletion of tropospheric ozone, gaseous elemental mercury and non-methane hydrocarbons in the European Arctic, and its relation to atmospheric transport, Atmos. Environ., 41, 8511-8526

EPA, (2008) Uses and Emissions of Liquid PFC Heat Transfer Fluids from the Electronics Sector, Environmental Protection Agency, Office of Air and Radiation, Office of Atmospheric Programs, Climate Change Division, EPA-430-R-06-901

Etheridge, D.M., L. P. Steele, R. J. Francey, and R. L. Langenfelds (1998) Atmospheric methane between 1000 A.D. and present: Evidence of anthropogenic emissions and climatic variability, J. Geophys. Res., 103(D13), 15979-15993

Etiope, G. and Ciccioli, P. (2009) Earth's Degassing: A Missing Ethane and Propane Source, Science, 323, 478

Eyring, V., I. Cionni, G. E. Bodeker, A. J. Charlton-Perez, D. E. Kinnison, J. F. Scinocca, D. W. Waugh, H. Akiyoshi, S. Bekki, M. P. Chipperfield, M. Dameris, S. Dhomse, S. M. Frith, H. Garny, A. Gettelman, A. Kubin, U. Langematz, E. Mancini, M. Marchand, T. Nakamura, L. D. Oman, S. Pawson, G. Pitari, D. A. Plummer, E. Rozanov, T. G. Shepherd, K. Shibata, W. Tian, P. Braesicke, S. C. Hardiman, J. F. Lamarque, O. Morgenstern, J. A. Pyle, D. Smale, and Y. Yamashita (2010) Multi-model assessment of stratospheric ozone return dates and ozone recovery in CCMVal-2 models, Atmos. Chem. Phys., 19, 9451-9472

Federal Highway Administration (2013) Traffic Volume Trends, Office of Highway Policy Information, Travel Monitoring, http://www.fhwa.dot.gov/policyinformation/travel_monitoring/tvt.cfm, last accessed 6 April, 2013

Finlayson-Pitts, B. J., and J. N. Pitts Jr (1977) Chemical basis of air quality: Kinetics and mechanisms of photochemical air pollution and application to control strategies, Adv. Environ. Sci. Technol., 7, 75-162

Finlayson-Pitts, B. J., and J. N. Pitts (1999) Chemistry of the Upper and Lower Atmosphere: Theory, Experiments, and Applications, Academic Press, Burlington, MA, USA, pp.992.

Fischer, R. G., J. Kastler, and K. Ballschmiter (2000) Levels and pattern of alkyl nitrates, multifunctional alkyl nitrates and halocarbons in the air over the Atlantic ocean. J. Geophys. Res., 105(D11), 14473-14494

Flocke, F., A. Volz-Thomas, H. -J. Buers, W. Pätz, H. -J Garthe, and D. Kley (1998) Long-term measurements of alkyl nitrates in southern Germany. General behaviour and seasonal and diurnal variation. Journal of Geophysical Research 103 (D5), 5729–5746

Forster, P., V. Ramaswamy, P. Artaxo, T. Berntsen, R. Betts, D.W. Fahey, J. Haywood, J. Lean, D.C. Lowe, G. Myhre, J. Nganga, R. Prinn, G. Raga, M. Schulz and R. Van Dorland, 2007: Changes in Atmospheric Constituents and in Radiative Forcing. In: Climate Change 2007: The Physical Science Basis. Contribution of Working Group I to the Fourth Assessment Report of the Intergovernmental Panel on Climate Change [Solomon, S., D. Qin, M. Manning, Z. Chen, M. Marquis, K.B. Averyt, M.Tignor and H.L. Miller (eds.)]. Cambridge University Press, Cambridge, United Kingdom and New York, NY, USA.

Fraser P., R. Langenfelds, N. Derek, and L. Porter (1991) Studies in air archiving techniques. Part 1: Long term stability of atmospheric trace gases in dry, natural air stored in high pressure, surface treated aluminium cylinders, Baseline 89, S. Wilson and J. Gras (eds.), 16-29, CSIRO/Bureau of Meteorology

Fraser, P.J., D. E. Oram, C. E. Reeves, S. A. Penkett, and A. McCulloch (1999) Southern hemispheric halon trends (1978-1998) and global halon emissions, J. Geophys. Res., 104, 15985-15999

Friedli, H. R., E. Atlas, V. R. Stroud, L. Giovanni, T. Campos, and L. F. Radke (2001), Volatile organic trace gases emitted from North American wildfires, Global Biogeochem. Cycles, 15, 435– 452.

Friedrich, R. and Obermeier, A. (1999) Anthropogenic emissions of volatile organic compounds, Academic, San Diego, California, 2–38

Fuller, E.N., Pd. Schettler, and J. C. Giddings (1966) A New method for Prediction of binary gas-phase diffusion coefficients, Ind. Eng. Chem., 58, 19-27

Gear, C. W. (1971) Numerical Initial Value Problems in Ordinary Differential Equations. Englewood Cliffs, NJ, Prentice-Hall.

Gillotay, D., P. C. Simon, and L. Dierickx (1988) Temperature dependence of ultraviolet abosorption cross-sections of brominated methanes and ethanes, Aeron. Acta, 335, 1-17

Gillotay, D., and P. C. Simon (1989) Ultraviolet adsorption spectrum of bromotrifluoromethane, dibromodifluoromethane and bromochlorodifluoromethane in the vapour phase, J. Atmos. Chem., 8, 41-62

Goldan, P. D., Parrish, D. D., Kuster, W. C., Trainer, M., McKeen, S., Holloway, J., Jobson, B., Sueper, D., and Fehsenfeld (2000) Airborne measurements of isoprene,CO, and anthropogenic hydrocarbons and their implications, J. Geophys. Res., 105, 9091–9105

Haagen-Smit A. J. (1952) Chemistry and physiology of Los Angeles smog. Ind. Eng. Chem., 44, 1342–1346

Haigh, J. D., A. R. Winning, R. Toumi, and J. W. Harder (2010) An influence of solar spectral variations on radiative forcing of climate, Nature, 467, 696-699

Harnisch, J., R. Borchers, P. Fabian, H. W. Gäggeler, and U. Schotterer (1996a) Effect of natural tetrafluoromethane, Nature, 384, 32, doi:10.1038/384032a0

Harnisch, J., R. Borchers, P. Fabian, and M. Maiss (1996b) Tropospheric trends for CF4 and C2F6 since 1982 derived from SF6 dated stratospheric air, Geophys. Res. Lett., 23, 1099–1102, doi:10.1029/96GL01198

Harte, S., H. Thewissen, and F. Illuzzi (2011) The European Semiconductor Industry's agreement to reduce 'Perfluorocompound' emissions: actions leading to results, 6th International Symposium on Non-CO$_2$ Greenhouse Gases (NCGG-6), Amsterdam, The Netherlands, 2-4 November 2011.

Hauglustaine, D. A., C. Granier, G. P. Brasseur, and G. Megie (1994) The importance of atmospheric chemistry in the calcualtion of radiative forcing on the climate system, J. Geophys. Res., 99, 1173-1186

Helmig, D., D. M. Tanner, R. E. Honrath, R. C. Owen, and D. D. Parrish (2008) Nonmethane hydrocarbons at Pico Mountain, Azores: 1. Oxidation chemistry in the North Atlantic region, J. Geophys. Res. Atmos., 113, 10.1029/2007JD008930

Helmig D., J. Hueber, and P. Tans (2011) Non-Methane Hydrocarbons from the NOAA ESRL Surface Network, 2004-2011 accessed April 2011 at http://www.esrl.noaa.gov/gmd/dv/data/index.php

Henderson, B.H., H. E. Jeffries, B. –U Kim, and W. G. Vizuete, (2010) The influence of model resolution on ozone in industrial volatile organic compound plumes, J. Air and Waste Management Assoc., 60, 1105-1117

Hirdman, D., J. F. Burkhart, H. Sodemann, S. Eckhardt, . Jefferson, P. K. Quinn, S. Sharma, J. Ström, and A. Stohl (2010) Long-term trends of black carbon and sulphate aerosol in the Arctic: changes in atmospheric transport and source region emissions, Atmos. Chem. Phys., 10, 9351-9368

Hogan, C (2012) Time Series of Atmospheric Halogenated Trace Gases from Arctic and Antarctic Firn Air, Ph.D. Thesis, University of East Anglia, Norwich

Honrath, R.E., M. C. Peterson, S. Guo, J. E. Dibb, P. B. Shepson, and B. Campbell (1999) Evidence of NOx production within or upon ice particles in the Greenland snowpack, Geophys. Res. Lett., 26, 695-698

Hopkins J. R., I. D. Jones, A. C. Lewis, J. B. McQuaid, and P. W. Seakins (2002) Non-methane hydrocarbons in the Arctic boundary layer, Atmos. Environ., 36, 3217-3229

Hough, A.M., and K. J. Woods (1988) Ozone concentrations in the global atmosphere. An analysis of data from the SBUV instrument on the Nimbus-7 satellite, AERE Report R-13271, 218 pp., Her Majesty's Stationery Office, London

Hough, A. M., (1988a) The calculation of photolysis rates for use in global tropospheric modelling studies, AERE Rep. R-13259, 52 pp., Her Majesty's Stn. Off., London, England, U.K.

Hough, A. M., (1989) The development of a two-dimension global tropospheric model, 1, The model transport, Atmos. Environ., 23, 1235-1261

Hough, A. M., and C. E. Johnson (1990) The development of a two-dimensional global tropospheric model, AERE Rep. R-13495, 116 pp., Her Majesty's Stn. Off., London, England, U.K.

Hough, A. M., (1991) Development of a two-dimension global tropospheric model: Model chemistry, J. Geophys. Res., 96, 7325-7362

Hough, A. M. and R. G. Derwent (1990) Changes in the Global Concentration of Tropospheric Ozone Due to Human Activities, Nature, 344, 645-650.

Hough, A. M. and C. E. Johnson (1991) Modelling the Role of Nitrogen Oxides, Hydrocarbons and Carbon Monoxide in the Global Formation of Tropospheric Oxidants, Atmos. Environ., 25A,1819-1836.

HTOC (Halon Technical Options Committee): Assessment Report of the Halon Technical Options Committee 1998, Ozone Secretariat, UNEP, Nairobi, Kenya, 1999.

HTOC (Halon Technical Options Committee): Assessment Report of the Halon Technical Options Committee 2006, Ozone Secretariat, UNEP, Nairobi, Kenya, 2007.

HTOC (Halon Technical Options Committee): Assessment Report of the Halon Technical Options Committee 2010, Ozone Secretariat, UNEP, Nairobi, Kenya, 2011.

Huang, L., L. Zhu, X. Pan, J. Zhang, B. Ouyang and H. Hou (2005) One potential source of the potent greenhouse gas $SF_5CF_3$: the reaction of SF6 with fluorocarbon under discharge. Atmos. Environ., 39, 1641–1653

International Aluminium Institute, (2005) IAI 2003 Anode Effect Survey Results and Analysis IAI Survey, International Aluminium Institute, New Zealand House, Haymarket, London SW1Y 4TE, United Kingdom

IPCC/TEAP, N. Campbell, R. Shende, M. Bennett, O. Blinova, R. Derwent, A. McCulloch, M. Yamabe, J. Shevlin, T. Vink, P. Ashford, P. Midgley, and M. McFarland (2005) HFCs and PFCs: current and future supply, demand and emissions, plus emissions of CFCs, HCFCs and halons, in: IPCC/TEAP Special Report on Safeguarding the Ozone Layer and the Global Climate System, edited by Hayman, G. and Kuijpers, L., Cambridge University Press, Cambridge, 2005

IPCC, 1990: Climate Change: The IPCC Scientific Assessment (1990). Report prepared for Intergovernmental Panel on Climate Change by Working Group I [J. T. Houghton, G. J. Jenkins, and J. J. Ephraums (eds.)], Cambridge University Press, Cambridge, Great Britain, New York, NY, USA and Melbourne, Australia, 410 pp.

IPCC, 2007: Climate Change 2007: The Physical Science Basis. Contribution of Working Group I to the Fourth Assessment Report of the Intergovernmental Panel on Climate Change [Solomon, S., D. Qin, M. Manning, Z. Chen, M. Marquis, K.B. Averyt, M.Tignor and H.L. Miller (eds.)]. Cambridge University Press, Cambridge, United Kingdom and New York, NY, USA.

IUPAC: (International Union of Pure and Applied Chemistry – Subcommittee for Gas Kinetic Data Evaluation) Evaluated kinetic data, http://www.iupac-kinetic.ch.cam.ac.uk (last access: March 2013)

Jacob, D. J., M. J. Prather, P. J. Rasch, R. –L. Shia, Y. J. Balkanski, S. R. Beagley, D. J. Bergmann, W. T. Blackshear, M. Brown, M. Chiba, M. P. Chipperfield, J. De Grandpré, J. E. Dignon, J. Feichter, C. Genthon, W. L. Grose, P. S. Kasibhatla, I. Köhler, M. A. Kritz, K. Law, J. E. Penner, M. Ramonet, C. E. Reeves, D. A. Rotman, D. Z. Stockwell, P. F. J. Van Velthoven, G. Verver, O. Wild, H. Yang, and P. Zimmermann (1997) Evaluation and intercomparison of global atmospheric transport models using $^{222}$Rn and other short-lived tracers, J. Geophys. Res., 5, 5953-5970

Jacob, D. J. (1999). Introduction to atmospheric chemistry. Princeton, N.J: Princeton University Press.

Jacobson, M. Z., (2005) Fundamentals of Atmospheric Modeling, Second Edition, Cambridge University Press, New York, pp. 813

Jaegle, L., L. Steinberger, R. V. Martin, and K. Chance (2005) Global partitioning of NOx sources using satellite observations: relative roles of fossil fuel combustion, biomass burning and soil emissions, Faraday Discuss., 130, 407-423.

Jenkin, M.E., S. M. Saunders, and M. J. Pilling, M.J. (1997) The tropospheric degradation of volatile organic compounds: A protocol for mechanism development, Atmos. Environ., 31, 81-104

Jobson B. T., H. Niki, Y. Yokouchi, J. Bottenheim, F. Hopper, and R. Leitch (1994) Measurements of C2–C6 hydrocarbons during the Polar Sunrise 1992 Experiment: evidence for Cl atom and Br atom chemistry. J. Geophys. Res. 99, 25355–25368.

Johnson, C. E., and R. G. Derwent (1996) Relative radiative forcing consequences of global emissions of hydrocarbons, carbon monoxide and $NO_x$ from human activities estimated with a zonally-averaged two-dimensional model, Climatic Change, 34, 439-462

Johnston, H., (1971) Reduction of stratospheric ozone by nitrogen oxide catalysts from supersonic transport exhaust, Science, 173, 517-522

Kahl, J. D. W., J. A. Galbraith, and D. A. Martinez (1999) Decadal-scale variability in long range atmospheric transport to the Summit of the Greenland Ice Sheet, Geophys. Res. Lett., 26, 481-484

Kai, F. M., S. C. Tyler, J. T. Randerson, and D. R. Blake (2011) Reduced methane growth rate explained by decreased Northern Hemisphere microbial sources, Nature, 476, 194-197

Kennedy, R.A., and C. A. Mayhew (2001) A study of low energy electron attachment to trifluoromethyl sulphur pentafluoride, SF5CF3: atmospheric implication. Int. J. Mass Spec. 206, i–iv.

Kesselmeier, J. and Staudt, M. (1999) Biogenic Volatile Organic Compounds (VOC): An Overview on Emission, Physiology and Ecology, J. Atmos. Chem., 33, 23–88

Khalil, M. A. K., R. A. Rasmussen, J. A. Culbertson, J. M. Prins, E. P. Grimsrud, and M. J. Shearer (2003) Atmospheric perfluorocarbons, Environ. Sci. Technol., 37, 4358-4361

Kirschke, S., P. Bousquet, P. Ciais, M. Saunois, J. G. Canadell, E. J. Dlugokencky, P. Bergamaschi, D. Bergmann, D. R. Blake, L. Bruhweiler, P. Cameron-Smith, S. Castaldi, F. Chevallier, L. Feng, A. Fraser, M. Heimann, E. L. Hodson, S. Houweling, B. Josse, P. J. Fraser, P. B. Krummel, J. F. Lamarque, R. L. Langenfelds, C. Le Quere, V. Naik, S. O;Doherty, P. I. Palmer, I. Pison, D. Plummer, B. Poulter, R. G. Prinn, M. Rigby, B. Ringeval, M. Santini, M. Schmidt, D. T. Shindell, I. J. Simpson, R. Spahini, L. P. Steele, S. A. Strode, K. Sudo, S. Szopa, G. R. Van Der Werf, A. Voulgarakis, M. Van Weele, R. F. Weiss, J. E. Williams, G. Zeng (2013) Three decades of global methane sources and sinks, Nature Geoscience, 10, 813-823

Kleinman, L. I. (1991) Seasonal dependence of boundary layer peroxide concentration: the low and high $NO_x$ regimes, J. Geophys. Res., 96, 20,721-20,734

Kleinman, L. I. (1994) Low and high-NO$_x$ tropospheric photochemistry, J. Geophys. Res., 99, 16,831-16,838

Klonecki, A., P. Hess, L. Emmons, L. Smith, J. Orlando, and D. Blake (2003) Seasonal changes in the transport of pollutants into theArctic troposphere – model study, J. Geophys. Res., 108, 8367, doi:10.1029/2002JD002199

Krivova, N. A., L. Balmaceda, and S. K. Solanki (2007) Reconstruction of solar total irradiance since 1700 from the surface magnetic flux, Astronomy and Astrophysics, 467, 335-346

Krol, M., and J. Lelieveld (2003) Can the variability in tropospheric OH be deduced from measurements of 1,1,1-trichloroethane (methyl chloroform)?, J. Geophys. Res., 108(D3), 4125, doi:10.1029/2002JD002423

Krol, M. C., J. Lelieveld, D. E. Oram, G. A. Sturrock, S. A. Penkett, C. A. M. Brenninkmeijer, V. Gros, J. Williams, and H. A. Scheeren (2003) Continuing emissions of methyl chloroform from Europe, Nature, 421, 131–135

Langenfelds, R. J., P. J. Fraser, R. J. Francey, L. P. Steele, L. W. Porter, and C. E. Allison (1996) The Cape Grim air archive: The first seventeen years, in Baseline 94-95, edited by R. J. Francey, A. L. Dick, and N. Derek, pp. 53-70, Bur. Meteorol. and CSIRO Atmos. Res., Melbourne, Victoria, Australia

Lantz, K. O., (1996) Theoretical, actinometric, and radiometric determinations of the photolysis rate coefficient of NO2 during the Mauna Loa Observatory Photochemistry Experiment 2, J. Geophys. Res. Atmos., 101, 14613-14629

Laube, J. C., A. Engel, H. Bönisch, T. Möbius, D. R. Worton, W. T. Sturges, K. Grunow, and U. Schmidt (2008) Contribution of very short-lived organic substances to stratospheric chlorine and bromine in the tropics – a case study, Atmos. Chem. Phys., 8, 7325–7334

Laube, J. C., P. Martinerie, E. Witrant, T. Blunier, J. Schwander, C. A. M. Brenninkmeijer, T. J. Schuck, M. Bolder, T. Röckmann, C. van der Veen, H. Bönisch, A. Engel, G. P. Mills, M. J. Newland, D. E. Oram, C. E. Reeves, and W. T. Sturges, **2010.** Rapid growth of HFC-227ea (1,1,1,2,3,3,3-Heptafluoropropane) in the atmosphere, Atm. Chem. Phys. Discuss., 10, 7675–7697

Laube, J. C., A. Engel, H. Bönisch, T. Möbius, D. R. Worton, W. T. Sturges, M. Braß, and T. Röckmann (2010) Fractional release factors of long-lived halogenated organic compounds in the tropical stratosphere, Atmos. Chem. Phys., 10, 1093–1103, doi:10.5194/acp-10-1093-2010

Laube, J. C., C. Hogan, M. J. Newland, F. S. Mani, P. J. Fraser, C. A. M. Brenninkmeijer, P. Martinerie, D. E. Oram, T. Röckmann, J. Schwander, E. Witrant, G. P. Mills, C. E. Reeves, and W. T. Sturges (2012) Distributions, long term trends and emissions of four perfluorocarbons in remote parts of the atmosphere and firn air, Atmos. Chem. Phys., 12, 4081–4090, doi:10.5194/acp-12-4081-2012

Laube, J. C., A. Keil, H. Bönisch, A. Engel, T. Röckmann, C. M. Volk, and W. T. Sturges (2013) Observation-based assessment of stratospheric fractional release, lifetimes, and Ozone Depletion Potentials of ten important source gases, Atmos. Chem. Phys., accepted, 12, 28525-28557

Lawrence, M. G, and P. J. Crutzen, (1999) Influence of NO$_x$ emissions from ships on tropospheric photochemistry and climate, Nature, 402, 167-170

Lawrence, M. G., P. Jöckel, and R. von Kuhlmann (2001) What does the global mean OH concentration tell us?, Atmos. Chem. Phys., 1, 37-49

Lean, J., G. Rottman, J. Harder, and G. Kopp (2005) SORCE contributions to new understanding of global change and solar variability, Solar Physics, 230, 27-53

Lewis, A. C., L. J. Carpenter, and M. J. Pilling (2001) Nonmethane hydrocarbons in Southern Ocean boundary layer air, J. Geophys. Res., D5, 4987-4994

Le Quéré, C., R. J. Andres, T. Boden, T. Conway, R. A. Houghton, J. I. House, G. Marland, G. P. Peters, G. van der Werf, A. Ahlström, R. M. Andrew, L. Bopp, J. G. Canadell, P. Ciais, S. C. Doney, C. Enright, P. Friedlingstein, C. Huntingford, A. K. Jain, C. Jourdain, E. Kato, R. F. Keeling, K. Klein Goldewijk, S. Levis, P. Levy, M. Lomas, B. Poulter, M. R. Raupach, J. Schwinger, S. Sitch, B. D. Stocker, N. Viovy, S. Zaehle, and N. Zeng (2012) The global carbon budget 1959–2011, Earth Syst. Sci. Data Discuss., 5, 1107-1157

Li, G., N. Bei, X. Tie, X., and L. T. Molina (2011) Aerosol effects on the photochemistry in Mexico City during MCMA-2006/MILAGRO campaign, Atmos. Chem. and Phys., 11 , 5169-5182

Liao, H., P. J. Adams, S. H. Chung, J. H. Seinfeld, L. J. Mickley, and D. J. Jacob (2003) Interactions between tropospheric chemistry and aerosols in a unified general circulation model, J. Geophys. Res. Atmos., 108, AAC 1-1 AAC 1-23

Liu, S. C., (1987) Ozone production in the rural troposphere and the implications for regional and global ozone distributions, J. Geophys. Res, 92 (D4), 4191-4207

Madronich, S., and J. G. Calvert (1990) Permutation reactions of organic peroxy radicals in the troposphere, J. Geophys. Res., 95, 5697-5715

Mahlman J. D., H. Levy, and W. J. Moxim (1980) Three-dimensional tracer structure and behaviour as simulated in two ozone precursor experiments, J. Atmos. Sci. 37. 655-685

Marland, G., T. A. Boden, and R. J. Andres (2005) Global, Regional, and National fossil fuel CO2 emissions, in Trends: A Compendium of data on global change. Carbon Dioxide Information Analysis Center, Oak Ridge National Laboratory, U.S. Department of Energy, Oak Ridge, Tenn., U.S.A.

Martin, R.V., D. J. Jacob, R. M. Yantosca, M. Chin, and P. Ginoux (2003) Global and regional decreases in tropospheric oxidants from photochemical effects of aerosols, J. Geophys. Res. Atmos., 108, ACH 6-1 - ACH 6-14

Martinerie, P., E. Nourtier-Mazauric, J. –M. Barnola, W. T. Sturges, D. R. Worton, E. Atlas, L. K. Gohar, K. P. Shine, and G. P. Brasseur (2009) Long-lived halocarbon trends and budgets from atmospheric chemistry modelling constrained with measurements in polar firn, Atmos. Chem. Phys., 9, 3911-3934

McConnell, J.R., R. Edwards, G. L. Kok, M. G. Flanner, C. S. Zender, E. S. Saltzman, J. R. Banta, D. R. Pasteris, M. M. Carter, and J. D. W. Kahl (2007) 20th-Century industrial black carbon emissions altered arctic climate forcing, Science, 317, 1381-1384

McCulloch, A. (1992) Global production and emissions of bromochlorodifluoromethane and bromotrifluoromethane (halons 1211 and 1301), Atmos. Environ., Part A, 26, 1325-1329

McCulloch, A., (2003) Fluorocarbons in the global environment: a review of the important interactions with atmospheric chemistry and physics. J. Fluorine Chem., 123, 21–29

McIntyre, H. P. (2001) The measurement and implications of short chain alkyl mononitrates in contemporary tropospheric and aged polar firn air, Ph.D. Thesis, University of East Anglia, Norwich

MCM, The Master Chemical Mechanism (http://mcm.leeds.ac.uk/MCM/home.htt) 2011.

Miller, T.M., S. T. Arnold, A. A. Viggiano, and W. B. Knighton, (2002) Electron attachment of $SF_5CF_3$ (296-563 K) and calculations of the neutral and anion thermochemistry. J. Chem. Phys., 116, 6021-6027

Molina, M. J., and F. S. Rowland, (1974) Stratospheric sink for chlorofluoromethanes: chlorine atom catalysed destruction of ozone, Nature, 249, 810-812

Montzka, S. A., Fraser, P. J. (Coordinating Lead Authors), Butler, J. H., Connell, P. S., Cunnold, D. M., Daniel, J. S., Derwent, R. G., Lal, S., McCulloch, A., Oram, D. E.,

Reeves, C. E., Sanhueza, E., Steele, L. P., Velders, G. J. M., Weiss, R. F., and Zander, R. J.: Scientific Assessment of Ozone Depletion: 2002, Global Ozone Research and Monitoring Project, Report No. 47, Chapter 1, Controlled Substances and Other Source Gases, World Meteorological Organization, Geneva, Switzerland, 2003.

Montzka, S. A., S. Reimann (Coordinating Lead Authors) A. Engel, K. Krüger, S. O'Doherty, W. Sturges, D. Blake, M. Dorf, P. Fraser, L. Froidevaux, K. Jucks, K. Kreher, M. Kurylo, A. Mellouki, J. Miller, O.-J Nielsen, V. Orkin, R. Prinn, R. Rhew, M. Santee, A. Stohl, and D. Verdonik (2011) Scientific Assessment of Ozone Depletion: 2010, Global Ozone Research and Monitoring Project, Report No. 52, 516 pp., Chapter 1, Ozone-Depleting Substances (ODSs) and Related Chemicals, World Meteorological Organization, Geneva, Switzerland

Montzka, S. A., and Elkins, J. W.: NOAA/ESRL/GMD halons flask data, Versions 2012-07-09 (H-1301) and 2012-07-16 (H-1211 and H-2402), available at ftp://ftp.cmdl.noaa.gov/hats/halons/flasks/ (last access August 2012)

Morris, R.A., T. M. Miller, A. A. Viggiano, J. F. Paulson, S. Solomon and G. Reid. (1995) Effects of electron and ion reactions on atmospheric lifetimes of fully fluorinated compounds. J. Geophys. Res., 100, 1287-1294

Mühle, J., A. L. Ganesan, B. R. Miller, P. K. Salameh, C. M. Harth, B. R. Greally, M. Rigby, L. W. Porter, L. P. Steele, C. M. Trudinger, P. B. Krummel, S. O'Doherty, P. J. Fraser, P. G. Simmonds, R. G. Prinn, and R. F. Weiss (2010) Perfluorocarbons in the global atmosphere: tetrafluoromethane, hexafluoroethane and octafluoropropane, Atmos. Chem. Phys., 10, 5145-5164

Muthuramu, K., P. B. Shepson, J. W. Bottenheim, B. T. Jobson, and H. Niki (1994) Relationships between organic nitrates and surface ozone destruction during Polar Sunrise Experiment 1992. J. Geophys. Res., 99(D12) 25369-25378.

Naik, V., A. Voulgarakis, A. M. Fiore, L. W. Horowitz, J. -F. Lamarque, M. Lin, M. J. Prather, P. J. Young, D. Bergmann, P. J. Cameron-Smith, I. Cionni, W. J. Collins, S. B. Dalsøren, R. Doherty, V. Eyring, G. Faluvegi, G. A. Folberth, B. Josse, Y. H. Lee, I. A. MacKenzie, T. Nagashima, T. P. C. Van Noije, D. A .Plummer, M. Righi, S. T. Rumbold, R. Skeie, D. T. Shindell, D. S. Stevenson, S. Strode, K. Sudo, S. Szopa, and G. Zeng (2013) Preindustrial to present-dat changes in tropospheric hydroxyl radical and methane lifetime from the Atmospheric Chemistry and Climate Model Intercomparison Project (ACCMIP), Atmos. Chem. Phys, 13, 5277-5298

National Statistics Office (2012) Statistical Release - Road traffic estimates: 2011 (Revised), Department for Transport.

Newland, M. J., C. E. Reeves, D. E. Oram, J. C. Laube, W. T. Sturges, C. Hogan, P. Begley, and P. J. Fraser (2013) Southern hemispheric halon trends and global halon emissions, 1978 – 2011, Atmos. Chem. Phys., in publication.

Nielsen, O.J., F. M. Nicolaisen, C. Bacher, M. D. Hurley, T. J. Wallington, and K. P. Shine, (2002) Infrared spectrum and global warming potential of $SF_5CF_3$. Atmos. Environ. 36, 1237–1240.

Novelli P. C., K. A. Masarie, and P. M. Lang (1998) Distributions and recent changes of carbon monoxide in the lower troposphere, J. Geophys. Res., 103, D15, 19015-19033

Nyeki, S., U. Baltensperger, I. Colbeck, D. T. Jost, E. Weingartner, and H. W. Gäggeler (1998) The Jungfraujoch high-alpine research station (3454 m) as a background clean continental site for the measurement of aerosol parameters, J. Geophys. Res. Atmos., 103 (D6), 6097-6107

Olivier, J. G. J., Bloos, J. P. J., Berdowski, J. J. M., Visschedijk, A. J. H., and Bouwman, A. F. (1999) A 1990 global emission inventory of anthropogenic sources of carbon

monoxide on 1°×1° developed in the framework of EDGAR/GEIA, Chemosphere, 1,1–17

Oltmans, S. J., and H. Levy II (1994) Surface ozone measurements from a global network, Atmos. Env., 28, 1-24

Oort, A. H. (1983) Global atmospheric circulation statistics, NOAA Prof. Pap. 14, Geophys. Fluid Dyn. Lab., Princeton, N.J.

Oram, D. E, C. E. Reeves, S. A. Penkett, and P. J. Fraser (1995) Measurements of HCFC-142b and HCFC-141b in the Cape Grim air archive: 1978-1993, Geophys. Res. Letts., 22, 2741-2744

Oram, D. E., (1999) Trends of long-lived anthropogenic halocarbons in the Southern Hemisphere and model calculations of global emissions. Ph.D. Thesis, School of Environmental Sciences, University of East Anglia, Norwich, U.K.

Oram, D.E., F. Mani, J. C. Laube, M. J. Newland, C. E. Reeves, W. T. Sturges, S. A. Penkett, C. A. M. Brenninkmeijer, T. Röckmann, and P. J. Fraser (2012) Long-term tropospheric trend of octafluorocyclobutane (c-$C_4F_8$ or PFC-318), Atmos. Chem. Phys., 11, 19089-19111

Parrish, D. D., C. J. Hahn, E. J. Williams, R. B. Norton, F. C. Fehsenfeld, H. B. Singh, J. D. Shetter, B. W. Gandrud, and B. A. Ridley (1992) Indications of photochemical histories of Pacific air masses from measurements of atmospheric trace species at Point Arena, California, J. Geophys. Res., 97 (D14), 15883-15901

Parrish, D. D., K. S. Law, J. Staehelin, R. Derwent, O. R. Cooper, H. Tanimoto, A. Volz - Thomas, S. Gilge, H.-E. Scheel, M. Steinbacher, and E. Chan (2012) Long-term changes in lower tropospheric baseline ozone concentrations at northern mid-latitudes, Atmos. Chem. Phys., 12, 11485-11504

Paul, A. G., K. C. Jones and A. J. Sweetman, (2009) A first global production, emission and environmental inventory for perfluorooctane sulfonate. Environ. Sci. Technol., 43, 386-392

Petrenko, V. V., P. Martinerie, P. Novelli, D. M. Etheridge, I. Levin, Z. Wang, T. Blunier, J. Chappellaz, J. Kaiser, P. Lang, L. P. Steele, S. Hammer, J. Mak, R. L. Langenfelds, J. Schwander, J. P. Severinghaus, E. Witrant, G. Petron, M. O. Battle, G. Forster, W. T. Sturges, J.-F. Lamarque, K. Steffen, and J. W. C. White (2012) A 60-yr record of atmospheric carbon monoxide reconstructed from Greenland firn air, Atmos. Chem. Phys. Discuss., 12, 18993-19037

Pfeilsticker, K., W. T. Sturges, H. Bösch, C. Camy-Peyret, M. P. Chipperfield, A. Engel, R. Fitzenberger, M. Müller, S. Payan, and B. -M. Sinnhuber (2000) Lower stratospheric organic and inorganic bromine budget for the Arctic winter 1998/99, Geophys. Res. Lett., 27, 3305–3308, doi:10.1029/2000GL011650

Pison, I., B. Ringeval, P. Bousquet, C. Prigent, and F. Papa (2013) Stable atmospheric methane in the 2000s: Key-role of emissions from wetlands, Atmos. Chem. Phys., 13, 11609-11623

Plass-Dulmer, C., Koppmann, R., Ratte, M., and Rudolph, J. (1995) Light non-methane hydrocarbons in seawater, Global Biogeochem.Cy., 9, 79–100

Plumb, A., and J. D. Mahlman (1987) The zonally-averaged transport characteristics of the GFDL general circulation/transport model, J. Atmos. Sci., 44, 298-327

Poisson, N., M. Kanakidou, and P. J. Crutzen (2000) Impact of non-methane hydrocarbons on tropospheric chemistry and the oxidizing power of the global troposphere: 3-dimensional modelling results, J. Atmos. Chem., 36, 157-230.

Pollmann, J., D. Helmig, J. Hueber, C. Plass-Dülmer, and P. Tans (2008) Sampling, storage, and analysis of C2-C7 non-methane hydrocarbons from the US National Oceanic and

Atmospheric Administration Cooperative Air Sampling Network glass flasks, J. Chromatogr. A, 1188, 75-87

Pozzer, A., Pollmann, J., Taraborrelli, D., Jöckel, P., Helmig, D., Tans, P., et al. (2010). Observed and simulated global distribution and budget of atmospheric C2-C5 alkanes. Atmos. Chem. Phys., 10(9), 4403-4422. doi: 10.5194/acp-10-4403-2010.

Prinn R. G., R. F. Weiss, B. R. Miller, J. Huang, F. N. Alyea, D. M. Cunnold, P. J. Fraser, D. E. Hartley, and P. G. Simmonds (1995) Atmospheric trends and lifetime of $CH_3CCl_3$ and global OH concentrations, Science, 269, 187-192

Prinn, R. G., R. F. Weiss, P. J. Fraser, P. G. Simmonds, D. M. Cunnold, F. N. Alyea, S. O'Doherty, P. Salameh, B. R. Miller, J. Huang, R. H. J. Wang, D. E. Hartley, C. Harth, L. P. Steele, G. Sturrock, P. M. Midgley, and A. McCulloch (2000) A history of chemically and radiatively important gases in air deduced from ALE/GAGE/AGAGE, J. Geophys. Res., 105, 17751–17792

Prinn, R. G., J. Huang, R. F. Weiss, D. M. Cunnold, P. J. Fraser, P. G. Simmonds, A. McCulloch, C. Harth, P. Salameh, S. O'Doherty, R. J. J. Wang, L. Porter, and B. R. Miller (2001) Evidence for substantial variations of atmospheric hydroxyl radicals in the past two decades, Science, 292, 1882–1888

Prinn, R.G., J. Huang, R. F. Weiss, D. M. Cunnold, P. J. Fraser, P. G. Simmonds, A. McCulloch, C. M. Harth, S. Reimann, P. K. Salameh, S. O'Doherty, R. H. J. Wang, L. W. Porter, B. R. Miller, and P. B. Krummel (2005) Evidence for variability of atmospheric hydroxyl radicals over the past quarter century, Geophys. Res. Lett., 32, L07809, doi:10.1029/2004GL022228

Ramacher B., J. Rudolph, and R. Koppmann, (1999) Hydrocarbon measurements during tropospheric ozone depletion events: evidence for halogen atom chemistry. J. Geophys. Res. 104, 3633–3653

Rand. S., and J. Marks (2011) Implications of Non-Anode Effect Related PFC Emissions from Primary Aluminium, 6th International Symposium on Non-$CO_2$ Greenhouse Gases (NCGG-6), Amsterdam, The Netherlands, 2-4 November 2011.

Ravishankara, A. R., S. Solomon, A. A. Turnipseed, and R. F. Warren (1993) Atmospheric lifetimes of longlived halogenated species, Science, 259, 194–199, doi:10.1126/science.259.5092.194

Raynaud, D. (1992) The Ice Core record of the Atmospheric Composition: A Summary, Chiefly of $CO_2$, $CH_4$, and $O_2$. In *Trace Gases in the Biosphere*. Edited by B. Moore and D. Schimel, Boulder, Colorado: UCAR Office for Interdisciplinary Studies.

Reimann and Lewis. (2007) Volatile Organic Compounds in the Atmosphere. Blackwell Publishing Ltd. 33-55

Reeves, C. E., W. T. Sturges, G. A. Sturrock, K. Preston, D. E. Oram, J. Schwander, R. Mulvaney, J. -M. Barnola, and J. Chappellaz (2005) Trends of halon gases in polar firn air: implications for their emission distributions, Atmos. Chem. Phys., 5, 2055–2064, doi:10.5194/acp-5-2055-2005

Reeves, C. E., J. Slemr, D. E. Oram, D. Worton, S. A. Penkett, D. J. Stewart, R. Purvis, N. Watson, J. Hopkins, A. Lewis, J. Methven, D. R. Blake, and E. Atlas (2007) Alkyl nitrates in outflow from North America over the North Atlantic during Intercontinental Transport of Ozone and Precursors 2004, J. Geophys. Res., 112, D10s37, doi:10.1029/2006jd007567

Rigby, M., R. G. Prinn, P. J. Fraser, P. G. Simmonds, R. L. Langenfelds, J. Huang, D. M. Cunnold, L. P. Steele, P. B. Krummel, R. F. Weiss, S. O'Doherty, P. K. Salameh, H. J. Wang, C. M. Harth, J. Mühle, and L. W. Porter (2008) Renewed growth of atmospheric methane, Geophys. Res. Lett., 35, Article number L22805

Roberts J. M., F. C. Fehsenfeld, S. C. Liu, M. J. Bollinger, C. Hahn, D. L. Albritton, and R. E. Sievers (1984) Measurements of aromatic hydrocarbon ratios and $NO_x$ concentrations in the rural troposphere – observation of air mass photochemical aging and $NO_x$ removal, Atmos. Environ., 18, 2421-2432

Roberts, J. M., S. B. Bertman, D. D. Parrish, F. C. Fehsenfeld, B. T. Jobson, and H. Niki (1998), Measurement of alkyl nitrates at Chebogue Point, Nova Scotia during the 1993 North Atlantic Regional Experiment (NARE) intensive, J. Geophys. Res., 103, 13,569–13,580.

Roberts, J. M., and R. W. Fajer (1989), UV absorption cross sections of organic nitrates of potential atmospheric importance and estimation of atmospheric lifetimes, Environ. Sci. Technol., 23, 945–951

Rommelaere V., L. Arnaud, and J. M. Barnola, (1997) Reconstructing recent atmospheric trace gas concentrations from polar firn and bubbly ice data by inverse methods. J. Geophys. Res. 102(D25), 30069-30083

Saito, T., Yokouchi, Y., and Kawamura, K. (2000) Distribution of C2–C6 hydrocarbons over the western north Pacific and eastern Indian Ocean, Atmos. Environ., 34, 4373–4381

Saito T., Y. Yokouchi, A. Stohl, S. Taguchi and H. Mukai (2010) Large emissions of perfluorocarbons in East Asia deduced from continuous atmospheric measurements, Environ. Sci. Technol., 44, 4089-4095

Saiz-Lopez, A., and R. von Glasow (2012) Reactive halogen chemsitry in the troposphere, Chem. Soc. Rev., 41, 6448-6472

Sander, S. P., Friedl, R. R., Abbatt, J. P. D., Barker, J. R., Burkholder, J. B., Golden, D. M., Kolb, C. E., Kurylo, M. J., Moortgat, G. K., Wine, P. H., Huie, R. E., and Orkin, V. L. (2011) Chemical kinetics and photochemical data for use in atmospheric studies, evaluation number 17, JPL Publ. 10-6, 4G-33

Santoro, M.A., (2000) Clarifying the SF5CF3 record, Science, 290, 935–936.

Schultz, M., S. Rast, M. van het Bolscher, T. Pulles, R. Brand, J. Pereira, B. Mota, A. Spessa, S. Dalsøren, T. van Nojie, S. Szopa, (2007) Emission data sets and methodologies for estimating emissions, RETRO project report D1-6, Hamburg, (http://retro.enes.org/reports/D1-6_final.pdf)

Schumann, U., and H. Huntrieser (2007) The global lightning-induced nitrogen oxides source, Atmos. Chem. Phys., 7, 3823-3907

Schwander, J., J. -M. Barnola, C. Andrie, M. Leuenberger, A. Ludin, D. Raynaud, and B. Stauffer (1993) The age of the air in the firn and the ice at Summit, Greenland. J. Geophys. Res. Atmos., 98, 2831-2838.

Schwander, J., (2001) North GRIP field report

Schwander J., T. Sowers, T. Blunier, and V. Petrenko, (2008) NEEM firn air sampling field report.

Seinfeld J. H. and Pandis S. N. (2006) Atmospheric Chemistry and Physics: From Air Pollution to Climate Change, J. Wiley, New York.

Shepson, P. B., K. G. Anlauf, J. W. Bottenheim, H. A. Wiebe, N. Gao, K. Muthuramu, and G. MacKay (1993), Alkyl nitrates and their contribution to reactive nitrogen at a rural site in Ontario, Atmos. Environ., 27, 749– 757.

Shia, R. L., M. K. W. Ko, D. K. Weisenstein, C. Scott, and J. Rodriguez Transport between the tropical and midlatitude lower stratosphere: Implications for ozone response to high-speed civil transport emissions, J. Geophys. Res., 103 (D19), 25435-25446

Shindell, D. T., M. Chin, F. Dentener, R. M. Doherty, G. Faluvegi, A. M. Fiore, P. Hess, D. M. Koch, I. A. MacKenzie, M. G. Sanderson, M. G. Schultz, M. Schulz, D. S. Stevenson, H. Teich, C. Textor, O. Wild, D. J. Bergmann, I. Bey, H. Bian, C. Cuvelier, B. N. Duncan, G. Folberth, L. W. Horowitz, J. Jonson, J. W. Kaminski,

E. Marmer, R. Park, K. J. Pringle, S. Schroeder, S. Szopa, T. Takemura, G. Zeng, T. J. Keating, and A. Zuber (2008) A multi-model assessment of pollution transport to the Arctic, Atmos. Chem. Phys., 8, 5353-5372

Sillman, S., J. A. Logan, and S. C. Wofsy (1990) The sensitivity of ozone to nitrogen oxides and hydrocarbons in regional ozone episodes, J. Geophys. Res., 95(D2), 1837-1851

Sillman, S. (1999) The relation between ozone, $NO_x$ and hydrocarbons in urban and polluted rural environments, Atmos. Environ., 33, 1821–1845

Simpson, I. J., S. Meinardi, D. R. Blake, N. J. Blake, F. S. Rowland, E. Atlas, and F. Flocke (2002), A biomass burning source of C1–C4 alkyl nitrates, Geophys. Res. Lett., 29(24), 2168, doi:10.1029/2002GL016290.

Simpson, I. J., T. Wang, H. Guo, Y. H. Kwok, F. Flocke, E. Atlas, S. Meinardi, F. Sherwood Rowland, and D. R. Blake (2006) Long-term atmospheric measurements of C1-C5 alkyl nitrates in the Pearl River Delta region of southeast China, Atmos. Environ., 40, 1619-1632

Solberg, S., C. Dye., N. Schmidbauer, A. Herzog and R. Gehrig (1996) Carbonyls and nonmethane hydrocarbons at rural European sites from the Mediterranean to the Arctic, J. Atmos. Chem., 25, 33-66

Spivakovsky, C.M., J. A. Logan, S. A. Montzka, Y. J. Balkanski, M. Foreman-Fowler, D. B. A. Jones, L. W. Horowitz, A. C. Fusco, C. A. M. Brenninkmeijer, M. J. Prather, S. C. Wofsy, and M. B. McElroy (2000) Three-dimensional climatological distribution of tropospheric OH: Update and evaluation J. Geophys. Res. Atmos., 105 (D7), 8931-8980

Stohl, A., T. Berg, J. F. Burkhart, A. M. Fjæraa, C. Forster, A. Herber, Ø. Hov, C. Lunder, W. W. McMillan, S. Oltmans, M. Shiobara, D. Simpson, S. Solberg, K. Stebel, J. Ström, K. Tørseth, R. Treffeisen, K. Virkkunen, and K. E. Yttri (2007) Arctic smoke - Record high air pollution levels in the European Arctic due to agricultural fires in Eastern Europe in spring 2006, Atmos. Chem. Phys., 7, 511-534

Stone, D., L. K. Whalley, and D. E. Heard (2012) Tropospheric OH and $HO_2$ radicals: field measurements and model comparisons, Chem. Soc. Rev., 41, 6348-6404

Stroud, C., S. Madronich, E. Atlas, B. Ridley, F. Flocke, A. Weinheimer, B. Talbot, A. Fried, B. Wert, R. Shetter, B. Lefer, M. Coffey, B. Heikes, and D. Blake (2003) Photochemistry in the arctic free troposphere: $NO_x$ budget and the role of odd nitrogen reservoir recycling Atmos. Environ., 37, 3351-3364

Sturges, W.T., Oram, D.E., Penkett, S.A., Fraser, P.J. and Engel, A.: Long-lived halogenated compounds in the stratosphere, Proceedings of 2nd International Symposium on Non-$CO_2$ Greenhouse Gases (NCGG-2), Noordwijkerhout, The Netherlands, 8-10 September 1999.

Sturges,W.T., T. J. Wallington, M. D. Hurley, K. P. Shine, K. Sihra, A. Engel, D. E. Oram, S. A. Penkett, R. Mulvaney, and C. A. M. Brenninkeijer (2000) A potent greenhouse gas identified in the atmosphere: SF5CF3, Science, 289, 611–613.

Sturges,W.T., H. P. McIntyre, S. A. Penkett, J. Chappellaz, J. -M Barnola, R. Mulvaney, E. Atlas, and V. Stroud (2001) Methyl bromide, other brominated methanes, and methyl iodide in polar firn air, J. Geophys. Res. Atmos., 106, 1595-1606

Sturges, W. T., D. E. Oram, J. C. Laube, C. E. Reeves, M. J. Newland, C. Hogan, P. Martinerie, E. Witrant, C. A. M. Brenninkmeijer, T. J. Schuck and P. J. Fraser (2011) Emissions halted of the potent greenhouse gas $SF_5CF_3$, Atmos. Chem. Phys., 12, 3653-3658

Sturrock, G. A., D. M. Etheridge, C. M. Trudinger, P. J. Fraser, and A. M. Smith (2002) Atmospheric histories of halocarbons from analysis of Antarctic firn air: major

Montreal Protocol species, J. Geophys. Res., 107, D24, 4765, doi:10.1029/2002/JD002548

Swanson, A, L., N. J. Blake, J. E. Dibb, M. R. Albert, D. R. Blake, and F. S. Rowland (2002) Photochemically induced production of $CH_3Br$, $CH_3I$, $C_2H_5I$, ethene, and propene within surface snow at Summit, Greenland, Atmos. Env., 36, 2671-2682

Swanson, A., Blake, N., Atlas, E., Flocke, F., Blake, D. R., and Sherwood, F. (2003) Seasonal variation of C2–C4 nonmethane hydrocarbons and C1–C4 alkyl nitrates at the Summit research station in Greenland, J. Geophys. Res., 108, 4065,doi:10.1129/2001JD001445.

Talbot, R. W., J. E. Dibb, E. M. Scheuer, J. D. Bradshaw, S. T. Sandholm, H. B. Singh, D. R. Blake, N. J. Blake, E. Atlas, and F. Flocke (2000) Tropospheric reactive odd nitrogen over the South Pacific in austral springtime, J. Geophys. Res., 105, 6681–6694.

Talukdar, R.K., Burkholder, J.B., Hunter, M., Gilles, M.K., Roberts, J.M., Ravishankara, A.R., (1997a) Atmospheric fate of several alkyl nitrates. 2. UV absorption cross sections and photodissociation quantum yields. J. Chem. Soc. Faraday T., 93, 2797-2805.

Talukdar, R.K., Herndon, S.C., Burkholder, J.B., Roberts, J.M., Ravishankara, A.R., (1997b) Atmospheric fate of several alkyl nitrates. 1. Rate coefficients of the reactions alkyl nitrates with isotopically labelled hydroxyl radicals. J. Chem. Soc. Faraday T., 93, 2787-2796.

Tang, Y., G. R. Carmichael, J. -H. Woo, N. Thongboonchoo, G. Kurata, I. Uno, D. G. Streets, D. R. Blake, R. J. Weber, R. W. Talbot, Y. Kondo, H. B. Singh, and T. Wang (2003) Influences of biomass burning during the Transport and Chemical Evolution Over the Pacific (TRACE-P) experiment identified by the regional chemical transport model, J. Geophys. Res. Atmos., 108, GTE 45- 1 - GTE 45-13

Thornberry, T., M. A. Carroll, G. J. Keller, S. Sillman, S. B. Bertman, M. R. Pippin, K. Ostling, J. W. Grossenbacher, P. B. Shepson, O. R. Cooper, J. R. Moody, and W. R. Stockwell (2001) Observations of reactive oxidized nitrogen and speciation of NOy during the PROPHET summer 1998 intensive. J. Geophys Res., 106(D20), 24359-24386

Tie, X,. S. Madronich, S. Walters, P. Rasch, and W. Collins (2003) Effect of clouds on photolysis and oxidants in the troposphere, J. Geophys. Res., 108, 4642, doi:10.1029/2003JD003659

Trudinger, C. M., I. G. Enting, D. M. Etheridge, R. J. Francey, V. A. Levchenko, and L. P. Steele (1997) Modeling air movement and bubble trapping in firn, J. Geophys. Res., 102, 6747–6763

Trudinger, C. M., D. M. Ethereidge, P. J. Rayner, I. G. Enting, G. A. Sturrock, and R. L. Langenfelds (2002) Reconstructing atmospheric histories from measurements of air composition in firn, J. Geophys. Res., 107, D24, Art. No. 4780

Tuma, P., and L. Tousignant (2001) Reducing Emissions of PFC Heat Transfer Fluids, EHS Challenges and Analytical Methodologies session at the SEMI Technical Symposium: Innovations in Semiconductor Manufacturing during SEMICON® West, July 16, 2001

UNEP (2009) Report on Implementation of Approved Projects, UNEP/OzL.Pro/ExCom/59/10

UNFCCC, (1997) United National Framework Convention on Climate Change Secretariat: National Greenhouse Gas Inventory Data for the Period 1990-1997 United Nations Office at Geneva, Geneva, Switzerland

Uppala, S. M., P. W. Kållberg, A. J. Simmonds, U. Andrae, V. Da Costa Bechtold, M. Fiorino, J. K. Gibson, J. Haseler, A. Hernandez, G. A. Kelly, X. Li, K. Onogi, S. Saarinen, N. Sokka, R. P. Allan, E. Andersson, K. Arpe, M. A. Balmaseda, A. C. M. Beljaars, L. Van de Berg, J. Bidlot, N. Bormann, S. Caires, F. Chevallier, A. Dethof, M.

Dragosavac, M. Fisher, M. Fuentes, S. Hagemann, E. Holm, B. J. Hoskins, L. Isaksen, P. A. E. M. Janssen, R. Jenne, A. P. McNally, J. -F. Mahfouf, J. J. Morcrette, N. A. Rayner, R. W. Saunders, P. Simon, A. Sterl, K. E. Trenberth, A. Untch, D. Vasiljevic, P. Viterbo, and J. Woollen (2005) The ERA-40 re-analysis, Quart. J. Royal. Met. Soc., 131, 2961-3012

Van Aardenne, J., Dentener, F., Olivier, J., Peters, J., and Ganzeveld, L. (2005) The EDGAR 3.2 Fast Track 2000 dataset (32FT2000), online available at: http://www.mnp.nl/edgar/model/v32ft2000edgar/docv32ft2000/

Van Aardenne, J. A., Dentener, F. J., Olivier, J. G. J., Klein Goldewijk, C. G. M., and Lelieveld, J. (2001) A 1deg×1deg resolution data set of historical anthropogenic trace gas emissions for the period 1890–1990, Global Biogeochem. Cy., 15, 909–928

Volk, C. M., J. W. Elkins, D. W. Fahey, G. S. Sutton, J. M. Gilligan, M. Loewenstein, J. R. Podolske, K. R. Chan, and M. R. Gunson (1997) Evaluation of source gas lifetimes from stratospheric observations, J. Geophys. Res., 102(D21), 25543–25564

Von Glasow, R. and P. J. Crutzen, (2007) Tropospheric Halogen Chemistry, Holland H. D. and Turekian K. K. (eds), Treatise on Geochemistry Update1, vol. 4.02, 1 - 67

Von Kuhlmann, R., (2001) Photochemistry of Tropospheric Ozone, Its Precursors and the Hydroxyl Radical: A 3D-Modeling Study Considering Non-Methane Hydrocarbons, Ph.D. thesis, Johannes Gutenberg-Universität Mainz, Mainz, Germany

von Schneidemesser, E., P. S. Monks, and C. Plass-Dülmer (2010) Global comparison of VOC and CO observations in urban areas, Atmos. Environ., 44, 5053-5064

Wallington, T.J., E. W. Kaiser, and J. T. Farrell (2006) Automotive fuels and internal combustion engines: A chemical perspective, Chem. Soc. Rev., 35, 335-347

Wang, H., L. Fu, Y. Zhou, X. Du, W. Ge (2010) Trends in vehicular emissions in China's mega cities from 1995 to 2005, Environmental Pollution, 158, 394-400

Warneke, C., J. A. De Gouw., J. S. Holloway, J. Peischl, T. B. Ryerson, E. Atlas, D. Blake, M. Trainer, and D. D. Parrish (2012) Multiyear trends in volatile organic compounds in Los Angeles, California: Five decades of decreasing emissions, J. Geophys. Res., 117, doi:10.1029/2012JD017899

Wayne, R. (2006) Chemistry of Atmospheres, Oxford University Press Inc., New York.

Weeks, I., R. Francey, D. Beardsmore, and L. Porter (1992) Studies in air archiving techniques. Part 2: Filling high pressure cylinders with baseline air, in: Baseline 90, S. Wilson and J. Gras, (eds.), 16-23, CSIRO/Bureau of Meteorology

Wehrli, C., (1985) Extraterrestrial Solar Spectrum, Technical Report

Wennberg, P. O., S. Peacock, J. T. Randerson, and R. Bleck (2004) Recent changes in the air-sea gas exchange of methyl chloroform, Geophys. Res. Lett., 31, L16112, doi:10.1029/2004GL020476

Wild, O., X. Zhu, and M. J. Prather (2000) Fast-J: Accurate simulation of in- and below-cloud photolysis in tropospheric chemical models, J. Atmos. Chem., 37, 245-282

Wilson, D. F., J. W. Swinnerton, R. A. Lamontagne, (1970) Production of carbon monoxide and gaseous hydrocarbons in seawater: Relation to dissolved organic carbon, Science, 168, 1577-1579

Wilson Jr., E.W., W. A. Hamilton, H. R. Kennington, B. Evans III, N. W. Scott, and W. B. Demore (2006) Measurement and estimation of rate constants for the reactions of hydroxyl radical with several alkanes and cycloalkanes, J. Phys. Chem. A, 110, 3593-3604

World Health Organization (2003), Health aspects of air pollution with particulate matter, ozone, and nitrogen dioxide, Rep. EUR/03/5042688, Bonn.

Worton, D. W. (2005) Alkyl nitrates (C$_1$-C$_5$), trihalomethanes and related compounds in contemporary air and air preserved in polar firn and ice, Ph.D. Thesis, University of East Anglia, Norwich

Worton, D. R., W. T. Sturges, L. K. Gohar, K. P. Shine, P. Martinerie, D. E. Oram, S. P. Humphrey, P. Begley, J. -M. Barnola, J. Schwander, and R. Mulvaney (2007) Atmospheric trends and radiative forcings of CF$_4$ and C$_2$F$_6$ inferred from firn air, Environ. Sci. Technol., 41, 2184-2189, doi:10.1021/es061710t

Worton, D.R., G. P. Mills, D. E. Oram, and W. T. Sturges (2008) Gas chromatography negative ion chemical ionization mass spectrometry: application to the detection of alkyl nitrates and halocarbons in the atmosphere. J. Chromatogr. A, 1201, 112-119

Worton, D. W., W. T. Sturges, C. E. Reeves, M. J. Newland, S. A. Penkett, E. Atlas, V. Stroud, K. Johnson, N. Schmidbauer, S. Solberg, J. Schwander, and J-M., Barnola. (2012) Evidence from firn air for recent decreases in non-methane hydrocarbons and a 20th century increase in nitrogen dioxides in the northern hemisphere, Atmos. Environ., 54, 592-602

Zhang, Y., D. H. Stedman, G. A. Bishop, P. L. Guenther, and S. P. Beaton (1995) Worldwide on-road vehicle exhaust emissions study by remote sensing, Env. Sci. Technol., 2286-2294

Zhang, Y., D. H. Stedman, G. A. Bishop, S. P. Beaton, and P. L. Guenther (1996) On-road evaluation of inspection/maintenance effectiveness, Environmental Science and Technology, 30, 1445-1450